Ecology of methanotrophs in a landfill methane biofilter

David Pearce

Thesis submitted as a requirement for the degree of

Doctor of Philosophy

University of East Anglia,

Norwich, UK

School of Environmental Sciences

February 2023

Acknowledgements

I would like to thoroughly thank my supervisors J. Colin Murrell and Andrew Crombie from the University of East Anglia and Charles Wright from Norfolk County Council. My primary supervisor, Colin Murrell, provided invaluable advice and guidance throughout this project and Andrew Crombie was always willing to share his remarkable insight and knowledge. This project would not have been possible without the support of my CASE supervisor, Charles Wright, who ensured the Strumpshaw biofilter, his team and his own expertise in landfill management were always available. I am also extremely grateful to NERC (via the EnvEast DTP) and Norwich County Council for funding my PhD. I additionally thank Daniel Rankin for his constant help with all manner of biofilter matters and Keziah Flack for agreeing to repeatedly help with biofilter monitoring, as well as the rest of the Norfolk County Council closed landfill team. My thanks also go out to Hui-Juan Xu from the South China Agricultural University, for her assistance characterising soil CH_4 oxidation profiles at different soil moisture contents. I would like to extend a special thanks to Farhan Muhammad Ul-Haque (University of the Punjab), who acted as an additional mentor and helped me find my feet in the lab. I also thank the past and present members of the ELSA lab, for both the input and friendship they offered. Finally, I want to thank my family and friends for their enduring support.

Abstract

Decomposing landfill waste is a significant anthropogenic source of the potent climate-active gas methane (CH_4). To mitigate fugitive methane emissions Norfolk County Council are trialling a landfill biofilter, designed to harness the methane oxidizing potential of methanotrophic bacteria. These methanotrophs can convert CH_4 to CO_2 or biomass and act as CH_4 sinks.

The most active CH_4 oxidising regions of the Strumpshaw biofilter were identified from *in-situ* temperature, CH_4, O_2 and CO_2 profiles. While soil CH_4 oxidation potential was estimated and used to confirm methanotroph activity and determine optimal soil moisture conditions for CH_4 oxidation. It was observed that most CH_4 oxidation occurs in the top 60cm of the biofilter (up to 50% of CH_4 input) at temperatures around 50ºC, optimal soil moisture was 10-27.5%. A decrease in *in-situ* temperature following CH_4 supply interruption suggested the high biofilter temperatures were driven by CH_4 oxidation.

The biofilter soil bacterial community was profiled by 16S rRNA gene analysis, with methanotrophs accounting for ~5-10% of bacteria. Active methanotrophs at a range of different incubation temperatures were identified by $^{13}CH_4$ DNA stable-isotope probing coupled with 16S rRNA gene amplicon and metagenome analysis. These methods identified *Methylocella*, *Methylobacter*, *Methylocystis* and *Crenothrix* as potential CH_4 oxidisers at the lower temperatures (30ºC/37ºC) observed following system start-up or gas-feed interruption. At higher temperatures typical of established biofilter operation (45ºC/50ºC), *Methylocaldum* and an unassigned *Methylococcaceae* species were the dominant active methanotrophs.

Finally, novel methanotrophs *Methylococcus capsulatus* (Norfolk) and *Methylocaldum szegediense* (Norfolk) were isolated from biofilter soil enrichments. *Methylocaldum szegediense* (Norfolk) may be very closely related to or the same species as one of the most abundant active methanotrophs in a metagenome from a 50ºC biofilter soil incubation, based on genome-to-MAG similarity. This isolate was capable of growth over a broad temperature range (37-62ºC) including the higher (*in-situ*) biofilter temperatures (>50ºC).

<u>Wordcount</u> = 52131

Abbreviations

aa	amino acid
AAI	average amino acid identity
AMRC	average MAG read coverage
ANI	average nucleotide identity
ASV	amplicon sequencing variant
BLAST	Basic Local Alignment Search Tool
CBB	Calvin-Benson-Bassham
DGGE	denaturing gradient gel electrophoresis
FID	flame ionisation detector
GC	gas chromatography
H_4F	tetrahydrofolate
H_4MPT	tetrahydromethanopterin
LFG	landfill gas
MAG	metagenome assembled genome
MFR	methanofuran
NAD^+/NADH	nicotinamide adenine dinucleotide
$NADP^+$/NADPH	nicotinamide adenine dinucleotide phosphate
NCBI	National Centre for Biotechnology Information
NGS	next-generation sequencing
NMS	nitrate mineral salts
OD	optical density
pMMO	particulate methane monooxygenase
RFLP	restriction fragment length polymorphism
RuMP	ribulose monophosphate
sMMO	soluble methane monooxygenase

List of Figures

List of Tables

Chapter 1: Introduction

1.1 Methane and Landfills

Methane (CH_4) is a climate active compound that contributes to radiative forcing. CH_4 possesses a global warming potential approximately 25 times that of carbon dioxide over a 100-year timescale (IPCC, 2014; IPCC, 2007). Reducing CH_4 emissions would help offset the increase in radiative forcing attributed to human activities observed over the previous 200 years and could lessen the increase in global temperatures expected over the next century (IPCC, 2014).

There are many different sources of CH_4 including natural wetlands, wild animals (especially termites) and geothermal processes. More than half of CH_4 emissions are thought to be from anthropogenic sources with landfills and waste estimated to be responsible for 10-25% of total anthropogenic CH_4 emissions (IPCC, 2007). Other major anthropogenic sources include CH_4 generated from ruminant enteric fermentation and manure in the agricultural sector, in addition to fossil fuel exploitation in the oil, gas and coal mining industries (Saunois et al., 2020).

The CH_4 emitted from landfills is generated through anaerobic methanogenesis by archaea during the anaerobic decomposition of organic waste. The amount of CH_4 produced and consequently the CH_4% content of total landfill gas (LFG) varies through the life cycle of a landfill: with high initial concentrations as anaerobic conditions are established in the Landfill, but then tailing off to very low concentrations after landfill closure as less and less organic matter is left to drive CH_4 production. This tailing off period of low CH_4 content LFG can last from decades to 100 years depending on the site and is a legacy that adds up to a sizeable amount of climate active CH_4 (illustrated in (**Figure 1.1**)) (Huber-Humer et al., 2008).

Conversion of landfill gas CH_4 to the less potent CO_2 via combustion (also generating heat and potentially electricity) is an appealing CH_4 mitigation strategy. However, such combustion becomes increasingly difficult to maintain as the CH_4 content of the landfill gas drops to low (<15%) levels. First combustion for energy generation can no longer be sustained and then even flaring the gas simply for CH_4 to CO_2 conversion becomes impractical. When flaring is discontinued the CH_4 containing LFG is commonly vented into the atmosphere. Considering the long duration of the landfill gas CH_4 tail-off, a cost-effective management strategy for low CH_4 content LFG streams could serve to materially reduce anthropogenic CH_4 emissions from landfill sites (Browell et al., 2009; Jardine et al., 2004).

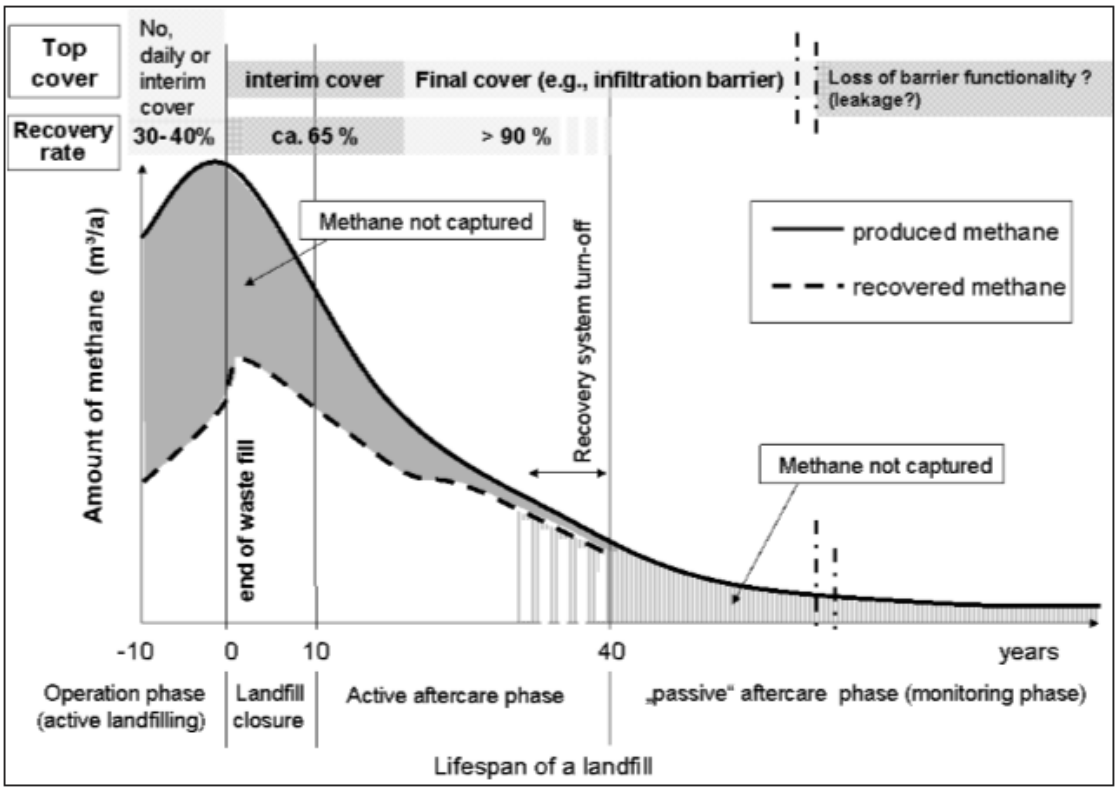

Figure 1.1 Production and recovery of landfill CH_4 over the lifetime of a landfill (Huber-Humer et al., 2008).

One such management strategy is the use of CH_4 biofilters, bioreactors containing CH_4 metabolising organisms called methanotrophs. Low content CH_4 LFG streams are directed through the bioreactor and the methanotrophs' metabolism can be harnessed to convert the CH_4 to CO_2 or incorporate the carbon into biomass. Effective design and efficient running of methanotroph biofilters requires a clear understanding of the biology of these key organisms (Huber-Humer et al., 2008; Scheutz and Kjeldsen, 2009).

1.2 Methanotrophs

Methanotrophs are organisms that derive their carbon and cellular energy from CH_4. They are predominantly gram-negative bacteria that oxidise CH_4 aerobically, (Anthony, 1982) although there are archaea capable of oxidising CH_4 through a reverse methanogenesis pathway (in association with sulphate reducing bacteria), as well as bacteria capable of generating molecular oxygen for CH_4 oxidation under anaerobic conditions (designated NC10) (Ettwig et al., 2010; Scheller et al., 2010). This project is primarily concerned with aerobic methanotrophs in protobacteria.

1.2.1 Methanotroph taxonomic hierarchy and morphology

Bacterial methanotrophs are grouped into four categories based on their morphology, physiology, biochemistry and phylogenetics. These categories are: Type I, Type II, Verrucomicrobia and NC10 (Hanson and Hanson, 1996; Semrau, 2011).

Type I methanotrophs are gamma proteobacteria. They assimilate carbon from CH_4 via the ribulose monophosphate (RuMP) cycle and possess distinctive intracytoplasmic membranes (ICMs) arranged in stacks (Hanson and Hanson, 1996). Type II methanotrophs are alpha proteobacteria. In these methanotrophs CH_4 derived carbon is assimilated through the serine cycle. Type II methanotrophs also have ICMs although in these bacteria they are arranged along the inside of- and parallel to the cell periphery (Hanson and Hanson 1996). While still widely used, it has been argued that the Type I and Type II terminology should be limited to a phylogenetic distinction between "gammaproteobacterial" and "alphaproteobacterial" methanotrophs due to the discovery of new genera and species that don't fit historical Type I and Type II classification criteria, such as fatty acid composition, ability to fix nitrogen and even the presence and arrangement of ICMs (Knief, 2015). Verrucomicrobia are mostly thermotolerant extremophiles often thriving at low pH (Dunfield et al., 2007; Sharp et al 2014). Although a number of mesophilic Verrucomicrobia have also been successfully isolated (Teeseling et al., 2014). They are autotrophic, using CH_4 oxidation to generate reducing equivalents and assimilating carbon from CO_2 through the Calvin-Benson-Bassham (CBB) cycle (Khadem et al 2011). Some appear to contain ICMs (Dunfield et al., 2007; Teeseling et al., 2014). NC10 consist of anaerobic organisms only available in enrichments, they can generate molecular oxygen for CH_4 oxidation from reduction of nitrite (Ettwig et al., 2010). Like Verrucomicrobia, NC10 organisms assimilate carbon from CO_2 through the CBB cycle and use CH_4 oxidation for reducing equivalent generation (Rasigraf et al., 2014). Candidatus *Methylomirabilis oxyfera* has an unusual polygonal rod shape and does not seem to possess ICMs (Wu et al., 2012), Candidatus *Methylomirabilis sinica* also has a polygonal (coccus) morphology (He et al., 2016).

(**Figure 1.2**) Shows the evolutionary relationship between members of these four different groups of methanotrophs based on their 16S rRNA sequences, demonstrating the phylogenetic rationale for separation into these categories.

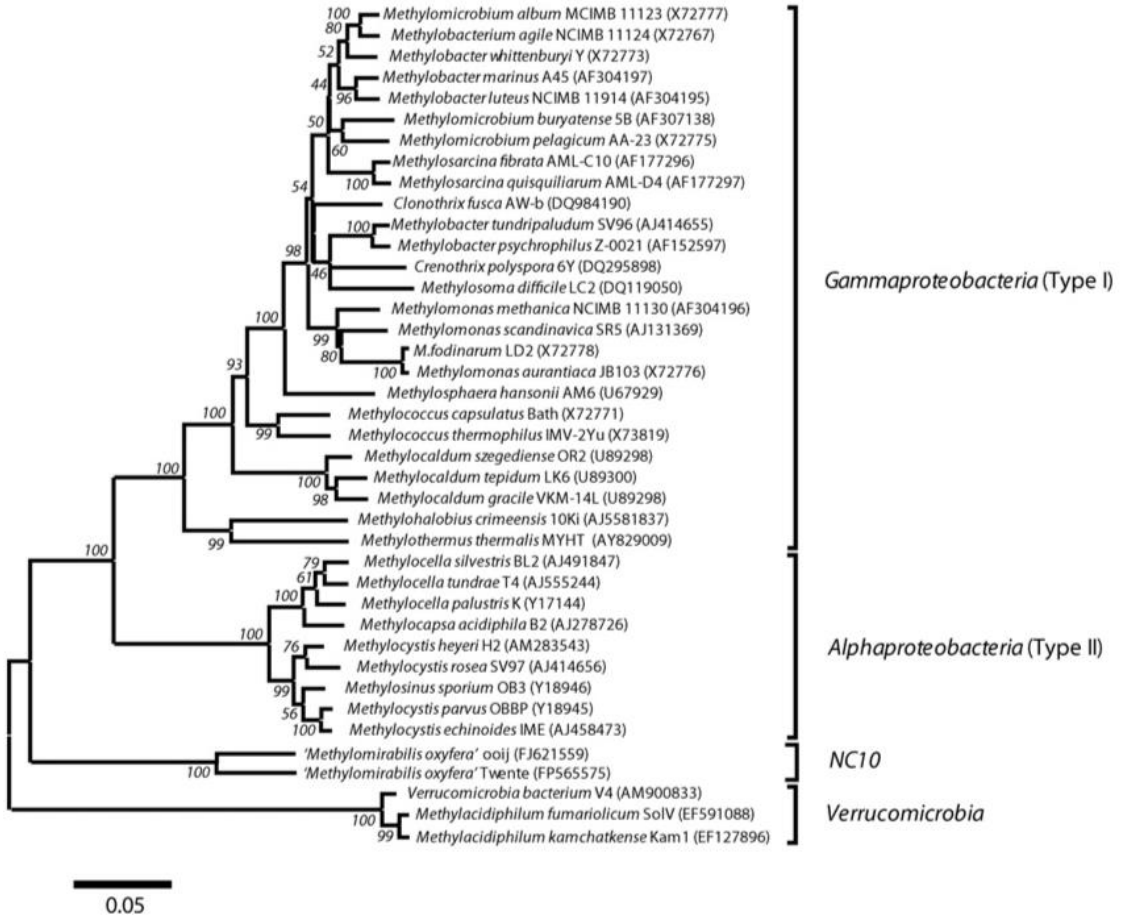

Figure 1.2 Phylogenetic tree of bacterial methanotrophs from the four categories, Type I, Type II, Verrucomicrobia and NC10 constructed from their 16S rRNA sequences. Includes a scale bar for evolutionary distance (nucleotide substitutions per site). From Wu et al. 2011 (Wu et al., 2011).

1.2.2 Methanotroph physiology

Methanotrophic bacteria are found in a wide range of environments from agricultural and forest soils, landfill cover soils, acidic peat bogs, marine/freshwater and soda lakes to volcanic mudpots and polar tundras (Cebron et al., 2007; Dedysh et al., 2000; Kizilova et al., 2013; Lin et al., 2004; Omelchenko et al., 1993; Pol et al., 2014; Radajewski et al., 2002; Vekeman et al., 2016; Zigah et al., 2015).

Writing in 1996 Hanson and Hanson noted that most methanotrophs seemed to grow at neutrophilic or slightly acidic conditions with no known methanotroph growing at a pH below 5, and all available isolates were mesophilic apart from relatives of the thermophilic *Methylococcus capsulatus* and psychrophilic arctic methanotrophs isolated by Omelchenko et al. in 1993 (Hanson and Hanson, 1996; Omelchenko et al., 1993). In the years since a number

of thermotolerant and thermophilic methanotrophs have been discovered, such as the thermotolerant (Type I) *Methylocaldum* strains which will grow at temperatures above 40˚C (Bodrossey et al., 1997). Methanotrophs belonging to the Verrucomicrobia have been found at considerably higher temperatures: Sharp et al. identified putative Verrucomicrobial methanotrophs in acidic geothermal environments at temperatures ranging from 22.5 to 81.6˚C (using 16S rRNA gene amplicon sequencing) (Sharp et al., 2014). More psychrophilic methanotrophs have also been found such as the Type I methanotrophs *Methylomonas scandinavica* with an optimal growth temperature of 15˚C, and *Methylosphaera hansonii* which had an optimum growth temperature around 10˚C but was also seen to grow well at 0˚C (Bowman et al., 1997; Kalyuzhnaya et al., 1999).

The number of acidophile methanotrophs has also increased with the discovery of such organisms as the Type II methanotrophs *Methylocella palustris* and *Methylocella silvestris* both of which are capable of growth at pH 4.5 (Dedysh et al., 2000; Dunfield et al., 2003). Verrucomicrobial bacteria have been isolated that are capable of oxidising CH_4 at pH 1 (Dunfield et al., 2007). Halotolerant alkaliphilic methanotrophs have also been found, a prime example being the Type I *Methylomicrobium alcaliphilum*, which demonstrated fastest growth at pH 9 and would not grow at pH 6.8 or lower (Kalyuzhnaya et al., 2008; Khmelenina et al., 1997).

Microaerobic and anaerobic bacterial methanotrophy is also known. Type I microaerobic methanotrophs such as Candidatus *Methylospira mobilis*, *Methylosoma difficile* and *Methyloglobulus morosus* have been recovered from the oxic-anoxic interface of a peat bog and lake sediments (Danilova et al., 2016; Deutzmann et al., 2014; Rahalkar et al., 2007). Anaerobic bacterial methane oxidisers are found in the NC10 phylum and include candidatus *M. oxyfera* and candidatus *M. sinica* (Ettwig et al., 2010; He et al., 2016).

1.2.3 Methanotroph biochemistry

1.2.3.1 The CH_4 oxidation pathway in methanotrophs

Aerobic oxidation of CH_4 to CO_2 by methanotrophs is a multi-step enzyme pathway with different routes available for carbon assimilation depending on the enzyme inventory of the methanotroph in question. (**Figure 1.3**) shows an overview of the methanotroph CH_4 oxidation pathways.

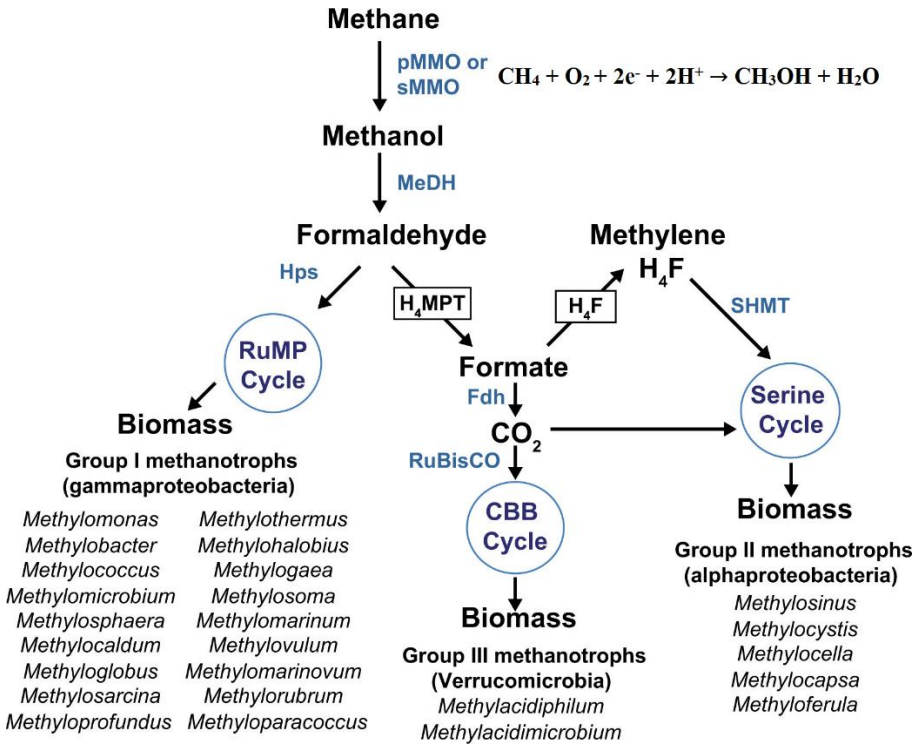

Figure 1.3 Assimilatory and dissimilatory pathways of CH_4 oxidation in methanotrophs. From Kalyuzhnaya et al. (Kalyuzhnaya et al. 2015) with CH_4 oxidation reaction added. Hps: hexulose phosphate synthase, pMMO: particulate methane monooxygenase, sMMO: soluble methane monooxygenase, Fdh: Formate dehydrogenase, SHMT: Serine hydroxymethyl transferase.

1.2.3.1.1 Methane Oxidation

The initial step in the pathway (oxidation of CH_4 to methanol) is carried out by a methane monooxygenase enzyme of which there are two types: the cytoplasmic soluble methane monooxygenase and the ICM associated particulate methane monooxygenase (Hanson and Hanson 1996; Nguyen et al., 1998). Methanotrophs can possess either or both of these MMOs although pMMO is the most widespread and relatively few methanotrophs (*Methylocella*, *Methyloferula* and *Methyloceanibacter*) rely solely on sMMO for CH_4 oxidation (Dedysh et al., 2000; Vekeman et al., 2016; Vorobev et al., 2011).

Soluble methane monooxygenase is a diiron monooxgenase (Rosenzweig et al., 1993). The gene map of the sMMO operon in *Methylosinus trichosporium* OB3b is shown in (**Figure 1.4**), the *mmoXYBZDC* arrangement is common to the majority of sMMO harbouring methanotrophs (Lee, 2016).

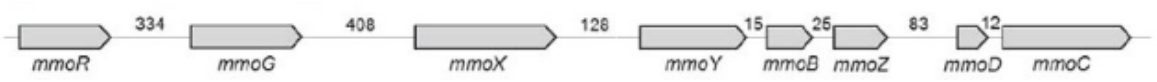

Figure 1.4 Gene map of the *M. trichosporium* (OB3b) sMMO operon adapted from Lee, 2016 (Lee, 2016).

The sMMO enzyme is made up of three structural elements (Stirling and Dalton, 1978): a hydroxylase, a reductase and a regulatory protein (Green and Dalton, 1985). The hydroxylase component MMOH (251 kDa) consists of three different subunits: an α-subunit encoded by *mmoX* (60.6kDa), a β-subunit encoded by *mmoY* (40.5kDa), and a γ-subunit encoded by *mmoZ* (19.8 kDa), arranged as an $\alpha_2\beta_2\gamma_2$ homodimer. The non-haem diiron active site is located in the α subunit of each homodimer and in the assembled protein these active sites are arranged within a hydrophobic pore (Rosenzweig et al., 1993). The reductase component MMOR (40kDa) encoded by *mmoC* contains flavin adenine dinucleotide (FAD) and 2Fe-2S centres that facilitate transfer of electrons from NADH to the diiron active site in the hydroxylase (Colby and Dalton, 1979; Fox et al., 1989; Lee, 2016). The regulatory component MMOB (16kDa) encoded by *mmoB* acts to improve the efficiency of CH_4 Oxidation by sMMO, the binding of MMOB to MMOH induces conformational changes that affect substrate access to the diiron active site of MMOH. MMOB also acts to modulate electron transfer by displacing the reductase after it is oxidised, allowing CH_4 oxidation to proceed (Lee, 2016; Walters et al., 1999; Wang et al., 2014). The other non-structural genes in the sMMO cluster are thought to have a regulatory function (Lee, 2016; Semrau et al., 2013).

Decades of research into the mechanism of CH_4 oxidation by sMMO have allowed a model for this process to be built up. The diiron active site (in MMOH) is sequentially reduced (by MMOR) and then goes through a series of transient states including the key dinuclear Fe^{IV} species Q that is capable of breaking the C-H bond in CH_4 (Lee et al., 1993b; Lee et al., 1993a). In the initial oxidised state (MMOHox) an Fe^{III} Fe^{III} state is observed, this is followed by reduction of one of the Fe atoms to produce an Fe^{II} Fe^{III} mixed valence intermediate, followed

by reduction of the other Fe atom to create the fully reduced (MMOHred) Fe^{II} Fe^{II} form (with electron transfer from MMOR driving both reduction steps) (Fox et al., 1989; Fox et al., 1988). MMOHred then reacts with O_2 to form O, in the presence of the regulatory component MMOB the rate of this reaction is increased by a factor of 1000 (Liu et al., 1995). O is the first of several transient species, followed by transformation to ($Fe^{II}Fe^{II}$) P*, then to P a peroxodiiron($Fe^{III}Fe^{III}$) species, then Q (the dinuclear Fe^{IV} species) which reacts with CH_4 leading to production of the product complex T (through predicted intermediates QS and R) and ultimately release of CH_3OH and regeneration of MMOHox (Banerjee et al., 2015; Banerjee et al., 2013; Brazeau and Lipscomb 2000; Tinberg and Lippard 2009). This mechanism is outlined in (**Figure 1.5**).

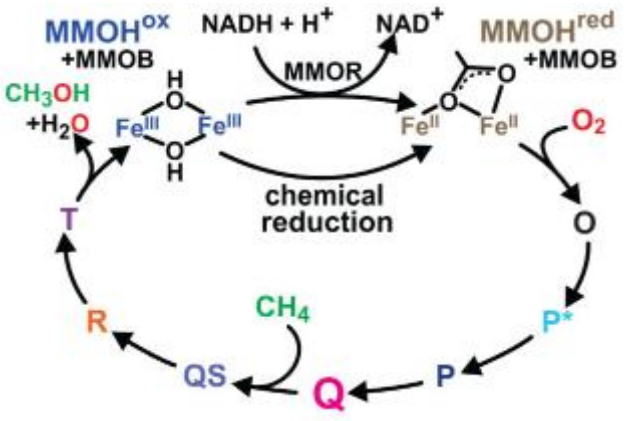

Figure 1.5 Proposed mechanism of sMMO CH_4 oxidation, from Banerjee et al (Banerjee et al., 2015).

In contrast to sMMO, Particulate methane monooxygenase is less well understood. The pMMO operon consists of a sequence of three genes *pmoA*, *pmoB* and *pmoC*, usually in the order *pmoCAB* (Lieberman and Rosenzeig, 2004). Some methanotrophs such as the Type II *Methylocystis* sp. Strain SC2 are known to encode more than one isozyme of pMMO with different affinities for CH_4 (Dam et al., 2012). The pMMO enzyme consists of three different subunits assembled as an $\alpha_3\beta_3\gamma_3$ trimer: the 47kDa α subunit (*pmoB*) originally thought to contain the active site, 24kDa β subunit (*pmoA*) and 22kDa γ subunit (*pmoC*) (Culpepper and Rosenzweig, 2012; Lieberman and Rosenzweig, 2005). While sMMO is regarded as a card-carrying diiron monooxygenase, there has been far less consensus regarding the metal content of the pMMO active site. Dinuclear Fe as well as mono-, di-, and tri-Cu active sites have all been proposed. Recent research by Cao et al suggests that a mononuclear copper site is more

compatible with current crystallographic information (Cao et al., 2018; Culpepper and Rosenzweig, 2012). While Chang et al. suggest the active site may in fact be a cavity between the *pmoA* and *pmoC* encoded subunits with a tri-Cu centre, based on their 2.5 Å cryo-EM structure of *holo*-pMMO (Chang et al., 2021). The mechanism of CH_4 oxidation in pMMO has not yet been identified although potential reductants include ubiquinol supplied by a NADH:quinone oxidoreductase or a methanol dehydrogenase coupled electron transfer (Culpepper and Rosenzweig, 2014).

Both sMMO and pMMO are capable of co-metabolising a range of other compounds besides CH_4, although sMMO has a broader substrate range than pMMO (Burrows et al., 1984). Significantly MMOs are capable of co-metabolising ammonia, with apparent km values in the 0.19-3.9 mM range (as estimated by Nyerges and Stein), which suggests methanotrophs may play a role in the global nitrogen cycle (Dalton, 1977; Nyerges and Stein, 2009; Stein et al., 2012). sMMO and pMMO also have different affinities for CH_4: pMMO usually has a higher affinity with rough km values of 1-2μM and 0.1μM for CH_4 and O_2, while for lower affinity sMMO these values are in the region of 3μM and 16.8μM respectively. This higher affinity of pMMO for CH_4 paints pMMO as the more efficient MMO for CH_4 oxidation (Trotsenko and Murrell, 2008).

1.2.3.1.2 Methanol oxidation

The second step (conversion of methanol to formaldehyde) is carried out by a methanol dehydrogenase (MDH) (Hanson and Hanson, 1996). Methanotrophs possess both Calcium (MxaFI) and Lanthanide (XoxF) dependant methanol dehydrogenases. MxaFI was long thought to be the primary enzyme catalysing methanol conversion, until the recent discovery of widespread methanotroph XoxF MDHs and their contribution to this step of the CH_4 oxidation pathway.

The Ca^{2+} dependant MxaFI methanol dehydrogenase is a periplasmic enzyme with a heterotetrameric structure ($\alpha_2\beta_2$) composed of large MxaF (α) and small MxaI (β) subunits (Anthony, 1992; Nunn et al., 1989). A pyrroloquinoline quinone (PQQ) prosthetic group and a Ca^{2+} cofactor are located in the active site of the α subunits (Goodwin and Anthony, 1995).

Methanol oxidation by MxaFI is coupled to reduction of the PQQ group, producing formaldehyde and reduced $PQQH_2$. The Ca^{2+} cofactor in the active site acts as a Lewis Base

and makes the PQQ C5 a better electrophile for attack and reduction by activated CH_3OH. PQQ is then regenerated from the reduced form $PQQH_2$ by a two round sequential transfer of individual electrons to cytochrome C_L, these electrons are then passed on to an additional cytochrome C_H and from there to a terminal oxidase that reduces oxygen to H_2O at the end of the electron transport chain (Anthony and Williams, 2003; Goodwin and Anthony, 1995).

XoxF is a homodimer, with subunits sharing a limited sequence similarity (50%) to the MxaF components of MxaFI (Chistoserdova, 2011). Significantly, XoxF features a bound Lanthanide ion (rather than Ca^{2+}) alongside the PQQ in each subunit (Gu et al., 2016; Nakagawa et al., 2012; Pol et al., 2014). The presence of a lanthanide rare earth element (REE) cofactor was surprising as REEs were not previously considered to be biologically essential (Nakagawa et al., 2012). The presence of a lanthanide REE rather than Ca^{2+} likely confers improved catalytic ability on XoxF MDHs as lanthanides are stronger Lewis Bases than Ca^{2+} and may further enhance the susceptibility of PQQ C5 to reduction by CH_3OH (Pol et al., 2014). *M. oxyfera* contains a more unusual form of XoxF MDH, this enzyme is composed of two XoxF subunits and two MxaI subunits in a heterotetramer arrangement (Wu et al., 2015).

1.2.3.1.3 Oxidation of formaldehyde

Methanotrophs have a number of enzymes capable of oxidising formaldehyde via different routes. Formaldehyde oxidation to CO_2 (via formate) generates a large proportion of the reducing equivalents required for CH_4 oxidation (Hanson and Hanson, 1996), additionally formaldehyde and formate represent branch points for C_1 assimilation (Crowther et al., 2008; Higgins et al., 1981).

Two major routes for methanotroph formaldehyde oxidation are the Tetrahydromethanopterin (H_4MPT) and Tetrahydrofolate (H_4F) linked pathways (Vorholt, 2002), with an additional route via a non-assimilatory branch of the RuMP pathway (Anthony, 1982). In the H_4MPT-linked pathway formaldehyde first combines with H_4MPT to form methylene H_4MPT through a condensation reaction catalysed by the formaldehyde activating enzyme (Fae). The methylene H_4MPT then undergoes a dehydrogenation reaction catalysed by the $NAD(P)^+$ methylene H_4MPT dehydrogenases (MtdB or MtdA), which also generates NADH or NADPH (Vorholt et al., 2000), the resulting methenyl-H_4MPT is then converted to formyl-H_4MPT through hydrolysis by the methenyl-H_4MPT cyclohydrolase enzyme (Mch). Finally, the formyl group from formyl-H_4MPT is transferred to methanofuran (MFR) by the formyl-transferase (Ftr)

present as subunit FhcD in the formyltransferase/hydrolase complex (FhcABCD), the formyl-MFR produced is then hydrolysed to formate and MFR by this complex (Vorholt, 2002).

The H_4F-linked pathway relies on the spontaneous coupling of formaldehyde to H_4F to form methylene-H_4F as its first step, which is then followed by a series of reversible reactions to produce formate. In the first of these methylene-H_4F is converted to methenyl-H_4F (and NADPH generated) in a reaction catalysed by the NADP-dependent H_4F dehydrogenase (MtdA). The methenyl-H_4F produced is then converted to formyl-H_4F using the methenyl H_4F cyclohydrolase enzyme (FchA). In the final step, formate H_4F ligase (Ftfl) catalyses the conversion of formyl-H_4F to formate (Vorholt, 2002).

The formate generated from formaldehyde oxidation can be directed into the serine cycle (for carbon assimilation) via conversion to methylene-H_4F using the reverse H_4F coupled (reductive pathway), with transfer to the serine cycle facilitated by the serine hydroxymethyltransferase encoded by *glyA* (Crowther et al., 2008). The use of this pathway in reverse to produce methylene-H_4F from formate generated through the H_4MPT-linked pathway may be essential in type II methanotrophs, which are dependent on the serine cycle for carbon assimilation, as the serine cycle using methylotroph *Methylobacterium extorquens* (AM1) was unable to grow on methanol as Δ*mtdA*, Δ*fchA* or Δ*ftfl* mutants (Crowther et al., 2008).

There is a possibility that some methanotrophs could possess cytochrome-linked formaldehyde dehydrogenases (FADH) capable of oxidising formaldehyde directly to formate. In *Methylococcus capsulatus* (Bath) an FADH containing a PQQ synthetic group was thought to be responsible for the majority of formaldehyde oxidation when grown in Cu rich conditions (Zahn et al., 2001), although this was later found to be due to the combined activity of methanol dehydrogenase and methylene-H_4MPT dehydrogenase (Adeosun et al., 2004).

1.2.3.1.4 Oxidation of formate to CO_2

The final step in the methanotroph CH_4 oxidation pathway, oxidation of formate to CO_2 (and concomitant production of the reducing equivalent NADH), is catalysed by a formate dehydrogenase (FDH) (Popov and Lamzin, 1994). The existence of multiple FDH isoforms in the same methanotroph is known (Ward et al., 2004).

1.2.3.1.5 Carbon assimilation via the RuMP, Serine and CBB cycles

Methanotrophs incorporate carbon into their central metabolism through one of three cycles: the ribulose monophosphate (RuMP) cycle, the serine cycle or the Calvin-Benson-Bassham (CBB) cycle (Hanson and Hanson, 1996; Khadem et al., 2011; Rasigraf et al., 2014). The entry points for each of these cycles are: formaldehyde for the RuMP cycle, methylene-H_4F for the serine cycle and CO_2 for the CBB cycle. (Crowther et al., 2008; Higgins et al., 1981). candidate phylum NC10 and verrucomicrobial methanotrophs use the CBB cycle, Type II (alphaproteobacterial) methanotrophs utilise the serine cycle and Type I (gammaproteobacterial) methanotrophs leverage the RuMP cycle. A subset of Type I methanotrophs belonging to the *gammaproteobacteria* possess genes for more than one carbon assimilation pathway, such as *Methylococcus capsulatus* Bath (which hosts genes belonging to all three pathways) (Chistoserdova et al., 2005).

The ribulose monophosphate cycle begins the process of carbon assimilation by first combining formaldehyde with ribulose-5-phosphate to form 3-hexulose-6-phosphate in an aldol condensation reaction, the product then undergoes an isomerization reaction to form fructose-6-phosphate, these two reactions are catalysed by a hexulose phosphate synthase (HPS) and hexulose isomerase (HPI) respectively (Anthony, 1982). The formaldehyde derived carbon can then be channelled into biosynthesis through either: conversion of fructose-6-phosphate to fructose-1,6-bisphosphate by a phosphofructokinase followed by splitting to produce glyceraldehyde-3-phosphate and glycerone phosphate (DHAP), catalysed by a fructose-bisphosphate aldolase (FBA); or by conversion of fructose-6-phosphate to glucose-6-phosphate using a glucose phosphate isomerase (GPI) and following the Entner-Douderoff, pathway to produce glyceraldehyde-3-phosphate and pyruvate from aldolase splitting of an intermediate 2-dehydro-3-deoxy-phosphogluconate (White, 2007). For every three formaldehyde molecules used to form 3-hexulose-6-phosphate one molecule of generated pyruvate or glycerone phosphate is directed into biosynthesis, while the glyceraldehyde-3-phosphate and remaining fructose-6-phosphate molecules are used to regenerate three molecules of ribulose-5-phosphate (through a series of rearrangement reactions) allowing the cycle to continue (Anthony, 1982).

Carbon enters the serine cycle for assimilation via condensation of methylene-H_4F from the reductive tetrahydrofolate (H_4F)-linked pathway with glycine to produce serine (catalysed by the *glyA* encoded serine hydroxymethyltransferase) (Crowther et al., 2008). Serine (containing

methylene-H_4F derived carbon) is next converted to hydroxypyruvate in a reaction catalysed by the serine-glyoxylate aminotransferase enzyme (SgaA) before being successively converted to glycerate, 2-phosphoglycerate and then phosphoenolpyruvate by the enzymes glycerate dehydrogenase (hprA), glycerate-2-kinase (Gck) and enolase (ENO) respectively (Anthony, 2011). Phosphoglycerate represents a major branch point in the serine cycle (Matsen et al., 2013), where 2-phosphoglycerate can be directed into biosynthesis (by conversion to 3-phosphoglycerate), with the remainder of the serine cycle concerned with regenerating glyoxylate and then glycine to accept further molecules of methylene-H_4F. In this regeneration segment phosphoenolpyruvate is first converted to oxaloacetate through incorporation of a CO_2 molecule catalysed by the phosphoenolpyruvate carboxylase (PPC) enzyme. The oxaloacetate is then converted to malate by malate dehydrogenase (Mdh), and the malate to malyl-CoA by malate thiokinase (MtkA and MtkB subunits). The malyl-CoA is then split into glyoxylate and acetyl-CoA by malyl-CoA lyase (MCL) and glycine is produced from the glyoxylate by the serine-glyoxylate aminotransferase enzyme (SgaA) (which also catalysed the serine to hydroxypyruvate reaction) (Anthony, 2011; Chistoserdova and Lidstrom, 1994). In addition to this primary serine cycle there is a glyoxylate regeneration cycle then serves to make up the balance of glyoxylate (and then glycine) lost from the cycle through diversion of intermediates (such as phosphoglycerate) for biosynthesis. This regeneration pathway takes the acetyl-CoA resulting from malyl-CoA lysis and produces additional glyoxylate molecules by CO_2 carbon addition in a multistep pathway (Anthony, 2011; Braakman and Smith 2013).

The carbon fixation step in the Calvin-Benson-Bassham cycle is catalysed by the crucial ribulose-1,5-bisphosphate carboxylase/oxygenase (RubisCO) encoded by the *cbbL* and *cbbS* genes (Baxter et al., 2002), this step sees the formation of two molecules of phosphoglycerate from ribulose-1,5-bisphosphate and CO_2. The phosphoglycerate is then reduced to glyceraldehyde-3-phosphate via two reactions catalysed by phosphoglycerate kinase (PGK) and glyceraldehyde 3-phosphate dehydrogenase (GAP) with a bisphosphate intermediate. The glyceraldehyde-3-phosphate is the branch point for carbon transfer to biosynthesis with one glyceraldehyde-3-phosphate molecule diverted to biosynthesis for every three CO_2 molecules fixed (Anthony, 1982; White, 2007), the remaining five molecules of glyceraldehyde-3-phosphate are used to regenerate the three molecules of ribulose-1,5-bisphosphate initially combined with the CO_2. This ribulose-1,5-bisphosphate regeneration is achieved through a series of reactions laid out in (**Table 1.1**) (White, 2007). It has been noted that sedoheptulose-1,7-bisphosphatase is missing in *Methylococcus capsulatus* (Bath) which instead possesses a

pyrophosphate-dependent 6-phosphofructokinase (PPi-PFK) which was found capable of catalysing the same step in the CBB cycle (Reshetnikov et al., 2008). Henard et al recently demonstrated that CO_2 and RubisCO are essential for growth in *Methylococcus capsulatus* (Bath) (Henard et al., 2021), with their isotope study suggesting *M.c.* (Bath) may be leveraging the oxidative pentose phosphate pathway, possibly for generation of reducing equivalents in the form of NADH.

In addition to the majority of methanotrophs which are obligate methanotrophs utilizing CH_4 for cellular energy and CH_4 (or CO_2) for carbon assimilation, there are also facultative methanotrophs capable of growing on compounds other than CH_4. One of the best-known examples of such an organism is *Methylocella silvestris*, the first methanotroph shown to be capable of growth on either CH_4 or a short chain alkane (propane) (Crombie and Murrell, 2014).

Table 1.1 Calvin-Benson-Bassham (CBB) cycle reaction pathway leading to ribulose-1,5-bisphosphate regeneration. The enzymes for each step are shown, along with an overall net reaction for the ribulose-1,5-bisphosphate regeneration section of the CBB cycle. (White 2007).

Ribulose-1,5-bisphosphate regeneration steps in the Calvin-Benson-Bassham (CBB) cycle	**Enzyme**
2 glyceraldehyde-3-phosphate -> 2 glycerone phosphate (DHAP)	triose phosphate isomerase (TPI)
glyceraldehyde-3-phosphate + glycerone phosphate (DHAP) -> fructose-1,6-bisphosphate	fructose bisphosphate aldolase (FBA)
fructose-1,6-bisphosphate + H_2O -> fructose-6-phosphate + Pi	fructose bisphosphate phosphatase (FBP)
fructose-6-phosphate + glyceraldehyde-3-phosphate -> erythrose-4-phosphate + xylulose-5-phosphate	transketolase (TKT)
erythrose-4-phosphate + glycerone phosphate (DHAP) -> sedoheptulose-1,7-bisphosphate	sedoheptulose-1,7-bisphosphate aldolase (SBPA)
sedoheptulose-1,7-bisphosphate + H_2O -> sedoheptulose-7-phosphate + Pi	sedoheptulose-1,7-bisphosphatase (SBP)
sedoheptulose-7-phosphate + glyceraldehyde-3-phosphate -> ribose-5-phosphate + xylulose-5-phosphate	transketolase (TKT)
2 xylulose-5-phosphate -> ribulose-5-phosphate	ribulose phosphate epimerase (RPE)
ribose-5-phosphate -> ribulose-5-phosphate	ribose phosphate isomerase (RPI)
3 ribulose-5-phosphate + 3 ATP -> 3 ribulose-1,5-bisphosphate + 3 ADP	phosphoribulokinase (PRK)
Overall:	
5 Glyceraldehyde-3-phosphate + 2 H_2O + 3 ATP -> 3 ribulose-1,5-bisphosphate + 2 Pi + 3 ADP	

1.2.3.2 Nitrogen pathways of methanotrophs

Methanotrophs can utilize ammonium as their nitrogen source with most also capable of using nitrate and nitrite with a subset capable of using urea, casamino acids and yeast extract (Whittenbury et al., 1970).

1.2.3.2.1 Ammonia incorporation in methanotrophs

Type II methanotrophs implement the GS/GOGAT glutamate cycle for NH_4^+ assimilation (Trotsenko and Murrell, 2008), this cycle is dependent on the glutamine synthetase (GS) and glutamate synthase (also known as glutamine-oxoglutarate aminotransferase, GOGAT) enzymes encoded by the *glnA* (GS) or *gltB* and *gltD* (GOGAT) genes (Mohammadi et al., 2017). Glutamine synthetase combines NH_4^+ with glutamate in an ATP driven reaction to form glutamine, while in the second stage of the cycle glutamate synthase produces two molecules of glutamate from glutamine and 2-oxoglutarate, for a net production of one molecule of glutamate from one molecule of NH_4^+ and 2-oxoglutarate (Murrell and Dalton, 1983b).

In Type I methanotrophs the mechanism of ammonia assimilation is dependent on the available N source: when grown on ammonia α-ketoglutarate or pyruvate reductive amination pathways are responsible for ammonium (NH_4^+) assimilation using glutamate dehydrogenase or alanine dehydrogenase, however when grown at very low ammonia levels (<0.5mM) or solely on nitrate Type I methanotrophs were observed to leverage the glutamate cycle for ammonia incorporation (Murrell and Dalton, 1983b). Additionally, under growth at higher ammonia concentrations GS is adenylylated, which makes the enzyme more sensitive to feedback inhibition (Murrell and Dalton, 1983a). This shift between ammonia levels is likely due to the glutamate cycle being a higher affinity but also more energy expensive assimilation mechanism due to the ATP requirement (Murrell and Dalton, 1983b).

Nitrate and nitrite assimilation is accomplished via conversion to ammonia utilising nitrate/nitrite reductases such as assimilatory NasA and NirB (Kits et al., 2015; Ren et al., 2000; Stein and Klotz, 2011).

1.2.3.2.2 Methanotroph nitrification

Nitrification in methanotrophs is linked to the detoxification of hydroxylamine generated by the cometabolic oxidation of ammonia by methanotroph MMOs (Stein and Klotz, 2011). Cometabolic oxidation of ammonia by sMMO or pMMO generates hydroxylamine (Dalton, 1977; Nyerges and Stein, 2009). The nitrification (detoxification) pathway then begins with oxidation of hydroxylamine to nitrite or nitric oxide by hydroxylamine oxidoreductase (Poret-Peterson et al., 2008) or cytochrome P460 (Elmore et al., 2007), followed by reduction of nitrite to nitric oxide by nitrite reductases NirK and NirS (Stein and Klotz, 2011) and finally reduction of nitric oxide to nitrous oxide by nitric oxide reductase (encoded by the *norB* and *norC* genes) (He et al., 2022; Stein et al., 2012). This Nitrification pathway is shown in (**Figure 1.6**).

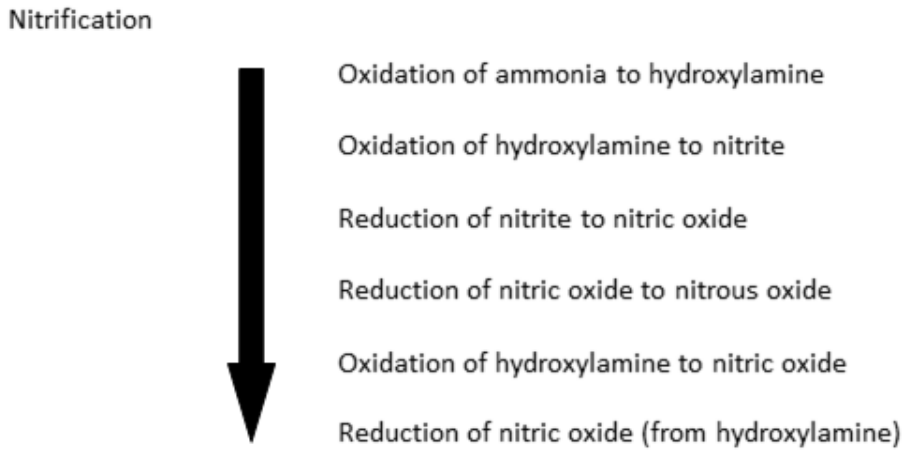

Figure 1.6 Nitrification pathway in methanotrophs, adapted from Stein and Klotz, 2011 (Stein and Klotz., 2011).

Some methanotrophs have also been found to possess putative hydroxylamine oxidoreductase genes (*hao*) for the detoxification of hydroxylamine through regeneration of ammonia (Dam et al., 2012; Stein et al., 2010).

1.2.3.2.3 Methanotroph denitrification

The exact role of denitrification in methanotrophs appears to be removal of toxic nitrogen compounds or respiratory denitrification to preserve O_2 for aerobic CH_4 oxidation under O_2 limited conditions (Kits et al., 2015; Nyerges et al., 2010). Denitrification in methanotrophs consists of the reduction of nitrate to nitrous oxide or dinitrogen (Stein and Klotz, 2011). Although complete denitrification to N_2 has so far only been observed in *Methylocystis* sp. (Dam et al., 2013), other methanotrophs lack a nitrous oxide reductase. See (**Figure 1.7**) for the full pathway and enzymes involved.

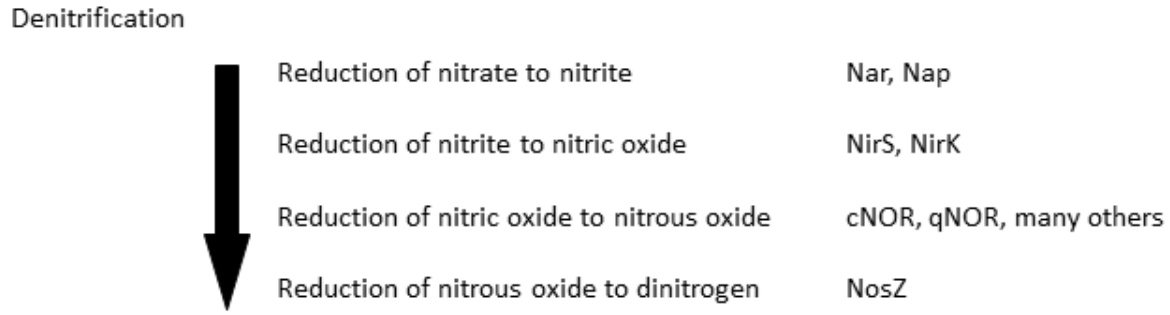

Figure 1.7 Denitrifying pathway in methanotrophs and enzymes responsible for each step, adapted from Stein et al 2011 (Stein and Klotz, 2011).

1.2.3.2.4 Potential for N_2O production in methanotrophs?

As we have seen the nitrifying and denitrifying pathways of methanotrophs can both produce N_2O (itself a potent climate active compound). Myung et al found that methanotroph enrichments were capable of generating significant amounts of nitrous oxide under high N and low O_2 conditions (Myung et al., 2015). The potential production of nitrous oxide by methanotrophs being used for greenhouse gas mitigation (CH_4 oxidation), would be counterproductive and needs to be evaluated and (ideally) eliminated. Similarly, research by Chang et al indicated that methanobactin from *Methylosinus trichosporium* OB3b inhibited reduction of nitrous oxide to dinitrogen in cocultured denitrifiers, resulting in increased accumulation of nitrous oxide. This was likely due to sequestration of environmental copper by methanobactin leading to downregulation of the denitrifiers' copper dependant NosZ nitrous

oxide reductase. This is another potential source of elevated nitrous oxide that would have to be accounted for within a biofilter setting (Chang et al., 2018).

1.2.3.2.5 Fixation of atmospheric dinitrogen in methanotrophs

Conversion of dinitrogen to ammonia (the ability to fix N_2) has been observed for members of the Type I, Type II and Verrucomicrobial methanotrophs (Auman et al., 2001; Hoefman et al., 2014; Khadem et al., 2010) although the presence or absence of this pathway has shown variability between strains of the same species (Hoefman et al., 2014). *nifH*, *nifK* and *nifD* are the nitrogenase structural genes, *nifH* encodes the Fe harbouring nitrogenase protein (Trotsenko and Murrell 2008).

1.2.3.2.6 NC10 - Coupling nitrite reduction to aerobic CH_4 oxidation

NC10 methanotrophs are able to carry out aerobic CH_4 oxidation in anaerobic environments by generating molecular oxygen (via nitrite reduction) for use in the oxidation of CH_4 to CH_3OH. They can perform such a feat due to expression of a nitric oxide dismutase: $2NO_2^-$ is first reduced to 2NO then nitric oxide dismutase converts the 2NO to N_2 and O_2 which is then available for aerobic oxidation of CH_4 (Ettwig et al., 2010).

1.2.3.2.7 Concluding remarks on nitrogen metabolism

The fitness of different methanotrophs over a range of N source conditions is likely to vary wildly as a study by Hoefman et al indicated a great deal of diversity in nitrogen metabolism within one methanotroph genus (and even within the same species) (Hoefman et al., 2014). Such potential differentiation in N metabolic capability should be born in mind when investigating the effects of different N sources as well as the potential for nitrous oxide generation. As an example: methanotrophs have variable ability to tolerate generated hydroxylamine depending on their inventory of enzymes. Some have detoxification pathways - others do not. Stein et al suggest that this could contribute to the observation of (CH_4 Ox) inhibitory effects of ammonia addition in some studies (substrate competition CH_4/NH_3 and toxic effects of hydroxylamine) and stimulatory effects on CH_4 oxidation in others (NH_3 addition relieving N limitation) (Stein et al., 2012).

1.2.4 Molecular “Switches” in methanotrophs

1.2.4.1 Methanobactin, pMMO, sMMO and the Copper switch

It has long been known that copper availability plays a key role in regulating which type of methane monooxygenase is expressed in organisms that carry the genes for both forms (the copper-containing pMMO and the iron-containing sMMO) although the mechanism behind this “copper switch” was not immediately apparent (Stanley et al., 1983). A shift from pMMO to sMMO expression is apparent when copper starved, with a return to pMMO expression when copper is no longer limited (Stanley et al., 1983; Murrell et al., 2000).

The expression of the higher affinity (copper containing) pMMO therefore comes with a copper requirement. A key mechanism for sequestering environmental Cu for use in pMMO is the production of post-translationally modified peptides called methanobactins. Methanobactins are chalkophores involved in methanotroph copper uptake, they have a high affinity for copper ions and quickly reduce Cu(II) to Cu(I) upon binding (Dispirito et al., 2016; Kim et al., 2004).

Methanobactins are secreted by methanotrophic bacteria, their high affinity allows binding to environmental copper, copper bound methanobactin is then actively transported back into methanotrophic bacteria helping to meet the copper demand of pMMO utilizing methanotrophs. Some of the proteins involved in methanobactin uptake have been found: the TonB dependant transporter MbnT is responsible for Cu-methanobactin uptake and MbnE is a methanobactin periplasmic binding protein, the MATE multidrug exporter MbnM has a suggested role in methanobactin export. All of these proteins are encoded on the methanobactin mbn operon which also host *mbnA* encoding the methanobactin precursor itself (Dassama et al., 2016; Dispirito et al., 2016; Kenney and Rosenzweig 2013).

The discovery and study of methanobactins led to the proposal of a detailed molecular mechanism for the MMO “copper switch” (Semrau et al., 2013). The overall result of this mechanism is that sMMO is expressed at high biomass to copper ratios while pMMO is expressed at low biomass to copper ratios. Semrau et al summarised their “copper switch” mechanism as follows: At high biomass to copper ratios the MmoD protein (encoded by *mmoD* on the sMMO operon, see **Figure 1.4**) suppresses the pMMO operon and upregulates expression of the sMMO operon as well as the methanobactin mbn operon, methanobactin (mb) also serves to upregulate the sMMO operon producing more MmoD and reinforcing pMMO

repression (the soluble MMO is expressed). At low biomass to copper ratios the mb binds the abundant copper and becomes unable to upregulate the sMMO operon which causes a reduction in both the levels of MmoD and mb expressed, the MmoD also binds copper and is unable to continue repressing the pMMO operon or upregulating the sMMO operon (the particulate MMO is expressed). An overview of this mechanism is shown in (**Figure 1.8**) (from Semrau et al., 2013).

Ul haque et al demonstrated that methanobactin from a *Methylocystis* strain affected regulation and activity of MMOs in *Methylosinus trichosporium* OB3b, suggest that "methanobactin piracy" may be common in mixed methanotroph communities (Ul Haque et al., 2015). This was further supported by the discovery that the MbnT Cu-methanobactin transporter is capable of binding non-native Cu-methanobactin (Dassama et al., 2016).

In OB3b a tetramer of four-helix bundles (122 aa subunits with 12 Cys residues each) called Csp1 stores Cu(I) within the cell. Csp1 and homologue Csp2 have signal peptides thought to facilitate export from the cytosol into the intracellular membrane structures that harbour pMMO. Capable of storing a total of 52 Cu(I) per tetramer through interaction with Cys residues, Csp1/Csp2 compromised mutants showed a faster "copper switch" shift from pMMO to sMMO expression when supplied with lower amounts of Cu: suggesting Csp1 Cu storage acts to extend pMMO function as environmental Cu becomes limited. Csp3 is another homologue which seems to lack a signal peptide and has a suggested role in cytosolic Cu(I) storage. The affinity of Csp1 for Cu(I) ($1x10^{17}$ M^{-1}) is considerably lower than the Cu(I) affinity of methanobactin ($6\text{-}7x10^{20}$ M^{-1}) (El Ghazouani et al., 2011). Vita et al propose a system whereby methanobactin is responsible for stripping Cu(I) from the storage protein (Csp1) then potentially releasing the Cu(I) for cellular use through Methanobactin degradation (Vita et al., 2015).

Dennison et al. pointed out that copper storage proteins, such as the Csps described above and MopE and MopE* from *Methylococcus capsulatus* (Bath) (Ve et al., 2012), are only found in ~40% methanotrophs and a methanobactin operon is present in roughly 13% of sequenced methanotroph genomes. A significantly different form of methanobactin or an alternative mechanism may well be responsible for Cu uptake in other pMMO containing methanotrophs (Dennison et al., 2018).

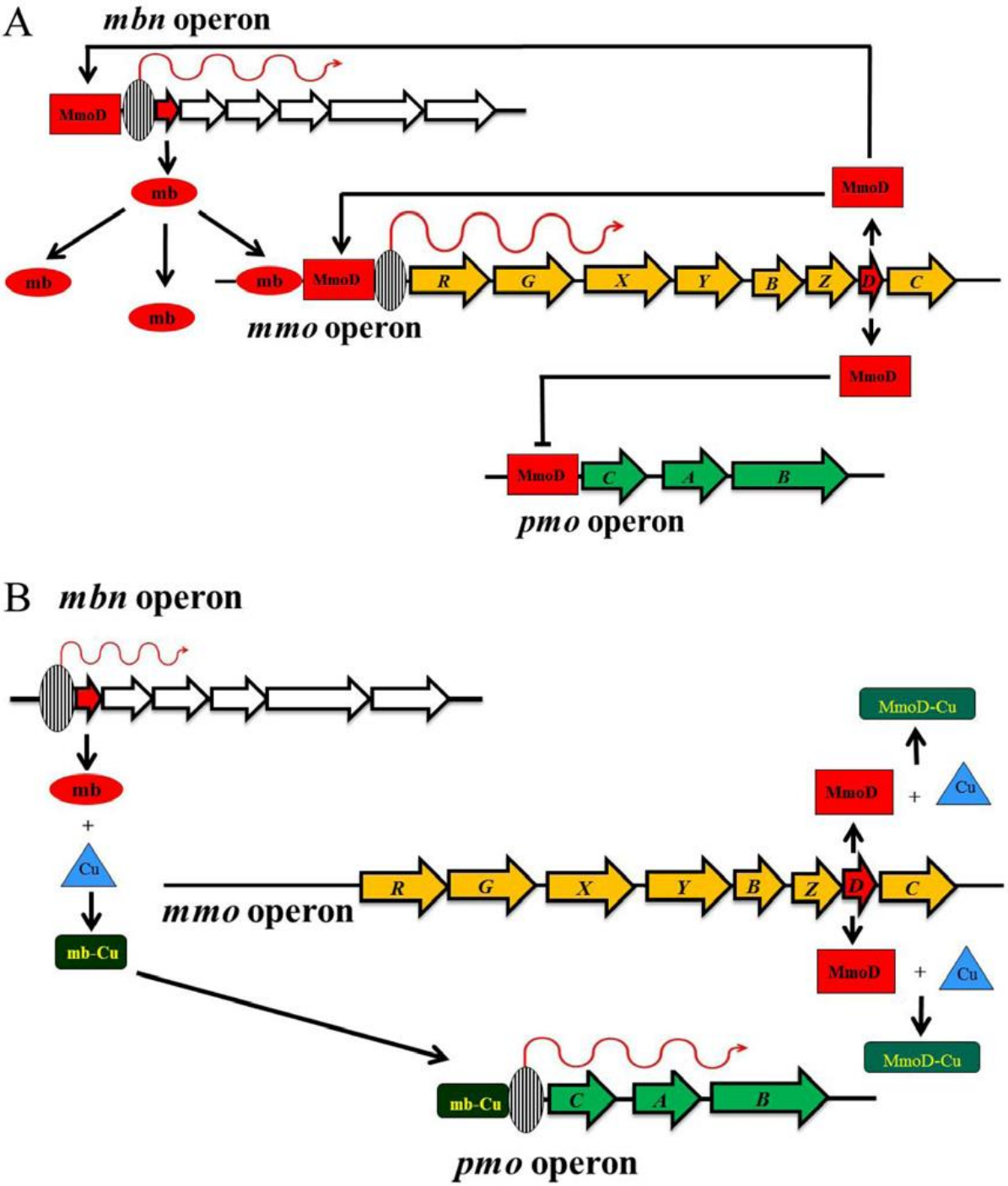

Figure 1.8 "copper switch" mechanism for controlling expression of sMMO and pMMO, figure from Semrau et al. (Semrau et al., 2013). Note: grey oval with curly red arrow (RNA polymerase and transcribed RNA) indicates activation (transcription) of downstream genes. **A)** high biomass: copper ratio (**sMMO expressed**); MmoD protein suppresses pMMO operon and upregulates sMMO and methanobactin operons, methanobactin also upregulates the sMMO operon producing more MmoD. **B)** low biomass: copper ratio (**pMMO expressed**); methanobactin and MmoD protein bind abundant copper and are unable to upregulate sMMO operon, MmoD is also unable to repress pMMO operon.

1.2.4.2 Methanol dehydrogenases and a "lanthanide REE switch"?

In a similar fashion to MMOs and the copper switch, the form of methanol dehydrogenase expressed in Methanotrophs (MxaFI or XoxF) seems to be regulated by environmental metal levels. In the case of MDH expression the abundance of Lanthanide rare earth elements (REEs) influences whether MxaFI or XoxF MDHs are expressed. Ca^{2+} dependant MDH (MxaFI) expression is supressed on addition of Lanthanides and expression of XoxF methanol dehydrogenase increases, this lanthanide dependant switch between MDH forms is partially controlled by the regulatory MxaB (Chu and Lidstrom, 2016).

XoxF containing methanotrophs demonstrated better growth when supplied with lower atomic weight lanthanide REEs such as Lanthanum, Cerium, Praseodymium and Neodymium than when provided with heavier lanthanides such as Gadolinium or Samarium (which could not support growth in a MxaFI knockout OB3b) (Gu et al., 2016; Pol et al., 2014).

Interestingly in *M. trichosporium* OB3b Cu was also seen to regulate MDH expression. Without copper present lanthanide suppression of MxaFI was observed, but in the presence of copper MxaFI expression was not reduced on addition of lanthanides (in either case XoxF was upregulated by lanthanide addition) (Gu et al., 2016). This copper dependant MDH regulation is so far restricted to OB3b and has not been observed in other methanotrophs that have been tested (Krause et al., 2017).

Studies suggest that in some environments lanthanide dependant XoxF dehydrogenases could be the dominant form of MDH expressed in methanotrophs (Chu and Lidstrom 2016; Gu et al., 2016; Taubert et al., 2015). In contrast, Krause et al identified suppression of XoxF and expression of MxaFI in a methanotroph grown in mixed culture with non-methanotroph methylotrophs supplemented with lanthanides. Experiments demonstrated methanotroph MxaFI driven CH_3OH oxidation to result in higher extracellular methanol concentrations than XoxF CH_3OH oxidation, additionally they observed high expression levels of MDH in the cocultured meythylotrophs when the synthetic community was provided CH_4 rather than CH_3OH as the carbon source. These results led to a hypothesis that the methylotrophs may be promoting this expression change from the potentially high affinity XoxF (Pol et al., 2014) to the leakier MxaF, perhaps through release of a signalling compound, chemical or lanthanide chelating agent: ultimately providing the methylotrophs with access to CH_4 derived CH_3OH metabolite that would otherwise have been unavailable under the CH_4-only culture conditions. These findings not only highlight the limitations of studies on pure cultures in isolation but

demonstrate a potentially significant route of C flow in methanotroph containing communities in high CH_4 environments (Krause et al., 2017).

1.3 Previous studies of landfill methanotrophs

The study of methanotrophs stretches back to the early 20th century with the isolation of *Pseudomonas methanica* by Söhngen in 1906 (Söhngen, 1906). Consequently, the early work on methanotrophs was dependant on the cultivation and study of methanotroph isolates (a "culture dependent" approach). Initial attempts at isolating methanotrophs from environmental samples proved difficult and for many years there were only a few success stories: such as the isolation of the thermotolerant *Methylococcus capsulatus* by Foster and Davis in 1966 (Foster and Davis, 1966). It wasn't until the landmark experiments by Whittenbury et al in the late 1960s that a significant number (over 100) of methanotrophs were available in pure culture. This was achieved by varying the inocula as well as the enrichment and isolation conditions, to select for a range of different methanotrophs (Whittenbury et al., 1970).

A solely "culture dependent" approach to exploring bacterial communities is limited by the researcher's ability to select appropriate growth conditions for potentially unknown and intractable organisms, with no real way of knowing what proportion of relevant organisms have been recovered from a sample (Amann et al., 1995). The development of increasingly powerful "culture independent" techniques including functional gene and 16S rRNA gene probing, as well as metagenome analysis have revolutionised environmental microbiology: not only providing an overview of the organisms present and their evolutionary relationship, but also allowing retrieved isolates to be seen in the context of their environmental communities. They have also highlighted the presence of abundant uncultivated bacteria in various environments (Amann et al., 1995; Meyer-Dombard et al., 2020; McDonald et al., 2008).

Such culture independent approaches have been successfully applied in the study of landfill cover soil methanotroph communities. Functional gene probing targeting methane monooxygenase genes *pmoA* (pMMO) and *mmoX* (sMMO) as well as 16S rRNA has been used to identify the most abundant methanotrophs present in the cover soils of different landfills. When combined with DNA Stable Isotope Probing (DNA-SIP) the dominant active methanotrophs can be identified. The results of a selection of these studies show various methanotrophs to be abundant in landfill cover soils including *Methylobacter*, *Methylomonas*, *Methylosarcina*, *Methylohalobius*, *Methylocaldum* and *Methylomicrobium* (Type I

methanotrophs) as well as *Methylocella*, *Methylocapsa*, *Methylocystis* and *Methylosinus* (Type II methanotrophs). Of these *Methylobacter*, *Methylocaldum*, *Methylosarcina*, *Methylohalobius* (Type I) and *Methylocystis*, *Methylocella*, *Methylocapsa* (Type II) were seen to be the dominant methanotrophs in studies on different landfills (Cebron et al., 2007; Chi et al., 2015; Henneberger et al., 2011; Su et al., 2014; Wang et al., 2017; Zhang et al., 2014). Type II methanotrophs appear to dominate over type I in more acidic cover soils, likely due to the mild-to-moderate acidophilic nature of many species belonging to the cover soil associated Type II methanotrophic genera (*Methylocystis*, *Methylocella*, *Methylocapsa* and *Methylosinus*). (Belova et al., 2013; Bowman et al., 1993; Cebron et al., 2007; Dedysh et al., 2004; Dunfield et al., 2010; Kong et al., 2013; Tikhonova et al., 2021). Shotgun metagenome sequencing represents a particularly powerful cultivation independent tool for microbial ecology: this technique uses high throughput next-generation sequencing of total community DNA and fragment assembly algorithms to reconstruct metagenome assembled genomes (MAGs) for individual members of the microbial community (Quince et al., 2017). While the uptake of metagenome analysis to study landfill cover soil methanotrophs has been slow, perhaps due to the existence of established functional gene markers, metagenomics has the potential to detect methanotrophs with sequence divergent or missing functional genes (Meyer-Dombard et al., 2020). In one metagenome-based study on landfill soil carried out by Singh et al. *Methylomonas*, *Methylococcus*, *Methylocella*, and *Methylacidiphilum* were identified as the most abundant methanotrophs (Singh et al. 2022). Perhaps the most compelling argument for metagenome analysis is the recovery of the gene complement within each MAG, which can be used to map metabolic potential.

The information on community structure (i.e. what is there?) gleaned from these culture independent investigations has enormous potential to inform and focus culture dependent efforts to obtain methanotroph isolates of interest. For example, if novel methanotrophs are detected that show functional gene sequence similarity to acidophilic and thermophilic methanotrophs such as *Methylacidiphilum fumariolicum* or microaerophiles like *Methylosoma difficile*, then enrichment conditions using low pH/high temperature or low O_2 concentration may have a greater chance of generating isolates (Khadem et al., 2010; Rahalkar et al., 2007). Such a strategy facilitates retrieval of methanotrophs that require tailored culturing conditions and that would perhaps be missed by a less specific enrichment regimen.

1.4 Biofilters

Biofilters for landfill CH_4 mitigation consist of open or closed bioreactors such as lined beds or tanks containing a methanotroph rich matrix or medium designed to support the growth and CH_4 metabolism of these organisms. Open biofilters are exposed to the air and gases fed into them will flow through the filter into the atmosphere without further regulation, while closed biofilters are fully contained systems with controlled gas flow and interaction with the atmosphere (Huber-Humer et al., 2008). A passive or active gas collection system is employed to channel generated landfill gas (containing CH_4) into the bioreactor where it is allowed to percolate through the matrix to facilitate CH_4 removal by the resident methanotrophs. Air can also be mixed with the LFG before it is piped into the biofilter reactor to help support the commonly aerobic methanotroph CH_4 oxidation, this is a requirement for closed biofilters that cannot rely on atmospheric O_2 (Dever et al., 2007; Turgeon et al., 2011). Closed reactor biofilter designs allow greater control and optimisation of the physical and chemical conditions under which biological CH_4 oxidation is taking place: variables such as O_2 and CH_4 flow as well as temperature and matrix H_2O content can be more easily regulated than with open air biofilter set-ups. However, such fine tuning capabilities come with a higher capital cost when compared with open air biofilter systems (Huber-Humer et al., 2008). The applications of biofilters for methane mitigation extend beyond closed landfill management, with different groups looking to apply a form of this technology to mitigate livestock methane emissions (Veillette et al., 2012), and fugitive methane emissions from coal mines (Limbri et al., 2014), methane biofiltration could also play a role in mitigating fugitive methane emissions released by the growing shale gas industry (Howarth, 2015).

1.5 The Strumpshaw biofilter

Strumpshaw Landfill (located roughly 8 miles east of Norwich) is an older closed landfill generating relatively low levels of CH_4 in its Landfill gas (LFG). Norfolk County Council (NCC) are responsible for managing this site and mitigating Landfill gas emissions from the breakdown of deposited waste. The site itself is a relatively small landfill with an area of 12 hectares that was in use (receiving waste) from 1972 to 1988, accumulating roughly 1 million tonnes of municipal solid waste. Strumpshaw has a network of LFG extraction wells that have been connected to gas flares and Stirling engines for the combustion of CH_4. In 2014 the NCC closed landfill team installed a biofilter to handle the low concentration of CH_4 in the LFG

from the site's migration (boundary) line. From 2017 to 2022 the biofilter was the only CH_4 mitigation platform operational at Strumpshaw, as the Stirling engines that normally take the well field LFG were out of action and a replacement low-cal flare has only recently been delivered. The biofilter has a volume of approximately 75m^3 and is currently supplied with 75m^3 h^{-1} air-diluted LFG with a final CH_4 and O_2 content of 8 and 16% respectively.

The biofilter is contained in an impermeable liner and has been built on a slight slope to allow collection of leachate at the lower end of the basal gravel layer as it drains through. A schematic of the Strumpshaw biofilter as designed is shown in (**Figure 1.9**), the air-diluted LFG enters the biofilter matrix soil via perforations in the gas distribution pipes shown. The biofilter matrix soil consists of a mix of expanded clay pellets (1-1.5 cm diameter spheres with honeycomb centre), coir (coconut fibre), wood chips (max size 40 mm) and compost, while the topsoil layer (separated from the matrix by a semi-permeable membrane) has a similar composition but lacks the clay pellets. The matrix was designed to support CH_4 consuming methanotrophic bacteria and to promote their bio-oxidation of CH_4 by providing good gas permeability and moisture retention as well as nutrients and trace minerals. It should be noted that while the biofilter was designed to feature a 30 cm deep topsoil layer, during soil sampling in the course of this project it was observed that this layer was more often 50 cm deep. One issue with biofilter operation at the start of this project was the requirement for continual (weekly) manual rebalancing of the inlet gas mix to maintain the 8%:16% ratio of CH_4 and O_2 in the diluted LFG, this process was later automated to provide a more stable flow of CH_4 and O_2 into the biofilter.

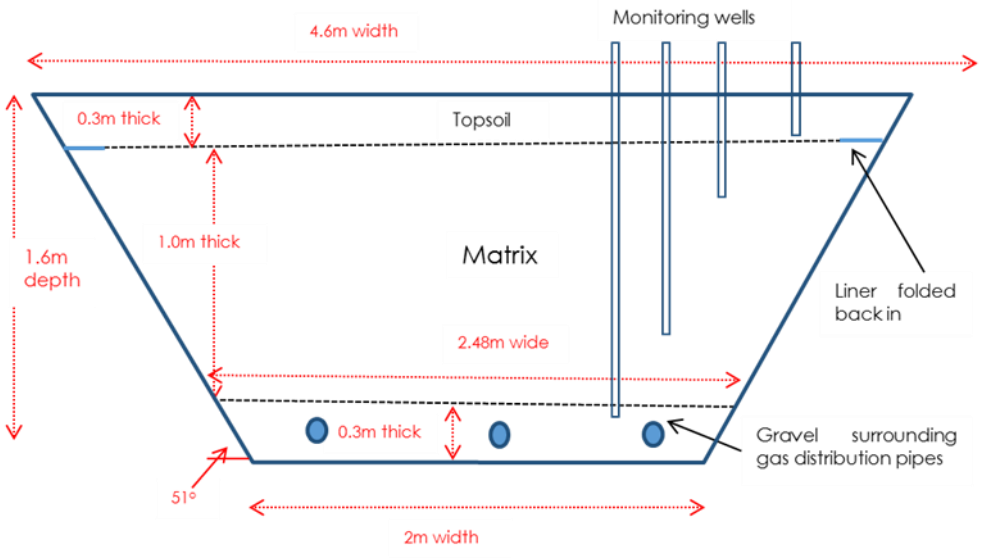

Figure 1.9 Strumpshaw biofilter design schematic, the biofilter length is 21 m.

1.6 Project aims and methodology

The aim of this project was to determine where and under what conditions CH_4 is oxidised within the Strumpshaw biofilter and to identify and isolate the most active CH_4 oxidising methanotrophs (responsible for the majority of CH_4 turnover). In addition to providing an academic insight into the performance of the Strumpshaw biofilter system, this information would also be used to inform future biofilter design and operating parameters.

The operational characteristics of the Strumpshaw biofilter were explored by monitoring biofilter temperature and in-situ CH_4, O_2 and CO_2 levels to determine the most active CH_4 oxidising regions of the biofilter. While CH_4 soil oxidation potential assays were employed to confirm resident methanotroph activity and optimal soil conditions.

16S rRNA amplicon sequencing and metagenome studies of biofilter matrix soil samples were used to build biofilter microbial community profiles. The active proportion of the methanotroph community was then highlighted through Stable-Isotope-Probing (SIP), using ^{13}C labelled CH_4 to label the DNA of those methanotrophs actively metabolising CH_4. Methanotroph isolates were obtained by serial dilution plating of biofilter matrix inoculated enrichment cultures. A key isolate shown to be active in biofilter CH_4 oxidation was sent for genome sequencing, and its growth temperature range was investigated.

The design of future biofilters could be guided by this research. The identification of the most active regions of the biofilter matrix in terms of depth from surface and distance from gas distribution pipes could lead to rethinking the required size of the biofilter (with impact on unit cost). Whereas potential improvements to CH_4 bio-oxidation efficiency dependant on an altered moisture or ambient temperature might require a biofilter to feature a cover, insulation or an irrigation system.

Chapter 2: Materials and methods

2.1 Chemicals and reagents

Analytical grade reagents used in this study were from Sigma-Aldrich, Fisher Scientific, Formedium, Oxoid, Melford laboratories, Acros Organics, Honeywell Riedel-de Haen, VWR international, Hopkin and Williams, BDH chemicals and Hanna instruments. Molecular biology grade reagents were from Roche life science, MP Biomedicals, Zymo Research, Promega, PCR Biosystems, MACHEREY-NAGEL, Thermo Fisher Scientific and Invitrogen. Gases used were provided by BOC apart from $^{13}CH_4$ (99%) which was supplied by Cambridge Isotope Laboratories.

2.2 Implementation of a grid system for biofilter sampling and monitoring

The surface of the biofilter was marked up with a grid system to aid in sample collection and physical monitoring. Grid references were marked across the width and length of the biofilter along the exposed edges of the black liner containing the biofilter matrix. Four 1.2 m sections were marked across the width of the biofilter and labelled A to D. Twenty-one 1 m sectors were marked along the length of the biofilter and labelled 1 to 21. These markings could then be used to divide the biofilter surface into eighty-four 1.2 m by 1 m sectors each with a grid reference (e.g A7, C18 and so on) (**Figure 2.1**).

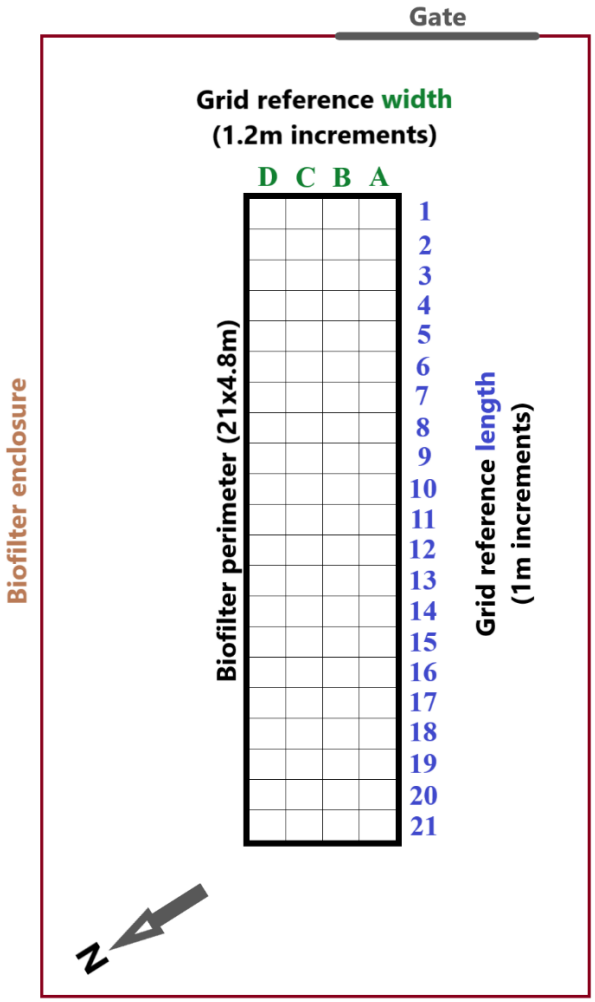

Figure 2.1 Aerial view of the biofilter and surrounding enclosure showing arrangement of the grid reference overlaid onto the biofilter surface. Note the grid itself is not marked onto the biofilter, grid sectors were identified by referring to the grid reference markings on the liner along the sides of the biofilter.

2.3 Monitoring temperature, pH and gas mix and flow within the biofilter

2.3.1 Measuring gas flow into the biofilter and adjusting CH_4:O_2 balance pre- and post-automation

Before biofilter gas feed automation, the CH_4:O_2 ratio of the gas mix (landfill gas mixed with air) was checked monthly by a member of the NCC closed landfill team. If necessary, the gas mix was then manually readjusted to the optimal ratio of 2:1 CH_4:O_2 as changes in atmospheric pressure would frequently affect the CH_4:O_2 balance. Automation of the biofilter gas feed

system implemented remote sensors to automatically detect changes in CH_4:O_2 balance and maintain a 2:1 ratio.

2.3.2 Monitoring gas composition and temperature within the biofilter

Four sets of fixed sampling ports were positioned across the biofilter when it was built to allow monitoring of gas composition and temperature at different depths. Each set of ports consisted of four capped pvc tubes sunk to the gravel layer, lower matrix, upper matrix and topsoil (**Figure 1.9**), gas content (CH_4, O_2, CO_2, H_2S) at each depth was measured by attaching a Geotech GA5000 gas analyzer (1000 ppmv limit of detection) to the top of each tube. The temperature at each depth was also measured by removing the tube caps and lowering a thermocouple to the base of each tube and measuring the temperature with an RS PRO RS 51 digital thermometer.

Both a temperature probe and combined temperature/gas probe (**Figure 2.2**) were used to obtain temperature depth profiles for the biofilter matrix at different grid positions. The probes consist of metal sheaths with a point at one end (manufactured by NCC) which houses a thermocouple connected to an RS Pro digital thermometer. Temperature depth profiles were built up by randomly picking a biofilter grid sector and inserting the temperature probe in the centre of the sector and measuring the *in-situ* temperatures at fixed depths (starting at the surface and then measuring at 5 or 10 cm increments) as the temperature probe was driven down vertically into the biofilter matrix.

Gas composition profiles as a function of depth were measured concomitantly with temperature profiles using the combined gas/temperature probe. A series of holes in the wall of the probe immediately above the tip allow biofilter gas to flow up the body of the probe to a port where it's composition could be detected with an attached Geotech GA5000 gas analyzer. A hairpin was used to clean out the holes between sets of readings to prevent clogging with biofilter soil.

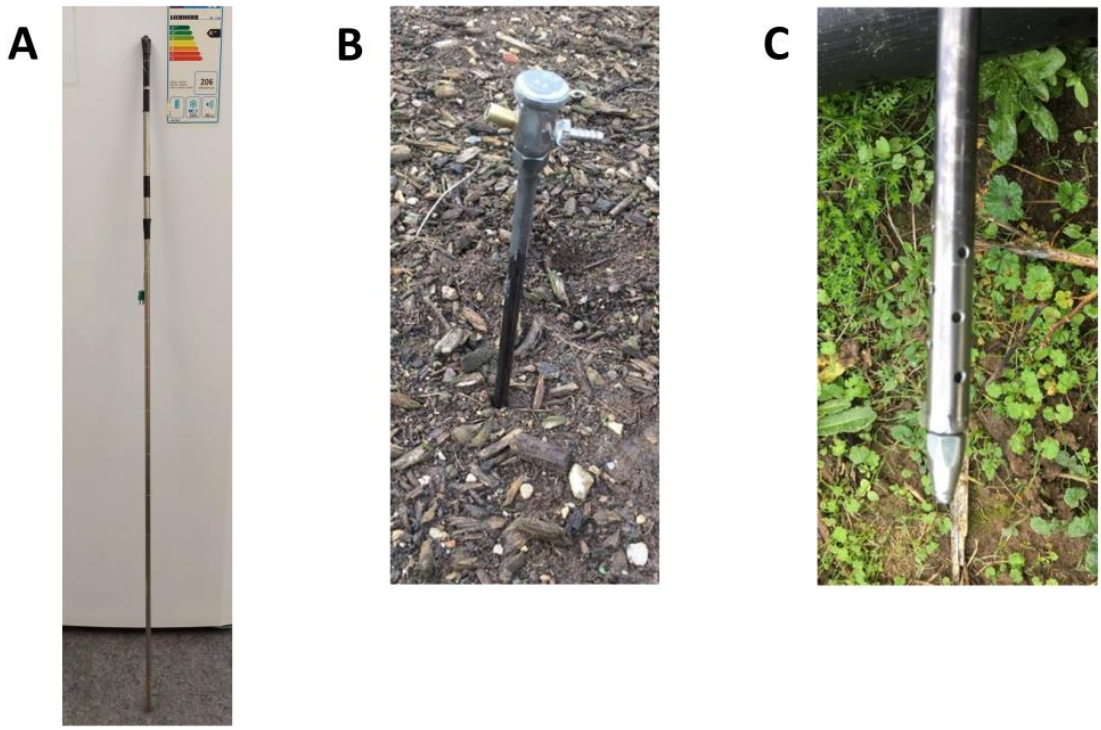

Figure 2.2 Temperature probe and combined temperature/gas probe used in this study. **A** temperature probe, 150 cm length with 10 cm intervals etched onto the outside of the sheath, detection end of probe ends in a sealed point containing the thermocouple sensor. **B** Combined temperature/gas probe inserted into biofilter matrix with the gas tight ports for digital thermometer and gas analyser connection visible below the cap, full length of probe is 110 cm. The detection end of the combined probe housing the thermocouple is shown in **C,** the holes allow gas flow to enter and reach the gas analyser through the sheath.

2.3.3 Measuring pH and oven-dry weight of soil samples

Matrix soil samples collected from the biofilter had their pH estimated by mixing an aliquot of soil with dH_2O in a 1:2 ratio and then measuring the pH of the resulting slurry with a Jenway 3505 pH meter.

Oven-dry weight of soil samples (the constant weight achieved following drying at 110 ±5 ˚C for 12-16 hours) was measured using the U.S.D.A. Soil Survey Field and Laboratory Method (U.S. Department of Agriculture Soil Survey Staff, 2009). 10 to 20 g of biofilter soil sample was transferred to an open container and oven dried at 115˚C overnight (14 hours) after which the sample was reweighed, the new mass of the soil was then used to calculate it's oven-dry weight.

2.4 Maintaining sterility of reagents and glassware

2.4.1 Autoclaving glassware and media

Autoclaving carried out at 121˚C for 15 minutes using a Dixons Vario 3028 autoclave.

2.4.2 Filtering liquid reagents

Liquid reagents were sterilised by passage through a 0.22 μm filter using a syringe or vacuum pump where specified.

2.5 Cultivation and maintenance of bacterial strains

2.5.1 Nitrate mineral salts methanotroph medium

The nitrate mineral salts (NMS) medium developed by Whittenbury et al (Whittenbury et al., 1970) was used to grow methanotrophic bacteria and enrichment cultures. This medium was routinely modified by addition of $LaCl_3$ to a final concentration of 5 μm. Methanotrophs were both grown in liquid NMS and on 1.5 or 1.8% (w/v) BD Bacto Agar NMS plates. In some cases, the NMS was supplemented with a filter-sterilized vitamin solution (for both liquid and agar NMS) see (**Table 2.1**). 1 ml L^{-1} of this vitamin solution was added to liquid NMS or freshly autoclaved NMS agar (ahead of plating).

Table 2.1 Vitamin solution ingredients added to 500 ml ddH_2O and then filter sterilised (**Chapter 2.4.2**)

Ingredient	Mass (mg)	Ingredient	Mass (mg)
Biotin	10	Cyanocobalamin	0.5
Folic acid	10	Riboflavin	25
Thiamine HCl	25	Nicotinic acid	25
Ca Pantothenate	25	4-aminobenzoic acid	10

2.5.2 Growth of methanotrophs on CH_4

Methanotrophs were routinely grown using solid or liquid medium supplied with CH_4 as a growth substrate. For liquid cultures, 20 ml of a 95%:5% mix of CH_4:CO_2 was aseptically injected into the headspace of a 120 ml serum vial containing 20 ml liquid medium plus inoculum. For solid medium, inoculated agar plates were closed and transferred to either an anaerobic jar (2.5 L) or air-tight Tupperware container (4 L) which was supplied with 95%:5% CH_4:CO_2 mix to fill approximately 50% of the container volume. Containers were then immediately sealed to prevent loss of CH_4.

2.5.3 Subculturing liquid cultures

Liquid bacterial cultures were subcultured by aseptic transfer of 1 ml of culture to sterile (autoclaved) 120 ml serum vial containing 20 ml of fresh culture. Newly inoculated subcultures were then gassed with 20 ml CH_4 and incubated with shaking at appropriate temperatures.

2.5.4 Measuring optical density of bacterial cultures

The optical density (OD) of bacterial cultures was measured using a Shimadzu UV-1800 UV spectrophotometer. 1 ml of culture was aseptically transferred to a Fisherbrand FB 55147 semi-micro polystyrene cuvette and the optical density (at 600 nm) measured, 1 ml of sterile medium was used as a blank to calculate corrected OD.

2.5.5 Cultivation of *Methylococcus capsulatus* (Norfolk) and *Methylocaldum szegediense* (Norfolk)

Methylococcus capsulatus (Norfolk) (isolated by Elliot Brooks) was routinely grown in liquid NMS medium supplied with CH_4 at 37˚C with shaking (160 RPM). *M.c* (Norfolk) was also grown on NMS plates containing 1.5% (w/v) agar supplied with CH_4 at 37˚C.

Methylocaldum szegediense (Norfolk) (isolated in this study) was grown in liquid NMS medium supplemented with vitamin solution and CH_4 at 50˚C with shaking (160 RPM). *M. szegediense* was also grown on NMS plates containing 1.8% (w/v) agar and vitamins supplied with CH_4 at 50˚C.

2.6 Bacterial purity checks and microscopy

The purity of bacterial cultures was regularly checked using microscopy, sequencing of 16S rRNA gene sequences from clone libraries and inspecting colonies on NMS serial dilution plates and R2A agar streak plates after incubation.

Cultures were first checked for contamination by phase contrast microscopy using a Zeiss Axio Scope.A1 microscope with oil immersion lens. Wet mounts of plate grown colonies or liquid cultures were set up and viewed under the microscope. The culture or colony was then screened for contamination based on the consistency of cell size, morphology and motility.

Contamination was also screened by extracting DNA from cultures and using it as a template in PCR or colony PCR (PCR modifications: 50 µl reaction volume, 27F and 1492R primers, 16S_72 or 16S_72col protocol) (Lane 1991). After carrying out PCR clean-up the PCR products were sent for Sanger sequencing with 27F and 1492R primers. The identity of the 16S rRNA gene could then be confirmed from this sequence using the NCBI Nucleotide BLAST search function and the quality of the sequencing chromatogram trace was used as a purity indicator (**Chapter 2.10** and **2.12.1**).

Additionally, serial dilutions of liquid cultures of putative isolates (**Chapter 2.7.3**) were spread onto NMS plates and examined for contamination by inspecting colonies after incubation with CH_4 at appropriate temperatures for 1-2 weeks. Observable differences in colony size, shape and colouration were taken as signs of contaminating microbes.

100 µl aliquots of bacterial cultures were also streaked onto separate R2A agar plates as a culture purity negative control (to check for contamination by aerobic heterotrophs). These were incubated at appropriate temperatures with and without CH_4 (**Chapter 2.5**) and checked for contaminant colonies after 1-2 weeks.

2.7 Isolation of methanotrophic bacteria from the biofilter

2.7.1 Collecting biofilter soil samples

Soil samples were retrieved from the biofilter initially with a 3 cm open-faced soil corer (which was found to be unsatisfactory (**Chapter 3.3.1**)), this was pushed into the biofilter soil using the operator's body weight and given a half turn *in situ*, before the corer was removed along

with the soil sample. Subsequently, soil sample retrieval was undertaken using a custom built 5 cm diameter soil corer (**Figure 2.3**) or manually using a spade when a larger volume of material was required. The 5 cm soil corer was first cleaned and assembled as shown in (**Figure 2.3 B**), the soil corer was then pushed firmly into the soil using body weight at the position to be sampled before being driven down to the depth required with a 7lb sledgehammer, the cap was then removed and the cross bar inserted to allow retrieval of the corer and the sample within, the sample core was then divided into 5 or 10 cm sections. When manually sampling with a spade, a profile was sampled by sequentially digging out 5 or 10 cm sections of the biofilter soil from the surface. Soil sections were then sealed in ziplock bags and taken back to the lab.

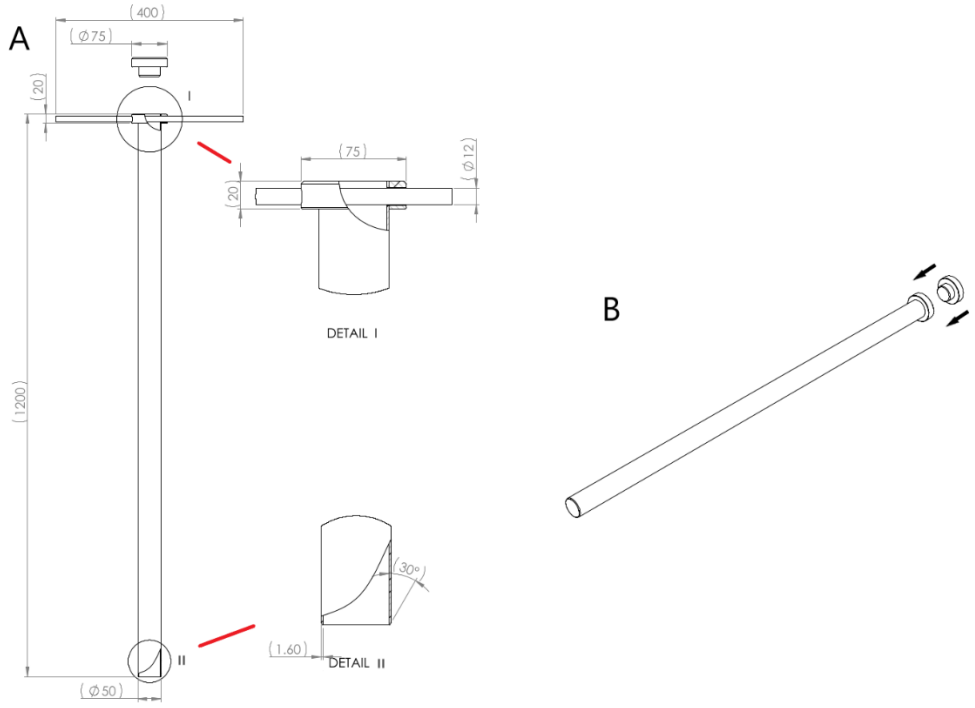

Figure 2.3 Diagram of soil corer built in the UEA workshop (adapted from quote schematic) **A** dimensions of corer components (in mm) **B** preparing corer for sampling, cap seated in place with retrieval cross bar removed.

2.7.2 Biofilter soil enrichment cultures

0.5 to 1 g of biofilter soil was transferred to sterile NMS medium in a 120 ml serum vial which was then sealed and gassed with CH_4 and incubated with shaking (160 RPM) at a given temperature. Enrichment cultures were subcultured every 1-2 weeks and phase contrast

microscopy was used to confirm bacterial growth, while decreasing headspace CH_4 was tracked by gas chromatography (**Chapter 2.8.1**). After a minimum of three subcultures, an aliquot from the latest enrichment subculture was then serially diluted.

2.7.3 Serial dilution and bacterial isolation from enrichment cultures

100 µl taken from the 3rd or subsequent enrichment subcultures were serially diluted six times with 900 µl volumes of NMS with or without vitamins, 100 µl aliquots of each dilution were then plated out onto NMS agar plates and incubated with CH_4 at the appropriate temperature until colonies appeared. Colonies were then restreaked onto fresh NMS agar and incubated under the same conditions. Once grown, cultures of putative isolates were generated by transferring individual colonies to sterile NMS medium in 120 ml serum vials. These were gassed with CH_4 and incubated at the appropriate temperature. Putative isolate cultures that demonstrated growth (observable turbidity or increase in OD) over the course of two weeks' incubation were scrutinised by microscopy to confirm cell proliferation. Purity and identity of isolates was then assessed.

Putative isolates that showed signs of contamination or confirmed isolates that had become re-contaminated were purified by repeated serial dilution and re-isolation from individual colonies. Identities were confirmed by extracting DNA and sequencing the 16S rRNA gene PCR products generated from it (**Chapter 2.9.2**).

2.8 Measuring culture and sample headspace CH_4 and calculation of CH_4 oxidation rates

2.8.1 Measuring headspace CH_4 concentration in soil sample incubations and cultures

The headspace CH_4 concentration of soil sample incubations and liquid bacterial cultures was measured by gas chromatography (GC) using an Agilent 7820A gas chromatograph fitted with a Supelco 80/100 Porapak Q column (length 1.8 m, outer diameter 3.175 mm, inner diameter 2.1 mm), with a limit of detection for CH_4 of 2 ppmv.

100 µl of headspace gas was withdrawn using a gas-tight syringe from a sealed serum vial and then injected down the GC septum and analysed using the following Methane Protocol: Inlet temperature 250ºC, oven temperature 80ºC for 4 minutes, column temperature 250ºC, using a

FID detector at 300ºC (approximate CH_4 retention time of 0.6 minutes). Serum vial standards with known headspace CH_4 content were used to create a standard curve of GC CH_4 retention peak area against headspace CH_4 volume. Using this standard curve, the concentration of headspace CH_4 for biofilter soil or methanotroph cultures could then be calculated from the area under the CH_4 retention peak on their GC traces.

2.8.2 Calculation of soil CH_4 oxidation rates.

CH_4 oxidation rates for biofilter soil were calculated for known masses of soil incubated with headspace CH_4 in sealed serum vials. The headspace concentration of CH_4 was measured over many timepoints and by plotting headspace CH_4 depletion against time, a CH_4 oxidation rate could be calculated for the sample. CH_4 oxidation rates per gram of field moist soil were calculated by transferring soil directly from sealed ziplock sampling bags to the serum vial, while CH_4 oxidation rates per gram of dry soil were calculated by establishing the oven-dry weight of the soil sample (**Chapter 2.3.3**).

2.9 Extraction of nucleic acids

2.9.1 DNA extraction from soil and humic acid removal

DNA was extracted from soil samples using an MP Biomedicals "Fast DNA SPIN Kit for Soil" and FastPrep system. The manufacturer's protocol was followed except, only 778 µl Sodium Phosphate Buffer (SPB) was added before the MT buffer and then a further 100 µl SPB was added after if there was still room in the tube.

DNA extracted from soil often included humic acid contamination (a potent PCR inhibitor), this was removed ahead of downstream nucleic acid manipulation using the Zymo "OneStep PCR Inhibitor Removal Kit" following the manufacturer's instructions.

2.9.2 DNA extraction from liquid culture and bacterial colonies

DNA was extracted from liquid cultures using a "Wizard Genomic DNA Purification Kit" (Promega) following the kit protocol. For *Methylocaldum szegediense* liquid cultures, cultures

were spun down and the pellet collected and transferred to a MP Biomedicals "Fast DNA SPIN Kit for Soil" bead beating tube and the DNA was extracted following the manufacturer's protocol except, substituting the cell pellet for the soil sample. DNA was extracted and amplified from colonies on agar plates by colony PCR (**Chapter 2.10.2**). DNA was also extracted by restreaking individual colonies onto fresh plates and incubating with CH_4 (**Chapter 2.5** and **2.7**), once colonies were fully grown the bacterial lawn was harvested aseptically with a sterile loop and transferred to an MP Biomedicals "Fast DNA SPIN Kit for Soil" bead beating tube and the DNA extracted following the manufacturer's protocol (substituting the bacterial cells for the soil sample).

2.10 Nucleic acid manipulation techniques

2.10.1 Quantification of DNA

DNA was quantified and quality checked using a Nanodrop 2000. Alternatively, DNA concentration was measured using Qubit 2.0 dsDNA broad range or high sensitivity kits (Life Technologies) to detect short DNA fragments or when higher sensitivity or accuracy was required.

2.10.2 Polymerase chain reaction (PCR) and purification of PCR products

Unless otherwise specified, PCR reactions used a standard reaction mix (**Table 2.2**) scaled up or down depending on total volume required, with the specific primer pair (**Table 2.3**) and PCR protocol (**Table 2.4**) used dependent on the DNA template targeted.

This information is given in the relevant methods or results sections in the format "PCR modifications: [total volume reaction mix], [primers used], [PCR protocol used]"

PCR reaction mixes were made up in 200 µl PCR tubes, mixed and briefly spun down in a Sprout mini centrifuge (Heathrow Scientific) before being transferred to the thermocycler (Bio-Rad DNA EngineTetrad 2).

PCR reactions that required further alteration to the above procedure included Nested PCR and Colony PCR. Nested PCR allowed increased specificity and sensitivity: Two successive PCR

reactions were carried out, with the second reaction using different primers and 1 µl of a 1-in-10 dilution of the first PCR product as template to amplify a shorter region within this sequence. Colony PCR was used to confirm and amplify the vector DNA inserts of transformed *E.coli* cells taken from colonies in clone libraries. For colony PCR, the PCR reaction mix was modified by replacing 10 ng μl^{-1} DNA template with an equal volume of molecular grade dH_2O. The template was instead provided by transferring a clone library colony to the modified reaction mix using a sterile woodpick. Colony PCR protocols also increase the duration of the initial 95˚C denaturation step to 10 minutes to facilitate lysis of cells and release of the vector containing the DNA template insert.

PCR products were purified using either a Roche High Pure PCR Product Purification Kit or Zymo OneStep PCR Inhibitor Removal kit following the manufacturer's instructions in both cases.

Table 2.2 Standard PCR reaction mix, volumes of reaction mix components were increased or decreased proportionally when a greater or lesser total reaction volume was required.

Reaction component	Volume (µl)
2XPCRBio Taq Mix Red	12.5
Forward primer (10 µM)	1
Reverse primer (10 µM)	1
DNA template (10 ng μl^{-1})	1
Molecular grade dH_2O	9.5
Total reaction volume	25

Table 2.3 PCR primer pairs used in this study.

Primer set	Target gene		Forward and Reverse primers	Product size (bp)	Reference	Notes
A189F, A682R	***pmoA***	A189F A682R	(5' to 3') GGN GAC TGG GAC TTC TGG (5' to 3') GAA SGC NGA GAA GAA SGC	525	(Holmes 1995)	
PmoC374, PmoA344	***pmoCA***	PmoC374 PmoA344	(5' to 3') AGC ARG ACG GYA CNT GGC (5' to 3') ANG TCC AHC CCC AGA AGT	850	(Ghashgavi 2017)	
A166F, B1401R then A206F, 886R	***mmoX***	A166F B1401R	(5' to 3') ACC AAG GAR CAR TTC AAG (5' to 3') TGG CAC TCR TAR CGC TC	1230	(Auman 2000)	**Nested PCR**
		A206F 886R	(5' to 3') ATC GCB AAR GAA TAY GCS CG (5' to 3') ACC CAN GGC TCG ACY TTG AA	719	(Hutchens 2004)	
27F, 1492R	***16S rRNA***	27F 1492R	(5' to 3') AGA GTT TGA TCM TGG CTC AG (5' to 3') TAC GGY TAC CTT GTT AGG ACT T	1465	(Lane 1991)	
341F, 785R	***16S rRNA***	341F 785R	(5' to 3') CCT ACG GGN GGC WGC AG (5' to 3') GAC TAC HVG GGT ATC TAA TCC	464	(Klindworth 2013)	***16S rRNA* amplicon sequencing**
341GC, 518R	***16S rRNA***	341GC	(5' to 3') CGC CCG CCG CGC GCG GCG GGC GGG GCG GGG GCA CGG GGG GCC TAC GGG AGG CAG CAG	177	(Muyzer 1993)	**341GC has GC clamp**
		518R	(5' to 3') ATT ACC GCG GCT GCT GG			
M13F, M13R	**pGEM-T insert**	M13F M13R	(5' to 3') TGT AAA ACG ACG GCC AGT (5' to 3') CAG GAA ACA GCT ATG AC	Dependent on insert	(Invitrogen, supplier)	**Amplifies pGEM-T vector insert**
T7, SP6	**pGEM-T insert**	T7 SP6	(5' to 3') TAA TAC GAC TCA CTA TAG GG (5' to 3') ATT TAG GTG ACA CTA TAG	Dependent on insert	(Invitrogen, supplier)	**Amplifies pGEM-T vector insert**
pmoCHF, pmoCHR1	***pmoC2* and flanking regions**	pmoCHF pmoCHR1	(5' to 3') TAG CTG CCC GAC AGC ATC A (5' to 3') CAT GAG GTT GGC TCA CGA		(This study)	**Designed to target *pmoC2* in *M.c.* (Bath)**
pmoCHF, pmoCHR2	***pmoC1* and flanking regions**	pmoCHF pmoCHR2	(5' to 3') TAG CTG CCC GAC AGC ATC A (5' to 3') GAA ACT ACC CCT GCG TCA A		(This study)	**Designed to target *pmoC1* in *M.c.* (Bath)**

Table 2.4 List of thermocycler PCR protocols used in this study.

Parameters		Thermocycler protocol			
		16S DGGE	**16S_72**	**16S_72col**	**PmoCABH1**
Initial Denaturation		95˚C, 5 min	95˚C, 3 min	95˚C, 10 min	95˚C, 3 min
PCR cycles	**Denaturation**	94˚C, 20 sec	94˚C, 20 sec	94˚C, 20 sec	94˚C, 20 sec
	Annealing	60˚C, 20 sec	55˚C, 20 sec	55˚C, 20 sec	52.8˚C, 20 sec
	Extension	72˚C, 20 sec	72˚C, 40 sec	72˚C, 40 sec	72˚C, 40 sec
Number of cycles		35	30	30	30
Finishing		72˚C, 5 min	72˚C, 5 min	72˚C, 5 min	72˚C, 5 min
Hold		10˚C	10˚C	10˚C	10˚C

2.10.3 Agarose gel electrophoresis and DNA extraction

Agarose gel electrophoresis was used to visualise DNA or RNA in samples, validate PCR products based on their migration and to separate DNA into bands for gel extraction.

Agarose gels were cast using gel cassettes. 0.5 or 1 g (for 1% and 2% (w/v) gels respectively). Agarose was melted in 50 ml 1 x TBE buffer (89 mM Tris Base, 89 mM boric acid, 2 mM EDTA) in a microwave and 3 µl ethidium bromide was added when hand hot. The mixture was then poured into a gel cassette and left to set with a well comb in place. When set, gels were covered with 1 x TBE buffer and the wells loaded with DNA ladder and sample DNA or PCR products were combined with loading buffer and run at a given voltage for the specified time. TBE buffer was used as it gives better resolution at small fragment sizes (< 300 bp) than TAE buffer (Miura et al., 1999).

After electrophoresis runs were completed, gels were imaged using a Bio-Rad ChemiDoc XRS System and Quantity One 4.6.9 (basic) software or transferred to a UV box for gel extraction.

For gel extraction, DNA bands corresponding to PCR products of interest were visualised using a UV lightbox. These bands were then excised with a sterile razor blade and their DNA content

extracted from the agarose slice using a MACHERY-NAGEL "Nucleospin Gel and PCR Clean-up kit" following the manufacturer's instructions.

2.10.4 *pmoCA* library construction, restriction digests and Restriction Fragment Length Polymorphism (RFLP) analysis

DNA was extracted from biofilter soil samples from three depths (0-10 cm, 10-20 cm and 20-30 cm) of core E (14.11.17) (**Chapter 3.3.1**) and used as templates for three *pmoCA* PCR reactions (PCR modifications: 20 µl reaction volume, PmoC374 and PmoA344 primers using 16S_72 protocol). PCR products (850 bp) were then ligated into pGEM-T easy vectors and the resulting constructs used to transform Top10 competent cells which were then plated and incubated overnight to produce a *pmoCA* library (**Chapter 2.10.5**). Resulting colonies from this library were then subjected to colony PCR (PCR modifications: 25 µl reaction volume, M13F and M13R primers using 16S_72col protocol) to amplify the *pmoCA* insert of each. A total of 90 colonies from the *pmoCA* library were used as templates for separate colony PCR reactions: 30 derived from 0-10 cm depth DNA, 30 derived from 10-20 cm depth DNA and another 30 derived from 20-30 cm depth DNA.

To generate restriction fragments of different lengths based on sequence polymorphisms, a restriction digest was carried out on each *pmoCA* colony PCR product. Two restriction enzymes were used: *Eco*RI with a 6 base recognition site (included to remove pGEM-T flanking regions from amplified *pmoCA*) and *Msp*I with a 4 base recognition site (which would be expected to make roughly three cuts in a random 850 bp nucleotide sequence). The restriction digest reaction mix (per reaction) consisted of: 2 µl 10X Fast digest buffer, 0.4 µl of EcoRI (1 U μl^{-1}), 0.4 µl of MspI (1 U μl^{-1}), 5 µl PCR product and 22.2 µl of molecular grade dH_2O. Digest reactions were incubated at 37˚C for 50 minutes. Resulting digest products for each reaction were visualised as banding patterns on 2% (w/v) agarose electrophoresis gels. *pmoCA* colony PCR products responsible for unique or highly similar sets of banding patterns underwent PCR clean-up and were then sent for single end Sanger sequencing with SF6 (pGEM-T insert) primer (**Chapter 2.10.6**).

2.10.5 Ligation of DNA and cloning PCR products

Ligation of DNA PCR products via the Promega pGEM-T Easy Vector System I was carried out according to the manufacturer's instructions (using 3 µl PCR product per reaction and reactions carried out overnight at 4˚C).

Ligated DNA in pGEM-T Easy Vectors was then used to transform Top10 chemically competent cells (Invitrogen). 4 µl of each ligation product was transferred to a separate 50 µl aliquot of Top10 competent cells in a 1.5 ml Eppendorf tube that had been allowed to thaw on ice, mixing each by tapping. Tubes immediately returned to ice for 3 minutes and then subjected to heat shock for 50 seconds at 42˚C before returning to ice for 2 minutes. 300 µl sterile SOC medium was then added to each tube and mixed by pipetting. Tubes were then incubated for 1 hour at 37˚C with shaking (160 RPM). After incubation, 100 or 50 µl aliquots of each transformation product were plated onto separate LB plates containing 1.5% agar, 100 µg ml^{-1} ampicillin and 40 µg ml^{-1} x-gal. Plates were then incubated overnight at 37˚C and vector harbouring colonies identified by blue/white screening.

2.10.6 DNA Sanger and amplicon sequencing of PCR products

Following DNA purification, PCR products were diluted and premixed with appropriate primers (as per the service instructions) and sent for Sanger sequencing using either the Eurofins Genomics Mix2Seq or TubeSeq services.

Amplicon sequencing of PCR products was carried out by either the Wilmes lab (Luxembourg) or mrDNA (Stillwater Texas USA). Sample DNA was amplified with appropriate primers via PCR and the PCR products subjected to PCR clean-up before being sent for amplicon sequencing. PCR products were prepared and shipped according to the service provider's guidelines.

2.10.7 Genome and metagenome sequencing

Genome sequencing was carried out by MicrobesNG (Birmingham UK) through their enhanced genome service. *Methylococcus capsulatus* (Norfolk) and *Methylocaldum szegediense* (Norfolk) cells were sent as per the submission guidelines.

For metagenome sequencing, soil DNA was extracted, separated from contaminating humic acid (**Chapter 2.9**) and then shipped for paired end metagenome sequencing (Illumina Novaseq 6000) by either mrDNA (Stillwater Texas USA) or Novogene (Cambridge UK) at the concentrations specified by the service provider.

2.11 DNA stable isotope probing

2.11.1 Preparation of biofilter soil samples

For each sample or sample treatment undergoing DNA-SIP, two aliquots of soil were required per replicate: one soil aliquot for incubation with the "heavy" $^{13}CH_4$ label and one soil aliquot to be incubated with "light" $^{12}CH_4$ as a negative control. Large stones, expanded clay pellets and woodchips were first removed from biofilter soil samples. Each sample was then thoroughly mixed and aliquots of soil of a specified weight were separated out for incubation. A small amount of sample soil was frozen at -20˚C for use as a pre-incubation Timepoint 0 (T0) sample.

2.11.2 Incubation of sample material with $^{13}CH_4$ and $^{12}CH_4$ and timepoint harvesting

For each incubation, a soil aliquot was transferred to a 120 ml butyl rubber stoppered serum vial along with a small volume of autoclaved dH_2O (in a 5 g soil:1 ml dH_2O ratio) to prevent soil drying out during the incubation period.

One set of replicates for each sample treatment was then gassed with one incubation volume of $^{13}CH_4$ (100%) into the headspace of each vial. A second set of replicates for each sample treatment was then gassed with one incubation volume of $^{12}CH_4$ (100%) into the headspace of each vial. Gas chromatography (**Chapter 2.8.1**) was used to confirm that the amount of CH_4 in each vial headspace was correct. Soil incubation vials were then incubated at appropriate temperatures without shaking.

Headspace CH_4 content was measured by GC every day. When headspace CH_4 was completely depleted, serum vials were opened and a small amount of soil was harvested from each and frozen at -20˚C (Timepoint 1, T1 sample). Serum vials were then allowed to re-equilibrate

headspace with air for 1 hour (to purge CO_2 and reintroduce O_2). Serum vials were then re-stoppered and injected with a fresh incubation volume of the same CH_4 (^{12}C or ^{13}C) and returned to the correct temperature incubation, with continued daily monitoring of headspace CH_4. After the second incubation volume of CH_4 was consumed, the above process was repeated: opening, Timepoint (T2) soil harvesting and freezing, re-equilibration, re-stoppering, incubation volume CH_4 injection, return to incubator and monitoring headspace CH_4. When the third incubation volume of CH_4 was consumed, serum vials were opened and all remaining soil frozen at -20˚C (Timepoint 3, T3 sample).

2.11.3 DNA-SIP soil DNA extraction

For each timepoint (T0, T1, T2 and T3) DNA was then extracted (**Chapter 2.9.1**) from a given mass of soil. DNA extracts were validated by PCR amplification using *pmoA* primers (PCR modifications: 20 µl reaction volume, A189F and A682R primers, 16S_72 protocol) and agarose gel electrophoresis of PCR products (**Chapter 2.10**). Where PCR was unsuccessful, corresponding DNA extracts then underwent humic acid removal followed by a second validation step (**Chapter 2.9.1**).

2.11.4 DNA ultracentrifugation and fractionation

Extracted DNA was separated into fractions following the protocol laid out by Neufeld et al (Neufeld et al., 2007). The "Gradient setup without EtBr" method was used to prepare the DNA for density gradient ultracentrifugation. Ultracentrifugation was then carried out as specified using a Beckman VTi 65.2 rotor (Neufeld et al., 2007).

The DNA was then separated out by gradient fractionation. The ultracentrifuge tube containing the CsCl:DNA gradient was fixed upright to a clamp, filtered dH_2O was pumped into the top of the ultracentrifuge tube via a 23 Gauge 1" needle (BD microlance 3) using a Watson Marlow 101U/R peristaltic pump (set to a flow rate of 425 µl min^{-1}). DNA fractions were then collected from the bottom of the ultracentrifuge tube through a hole made by a second needle. Fractions were collected in 1.5ml tubes, which were switched for a fresh tube every minute, resulting in a total of 12 consecutive fractions (from high to low density) in separate tubes. The refractive

index of each fraction was then measured with a Reichert refractometer, 35 µl sample aliquots were measured using the nD-TC setting following the manufacturer's instructions.

DNA was finally recovered from the separate fractions by precipitation following the Neufeld protocol (Neufeld et al., 2007) using 3 µl of linear polyacrylamide (5 mg ml^{-1}) instead of glycogen (Bartram et al., 2009). Precipitated gradient fraction DNA was quantified using Qubit 2.0 with the dsDNA high sensitivity kit and then kept at -4˚C (or -20˚C for longer term storage).

Fractions containing heavy (^{13}C labelled) and light (^{12}C labelled) DNA were identified by plotting fraction DNA concentrations against refractive indices for each set of sample fractions (**Figure 2.4**). Heavy fractions were identified amongst the earlier (high density) fractions where the $^{13}CH_4$ incubated sample DNA concentrations are initially higher than for the corresponding $^{12}CH_4$ incubated sample. The light fractions are the following fractions which produce the major peak on the DNA concentration vs refractive index plot. The heavy and light fractions were then confirmed by comparison with 16S rRNA gene DGGE profiles (**Chapter 2.11.6**).

A

Fraction number	$^{13}CH_4$ incubation extract		$^{12}CH_4$ incubation extract	
	Refractive Index	DNA conc (ng ml^{-1})	Refractive Index	DNA conc (ng ml^{-1})
1	1.4055	0	1.4053	0
2	1.4053	0	1.4051	0
3	1.4047	107	1.4047	0
4	1.4044	507	1.4043	0
5	1.4039	1660	1.4037	111
6	1.4034	2790	1.4034	531
7	1.4029	18900	1.4029	6650
8	1.4024	32100	1.4024	38000
9	1.4019	14500	1.402	16100
10	1.4016	4390	1.4016	4560
11	1.4004	1630	1.3981	2120
12	1.3787	867	1.3688	1190

B

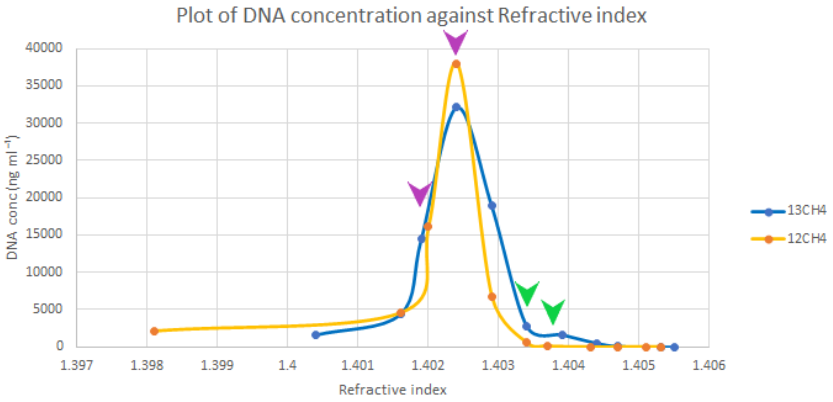

C

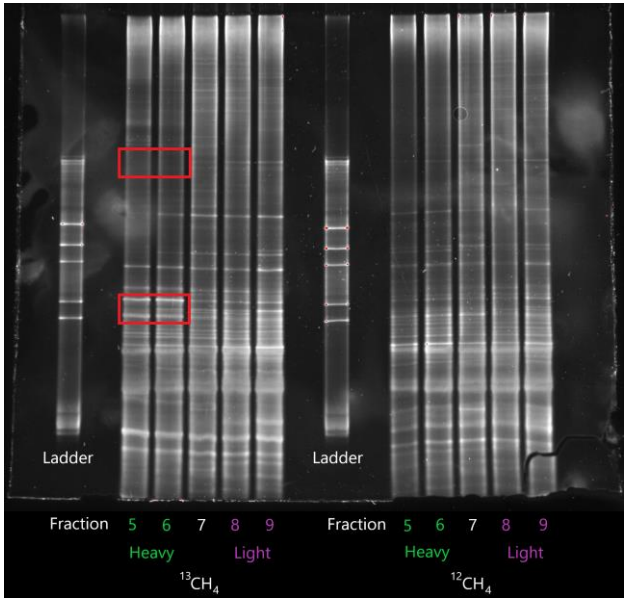

Figure 2.4 A) and **B)** Identifying heavy and light fraction DNA from a $^{13}CH_4$ incubated soil sample and it's $^{12}CH_4$ incubated control sample. heavy fractions (green) were identified where the $^{13}CH_4$ fractions initially showed higher DNA concentrations compared to the corresponding $^{12}CH_4$ fractions. Light fractions (purple) follow on from the heavy fractions. Intermediate fractions were considered a mix of heavy and light DNA.

C) Confirming identity of heavy (^{13}C-labelled) DNA fractions. 16S rRNA gene PCR products from putative heavy and light fractions of $^{13}CH_4$ incubated soil sample and corresponding $^{12}CH_4$ incubated control were run on a DGGE gel. A noticeable difference (red boxed area) between the banding pattern of the $^{13}CH_4$ incubated heavy fractions compared with all other fractions was expected.

2.11.5 Denaturing gradient gel electrophoresis (DGGE) analysis of 16S rRNA genes

PCR (**Chapter 2.10.2**) was carried out on precipitated gradient fraction DNA samples thought to contain heavy (^{13}C labelled) or light (^{12}C labelled) DNA. These PCR reactions used a 50 µl reaction volume, 341GC and 518R primers with precipitated gradient fraction DNA as template. The volume of template used was adjusted depending on the concentration of precipitated DNA: 3 µl template was used if the concentration was under 1 ng μl^{-1}; 2 µl was used if the concentration was between 1 and 3 ng μl^{-1} ; 1 µl was used if the concentration was above 3 ng μl^{-1}. Depending on the volume of template added, the amount of molecular grade dH_2O to take the reaction volume to 50 µl was modified accordingly. The reaction mixes were then subjected to the 16SDGGE PCR protocol (**Table 2.3**). The resulting PCR products were then run on DGGE gels.

DGGE gels were cast and run using a Bio-Rad DCode universal mutation detection system. Plates were cleaned with ethanol and assembled with greased spacers in the casting stand. These plates were used to cast 10% (w/v) agarose gels with a 30-70% denaturant gradient and a stacking gel without denaturant. The solutions used are shown in (**Table 2.5**).

Table 2.5 DGGE gel solutions. 12 ml 30% denaturant solution and 12 ml 70% denaturant solution (with 120 µl DGGE dye) were used to make the 30-70% denaturant gel. Stacking gel was then added using 5 ml of 0% denaturant stacking gel solution.

Solution component	DGGE solutions		
	30% denaturant solution	70% denaturant solution	0% denaturant stacking gel
40% acrylamide/bis 37.5:1 (ml)	12.5	12.5	0.75
50X TAE (ml)	1	1	0.1
formamide (ml)	6	14	-
urea (g)	6.3	14.7	-
filtered dH_2O (ml)	balance of 50 ml	balance of 50 ml	4.1
10 % ammonium persulfate solution (µl)	126	126	50
Tetramethylethylenediamine (µl)	12.6	12.6	5

Once DGGE gels had set, they were transferred to the gel tank filled with 1 x TAE buffer (40 mM Tris base, 20 mM acetic acid, 1mM EDTA) preheated to 60˚C. DGGE gel wells were then loaded with either 10 µl of each PCR product mixed with 4 µl of 6 x loading dye or 10 µl of an

in-house DNA ladder premixed with 10 µl 6 x loading dye. After all samples were loaded, the tank lid was replaced and the DGGE gels were run at 75 V, 200 mA for 16 hours at 60˚C with stirring of the buffer.

After DGGE gels had run they were removed from the gel tank and stained by incubation in the dark with a mixture of 300 ml 1 x TAE buffer and 4 ml SYBR Gold (Thermo Fisher Scientific) for 1 hour. The buffer and stain were then discarded and the DGGE gels were gently rinsed three times with dH_2O before being imaged using a Bio-Rad Gel Doc XR+ system.

2.12 Bioinformatics

2.12.1 *In silico* analysis of genomes and short nucleic acid and protein sequences

Genomes were visualised, annotated and analysed using a combination of the Microscope platform (Vallenet et al., 2020), Prokka ver1.14.6 (Seemann, 2014) and NCBI-BLAST ver2.10.1 (Camacho et al., 2009). BioEdit ver7.6.2.1 (Hall, 1999) was used to read, align and manipulate protein and nucleic acid sequences as well as to view Sanger sequencing chromatogram traces. Protein and Nucleotide BLAST searches hosted on the National Center for Biotechnology Information (NCBI) website (National Center for Biotechnology Information, 1988) were used to identify unknown nucleotide and protein sequences. Top hits from NCBI searches were also used to infer the taxonomy of the bacterium. The similarity of recovered MAGs and genomes (and the likelihood of them being the same species or subspecies) was estimated using the Genome-to-Genome Distance Calculator ver3.0 (Meier-Kolthoff, 2021).

2.12.2 Constructing *pmoCA* phylogenetic trees

Nucleotide and translated nucleotide maximum likelihood phylogenetic trees were constructed for *pmoCA* sequences generated from the clone library used for RFLP analysis. The *pmoCA* sequences were first trimmed down to their *pmoA* component and aligned alongside *pmoA* sequences from available methanotroph genome assemblies as well as *amoA* from *Nitrosomonas europaea.* Nucleotide and nucleotide-derived amino acid sequences were used to generate MUSCLE multiple sequence alignments using default parameters in MEGA ver11

(Tamura et al., 2021). Modeltest-NG ver.x.y.z (Darriba et al., 2019) was used to select an appropriate evolutionary model for the amino acid and nucleotide alignments with the "-t ml" flag. The optimal model based on the corrected Akaike information criterion (AICc) was then implemented to generate a maximum likelihood tree for both the nucleotide and amino acid alignments using PhyML ver3.3.20200621 (Guindon et al., 2010) with 1000 bootstrap replicates using *amoA* from *Nitrosomonas europaea* as a root.

2.12.3 16S rRNA gene amplicon analysis

16S rRNA V3V4 amplicons were analysed using the DADA2 platform ver1.16 (Callahan et al., 2016). For all amplicons the quality of the forward and reverse reads was first assessed and used to guide the "truncLen" values selected for the DADA2 filterAndTrim settings ensuring a minimum overlap of 35bp between the paired reads. Otherwise default filterAndTrim parameters were used: truncLen=c(<forward trim value>,<reverse trim value>), maxN=0, maxEE=c(2,2), truncQ=2. Amplicon reads were then denoised and paired reads merged. Very long (>460bp) and very short (<360bp) merged pairs were discarded and chimaeras removed. Taxonomy was then assigned to the resulting amplicon sequence variants (ASVs) using the Silva NR 99 138.1 dataset (Quast et al., 2013).

2.12.4 Metagenome assembly and analysis

Metagenome sequencing raw reads from Novogene and MrDNA were first trimmed using the Cutadapt wrapper Trim Galore ver0.6.5 (Martin, 2011) and underwent further light trimming following the suggestions of Minoche et al. (Minoche et al., 2011) using the illumina-utils minoche script developed by Eren et al. (Eren et al., 2013). Trimmed reads were then assembled using MEGAHIT ver1.2.9 (Dinghua et al., 2015) or SPAdes ver3.14.0 with the metagenome flag (Nurk et al., 2017) and the assembled contigs or scaffolds were then binned with metaBAT2 ver2.12.1 (Kang et al., 2019) and MaxBin2 ver2.2.6 (Wu et al., 2016) using the MetaWRAP wrapper ver1.2.1 (Uritskiy et al., 2018). The assembled contigs or scaffolds were also binned using CONCOCT ver1.0.0 (Alneberg et al., 2013), either alongside the other binning programs in MetaWRAP for the SPAdes assembly or separately for the MEGAHIT assembly, as the MEGAHIT contig format conflicts with the implementation of CONCOCT in the MetaWRAP binning module. The three sets of bins were then interrogated and curated into

an optimized bin set using the MetaWRAP bin refinement module. The completeness and contamination of the optimized bins was then estimated using CheckM ver1.0.12 (Parks et al., 2015) and taxonomy assigned to each using MIGA online (Rodriguez et al., 2018). The optimised bins were then annotated using Prokka ver1.14.6 (Seemann, 2014) and further screened for individual genes of interest using NCBI-BLAST ver2.10.1 (Camacho et al., 2009). K numbers identifying orthologues of experimentally determined enzymes were assigned to the translated coding sequences found by Prokka using BlastKoala (Kanehisa et al., 2016), to allow metabolic pathway enzyme mapping using the KEGG pathway reconstruct tool (Kanehisa 2019). The taxonomic origin of raw reads and assembled contigs or scaffolds was assessed with Kraken2 ver2.1.2 (Wood et al., 2019) and visualised with KronaTools ver2.8.1 (Ondov et al., 2011). CheckM was used to estimate the relative abundance of recovered bins from each metagenome assembly. Finally, average MAG read coverage (AMRC), per million paired reads, was calculated using the MetaWRAP quant_bins function.

Chapter 3: Biofilter soil sampling and monitoring

3.1 Biofilter soil sampling and monitoring

The Strumpshaw biofilter is effectively a 75m^3 matrix of soil material through which landfill gas is pumped to facilitate the bio-oxidation of CH_4 to CO_2 and biomass by methanotrophic bacteria residing in the biofilter soil. Understanding the operation and behaviour of the biofilter system involved investigation of gas flow and CH_4 removal within the biofilter alongside soil temperature and moisture content. Over the course of this project biofilter soil material was repeatedly sampled both to obtain measurements of these parameters as well as to study the methanotrophs inhabiting it. Experiments characterising soil CH_4 oxidation profiles at different soil moisture contents were carried out in conjunction with Dr Hui-Juan Xu from the Joint Institute for Environmental Research & Education, South China Agricultural University, Guangzhou, China. Biofilter combined temperature/gas depth profiles were taken with the help of Daniel Rankin or Keziah Flack from NCC.

3.2 Temperature and gas measurements within the Strumpshaw biofilter

3.2.1 Historical biofilter monitoring

Gas flow within the Strumpshaw biofilter has been monitored by the NCC on a monthly to weekly basis since 2014, with a 9-month break (May 2018 to February 2019) while the system was turned off for an upgrade (automated balancing of the inlet air and landfill gas mix). This monitoring consisted of gas composition measurements taken using a gas analyser from the biofilter gas inlet port, as well as from the four sets of four fixed sampling ports sunk to different depths within the biofilter matrix. Temperature readings were also taken by lowering a thermocouple down each of the ports, although this was done far less frequently (17 sets of temperature readings over a seven year period) (**Chapter 2.3**). These measurements were very useful to confirm the successful delivery of CH_4-containing gas within the biofilter and also highlighted that *in situ* temperatures were sometimes elevated above ambient air temperature. Unfortunately, the permanent nature of the sampling ports restricted gas and temperature measurements to the exact same positions across the biofilter for each iteration of readings.

There was also concern that the action of unscrewing the port caps could disturb the PVC tubing sunk into the biofilter matrix, potentially creating preferential pathways along the outside of the tubing for biofilter gas to escape to the surface, thus affecting the resulting readings taken from the port. Dilution of the biofilter gas samples with air when taking readings from the monitoring ports was an issue, as the artificially lowered CH_4 content of the measured gas would incorrectly imply higher CH_4 oxidation efficiency within the biofilter than was actually the case. (**Table 3.1**) shows just such a case, with the gas measurements taken from the n.o. 4 upper and lower matrix monitoring ports extremely close to atmospheric air composition. One further disadvantage of the monitoring ports was that for each set, the different depth ports were placed in straight lines across the biofilter surface with each several inches away from the next, this prevented the data from any one set being viewed as a true depth profile of gas or temperature measurements as the different depth readings were all offset horizontally. In order to address these issues, a temperature probe as well as a combined temperature/gas probe were commissioned from the NCC workshop (**Chapter 2.3.2**). These allowed temperature and gas measurements to be taken at any single point within the biofilter, as well as the construction of depth profiles to assess changes in gas composition and temperature as the inlet gas rises within the biofilter. The sturdier (steel) construction of the temperature/gas probe also allowed for compaction of the biofilter soil around the probe to limit preferential pathways along the outer edge of the probe, which might facilitate biofilter gas mixing with above surface air, leading to skewed gas readings (especially at shallower depths). In future biofilter designs, fixed monitoring ports could be improved by reducing the stiffness of their caps to limit disturbances to gas flow and increasing the number of monitoring positions to provide greater coverage, but a portable temperature/gas probe. would remain essential .

Table 3.1 Biofilter gas measurements taken from the biofilter gas inlet and the position 4 monitoring ports on 25.4.18. The lower and upper matrix measurements are almost certainly the result of the biofilter gas becoming contaminated and diluted with atmospheric air.

Sampling Port	CH_4 (%)	CO_2 (%)	O_2 (%)
Biofilter Inlet	6.7	3.7	18.2
BF4 Gravel layer	8.5	4.5	16.5
BF4 Lower matrix	0.0	0.5	21.2
BF4 Upper Matrix	0.0	0.0	21.4
BF4 Top layer	6.8	5.7	15.3

3.2.2 Monitoring changes in biofilter temperature following system restart

While the Strumpshaw biofilter is not actively heated, the historical temperature readings taken from monitoring ports by members of the NCC included a high of 60.7˚C measured within the biofilter matrix. The most likely explanation for these elevated temperatures was believed to be biological activity within the biofilter, with two main theories as to the cause. The first possibility was heat generation from general microbial activity associated with the break-down of organic soil components and respiration within the biofilter matrix, this seemed plausible as the biofilter soil matrix features a significant compost component and is actively aerated by the oxygen rich inlet gas (~16% O_2) (Bertoldi, 1983). The alternative theory was that it could be a CH_4-dependant temperature increase driven by CH_4 oxidation by methanotrophs as the bioconversion of CH_4 to CO_2 and H_2O is exothermic ($CH_4 + 2O_2 \rightarrow CO_2 + 2H_2O$ = + 882.6 kJ) and methanotrophic activity has been associated with elevated soil temperatures (Cappelletti 2016; Pehme 2020). Beyond the exothermic oxidation of CH_4, the production of carbon source metabolites such as methanol, formate and generation of reducing equivalents (through the methane oxidation pathway) may support heat generation through catabolism and aerobic respiration in both methanotrophs and non-methanotroph cross-feeders. The planned shutdown of the biofilter between May 2018 to February 2019 provided an opportunity to monitor temperatures within the biofilter soil matrix both before and after the system restart and to see how it would change as the CH_4-containing gas mix was supplied once more.

The effect of methane driven biological activity on *in situ* temperature was explored by generating temperature depth profiles at different points across the biofilter following biofilter switch on (14.2.19). Temperature profiles from different sampling days shown overlaid onto biofilter reference grid in (**Figure 3.1 A**,**B and C**).

Very high temperatures were observed on 8.3.19 (temperatures up to 61˚C) and steam could be seen rising from the biofilter (perhaps indicative of microbial activity generating heat within the biofilter matrix).

Unfortunately, due to a failure in the supply of CH_4 to the biofilter on a subsequent sampling trip, the biofilter (26.3.19) temperatures were around ambient air temperature (15˚C). Presumably this was due to a cessation of methanotroph activity (when deprived of CH_4).

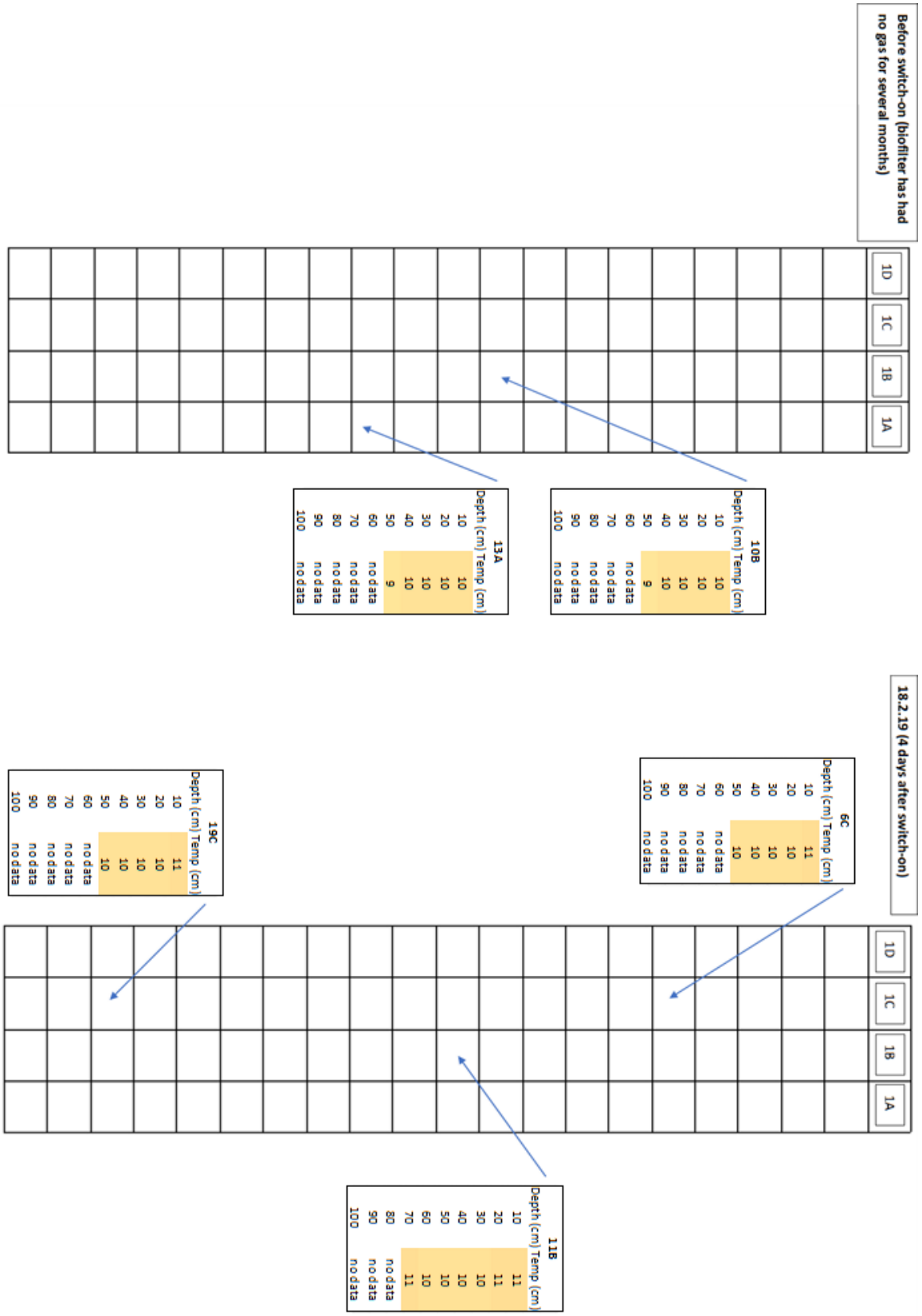

Figure 3.1 A) Temperature profiles recorded at Strumpshaw biofilter before and shortly after switch on (14.2.19).

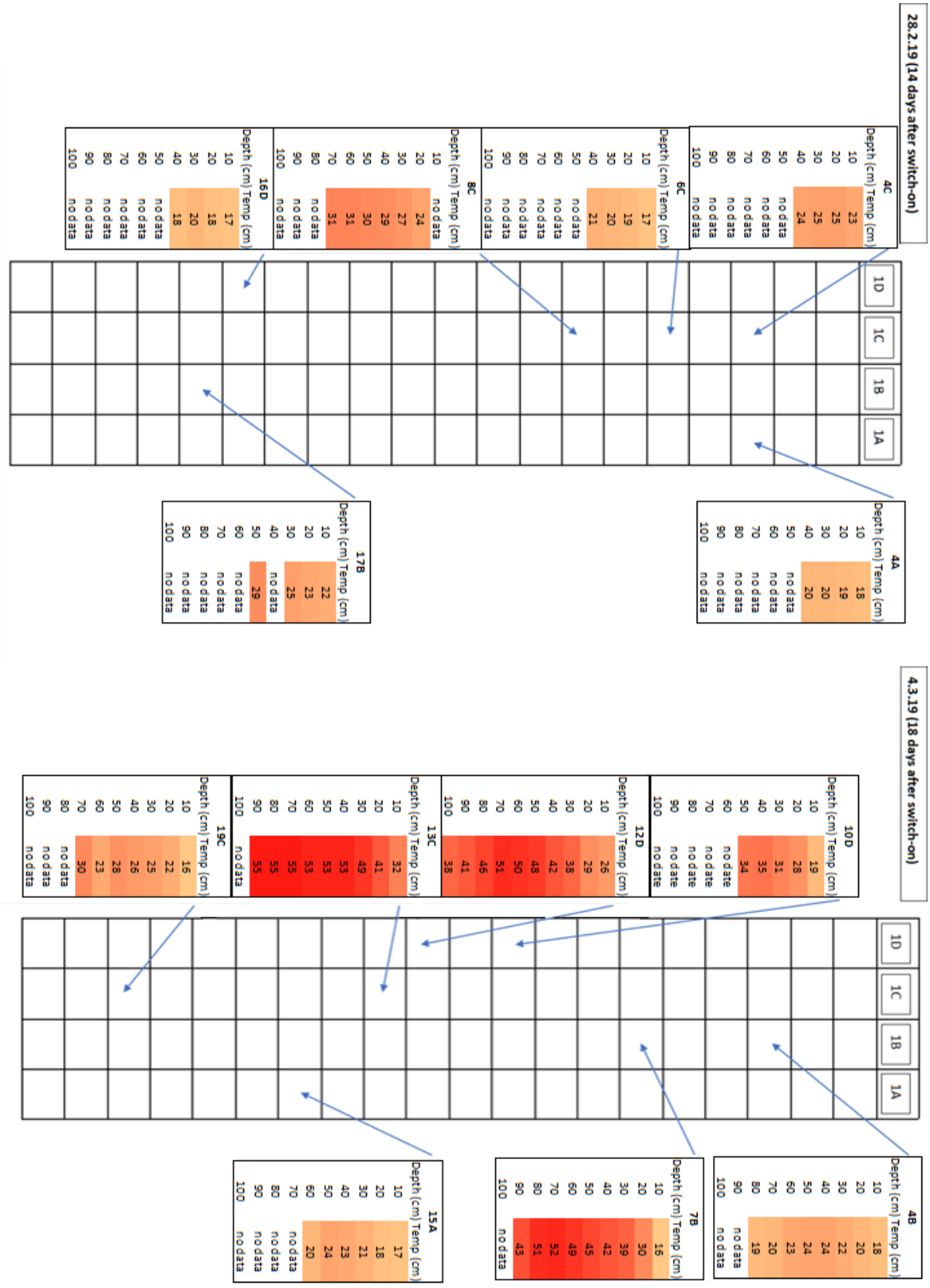

Figure 3.1 B) Temperature profiles recorded at Strumpshaw biofilter following switch on (14.2.19), note increase in measured temperatures compared with **Figure 3.1 A**).

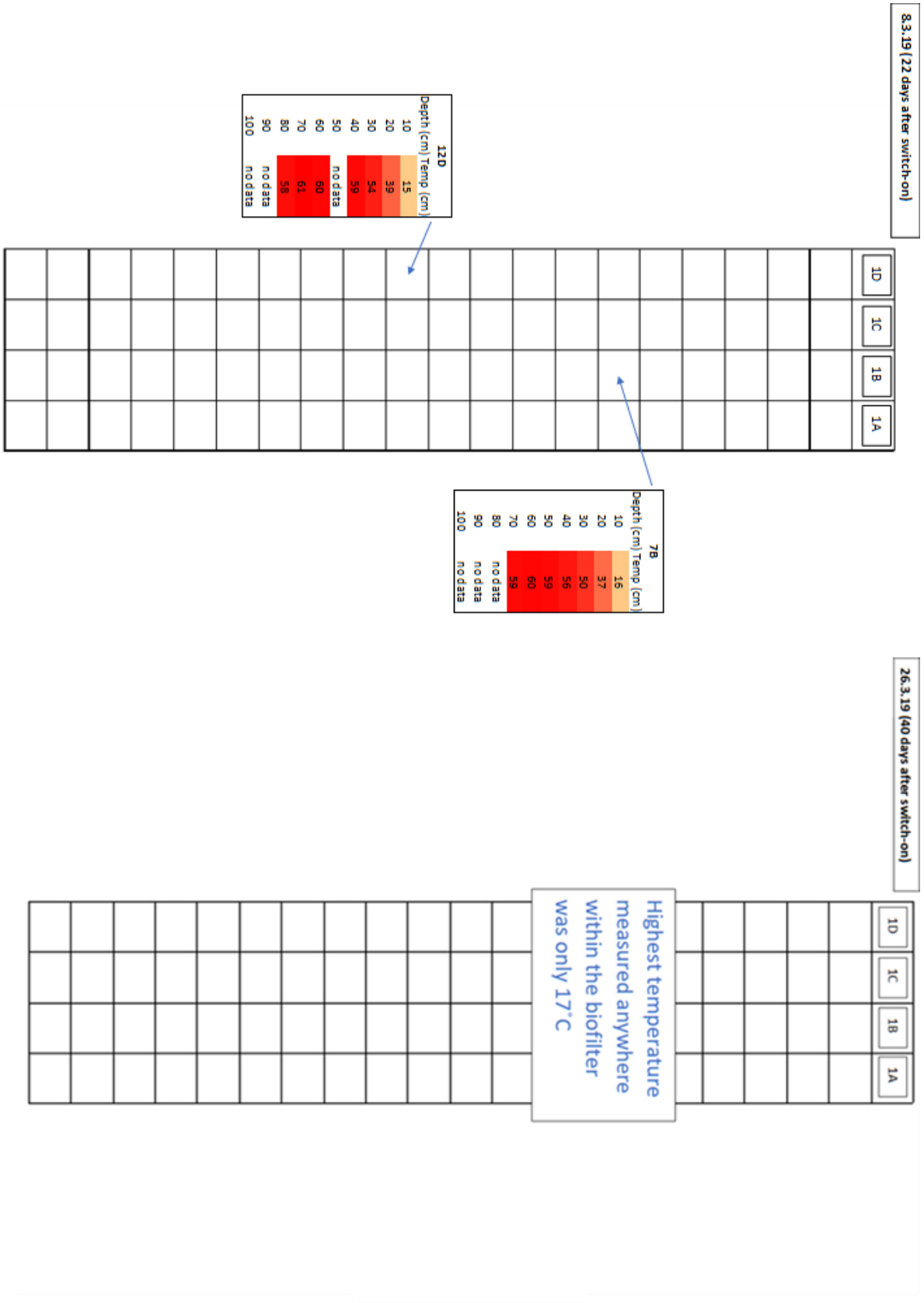

Figure 3.1 C) Follow up temperature measurements taken on subsequent trips, the low temperatures seen on 26.3.19 were measured following disruption to the biofilter CH_4 supply.

These results were very interesting as they suggested a CH_4 dependant increase in temperature within the biofilter. After the system restart began supplying the CH_4 and O_2 mix (on 14.2.19) there was a gradual increase in temperatures measured within the biofilter until by 8.3.19, temperatures as high as 61ºC were recorded (well above the East Anglia average maximum air temperatures for February, 8.06ºC (Met Office n.d.)). This heat was presumably due to methanotroph oxidation of CH_4 rather than bacterial breakdown of organics and respiration as the elevated temperatures disappeared when the CH_4 supply failed (even though O_2 was still being fed into the biofilter).

3.2.3 Temperature depth profiles

A temperature depth profile was generating using the temperature probe at the position from which a soil core was sampled on 8.3.19 in sector 12D of the biofilter (**Table 3.2**). This soil was intended for use as an enrichment inoculum in an attempt to isolate thermotolerant methanotrophs, this soil was considered suitable based on the high temperatures recorded.

Table 3.2 Temperature depth profile at sampling position of sector 12D on 8.3.19.

Sector **12D**	
Depth below surface (cm)	Temperature (˚C)
10	15.1
20	39.0
30	54.4
40	58.9
50	60.2
60	61.5
70	58.3
80	52.6

A set of temperature depth profiles were taken with the temperature probe on 3.5.19 to assess temperatures within the biofilter (**Table 3.3**). The ambient air temperature was 9.7˚C. The measured temperatures are very high with all temperature profiles taken reading over 60ºC for at least one depth measurement, with the temperature profile from sector 2C exhibiting a temperature high of 67.8ºC.

Table 3.3 Temperature depth profiles taken on 3.5.19 (ambient air temperature 9.7ºC).

Sector **2C**	
Depth below surface (cm)	Temperature (˚C)
10	10.5
20	38.0
30	61.5
40	66.0
50	67.8
60	62.0
70	60.6
80	56.0
90	58.0
100	no data

Sector **7A**	
Depth below surface (cm)	Temperature (˚C)
10	11.6
20	40.9
30	53.1
40	57.6
50	59.4
60	60.2
70	61.3
80	58.8
90	55.5
100	50.9

Sector **12D**	
Depth below surface (cm)	Temperature (˚C)
10	12.2
20	52.0
30	61.5
40	64.1
50	64.9
60	63.7
70	63.2
80	60.1
90	59.2
100	57.0

Sector **17B**	
Depth below surface (cm)	Temperature (˚C)
10	12.1
20	50.0
30	62.2
40	65.3
50	58.4
60	52.3
70	44.6
80	no data
90	no data
100	no data

Sector **19D**	
Depth below surface (cm)	Temperature (˚C)
10	11.7
20	38.8
30	53.8
40	58.8
50	60.2
60	56.9
70	51.0
80	no data
90	no data
100	no data

A further set of temperature depth profiles was taken on 20.7.19, when the ambient air temperature was 24ºC (**Table 3.4**). However, on this occasion the measured temperatures were

barely above the ambient air temperature. This was likely due to an incident of the biofilter shutting down at the end of the previous month, disrupting CH_4 supply to the biofilter soil and it's resident methanotrophs.

Table 3.4 Temperature depth profiles taken on 20.7.19 ambient air temperature 24ºC.

Sector **4A**	
Depth below surface (cm)	Temperature (˚C)
10	27.7
20	28.8
30	25.4
40	24.5
50	24.5
60	25.1
70	25.0

Sector **8B**	
Depth below surface (cm)	Temperature (˚C)
10	25.5
20	25.7
30	25.9
40	25.9
50	25.8
60	24.6
70	25.3

Sector **13C**	
Depth below surface (cm)	Temperature (˚C)
10	26.3
20	26.4
30	26.5
40	26.8
50	27.3
60	27.1
70	27.0

Sector **19D**	
Depth below surface (cm)	Temperature (˚C)
10	27.1
20	26.9
30	26.7
40	26.2
50	26.6
60	26.3
70	26.8

Assessing all these temperature depth profiles, as well as those taken as part of the system restart experiment, elevated temperatures well above ambient air temperature are observed within the biofilter, when the biofilter is receiving an uninterrupted supply of CH_4. But when the biofilter's supply of CH_4 fails, the *in situ* temperatures drop and take an extended period of time to rise again (several weeks judging by the system restart experiment).

3.2.4 Combined temperature and gas biofilter depth profiles

All temperature/gas depth profile measurements were taken with the help of Daniel Rankin or Keziah Flack from the NCC. The combined temperature/gas probe was first tested on 30.10.19.

A number of temperature depth profiles were recorded and *in situ* % CH_4 was measured at several different points (**Table 3.5**). While the biofilter appeared to be back up to higher temperatures again, there was some concern that the low CH_4 readings taken at the shallower depths may have been anomalous and caused by air dilution of the landfill gas. This might have been due to a shallower seal of soil around the probe inflow vents just behind the tip of the probe. To mitigate this in the future, it was decided to take measurements of CH_4, CO_2 and O_2 alongside temperature. If CH_4 was oxidised by methanotrophs as it rose through the biofilter, one would expect to see the CH_4 and O_2 levels drop as the gas moves up through the biofilter and one would expect the % CO_2 to increase as CH_4 and O_2 are used up and CO_2 generated, by the methanotroph driven bio-oxidation of CH_4 (Whittenbury et al., 1970). Conversely if air dilution occurred one would expect to see a drop in both CO_2 and CH_4 and an increase in % O_2 (as the 21% O_2 in air is higher than the % in the air/CH_4 mix). By looking for an increase in % O_2 and a decrease in CO_2 near the biofilter surface, where % CH_4 is seen to drop suddenly, the profiles could be screened for potential anomalies due to air dilution.

Six combined temperature, CH_4, O_2 and CO_2 depth profiles were taken with the temperature/gas probe on 7.11.19. These are displayed in (**Figure 3.2**). These profiles were very useful to again show the high in-situ temperatures previously seen when using the temperature-only probe. The gas depth profiles indicate that most CH_4 removal was occurring in the top 35 cm of these profiles. However, judging by the increase in % O_2 just below the surface (0cm depth) in all but 12B and 17B profiles, it is likely that the large decrease in CH_4 from 5 cm to 0 cm depth below surface was due to air dilution of the CH_4 containing gas mix. In fact, even for the 12B and 17B profiles, such a shallow depth reading is likely biased due to partial air dilution, with the decrease in O_2 smaller and the decrease in CH_4 being larger than they actually are.

Table 3.5 Combined temperature and gas profiles taken on 30.10.19. n.d. = measurement not determined.

Sector **3B**		
Depth below surface (cm)	Temperature (˚C)	CH_4 (%)
10	30.3	(15cm) **4.2**
20	32.5	
30	33.6	n.d.
40	37.2	n.d.

Sector **2A**		
Depth below surface (cm)	Temperature (˚C)	CH_4 (%)
10	30.1	**2.8**
40	37.6	**4.1**

Sector **5B**		
Depth below surface (cm)	Temperature (˚C)	CH_4 (%)
10	47.9	(15cm) **2.8**
20	54.0	
30	54.3	n.d.
40	50.5	**4.1**
50	46.1	n.d.
60	35.6	n.d.
70	31.2	n.d.

Sector **17B**		
Depth below surface (cm)	Temperature (˚C)	CH_4 (%)
10	54.2	**0**
20	59.0	n.d.
30	60.0	(35cm) **3.4**
40	59.9	
50	57.9	**6.8**
60	52.5	n.d.

17B Not sure if 0% CH_4 at 10cm depth was due to no CH_4 or bad probe/soil seal allowing air dilution

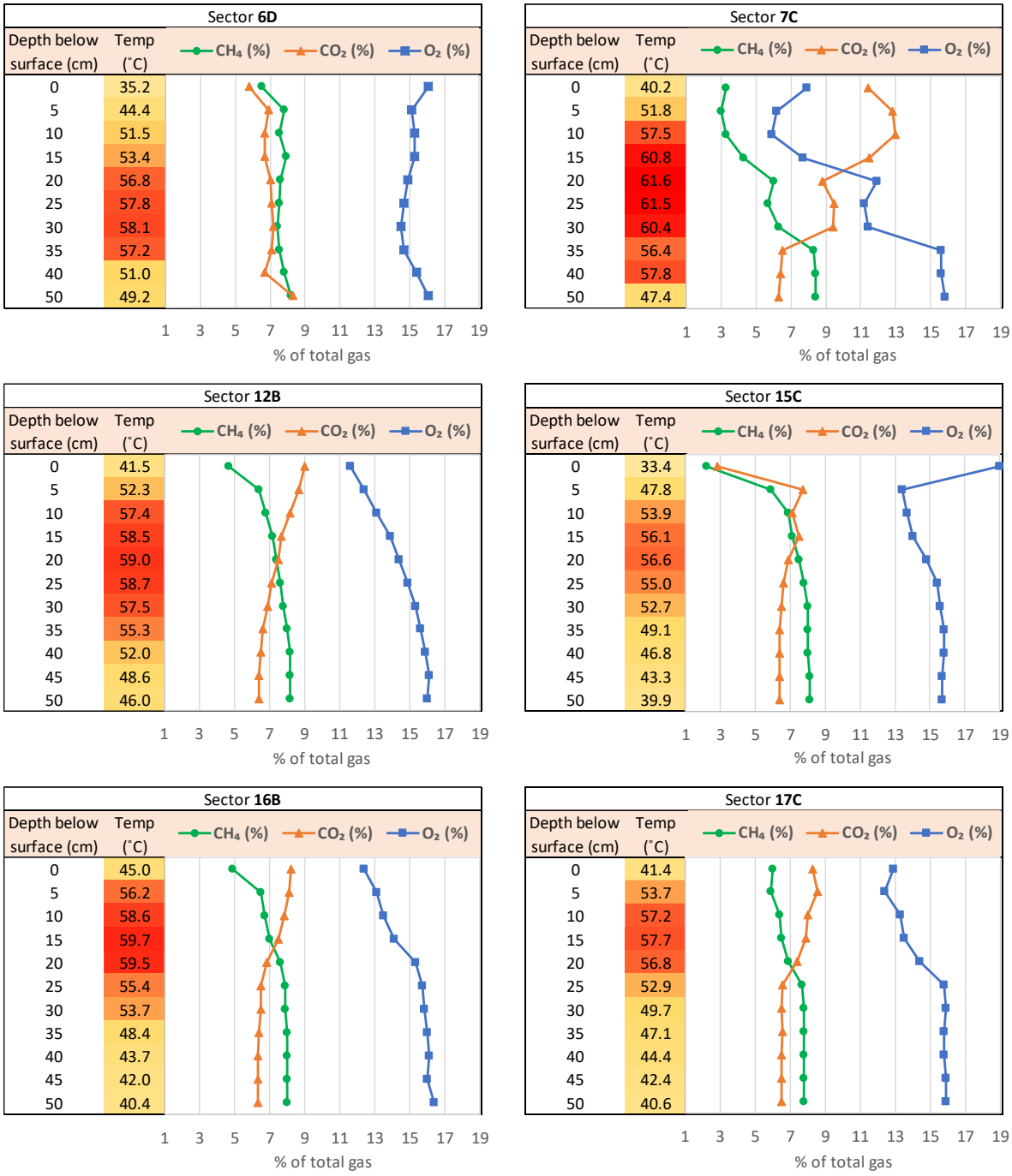

Figure 3.2 Combined biofilter temperature/gas depth profiles measured on 7.11.19. Note the temperature colour gradation was altered from that used in **Tables 3.2**, **3.3**, **3.4**, **3.5** and **Figure 3.1** to allow clearer resolution of the highest temperatures.

A further set of four combined temperature, CH_4, O_2 and CO_2 depth profiles (from sectors 3C, 7A, 13C and 18B) were taken on 13.11.19 at the same positions that soil samples were retrieved for soil moisture experiments (**Chapter 3.3.5.2**). These profiles served a double function: as

both additional profile datasets and as confirmation of CH_4 removal (methanotroph activity) in the sampled soil (**Figure 3.3**).

While the combined temperature/gas profiles show that most CH_4 removal was occurring in the top 35 cm of the biofilter, by combining the information from the temperature and combined temperature/gas depth profiles it seemed likely that most CH_4 removal was occurring in the top 60 cm of the biofilter. This conclusion was reached due to the correlation between maximal temperature and CH_4 removal seen in the combined temperature/gas depth profiles and the appearance of maximal temperature at an approximate depth of 50-60 cm in many of the temperature-only probe temperature depth profiles.

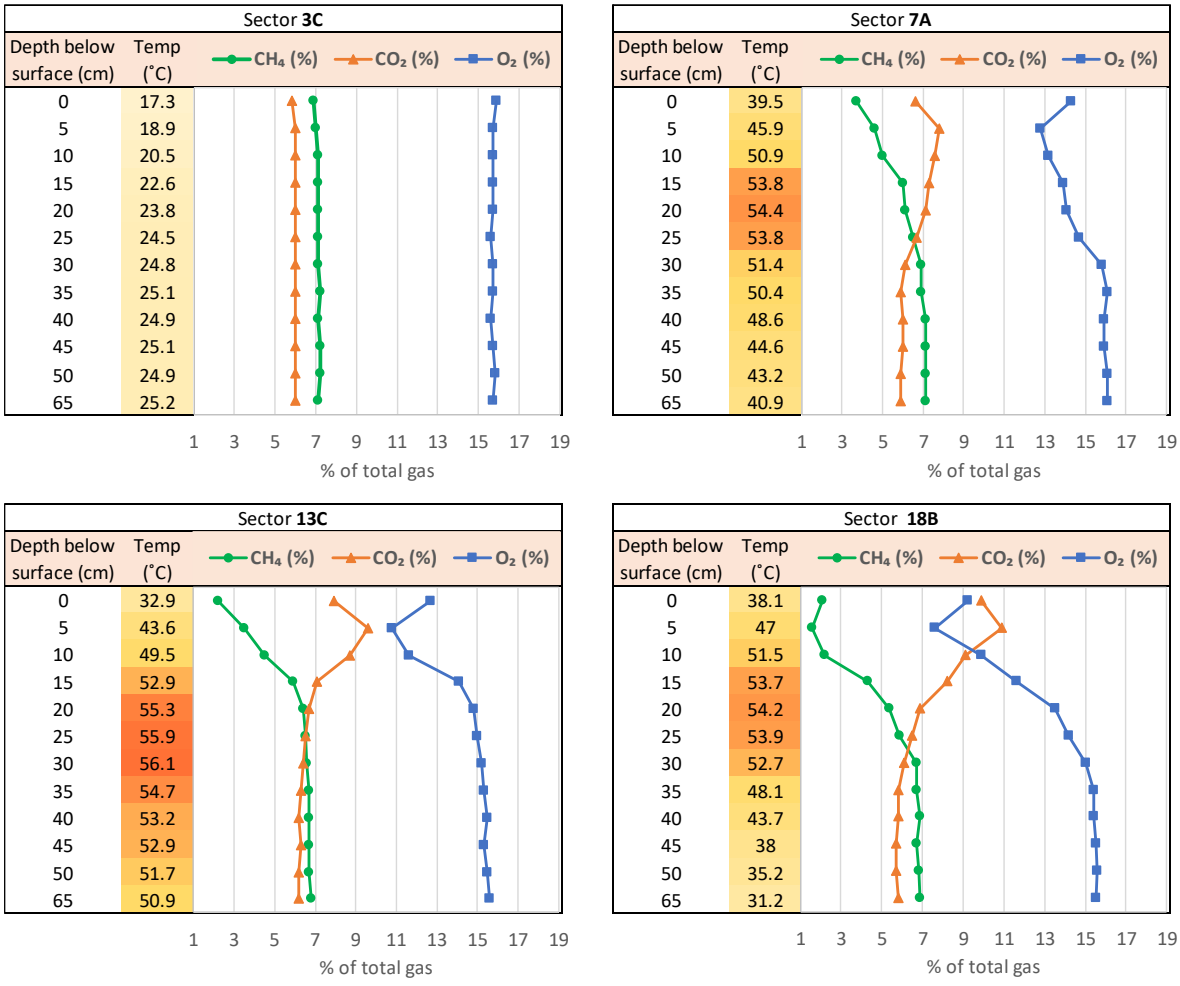

Figure 3.3 Combined biofilter temperature/gas depth profiles measured 13.11.19 taken in conjunction with soil sampling for soil moisture experiments. Note the temperature colour gradation was altered from that used in **Tables 3.2**, **3.3**, **3.4**, **3.5** and **Figure 3.1** to allow clearer resolution of the highest temperatures.

3.3 Biofilter soil sample retrieval and CH_4 oxidation potential measurements

3.3.1 Retrieving soil samples for PCR detection of methanotroph functional gene markers and *pmoCA* clone library and RFLP analysis

An open-faced soil corer (3 cm diameter) was obtained from the UEA field store and used to recover a soil core from sector 11C on 14.11.17, to provide biofilter soil bacterial DNA for use in PCR reactions to detect methanotroph functional gene markers. This soil core was taken from the surface of the biofilter down to a depth of 40 cm and divided into four 10 cm sections of increasing depth (0-10 cm, 10-20 cm, 20-30 cm and 30-40 cm) which were separately mixed. PCR primer pairs targeting regions of the *pmoA*, *pmoCA* (particulate methane monooxygenase) and *mmoX* (soluble methane monooxygenase) genes were then used to screen extracted soil DNA for the presence of methanotrophs. Additionally, DNA extracted from this soil core was used to generate a *pmoCA* clone library, which was then used for RFLP analysis of the methanotroph community (**Chapter 4.3**). Retrieval of biofilter soil cores proved difficult using this soil corer, as the open face resulted in poor soil retention during extraction. It was also decided that the 3 cm diameter would provide too little soil material from a given depth to facilitate soil CH_4 oxidation potential estimation assays. Therefore, a fully enclosed 5 cm diameter soil corer was ordered from the UEA workshop (**Chapter 2.7.1**).

3.3.2 Retrieving soil samples for 16S rRNA amplicons and initial DNA-SIP

A soil core was retrieved from the Strumpshaw biofilter on 19.2.18 to provide soil material for both 16S rRNA gene amplicon sequencing to explore the taxonomy of the total bacterial community (**Chapter 4.4**) and for a DNA-SIP labelling experiment to label, separate and identify the DNA of active methanotrophs within this community (**Chapter 5.2**).

The soil core was retrieved from the surface of the biofilter down to a depth of 60cm, taken at the midpoint of the sector 11B/11C boundary (the centre-most point of the biofilter surface). This 60 cm core was divided into six 10 cm sections: 1 (top of core) down to 6 (bottom of core). The bulk soil from each section was then mixed separately. A portion of soil from each section was then used to determine their soil CH_4 oxidation potentials. Remaining soil was then set aside for the bacterial community studies: All six sections were used for the 16S rRNA gene

amplicon community experiment (**Chapter 4.4**) while the topmost section (1) was used for the DNA-SIP labelling experiment (**Chapter 5.2**).

To determine the soil CH_4 oxidation potential of these soils, three sets of duplicate assays were created for each of the top four sections (1,2,3,4) and three sets of single assays were made up for the bottom two sections (5,6) due to slightly less material for the lower depths (large stone present). Each set of assays was incubated at one of three temperatures (30˚C, 37˚C or 45˚C), so that all soil core sections had one (5,6) or two (1,2,3,4) assays at each temp. The CH_4 oxidation assays were done in 120ml serum vials containing 5g of core section soil, gassed with 1% (1.2ml) headspace CH_4, and incubated at the desired temperature. Decrease in headspace CH_4 was measured over time to calculate the soil CH_4 oxidation potential. Results are shown in (**Table 3.6**).

The day after this initial soil CH_4 oxidation potential experiment, assay serum vials were opened, and their headspace allowed to re-equilibrate with air for 1 hour. Vials were then recapped and regassed with 1% (1.2ml) headspace CH_4 and the soil oxidation potential experiment (measuring CH_4 depletion over time) repeated on the same soil samples with the same temperature treatments. Results are shown in (**Table 3.7**).

Table 3.6 Sector 11B/11C boundary soil core CH_4 oxidation potentials calculated from the first CH_4 incubation.

1st Assay Run - February 2018 Core

Soil core section	Soil CH_4 oxidation potential at each incubation temperature (nmoles h^{-1} g $soil^{-1}$)		
	30˚C	**37˚C**	**45˚C**
Section 1 (0-10 cm depth)	240.81	291.31	184.65
	309.30	225.45	195.13
Section 2 (10-20 cm depth)	119.98	117.42	105.57
	116.52	33.94	81.04
Section 3 (20-30 cm depth)	109.89	28.08	26.93
	66.13	72.57	24.90
Section 4 (30-40 cm depth)	315.83	120.35	NRC
	347.14	92.12	10.54
Section 5 (40-50 cm depth)	479.79	134.76	18.35
Section 6 (50 -60 cm depth)	65.94	44.21	NRC

Table 3.7 11B/11C boundary core soil CH_4 oxidation potentials calculated from the second CH_4 incubation.

2nd Assay Run - February 2018 Core

Soil core section	Soil CH_4 oxidation potential at each incubation temperature (nmoles h^{-1} g $soil^{-1}$)		
	30˚C	**37˚C**	**45˚C**
Section 1 (0-10 cm depth)	343.05	413.06	435.36
	364.79	432.06	622.69
Section 2 (10-20 cm depth)	142.48	242.62	249.26
	139.18	209.29	135.74
Section 3 (20-30 cm depth)	409.67	23.80	NRC
	489.33	46.17	65.39
Section 4 (30-40 cm depth)	422.54	200.90	41.40
	407.51	207.22	NRC
Section 5 (40-50 cm depth)	79.86	17.05	45.38
Section 6 (50 -60 cm depth)	NRC	10.86	29.29

These results indicated that CH_4 was being oxidised by methanotrophs present within the incubated biofilter soil, and that this soil was suitable for use in the DNA-SIP labelling experiment as there were active methanotrophs present to oxidise $^{13}CH_4$ and label DNA. Of equal interest however, was the increase in CH_4 oxidation potential for most samples (except for section 5) during the second incubation. One possible explanation for this might be that the methanotroph communities were adapting to the lab incubation conditions. *In situ* biofilter temperature may have been different and the percentage of CH_4 in these layers may have been different in the biofilter (higher or lower than 1%, perhaps none?). It therefore seemed sensible to start monitoring temperature and perhaps gas flow within the biofilter when sampling, to gain a clearer understanding of the methanotrophs' environment within the biofilter.

3.3.3 Effect of headspace CH_4 concentration in vials on estimates of soil CH_4 oxidation potential

Biofilter soil was retrieved from a hot region of the biofilter (temperatures of around 50˚C) on 8.3.19 for use as an inoculum for the enrichment and isolation of methanotrophs. A soil core

sample was recovered from sector 12D. The soil core sample was then split into four sections of increasing depth below the biofilter surface: (1) 0-20 cm depth, (2) 20-40 cm depth, (3) 40-60 cm depth and (4) 60-80 cm depth. Each soil section was then thoroughly mixed and half of the material from each section was incubated at 50˚C in separate 2.32 L sidearm flasks containing 0.1% headspace CH_4, to allow estimation of soil section CH_4 oxidation potential. Soil section CH_4 oxidation potential was calculated per section rather than per gram to allow comparison of CH_4 oxidation efficiency between equal volumes of soil at the different depths. This is necessary to account for differences in soil bulk density caused by the presence of pellets in the deeper soil (**Chapter 1.5**). Results of these experiments are shown in (**Table 3.8**).

The calculated soil CH_4 oxidation potential for these sections seemed very low when compared with those calculated for the 19.2.18 11B/11C soil core (**Tables 3.8** and **3.9**) especially considering that the values given for the 19.2.18 material are per gram soil, while for the 12D samples it is per 1,570 cm^3 soil with total weights of soil varying between 134-347 g.

This suggested that either the methanotrophs in the 12D soil were considerably less active than those in the 11B/11C soil core, the difference in assay set up (45 vs 50˚C incubation or 1.2 vs 0.1% headspace CH_4) has influenced the calculated oxidation potential or both.

Table 3.8 12D core section soil CH_4 oxidation potentials calculated from 50˚C incubations with 0.1% headspace CH_4, note that the volume of each section was 1570 cm^3.

Core section and depth	Soil CH_4 oxidation potential (nmoles h^{-1} $section^{-1}$)
Section 1 (0-20 cm)	5.86
Section 2 (20-40 cm)	9.53
Section 3 (40-60 cm)	14.08
Section 4 (60-80 cm)	8.74

To investigate this, a second soil core sample (0-90 cm depth) was taken from 12D on 26.3.19, although on this day (2.5 weeks after first core) the biofilter as a whole was found to be very cold (ambient temperature or below) apparently due to a fault in the gas supply automation stopping CH_4 from entering the biofilter. Again, the core was split into 4 sections: Section 1 (0-20cm), Section 2 (20-40cm), Section 3 (40-60cm), Section 4 (60-90cm). Each section was

homogenised by thorough mixing. The sections with depth ranges matching the previous core (sections 1 to 3) were then used to set up soil CH_4 oxidation potential assays with different starting % headspace CH_4 to see if this would affect the calculated oxidation potentials. For each section two assays were set up each consisting of a 120 ml serum vial containing 30 g of the appropriate soil section and initial headspace CH_4 of 1% (1.2 ml) or 0.1% (0.12 ml) (v/v). These were then incubated at 50˚C and soil CH_4 oxidation potential values calculated based on headspace CH_4 depletion over time. The results are shown in (**Table 3.9**).

Table 3.9 Calculated CH_4 oxidation potential for (26.3.19) soil core material from each section when incubated at 50˚C with either 1% or 0.1% headspace CH_4

Core section and depth	Initial headspace CH_4 (% v/v)	Soil CH_4 oxidation potential (nmoles h^{-1} g $soil^{-1}$)
Section 1 (0-20cm)	1	96
	0.1	7
Section 2 (20-40cm)	1	75
	0.1	5
Section 3 (40-60cm)	1	133
	0.1	10

It appeared that the headspace CH_4 concentration (%) has a major effect on calculated soil CH_4 oxidation potential with more than an order of magnitude increase in the calculated oxidation potential for the assays starting with 1% headspace CH_4 compared with the assays starting with 0.1% headspace CH_4. One possible explanation for this is that CH_4 diffusion into the methanotroph cells is increased at higher headspace CH_4 concentrations, another potential factor could be that the methanotrophs responsible for CH_4 oxidation in the biofilter may possess lower affinity methane monooxygenases.

After discovering this effect of increasing headspace CH_4 on estimated soil CH_4 oxidation potential, it was necessary to ensure that future assays would use a consistent and environmentally relevant % CH_4 in the incubation headspace, ideally around 4-5% to limit incubation headspace flammability (flammability range of CH_4 is 5.3-14%) (National Research Council Committee on Toxicology 1984). This would hopefully give soil CH_4 oxidation potential estimates that more accurately reflect CH_4 turnover within the biofilter and that are comparable to one another.

3.3.4 Retrieving soil cores for 16S rRNA amplicon and metagenome sequencing

With temperature probe measurements indicating the biofilter was often running at an elevated temperature (circa 50˚C) and the observation that the temperature dropped without a CH_4 supply, suggesting that this high temperature may be driven by CH_4 oxidation, it became clear that identifying the methanotroph and bacterial community present at such higher temperatures was of critical importance. Two soil cores were retrieved from positions within the biofilter that were operating at temperatures above 50˚C. Cores from sectors 2C and 11B were extracted on 17.5.19 and sections of core of depth 10-30cm and 30-50cm were separated and retained from both. Each of these sections was well mixed and a small amount of bulk soil was retained for each section to determine soil CH_4 oxidation potential and pH. Remaining soil from each section was then separately processed through a 4 mm grade sieve to remove stones and pieces of wood and then split into three aliquots (replicates, A,B and C) of soil for DNA extraction. DNA used for 16S rRNA gene amplicon and metagenome sequencing (**Chapter 4.4.2**). The soil core sections all had pH values in the 7.5-7.8 range (determined by pH probe (**Chapter 2.3.3**)) indicating very slightly alkaline soil. Assays to determine soil CH_4 oxidation potential were set up with 30 g bulk soil in 2.32 L sidearm flasks and 4% headspace CH_4, with one assay flask per soil core section. The assay flasks were then incubated at 50˚C, headspace CH_4 depletion was measured by GC and the soil CH_4 oxidation potential calculated for each soil core section. The results are shown in (**Figure 3.4**).

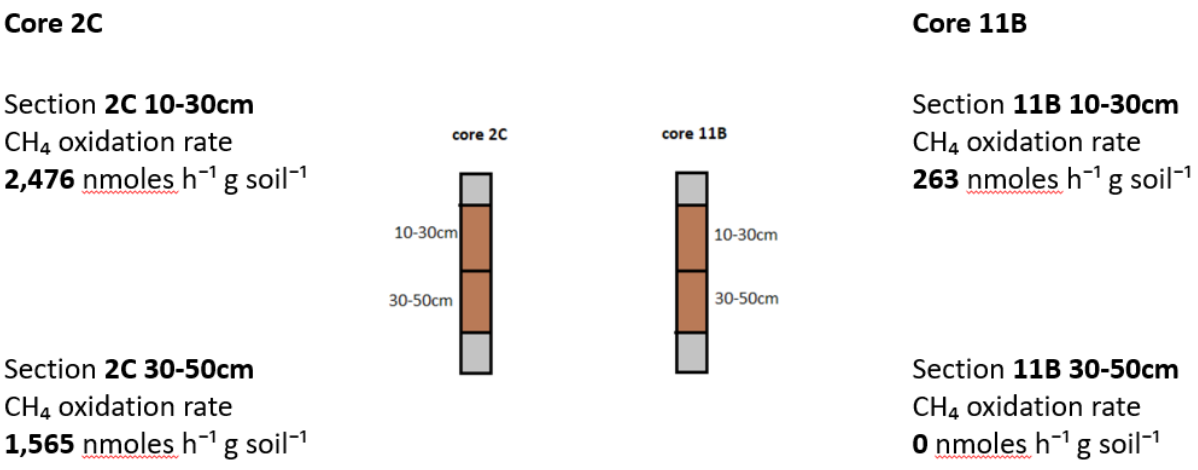

Figure 3.4 soil core 2C and 11B soil CH_4 oxidation potential calculated at 50˚C

The oxidation potentials calculated for the 2C core sections were in the low µmolar range in line with active CH_4 oxidising landfill cover soil microcosms (Knightly et al., 1995), while the 11B soil demonstrated very low to no CH_4 oxidation. It was interesting to see such a difference in calculated soil CH_4 oxidation potential for soil taken from cores that were both at an elevated temperature (>50˚C), especially considering our hypothesis that the elevated temperature was due to CH_4 oxidation. However, just by looking at the 2C and 11B soil material, a difference between the samples could be observed. The soil material from the 2C core looked darker and appeared to be more moist than the drier, lighter-coloured soil material from core 11B (**Figure 3.5**). This immediately raised the question: could the lack of CH_4 oxidation in soil core 11B be caused by the soil drying out? Perhaps exacerbated by the heat generated by methanotroph activity? An investigation into the effects of moisture on CH_4 oxidation was therefore carried out.

Figure 3.5 Soil from core 2C and 11B sections. Left to right: Core 2C 10-30 cm, core 2C 30-50 cm, core 11B 10-30 cm and core 11B 30-50 cm. The wetter darker soil from core 2C (left) is easily distinguishable from the drier lighter soil from core 11B (right).

3.3.5 Effects of biofilter soil moisture on CH_4 oxidation

Soil cores 2C and 11B were taken from locations within the biofilter with *in situ* temperatures above 50˚C. The calculated methane oxidation potentials for core 2C sections were considerably higher than those for core 11B. The soil samples themselves appeared noticeably

different, with the soil from core 11B being clearly drier than the soil from core 2C. This can be seen in (**Figure 3.5**). The effects of biofilter soil moisture on soil CH_4 oxidation potential were then explored.

3.3.5.1 Rewetting (dry?) inactive core 11B

Initially, the effect of rewetting the seemingly dry 11B soil samples with dH_2O on CH_4 oxidation was explored. The following experiment was set up: 10 g soil aliquots from each core section were transferred to 120 ml serum vials, two vials for each section (2C 10-30cm, 2C 30-50cm, 11B 10-30cm, 11B 30-50cm). For each section, one serum vial contained untreated soil (Control), the other soil with 2.5ml sterile dH_2O added (Rewetted). All serum vials were then sealed and gassed with 5% headspace CH_4. Disappearance of CH_4 from headspace was measured by GC. The soil CH_4 oxidation potentials calculated for the rewetted and control soils are shown in (**Figure 3.6**).

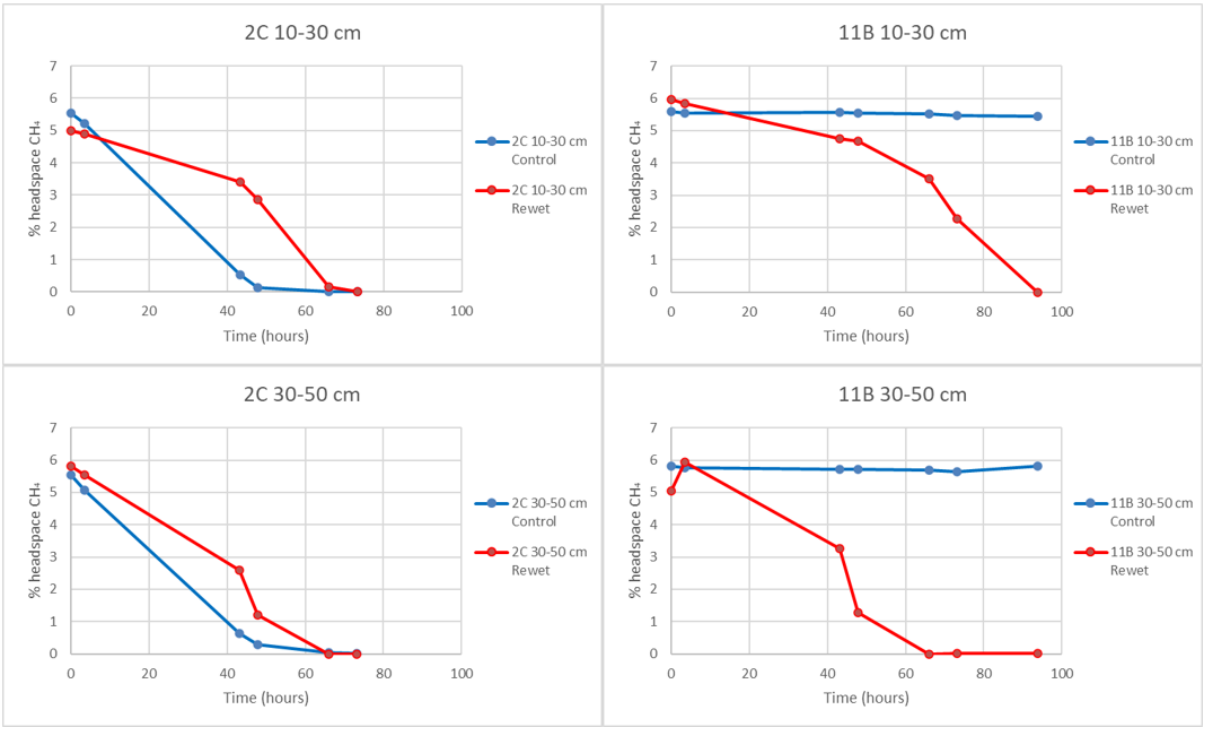

Figure 3.6 Headspace CH_4 depletion in rewetted and control 2C and 11B soil sections

Rewetting of the already active (CH_4 oxidising) soil samples 2C 10-30cm and 2C 30-50cm had little effect on CH_4 oxidation (control and rewetted soil performed similarly). However, a drastic increase in CH_4 soil oxidation was observed for the (formerly inactive) soil samples 11B 10-30cm and 11B 30-50cm after rewetting, with the methane oxidation potential approaching that calculated for the more active 2C core sections.

The recovery of CH_4 oxidation activity in the 11B soil upon adding water suggested that the soil had dried out to such a degree that the ability of the resident methanotrophs to oxidise CH_4 was compromised. This perceived reduction in fitness due to low water stress could be caused by an increase in macromolecular crowding effecting protein interaction and function, loss of membrane integrity or increased oxygen concentration leading to oxidative stress (Lee et al., 2016). Due to the poor aqueous solubility of CH_4 the reduction in soil water could also reduce the retention time of CH_4 within the biofilter, resulting in less opportunity for CH_4 oxidation (Manzanera, 2021).This had serious implications with regards to biofilter operation since drying out of the biofilter could adversely affect biofilter CH_4 oxidation efficiency. At this point it was clear that soil moisture content was an important parameter to measure in future sampling endeavours, alongside CH_4 oxidation potential and *in situ* temperature.

3.3.5.2 Soil moisture CH_4 oxidation profiles

To relate measured biofilter soil moisture to soil CH_4 oxidation efficiency, soil CH_4 oxidation profiles were measured across a range of soil moisture contents. This work was carried out in conjunction with Dr Hui-Juan Xu.

Biofilter soil material was retrieved for initial soil moisture measurement and investigation of effect on CH_4 oxidation on 4.9.19. Soil was manually collected with a spade from sector 16D. Soil material from a depth of 20-40cm and at 50-60 cm directly below this was excavated and retained. Additionally, another 20-40cm depth section was taken adjacent to the first 20-40cm soil sample from a position where the soil was noticeably drier (called “16D dry”). The soil was recovered from a region of the biofilter which was at approximately 38˚C. While not as high as some temperatures recorded in the biofilter (>60˚C), this was still well above ambient air temperature (18˚C). Once back in the lab, these soil samples were mixed separately, and their moisture content determined by oven drying. The following soil moisture contents were recorded:16D 20-40cm soil 11% moisture content, 16D 50-60 cm soil 7% moisture content and 16D Dry soil 7% moisture content.

Soil CH_4 oxidation potential assays were then set up for each of the 16D soil samples, with all soil used being first sieved through a 4mm sieve. For each sample, triplicate assays were set up for both field moist (either 7% "Dry", "50-60 cm" or 11% "20-40cm") and dH_2O wetted (to 25% moisture content) soil sample material, to observe if increasing soil moisture effected CH_4 oxidation potential, particularly in the case of the drier (7% moisture content) soils. Assays were set up in Suba-sealed 325 ml flasks with 5% CH_4 and incubated at 50˚C. 20g of field moist soil was used in each assay, with the moisture content being adjusted by addition of filter sterilised dH_2O for the wetted (rewet) assays. "No soil" control assays were also incubated with CH_4. The calculated soil CH_4 oxidation potentials are shown in (**Table 3.10**).

Table 3.10 Soil CH_4 oxidation potential for 16D soil samples at field moist and rewetted (25%) moisture content.

16D soil assay	CH_4 oxidation potential (nmoles h^{-1} g $soil^{-1}$)
Dry A	435
Dry B	551
Dry C	861
rewet Dry A	2530
rewet Dry B	2876
rewet Dry C	1680
20-40 cm A	3132
20-40 cm B	2800
20-40 cm C	2796
rewet 20-40 cm A	2823
rewet 20-40 cm B	1878
rewet 20-40 cm C	2664
50-60 cm A	869
50-60 cm B	538
50-60 cm C	3458
rewet 50-60 cm A	1635
rewet 50-60 cm B	1628
rewet 50-60 cm C	1427
Air + CH_4 Blank 1	22
dH_2O Air + CH_4 Blank 2	224

It was apparent that CH_4 oxidation rate was increased when soil moisture was raised from 7% to 25% (high rate calculated for 50-60 cm C possibly due to CH_4 leakage from flask). While 11% to 25% moisture content did not show such an increase, this experiment provided a useful initial indication that soil moisture content at 7% restricted methanotroph CH_4 oxidation.

Since the 16D 20-40 cm soil sample demonstrated a moderate amount of methanotroph activity, this soil sample was used to construct a soil moisture CH_4 oxidation profile. By adjusting the moisture content of 16D 20-40 cm soil samples to cover a broad range of values, the soil CH_4 oxidation potentials calculated for each after incubation with CH_4 should indicate the optimal moisture content for methanotroph CH_4 oxidation in the biofilter. Sieved (4mm) 16D 20-40cm soil was air-dried at room temp for three days and triplicate soil CH_4 oxidation potential assays were set up with the soil rewetted to a range of soil moisture content (5-35%). The equivalent of 20 g dry weight soil was used per assay in a 325 ml flask with 5% headspace CH_4, incubated at 50˚C. A (no soil) dH_2O only negative control was also included. Additionally, assays of air-dried soil rewetted to 12% soil moisture were included alongside assays of fridge stored and sieved ("Fridge") soil (which had a moisture content of 12% when checked on the day) to determine the effect of the air-drying and rewetting process on CH_4 oxidation potential. Depletion of headspace CH_4 was monitored and soil CH_4 oxidation potentials calculated; results shown in (**Table 3.11**).

Table 3.11 Soil CH_4 oxidation potential for 16D 20-40 cm soil samples air dried and rewetted to between 5-35% soil moisture content.

Assay (% soil moisture content)	CH_4 oxidation potential (nmoles h^{-1} g $soil^{-1}$)		CH_4 oxidation potential (nmoles h^{-1} g $soil^{-1}$)
5% A	108		
5% B	-47	**5% average**	30
5% C	30		
10% A	3389		
10% B	3266	**10% average**	3265
10% C	3139		
15% A	3356		
15% B	3640	**15% average**	3511
15% C	3538		
20% A	3317		
20% B	3159	**20% average**	3353
20% C	3583		
25% A	1867		
25% B	3295	**25% average**	2825
25% C	3315		
30% A	2055		
30% B	2185	**30% average**	2377
30% C	2893		
35% A	1690		
35% B	2217	**35% average**	2017
35% C	2145		
12% A	2979		
12% B	3221	**12% average**	3259
12% C	3579		
Fridge 12% A	2795		
Fridge 12% B	2689	**Fridge 12% average**	2829
Fridge 12% C	3005		
H_2O only	29	**H_2O only**	29

From these results it appears that the optimum soil moisture for CH_4 oxidation is between 10 and 20%. While CH_4 oxidation activity is still fairly high up to 35% moisture, there does seem to be a sharper drop-off in CH_4 oxidation between 10 and 5% moisture content. The fridge-stored-from-fresh soil CH_4 oxidation potential matched quite closely with that for the air-dried soil made up to equal moisture content (12%), indicating that there was not a significant effect on CH_4 oxidation potential from the air-drying and rewetting process. The detection of biofilter soil with a soil moisture content as low as 7% in the biofilter made the noticeable reduction in CH_4 oxidation between 10 and 5% of great interest, so a further soil moisture CH_4 oxidation profile experiment with greater resolution at soil moistures below 10% was undertaken.

Fresh biofilter soil material was collected for this second soil moisture CH_4 oxidation profile experiment on 13.11.19. Four positions were chosen on the biofilter (3C, 7A, 13C, 18B) and at each position soil samples were recovered from 10-30cm depth below the surface (a couple of kilograms for each). Temperature, CH_4, O_2 and CO_2 profiles were also taken with the combined temperature/gas probe at all four points that were sampled to confirm at least some *in situ* CH_4 removal (**Chapter 3.2.4**). The pH of these soils were then measured with a pH probe (**Chapter 2.3.3**) and found to be very close to one-another (pH 7.7-8.0).

The 3C, 7A, 13C and 18B 10-30 cm soil samples were then air-dried. It took considerably longer to air-dry the soil on this occasion as there was greater humidity than previously. It took over a week to reduce to suitable soil moisture content (<5%). Each soil was sieved after partial drying (they were too wet initially) using a 4mm grade sieve.

After 1.5 weeks, separate air-dried 10-30cm soil samples (3C, 7A, 13C and 18B) were mixed in a 1:1:1:1 ratio (oven dry weight). Resulting in "mixed air-dried soil".

19.5g (oven dry weight) aliquots of "mixed air-dried soil" were then transferred to 325ml conical flasks and rewet to set up a range of % soil moisture CH_4 oxidation potential assays (in duplicate): 2.4%, 5%, 6.25%, 7.5%, 8.75%, 10%, 12.5%, 15%, 17.5%, 20%, 27.2%, 35%, 40%, 45%. Duplicate aliquots (19.5g oven dry weight) of fridge stored soil (27.2% moisture) were also set up as a control to compare with the "mixed air-dried soil" aliquots rewet to 27.2% moisture, in order to assess activity loss due to the air-drying/rewetting process. "No soil" CH_4-only control flasks were also included as negative controls. Flasks were sealed as soon as filter-sterilised dH_2O was added (to rewet soil to correct moisture level). Flasks were then gassed with 5% CH_4 immediately before time 0 GC measurement of headspace CH_4 content. Flasks incubated at 50˚C and depletion of headspace CH_4 was tracked using the GC. Calculated soil CH_4 oxidation potentials shown in (**Table 3.12**). Average soil CH_4 oxidation potential is shown plotted against % soil moisture in (**Figure 3.7**).

Table 3.12 Soil CH_4 oxidation potentials calculated for "mixed air-dried soil" adjusted to a range of soil moisture %.

Assay (% soil moisture content)	CH_4 oxidation potential (nmoles h^{-1} g soil $^{-1}$)
2.4% A	236
2.4% B	242
2.4% Average	**239**
5% A	184
5% B	214
5% Average	**199**
6.25% A	149
6.25% B	294
6.25% Average	**222**
7.5% A	935
7.5% B	958
7.5% Average	**947**
8.75% A	771
8.75% B	1482
8.75% Average	**1127**
10% A	1918
10% B	1690
10% Average	**1804**
12.5% A	2744
12.5% B	2813
12.5% Average	**2779**
15% A	2716
15% B	2133
15% Average	**2425**
17.5% A	2631
17.5% B	3147
17.5% Average	**2889**
20% A	2958
20% B	2801
20% Average	**2880**
27.2% A	2235
27.2% B	1675
27.2% Average	**1955**
27.2% Fridge A	1824
27.2% Fridge B	1895
27.2% Fridge Average	**1860**
35% A	1156
35% B	1533
35% Average	**1344**
40% A	232
40% B	494
40% Average	**363**
45% A	221
45% B	294
45% Average	**257**
Control 1	-70
Control 2	-25
Control Average	**-48**

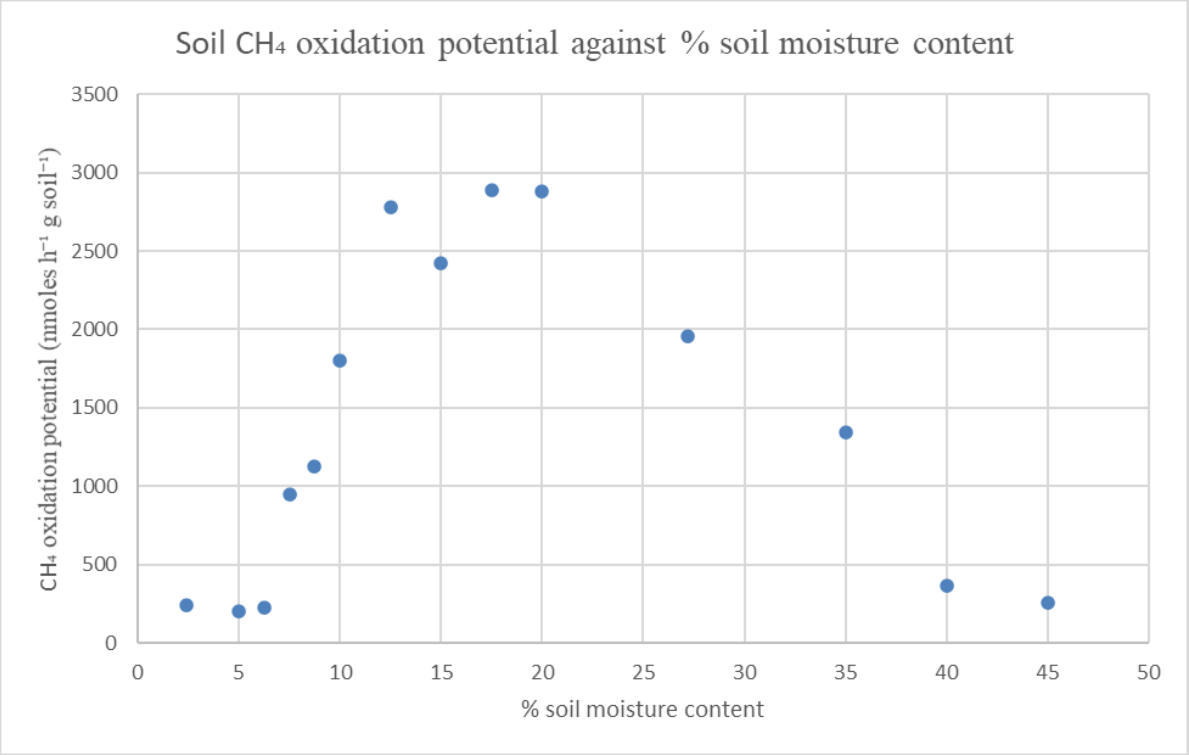

Figure 3.7 "Mixed air-dried soil" average soil CH_4 oxidation potential against % soil moisture.

The greater number of data points below 10% soil moisture content in this experiment better describe the drop in soil CH_4 oxidation potential at very low soil moisture content. At a soil moisture content of 7.5%, the CH_4 oxidation potential was roughly a third of that at the more optimal moisture contents of 17.5-20%. If the soil moisture content dropped to 6.25% that drop in CH_4 oxidation potential was down to one tenth. From these results it appeared that the drying out of biofilter soil poses a real threat to efficient biofilter CH_4 turnover.

The "Mixed air-dried soil was also used for another soil moisture CH_4 oxidation profile experiment the following month. Triplicate assays were set up for each % moisture investigated. Air-dried soil (20g aliquots) was placed in 325ml flasks and filtered dH_2O was added to each to give a range of triplicate assay flasks at different moisture levels. Each flask was quickly sealed with a Suba seal to prevent moisture loss and then gassed with 5% CH_4 immediately before the first GC measurement of headspace CH_4. Depletion of headspace CH_4 over time was used to calculate potential CH_4 oxidation rate of soil samples. Soil moisture content values used in this experiment as well as the calculated soil CH_4 oxidation potentials are shown in (**Table 3.13**). Average soil CH_4 oxidation potential is shown plotted against % soil moisture in (**Figure 3.8**).

Table 3.13 Soil CH_4 oxidation potentials calculated for second "mixed air-dried soil" soil moisture range CH_4 incubation experiment.

Assay (% soil moisture content)	CH_4 oxidation potential (nmoles h^{-1} g $soil^{-1}$)
6.25% A	570
6.25% B	660
6.25% C	625
6.25% Average	**618**
7.5% A	1339
7.5% B	915
7.5% C	1815
7.5% Average	**1356**
8.75% A	598
8.75% B	1879
8.75% C	1720
8.75% Average	**1399**
10% A	1241
10% B	2177
10% C	2095
10% Average	**1837**
12.5% A	1580
12.5% B	2311
12.5% C	2458
12.5% Average	**2116**
15% A	2365
15% B	2413
15% C	1315
15% Average	**2031**
17.5% A	2214
17.5% B	2250
17.5% C	1975
17.5% Average	**2146**
20% A	2483
20% B	2734
20% C	2159
20% Average	**2459**
27.7% A	1665
27.7% B	1734
27.7% C	1619
27.7% Average	**1673**
27.7% Fridge A	2697
27.7% Fridge B	2650
27.7% Fridge C	2547
27.7% Fridge Average	**2631**
35% A	797
35% B	1394
35% C	1349
35% Average	**1180**
Cont 1	**664**

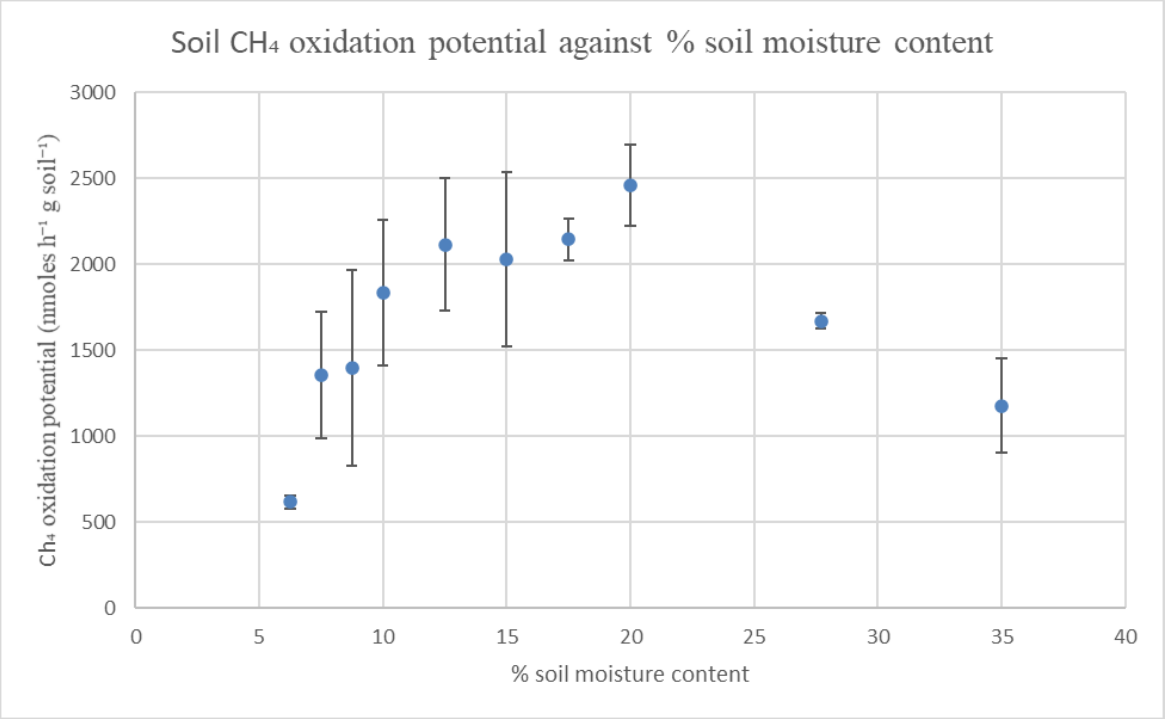

Figure 3.8 Second "mixed air-dried soil" soil moisture range CH_4 incubation experiment, average soil CH_4 oxidation potential against % soil moisture. Error bars show standard deviation.

This second attempt at rewetting experiment on "mixed air-dried soil" (3C, 7A, 13C and 18B 10-30 cm depth) had some issues. Including variability between replicates (see error bars in (**Figure 3.8**)) and a measurable rate for the negative control (no soil in flask, only CH_4), found to be caused by a slow leak in the Suba seal. This led to suspicion that some of the Suba seals may have been leaking during this experiment due to repeated headspace sampling with a syringe; not only did the control show a reduction of headspace CH_4, but the very dry soil treatments (6.25 and 7.5% moisture) consumed CH_4 at faster rate than in the previous experiment when the soil was fresher.

Overall, these soil moisture experiments resulted in a set of CH_4 oxidation profiles across a range of soil moistures. These demonstrated that the optimal soil moisture content for CH_4 oxidation in sieved biofilter soil lies somewhere in the range 12.5-20% with a broader range of 10-27.5% where CH_4 oxidation was at least 50% of maximum efficiency. Rewets also show a sharp drop-off in CH_4 oxidation potential at moisture contents below 10%, which is very relevant to biofilter function since soil moisture contents of 7% have been observed within the biofilter. The potential for the biofilter soil to dry out could be exacerbated by heat generation from the methanotrophs as they oxidise CH_4, which in turn could accelerate moisture

evaporation from the biofilter. In fact, when the biofilter was operating with high *in situ* temperatures, steam could be seen rising from the soil surface (**Figure 3.9**).

Figure 3.9 Photograph of the biofilter surface with soil corer in the foreground. Steam rising from the biofilter surface is visible.

If this is a system where methanotrophs raise the *in-situ* temperature through CH_4 oxidation to a point where the resulting elevated temperature leads to moisture loss from the biofilter soil, then this drop in soil moisture would result in a decline in CH_4 oxidation efficiency. This may

cause temperature fluctuations within the biofilter as the temperature drops due to reduced CH_4 oxidation. One potential solution to the biofilter soil drying out would be to install a simple sprinkler system that could be turned on to increase soil moisture within the biofilter, this would likely be particularly effective in improving biofilter performance during low rainfall periods.

3.3.6 Investigating the CH_4 oxidation potential of biofilter matrix clay pellets

Biofilter soil was sampled from sector 2C on 6.8.19 for further biofilter soil CH_4 oxidation potential calculations. Two soil sample depths were retrieved manually with a spade: 20-30cm (above liner, no pellets) and 30-40cm below liner, includes pellets). It was unusual for the pellet layer to be so close to the surface, elsewhere the top 50 cm of the biofilter is above the liner and does not contain pellets.

Initial investigation of 2C (6.8.19) soil CH_4 oxidation potential (carried out on day of sampling). Soil from each sample depth was mixed separately before 20g soil aliquots were transferred to 325 ml flasks and sealed with Suba seals. 20-30cm (pellets-) and 30-40cm (pellets+) soil sections tested at both 37 and 50˚C incubation temperatures. Duplicate flasks were set up for each depth and temperature treatment. Each flask was gassed with 5% CH_4 and depletion of headspace CH_4 monitored by GC. Average calculated soil CH_4 oxidation potentials are shown in (**Table 3.14**).

Table 3.14 Average soil CH_4 oxidation potentials for 2C soil sections taken on 6.8.19.

Soil samples	Average CH_4 oxidation rate (nmoles h^{-1} g $soil^{-1}$)
2C 20-30cm 37˚C	2443
2C 20-30cm 50˚C	3975
2C 30-40cm 37˚C	2185
2C 30-40cm 50˚C	2036

Soil moisture content for the two 2C soil samples was determined by oven drying. Field moist soil moisture contents were 21.75% for 2C 20-30 cm and 11.63% for 2C 30-40 cm. Determined moisture contents were close to optimal.

With the calculated soil CH_4 oxidation potentials indicating an active methanotroph community, the contribution of the pellets (present in the 30-40 cm soil) to CH_4 oxidation within the biofilter was investigated. With the expanded clay pellets containing a large internal surface area, it was important to determine if they were harbouring significant methanotroph populations, or if most of the methanotroph activity was located in a different fraction of the soil. Four soil CH_4 oxidation potential assays were set up in Suba sealed 325 ml conical flasks with 5% headspace CH_4, three of these assays contained 20 g of 2C 30-40 cm soil (replicates A, B and C), and one flask containing only 20 g of expanded clay pellets taken from the 2C 30-40 cm soil sample (no replicates due to limited amount of pellets in remaining sample) . The pellets were wiped to remove any methanotroph-containing soil on their outer surface. All four assays were then incubated at 50ºC and change in headspace CH_4 was measured and used to calculate soil (and pellet) CH_4 oxidation potential, results shown in (**Table 3.15**).

Table 3.15 Soil CH_4 oxidation potentials calculated for 20 g 2C 30-40 cm bulk soil aliquots and a 20 g expanded clay pellet only aliquot recovered from 2C 30-40 cm bulk soil.

Sample	Soil CH_4 oxidation potential (nmoles h^{-1} g $soil^{-1}$)
30-40 cm A	2486
30-40 cm B	2347
30-40 cm C	2601
Pellets only	372

Results show that the expanded clay pellets do not host a significant portion of the methanotroph community in the biofilter soil, as they had a calculated soil CH_4 oxidation potential of less than a sixth of that for the bulk soil. Even if they don't harbour a significant proportion of methanotrophs, the clay pellets may still serve a valuable function as a structural component of the biofilter matrix. A matrix solely composed of compost, coconut fibre and small woodchip is likely to suffer from compaction and poor gas diffusion.

3.3.7 Retrieving soil samples from a deeper, hotter region of the biofilter for DNA-SIP labelling of active methanotrophs

It was decided to retrieve a soil sample from the Strumpshaw biofilter to provide soil material for a second DNA-SIP labelling experiment, this time leveraging a greater understanding of the biofilter's operational characteristics to select an active (hot, 50ºC) region of the biofilter matrix where a good proportion of CH_4 oxidation is known to occur (50 cm depth) and to ensure that the soil's moisture content is at least within the active range (10-27.5%). This would allow isolation and study of the DNA belonging to methanotrophs active under conventional conditions (**Chapter 5.3**).

Prof. Colin Murrell retrieved a soil sample from 45-55cm below the surface of biofilter grid sector B19 using a spade on 26.6.20. A temperature of 50ºC was measured at the sampling point with a temperature probe. Once back in the lab this soil sample was first thoroughly mixed, before half the sample was processed through a 4mm sieve into "large sieved" and "small sieved" fractions and the other half retained as "bulk soil". The suitability of this soil sample for use in the DNA-SIP experiment to isolate active methanotroph DNA (**Chapter 5.3**) was then assessed. Soil CH_4 oxidation potential and moisture content were calculated for each of the bulk, sieved large and sieved small soil portions, to evaluate methanotroph activity and to ensure moisture content was within the active range of 10-27.5%.

Initial CH_4 oxidation potential was calculated for bulk soil, small sieved and large sieved soil fractions at incubation temperatures of 37 and 50 ºC. For both temperatures, duplicate assays for each soil type containing approximately 10 g of material were set up in sealed 120 ml serum vials, alongside a single empty vial (as negative control), all vials were then gassed with 5% headspace CH_4 and depletion of headspace CH_4 at the different incubation temperatures was tracked using on-line GC and estimates of soil CH_4 oxidation potential calculated. The results are shown in **Table 3.16**.

Table 3.16 Calculated soil CH_4 oxidation potentials at 37 and 50ºC for B19 bulk soil and soil fractions.

B19 soil fraction	CH_4 oxidation potential at 37˚C (µmoles hour^{-1} g soil^{-1})	CH_4 oxidation potential at 50˚C (µmoles hour^{-1} g soil^{-1})
small seived A	1.62	3.15
small sieved B	1.86	3.35
small sieved average	1.74	3.25
bulk A	1.29	2.71
bulk B	1.40	2.50
bulk average	1.35	2.61
large sieved A	0.71	1.20
large sieved B	0.67	1.37
large sieved average	0.69	1.29

As was expected, the CH_4 oxidation potentials were higher in the assay vials incubated at 50˚C (the *in-situ* temperature during sample retrieval) compared with those incubated at 37˚C. The highest CH_4 oxidation activity appeared to be in the small sieved fraction, therefore this fraction was chosen for DNA-SIP incubation and ^{13}C labelling. This higher observed activity is likely due to the large sieved soil containing small stones and pieces of wood which, compared to finer compost and coir pieces, provide a lower surface to volume ratio to accommodate methanotrophs.

Triplicate moisture assays were set up for each of the bulk, large sieved and small sieved soil portions. Each moisture assay consisted of a known weight of the respective soil in a pyrex beaker and moisture content was determined by oven drying (**Chapter 2.3.3**). The average moisture content calculated for each soil fraction is shown in **Table 3.17**.

Table 3.17 Calculated moisture content for B19 bulk soil and soil fractions.

Sample	Average moisture content (%)
B19 bulk soil	25.76
B19 small sieved	27.30
B19 large bits (crushed)	19.65

Measured moisture content for the different soil fractions were all within the required moisture range of 10-27.5%. In addition the pH of the bulk soil was measured using a pH probe (**Chapter 2.3.3**) and found to be 7.7, similar to the pH values returned for previous soil samples (**Chapter 3.3.4**).

3.4 Discussion

From the experiments carried out in this chapter a basic model of biofilter CH_4 oxidation has been elucidated. During typical operation, the biofilter establishes an active methane oxidising zone at a temperature of 50°C in the top 60cm of the biofilter, methanotrophs in this zone appear to be capable of oxidising >50% of CH_4 fed into the biofilter. Additionally, soil moisture content has a significant impact on biofilter CH_4 oxidation potential. The pH within the biofilter soil was fairly consistent when measured across three different sets of biofilter soil samples (**Chapter 3.3.4**, **3.3.5.2**, **3.3.7**) with all soil samples within the (slightly alkaline) pH 7.5-8.0 range, this is perhaps unsurprising as the biofilter soil has a sizeable compost component. Compost often has a pH between 7 and 8 and has been shown to improve the buffering capabilities of soils (Costello and Sullivan 2014; Latifah et al., 2014).

Although it appears that the clay pellets are not themselves hosting an abundance of active methanotrophs (**Table 3.15**), they may contribute to the structure of the biofilter and help prevent compaction of the finer soil and coconut coir components. Interestingly the majority of a biofilter studied by Gerbert et al. was composed of expanded clay pellets which had been crushed (Gerbert et al., 2003). It would make a great deal of sense to partially crush the clay pellets to expose their honeycomb structured centre, as this could potentially provide both a large surface area to accommodate methanotrophs and excellent channels to promote gas diffusion, unlike the smooth outer surface of uncrushed pellets. Perhaps future NCC biofilter designs should make use of crushed expanded clay pellets.

Designing shallower biofilters could potentially reduce future biofilter start-up costs by using less of the expensive expanded clay and coir components of the biofilter soil. As most CH_4 oxidation seemed to occur in the top layer (0-50 cm depth) of the biofilter. Possibly due to differences in the biofilter soil matrix at this depth (no pellets), or different physico-chemical

conditions nearer to the surface such as moisture content or a lower soil compaction allowing unrestricted gas flow.

While it is possible that a higher CH_4 oxidation rate might be obtainable by maintaining the biofilter at a lower temperature, the practicality of cooling a self-heating 75m^3 soil biofilter suggests this would be very inefficient for any gains that may (or may not) be achievable.

Another interesting observation was that loss of O_2:CH_4 supply to the biofilter due to system failure or suboptimal gas ratio, can result in a drop in biofilter temperature and soil CH_4 oxidation potential (when the supply resumes). Depending on the length of the shutdown, the system can take weeks to recover optimal performance. Gas balance automation has no doubt helped reduce interruptions to biofilter CH_4 oxidation, as loss of the optimal O_2:CH_4 feedgas ratio was often identified as the likely cause of low methanotroph activity and in-situ temperature during this project.

One of the clearest conclusions in this chapter is that biofilter soil moisture can have a significant effect on methane oxidation potential. Managing biofilter soil moisture content during particularly wet or dry weather would also improve biofilter CH_4 oxidation efficiency, by avoiding the dramatic drop in methanotroph CH_4 oxidation potential observed outside the optimal soil moisture range (10-27.5%). It may well be enough to simply turn on a basic sprinkler system for short periods during dry spells, or opening the biofilter leachate valve for greater drainage during prolonged wet weather.

Chapter 4: Initial molecular work on biofilter soil samples

4.1 Initial molecular work on biofilter soil samples

The Strumpshaw biofilter is a functioning bioreactor capable of removing methane from landfill gas mixed with oxygen, through the oxidation of methane to methanol by methanotrophs resident in the biofilter soil. However, at the start of this project, the methanotrophs present in the biofilter soil were mostly unknown, with the sole exception of *Methylococcus capsulatus* (Norfolk), which had been successfully isolated from the top 5 cm of biofilter soil by Elliot Brooks.

To gain insight into the methanotroph community present in the biofilter soil, a range of cultivation-independent molecular ecology techniques were employed. Initially, PCR amplification of the methanotroph functional gene markers *pmoA* and *mmoX*, encoding subunits of the particulate methane monooxygenase (pMMO) and soluble methane monooxygenase (sMMO) respectively (McDonald et al., 2008), was used to screen for the presence of methanotrophs in the biofilter soil. A methanotroph functional gene clone library and restriction fragment length polymorphism (RFLP) digest was then set up. This allowed sequencing and taxonomic assignment of methanotroph functional marker genes from individual members of the methanotroph community, as well as assessment of the viability of an RFLP approach to methanotroph community profiling. Following this, gene amplicon sequencing targeting the ubiquitous and phylogenetically conserved bacterial 16S rRNA gene (Tringe and Hugenholtz, 2008) was used to construct taxonomic profiles of the biofilter soil methanotroph and wider bacterial community. Finally, metagenome sequencing and analysis of biofilter soil DNA was carried out, to retrieve metagenome assembled genomes (MAGs) of biofilter soil methanotrophs that could prove difficult to isolate for direct study. Total RNA sequencing and transcriptome analyses were also planned to supplement metagenomic analysis in both this chapter and **Chapter 5**, unfortunately this was not possible within the timeframe of the project following the 2020 pandemic. This was unfortunate, as metagenome and transcriptome analysis complement one another very well: The transcriptome analysis can give an indication of what organisms might be doing in an environment by identifying actively transcribed genes; while the metagenome analysis allows reconstruction of the structure, organisation and complement of genes belonging to community members but cannot indicate

their activity. Similarly, planned qPCR experiments to quantify absolute abundance of methanotrophs in the soil samples used for the DNA-SIP incubations could not be carried out.

4.2 PCR amplification of pMMO and sMMO gene fragments from biofilter soil DNA

A preliminary experiment was carried out to detect methanotroph pMMO and sMMO functional gene markers (*pmoA* and *mmoX*) in biofilter soil DNA. This would serve to confirm the presence of methanotrophic bacteria in the biofilter soil.

A biofilter soil core was retrieved on 14.11.17 and divided into four 10 cm sections over a 0-40 cm depth range (**Chapter 3.3.1**). DNA was then extracted from each soil section and used as a template for *pmoA* and nested *mmoX* PCR amplification. For *pmoA* amplification, the PCR modifications were: [50 µl], [A189F and A682R primers], [16S_72]. For nested *mmoX* amplification the PCR modifications were: Nested [50 µl], [A166F and B1401R then A206F and 886R primers], [16S_72]. (**Chapter 2.9.1** and **2.10.2**) The resulting PCR products were then run on agarose gels alongside positive control PCR reactions which used genomic DNA of an sMMO- (*Methylocella silvestris*) or pMMO-containing (*M. trichosporium* OB3b) methanotroph as a template. (**Chapter 2.10.3**) The presence of a PCR product of the correct size (719 bp for *mmoX* and 525 bp for *pmoA*) in both the biofilter DNA and positive control PCR products, was used to indicate successful amplification of sMMO or pMMO gene fragments from the biofilter soil DNA. This served as both an initial confirmation of the presence of methanotrophs in the biofilter as well as to validate the suitability of a PCR amplification approach in exploring methanotroph diversity. The resulting agarose gels run with either the *mmoX* or *pmoA* PCR product are shown in **Figures 4.1** and **4.2**.

pmoA and *mmoX* DNA sequences were successfully amplified from all four 10 cm depth increments of biofilter soil from the 0-40 cm depth range of this soil core. This both reveals the presence of potential methanotrophs containing *pmoA* and/or *mmoX* within the biofilter soil, and validates the use of PCR amplification with methanotroph specific PCR primers for detection and analysis of the biofilter methanotroph community.

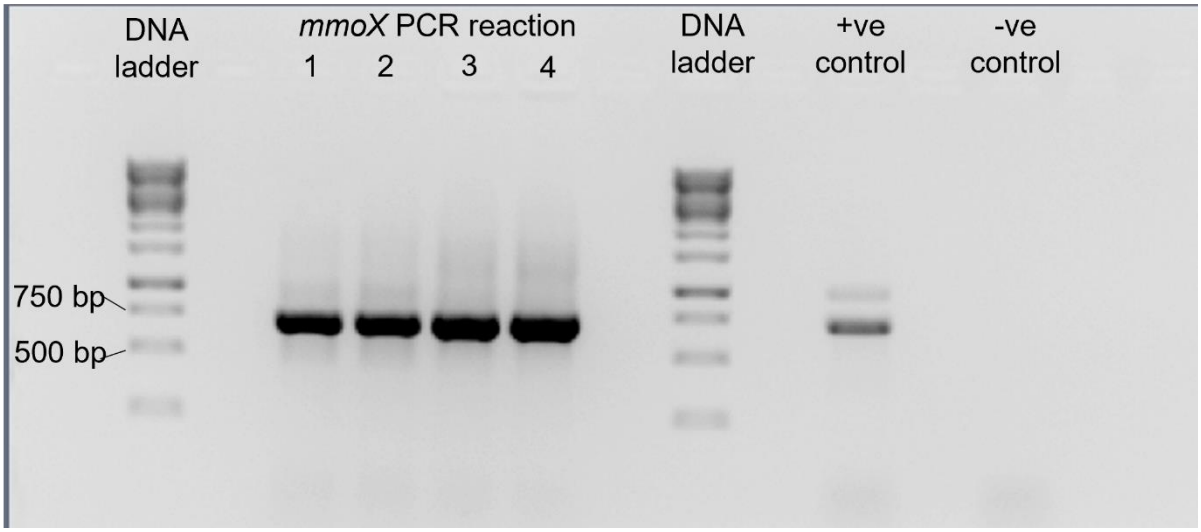

Figure 4.1 Nested *mmoX* PCR products, generated from template DNA extracted from 14.11.17 soil core. *mmoX* PCR reactions 1-4 use DNA from soil sections of increasing depth as template: 0-10 cm (1), 10-20 cm (2), 20-30 cm (3), 30-40 cm (4). *Methylocella silvestris* genomic DNA was used as the PCR template for the positive control.

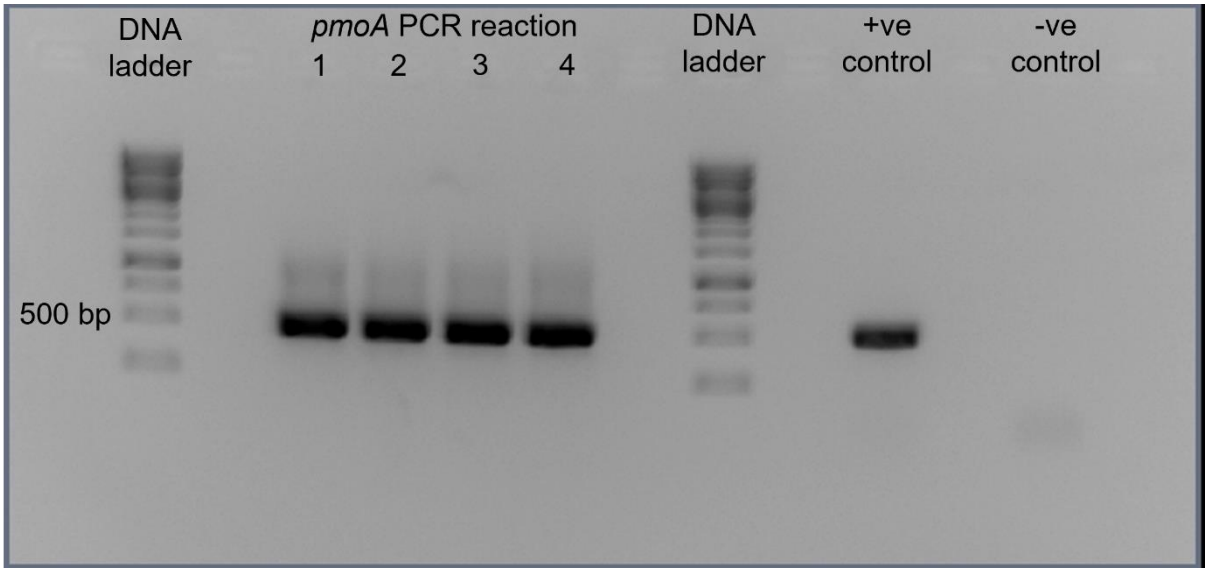

Figure 4.2 *pmoA* PCR products, generated from template DNA extracted from 14.11.17 soil core. *pmoA* PCR reactions 1-4 use DNA from soil sections of increasing depth as template: 0-10 cm (1), 10-20 cm (2), 20-30 cm (3), 30-40 cm (4). *Methylosinus trichosporium* (OB3b) genomic DNA was used as the PCR template for the positive control.

4.3 Biofilter soil DNA *pmoCA* clone library and RFLP analysis

Particulate methane monooxygenase is nearly ubiquitous across known methanotrophs and is therefore a particularly useful methanotroph functional gene marker (Mcdonald et al., 2008). A clone library of pMMO gene PCR products was generated from biofilter soil DNA extracts to explore methanotroph diversity. The recently developed *pmoCA* primer set (pmoC374 and pmoA344, 850bp product) was selected for its ability to target a wider range of methanotrophs in different environments than other pMMO gene primer sets (Ghashgavi et al., 2017). While still biased in favour of alpha- and gammaproteobacterial methanotrophs, these primers do have a limited capability to detect methanotrophs from the *Verucomicrobia* and NC10 phyla. This primer set targets a region spanning part of the *pmoA* and adjacent *pmoC* (5' of *pmoA*) (Ghashgavi et al., 2017).

DNA was extracted from three different depths (0-10cm, 10-20cm and 20-30cm) of the biofilter soil core retrieved on 14.11.17 (**Chapter 3.3.1**) and used to generate separate *pmoCA* clone libraries. Colony PCR was then carried out on 30 colonies from each of the three different depth clone libraries to amplify the *pmoCA* insert and flanking regions. These colony PCR products were then subjected to a restriction digest with a 6-base (*Eco*RI) and a 4-base (*Msp*I) recognition site restriction enzyme, to remove flanking regions and cut the *pmoCA* insert into restriction fragments based on its sequence (**Chapter 2.10.4**). The resulting digest banding patterns were then visualized on gels as shown in (**Figure 4.3**).

A subset of these PCR products was selected and undigested product was sent for Sanger sequencing (**Chapter 2.10.4**) to provide both a taxonomic identity for the organism of origin and to assess the suitability of the chosen restriction enzymes for use in community RFLP analysis. A total of 16 sequences were selected, including a mix of sequences with unique banding patterns as well as pairs of sequences with indistinguishable banding patterns, (**Figure 4.3**). The three pairs of PCR products that were selected for their similar RFLP banding patterns (B8 and D8, G4 and H4, B9 and D9), were checked to determine their nucleotide sequence similarity. For each pair, the sequences were trimmed down to the higher quality sequenced bases (positions 20-500) and then blasted against each other using the NCBI Blastn program (NCBI). The % average nucleotide identity for each pair was very high (98.75-99.58% ANI), which suggests that *pmoCA* RFLP fingerprinting with *Msp*I and *Eco*RI could be a viable strategy.

Maximum likelihood trees were then constructed to infer the phylogeny of the sequenced PCR product, by aligning these sequences with reference sequences taken from methanotrophs of known taxonomy. The *pmoCA* PCR product nucleotide sequences were trimmed down to their *pmoA* component (*pmoA*1-*pmoA*344) to remove the flanking vector sequence at the start of the reads as well as the intergenic region and following lower quality bases from the rear portion of the reads. Trimmed nucleotide and nucleotide-derived amino acid sequences were then aligned with a range of reference *pmoA* sequences from different methanotrophs, for both the nucleotide and amino acid alignment. An *amoA* sequence from *Nitrosomonas europaea* was included as an outgroup. Appropriate evolutionary models for the two alignments were then identified and a maximum likelihood phylogenetic tree was constructed for each alignment (**Figures 4.4** and **4.5**). The phylogenetic trees were then assessed by bootstrap test with 1000 replicates. For methods see (**Chapter 2.12.2**). The bootstrap test determines how frequently the same clades in a phylogenetic tree are recovered when the tree is reconstructed from a resampling of the sequence alignment. For each resample different positions are randomly selected from the sequence alignment up to the total number of positions in the full-length alignment: due to the random selection, each position may feature more than once or not at all, altering its impact on the reconstructed tree. The number of tree reconstructions used is referred to as the number of bootstrap replicates. The resulting bootstrap value for each tree branch is the proportion (%) of resampled trees in which these branches are also observed. The level of branch consistency across resampled trees can give an indication of the strength of the inferred phylogenetic relationships (Russo and Selvatti, 2018).

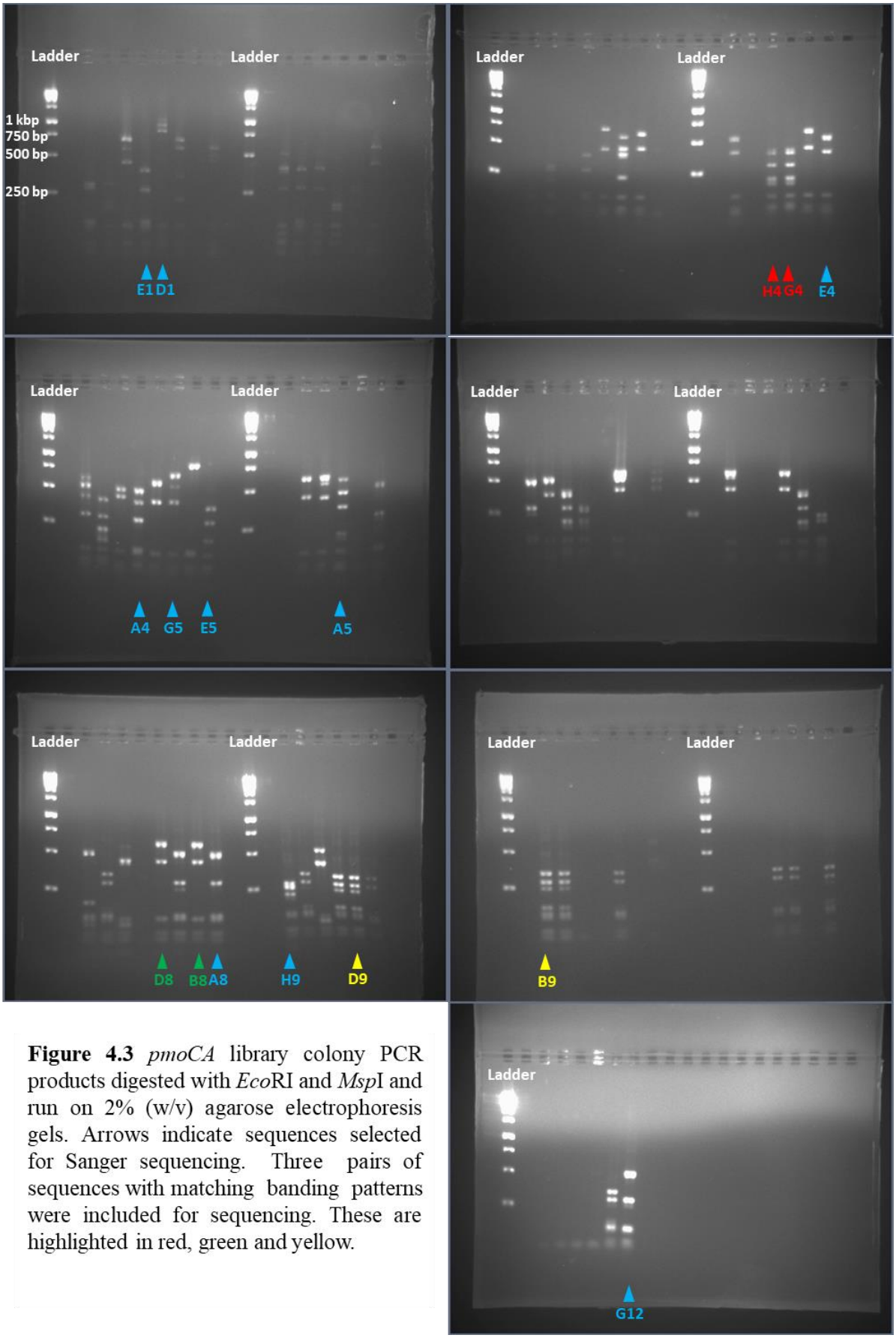

Figure 4.3 *pmoCA* library colony PCR products digested with *Eco*RI and *Msp*I and run on 2% (w/v) agarose electrophoresis gels. Arrows indicate sequences selected for Sanger sequencing. Three pairs of sequences with matching banding patterns were included for sequencing. These are highlighted in red, green and yellow.

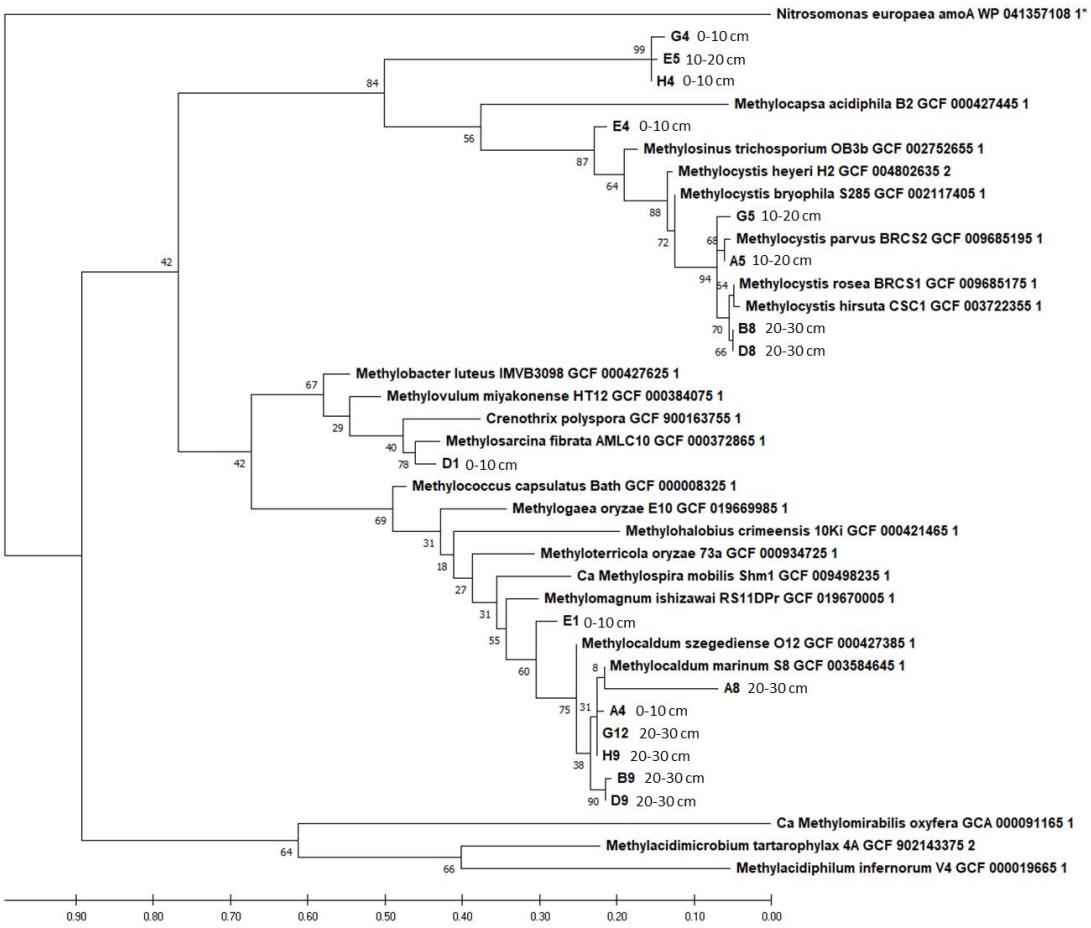

Figure 4.4 Maximum likelihood nucleotide-derived amino acid tree featuring translated *pmoA* region of *pmoCA* PCR products alongside *pmoA* sequences from known methanotrophs rooted against the outgroup ammonia monooxygenase subunit A (*amoA*) from *Nitrosomonas europaea*. Bootstrap values shown at each node.

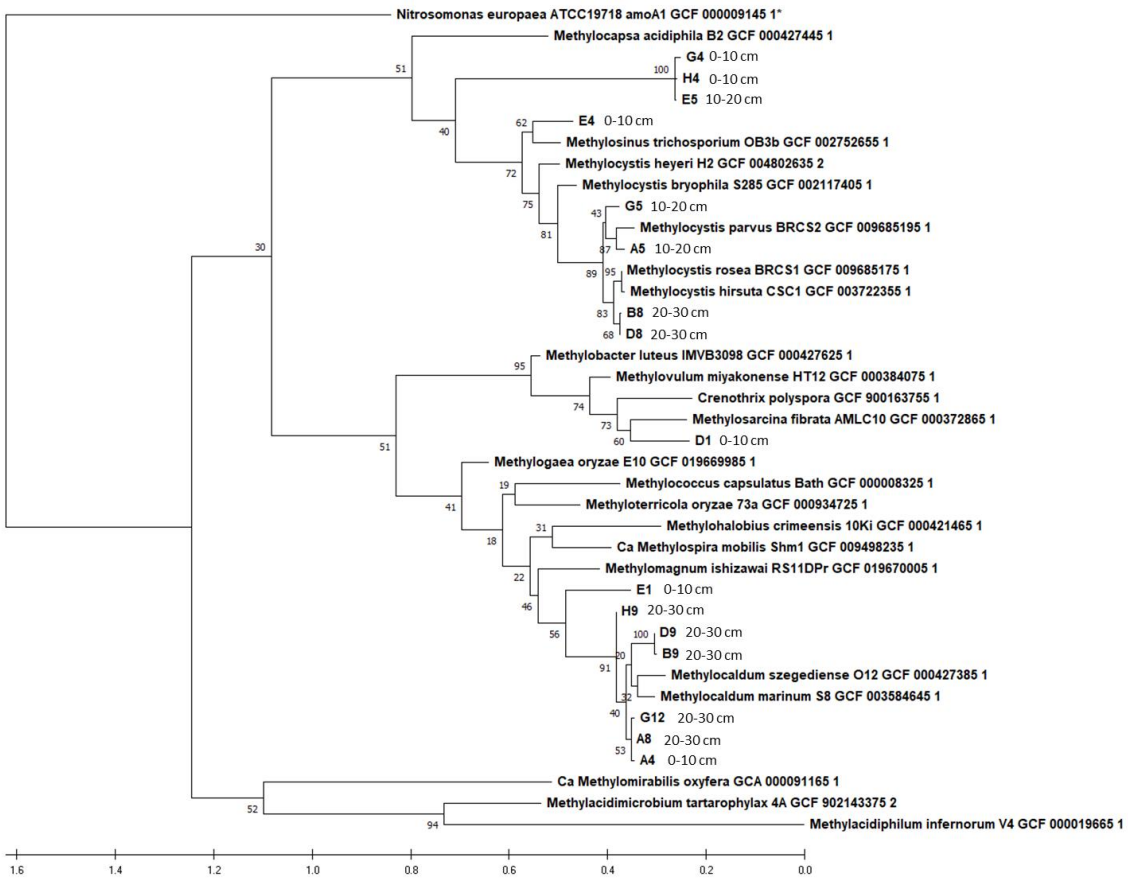

Figure 4.5 Maximum likelihood nucleotide tree featuring the *pmoA* region of *pmoCA* PCR products alongside *pmoA* sequences from known methanotrophs rooted against the outgroup ammonia monooxygenase subunit A (*amoA*) from *Nitrosomonas europaea*. Bootstrap values shown at each node.

When interpreting these trees, it is important to take into account the relatively short length of the truncated *pmoA* sequences used for the nucleotide (344 bp) and nucleotide derived amino acid (112 aa) alignments. This inherently makes placement within the tree less robust, and this is reflected in the low bootstrap values present in parts of these trees. However, these trees can still provide a good initial indication of the relationship between the methanotrophs these sequences originate from and the wider methanotroph guild.

A5, B8, D8 and G5 cluster within the *Methylocystis pmoA* reference sequences, with these positions supported by key bootstrap values in the 70s, 80s and 90s. Blasting the amino acid sequence (Blastp) of each against the NCBI database returns top hits from the *pmoA* sequence of *Methylocystis* species with % amino acid identities in the range of 97.44 to 99.15%. Several sequences (A4, A8, B9, D9, H9 and G12) cluster around or within the *Methylocaldum marinum* and *Methylocaldum szegediense* reference sequences in the nucleotide and amino acid trees. Blasting the amino acid sequence of each found closest hits amongst *Methylocaldum* species with a similarity of 96.43 to 100% amino acid identity. For both alignments, the D1 *pmoA* sequence was placed close to the *Methylosarcina fibrata* reference sequence in the resulting tree. This was interesting as one of the first methanotroph isolates retrieved from the biofilter was a *Methylosarcina fibrata*-like species (subsequently lost due to a glassware/detergent issue), enriched and isolated in a similar manner to the *Methylocaldum* isolate (**Chapter 6.2**) but at a lower incubation temperature (25ºC). However, a Blastp search against the NCBI database suggests this sequence could be derived from a *Methylobacter* (96.43% amino acid identity) rather than a *Methylosarcina* (94.64%) species. The E4 *PmoA* sequence was placed near the *Methylosinus trichosporium* OB3b reference, which is supported by the NCBI Blastp top hit of a *Methylosinus* species (96.58% amino acid identity).

The taxonomic identities of the remaining sequences E1, E5, G4 and H4 are less clear. E1 is closest to *Methylomagnum* and *Methylocaldum pmoA* reference sequences in the two trees. When the nucleotide-derived *pmoA* amino acid sequence of E1 was used as a query in a Blastp search, the closest matches from known species in the NCBI database were from *Methylomagnum ishizawai* and *Methylocaldum szegediense* with 91.96 and 92.86% aa identity respectively. The E5, G4 and H4 sequences cluster together by themselves in both trees. Blastp searches of each did not return any high similarity sequences of known taxonomy. The closest hit with assigned taxonomy in each case was *Methylocystis*, but the amino acid identity was limited to between 81.08 to 82.88%.

Methylocystis and *Methylosinus* are alphaproteobacterial methanotroph genera. Members of the *Methylocystis* include both obligate and facultative mesophilic methanotrophs capable of growth at 4-40°C. While members of the genus *Methylosinus* grow at 20-37ºC (Belova, 2013; Bowman et al., 1993; Tikhonova, 2021).

Methylocaldum, *Methylosarcina*, *Methylobacter* and *Methylomagnum* are gammaproteobacterial methanotrophs. *Methylocaldum* is a genus of thermotolerant or thermophilic methanotrophs with members capable of growth at over 60°C (Takeuchi 2014b). *Methylosarcina* and *Methylomagnum* are mesophilic methanotrophs with growth optima in the range of 22-37ºC and 15-37ºC respectively (Frindte et al., 2017; Wise et al., 2001). The genus *Methylobacter* contains both mesophilic methanotrophs with optimal growth around 20-37ºC (Bowman et al., 1993) as well as psychrophilic methanotrophs (Omel'chenko, 1996).

Methylocaldum, *Methylocystis*, *Methylobacter*, *Methylosinus*, *Methylosarcina* have all been found to be abundant methanotrophs in different landfill cover systems, indeed *Methylosarcina fibrata* was originally isolated from a landfill cover soil (Gebert et al., 2009; Wise et al., 2001; Zhang et al., 2014).

While this was only a small non-representative sample of sequenced *pmoCA* PCR products (16 sequences), several appeared highly similar to *Methylocystis* and *Methylocaldum* sequences. This experiment provided an initial indication that these could be abundant methanotroph genera in the biofilter. The presence of pMMO sequences from a genus containing thermotolerant and thermophilic methanotrophs (*Methylocaldum*), alongside Elliot Brooks' isolation of a thermotolerent *Methylococcus* from the top 5cm of the biofilter (**Chapter 6**) matched well with the high temperatures sometimes recorded at depth within the biofilter (**Chapter 3.2**). This supported the idea that the biofilter may often oxidise CH_4 at elevated temperatures and informed the decision to include hotter 45ºC incubations in initial DNA-SIP experiments (**Chapter 5**).

One limitation of using a PCR approach with primers targeting the *pmoC* and *pmoA* genes to explore the biofilter methanotroph community, is that it will not detect those methanotrophs containing only the soluble methane monooxygenase. Methanotrophs belonging to the *Methylocella* (Chen et al., 2010), *Methyloferula* (Dedysh et al., 2015), or *Methyloceanibacter* (Vekeman et al., 2016) do not contain any particulate methane monooxygenase genes for these primers to amplify. To address this potential bias, the ubiquitous bacterial 16S rRNA gene was targeted as a taxonomic marker for biofilter methanotroph community analysis. Furthermore,

with the reduction in cost of amplicon sequencing in recent years, 16S rRNA gene amplicon sequencing was selected over RFLP fingerprinting as it would facilitate the taxonomic analysis of a larger sample of the biofilter community. While the 16S rRNA gene is a good taxonomic marker for identifying potential methanotrophs belonging to known methanotroph genera. It offers no direct detection of MMO gene presence (Dumont, 2014; McDonald et al., 2008). One important consequence of this is an inherent inability to identify novel methanotrophs belonging to taxonomic groups with no known methanotrophic members. This is highlighted by the discovery of an sMMO containing *Methyloceanibacter* isolate, a genus not previously thought to contain methanotrophic strains, by Vekeman et al. (Vekeman et al., 2016). Their speculation that sMMO genes may be relatively amenable to horizontal gene transfer, raises the possibility that sMMO might be present in individual strains across multiple supposedly non-methanotrophic genera; and these methanotrophs would be undetectable by 16S rRNA gene amplicon analysis (Vekeman et al., 2016). One way to mitigate this is by complementing 16S rRNA analysis with metagenome analysis to allow reconstruction and identification of the genomes belonging to members of novel methanotrophic clades. In this approach, 16S rRNA analysis allows profiling of known methanotrophic genera, while metagenomics can identify unknown novel *smmo/pmmo* containing methanotrophs with more divergent phylogeny.

4.4 Soil DNA extract 16S rRNA gene amplicon sequencing

Variable regions within the bacterial 16S rRNA gene sequence are often used to provide taxonomic resolution for bacteria in environmental microbial communities. This is due to the evolutionarily conserved and ubiquitous nature of the 16S rRNA gene in bacteria, which is required for prokaryotic protein synthesis (Tringe and Hugenholtz, 2008). NGS amplicon sequencing couples PCR amplification of a target DNA sequence with high throughput sequencing. This allows the capture of all but the rarest sequences from a mixed community of different organisms (Sanschagrin and Yergeau, 2014). 16S rRNA amplicon sequencing was selected as an efficient method of generating a taxonomic snapshot of the bacterial community in the biofilter soil. The hypervariable 16S rRNA gene V3-V4 region was selected as the target for PCR amplification as it demonstrates good coverage across the bacterial domain (Klindworth et al 2013).

4.4.1 16S rRNA gene amplicon depth profile below the centre of the biofilter surface

A 16S rRNA amplicon sequencing experiment was set up to generate a depth profile of the resident microbial community below the centre of the biofilter surface. A 60cm deep soil core was taken from the midpoint of the boundary between sectors 11B and 11C on the surface of the biofilter on the 19.2.18 (11B/11C boundary core). This soil core was then split into six equal 10cm segments from successive depths below the biofilter surface (0-10cm, 10-20cm, 20-30cm, 30-40cm, 40-50cm and 50-60cm depth from surface) (**Chapter 3.3.2**). Note that soil from the topmost section of this soil core (0-10cm depth from surface) was also used concurrently in a DNA-SIP labelling experiment (**Chapter 5.2**).

DNA was extracted from each depth and used as a template for 16S rRNA V3-V4 PCR as described in **Chapter 2.10.2**, with PCR modifications: [50 µl], [341F and 785R primers], [16S_72]. The resulting PCR products were then cleaned and sent for sequencing by the Paul Wilmes group in Luxembourg. The resulting 16S rRNA amplicon sequences were then analysed using DADA2 as described in **Chapter 2.12.3**.

The most abundant bacteria identified at the genus level (≥2% relative abundance) are shown for each individual amplicon in **Figure 4.6**. This figure also shows similarly abundant groups of ASVs of unknown genera which could be grouped at a Average Nucleotide Identity (ANI) of 95% or above, with each group representing a putative unknown genus (Schloss and Handelsman, 2005). These putative genera are displayed as "<Lowest identified taxonomic rank> genus".

Methylocaldum, *Crenothrix* and *Methylobacter* are the only methanotrophic genera present at a relative abundance of 2% or higher. As discussed previously, *Methylocaldum* are thermotolerant or thermophilic methanotrophs, while most *Methylobacter* species are mesophilic with a few psychrophilic members. *Crenothrix* have been identified as potentially facultative methanotrophs containing a phylogenetically distinct *pmoA* sequence (Stoecker, 2006). A *Crenothrix* species has yet to be isolated in pure culture but they have been found in a number of different environments including agricultural soils, freshwater lakes and microbial mats within a goldmine (Dörr et al., 2010; Drewniak et al., 2012; Oswald et al., 2017). In addition the methylotrophic genera *Methylotenera* was detected at over 2% relative abundance.

16S rRNA gene sequences were then searched for all known methanotrophic genera present and those found are displayed along with their relative abundance in **Figure 4.7**.

Across all depths the proportion of total bacteria assigned to methanotrophic genera ranges from approximately 5 to 12%. Based on this 16S rRNA gene analysis, the most abundant methanotroph at each depth is either *Methylocaldum* or *Methylobacter*. *Methylocaldum* is the most abundant methanotroph from the biofilter surface down to a depth of 20cm. From 20 to 30cm *Methylocaldum* is only slightly more abundant than *Methylobacter*. Further down from 30 to 50cm, *Methylobacter* is the more plentiful and at the lowest depth *Methylocaldum* is once again the most abundant methanotroph. There is also a noticeable contribution from *Crenothrix* in the methanotroph community at the shallower depth range of 0-20cm. Of the other methanotrophs, *Methylocella* was only detected in the shallowest soil section (0-10cm) at a relative abundance of 0.7%, alongside *Methylomicrobium* and *Methylosarcina* at less than 0.2% each and *Methylomagnum* which was identified at less than 0.1% relative abundance in the 30-40cm depth amplicon.

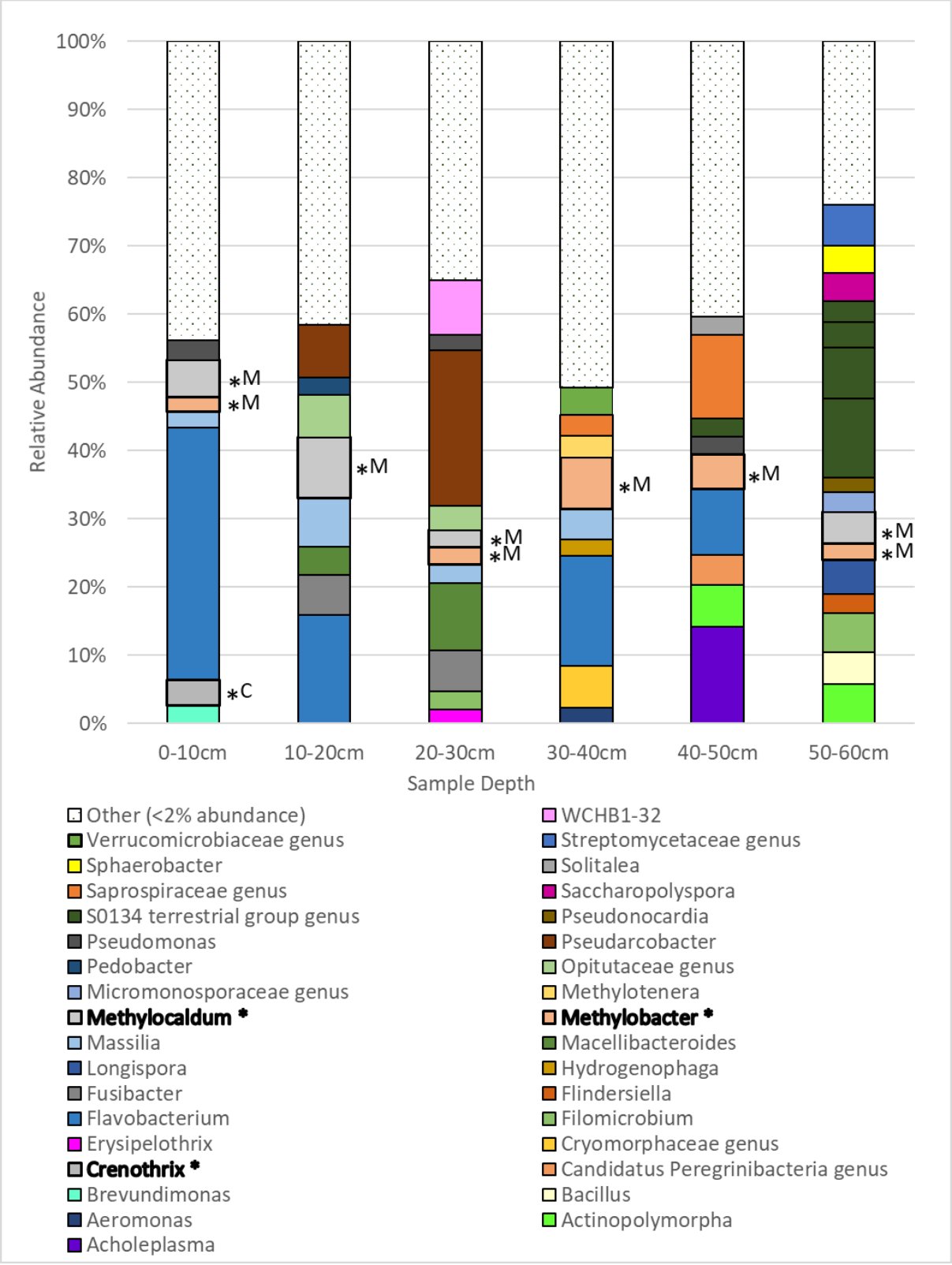

Figure 4.6 All bacteria identified at the genus level with 16S rRNA gene relative abundance above 2% across the depth profile amplicons from the 11B/11C boundary soil core. Also shown are similarly abundant groups of ASVs of unknown genera which could be grouped at a sequence similarity of 95% or above with each group representing a putative unknown genus (listed as "<Lowest identified taxonomic rank> genus"). Known methanotrophic genera are highlighted (*).

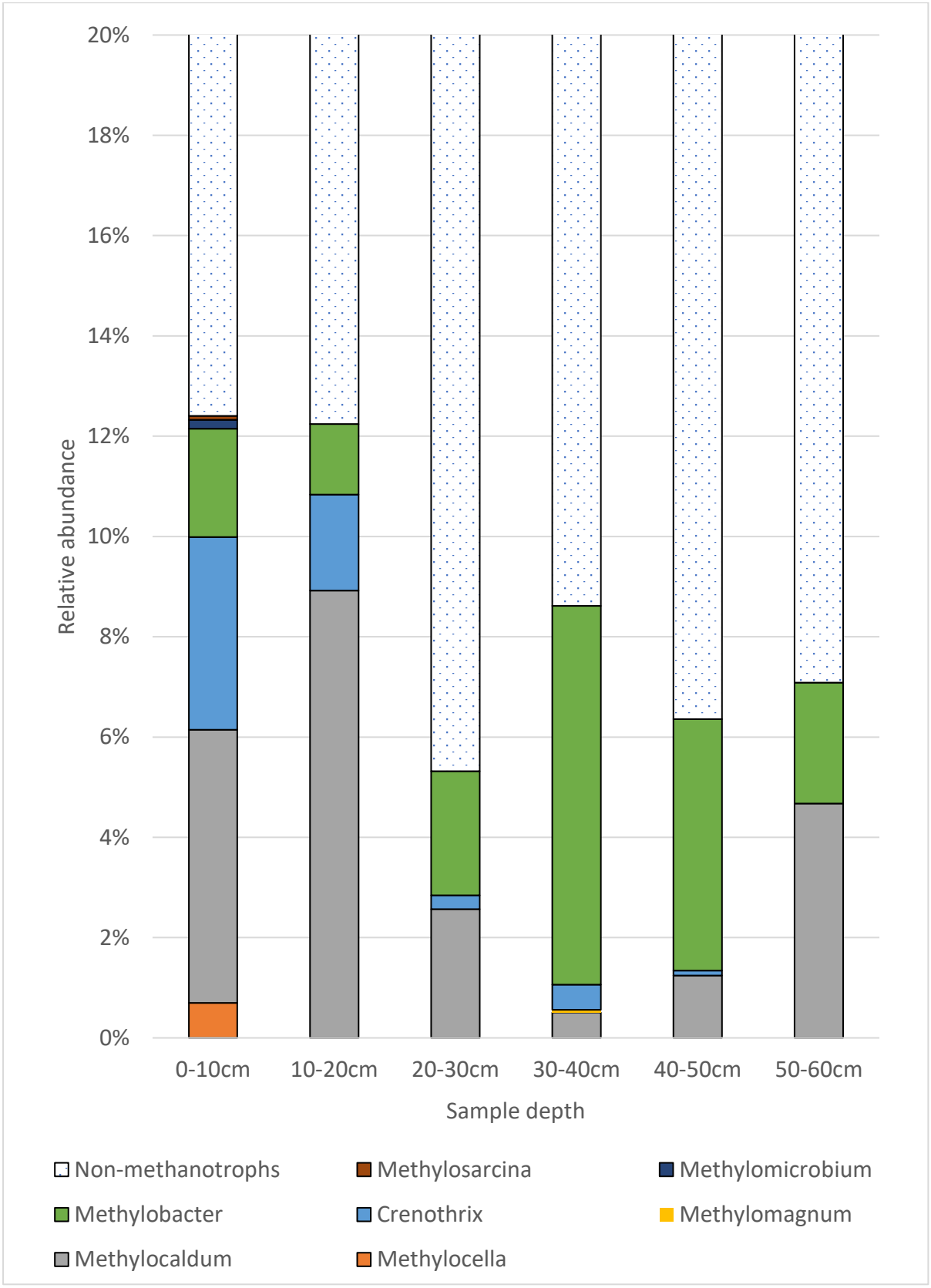

Figure 4.7 16S rRNA gene relative abundance (%) for all known methanotrophic genera identified in the depth profile 16S rRNA amplicons from the 11B/11C boundary soil core.

In addition to *Crenothrix*, *Methylocella* and *Methylomicrobium* are methanotroph genera that weren't assigned to any of the sequences from the *pmoCA* library. The alphaproteobacterial genus *Methylocella* contains mesophilic methanotrophs that grow at temperatures between 4 and 30ºC (Dedysh, 2004). While *Methylomicrobium* consists of mainly mesophilic gammaproteobacterial methanotrophs with growth temperatures over the range 4-37ºC (Orata et al., 2018), both *Methylocella* and *Methylomicrobium* have been found in landfill cover soils (Chen et al., 2007; Su et al., 2014).

The higher relative abundance of potentially thermophilic *Methylocaldum* in the top two sections of soil (0-10 and 10-20 cm depth) could explain the greater increase in estimated soil CH_4 oxidation potential between the first and second assay runs when incubating these soils at higher temperatures (**Chapter 3 Figures 3.8** and **3.9**). As the vials and resident soil had their headspace re-equilibrated with air and then re-gassed with CH_4 for the second CH_4 oxidation potential assays, each soil sample had effectively been pre-incubated with CH_4 at the given incubation temperature. The greater increase in soil CH_4 oxidation potential at the higher temperatures (37, 45ºC) on subsequent incubations could just be an effect of sampling and temporarily storing the soil at a (potentially lower) ambient temperatures while the assays were set up. Alternatively, it might indicate that the biofilter soil from these depths was at a lower temperature *in situ* and the preincubation was necessary to stimulate activity in the thermophilic methanotrophs.

In contrast, the greater relative abundance of *Methylobacter* in the lower depths (20-50 cm depth range) could be due to this soil having spent an extended time at a lower temperature that favoured the more mesophilic *Methylobacter*. Another explanation could be that the CH_4: O_2 balance of the inflow gas had shifted (sampling pre-gas balance automation), resulting in low O_2 content in the landfill gas at these depths. The well-developed hypoxia response of some species of *Methylobacter* allows them to outcompete other aerobic methanotrophs under microaerophilic conditions, and this may have given them the edge to become more dominant in the methanotroph community (Yu et al., 2020).

Further exploration of these theories was prevented by the lack of *in-situ* temperature or gas measurements, making it impossible to know how the biofilter was operating immediately prior to sampling both in terms of *in situ* temperature and gas flow. The detection of potentially thermophilic methanotrophs (*Methylocaldum* spp.) in both the *pmoCA* clone library (**Chapter 4.3**) and these 16S rRNA gene amplicons, reinforced the importance of producing a

temperature and gas probe capable of providing temperature profiles within the biofilter soil matrix (**Chapter 2.3.2** and **Chapter 3.2**).

Finally, while these 16S rRNA amplicons can tell us what methanotrophic genera are present in the region of the biofilter under investigation, they cannot tell us which of them are actively oxidising CH_4 under *in situ* conditions. To answer this a DNA-Stable Isotope Probing experiment was conducted to label the DNA of active methanotroph's from the biofilter soil with ^{13}C, this then allowed resolution and 16S rRNA gene amplicon analysis of the key players underpinning CH_4 oxidation (**Chapter 5**).

4.4.2 16S rRNA gene amplicons generated from biofilter cores at 50ºC

Surveying the biofilter with temperature probes, highlighted that the biofilter generally runs at elevated temperatures (**Chapter 3.2**). By using soil taken from a region of the biofilter known to be operating at high temperature for a 16S rRNA V3-V4 amplicon study, the taxonomy of the most abundant methanotrophs present at these hotter temperatures (around 50ºC) could be determined.

Two points in the biofilter with temperatures measured at 50ºC were selected for biofilter soil sample retrieval, one from the midpoint of sector 2C and one from the midpoint of 11B. Soil cores were retrieved from both positions on 17.5.19 (**Chapter 3.3.4**), and the 10-30cm and 30-50cm depth sections of each were retained for amplicon (and metagenome (**Chapter 4.5**)) analysis.

The remaining soil from each section (2C 10-30cm, 2C 30-50cm, 11B 10-30cm and 11B 30-50cm) was then divided into three aliquots (A,B,C). Triplicate DNA extractions were carried out on each aliquot for all sections. Extracted DNA quality was validated through 16S rRNA PCR and agarose gel electrophoresis of PCR products, PCR modifications: [50 µl][27F and 1492R] [16S_72]. Poor amplification with the 30-50cm section DNA extracts as template was observed, this was suspected to be due to humic acid contamination in the DNA extracts. As a result, the triplicate DNA extracts were pooled together for each section aliquot and subjected to a humic acid clean-up step using a Zymo One-step kit. These cleaned-up DNA extracts were revalidated and found to be satisfactory. After this the concentration of each pooled DNA extract was quantified via Qubit, and then each aliquot of pooled DNA extracts from each core section was used as a template in triplicate sets of V3V4 16S rRNA PCR reactions, PCR

modifications: [50 µl][341F, 785R][16S_72]. These were validated and the triplicate PCR reactions pooled for each aliquot and prepared for amplicon sequencing by High Pure PCR cleanup. 20µl of 20ng μl^{-1} PCR product from each pooled aliquot (2C 10-30cm A,B and C; 2C 30-50cm A,B and C; 11B 10-30cm A,B and C; 11B 30-50cm A,B and C) was then sent to mrDNA for amplicon sequencing (**Chapters 2.9.1** and **2.10**).

Amplicon analysis was then carried out using DADA2 as described in **Chapter 2.12.3**. The most abundant bacteria identified at the genus level (≥2% relative abundance) are shown for each individual amplicon in (**Figure 4.8**). This figure also shows similarly abundant putative genera made up from ASVs identified at higher taxonomic levels and grouped at 95% ANI 16S rRNA sequence similarity (Schloss and Handelsman, 2005), displayed as "<Lowest identified taxonomic rank> genus". The only known methanotrophic genus detected above 2% relative abundance in any of these amplicons was *Methylocaldum*. Known methanotrophs found amongst the identified genera in each amplicon are displayed along with their relative abundance (**Figure 4.9**). The methanotrophic community was overwhelmingly composed of *Methylocaldum* over the 10-50cm soil depth range explored in both core 2C and 11B. Of the two cores, 11B demonstrated slightly more methanotroph diversity with a 0.2-0.5% relative abundance of *Methylocystis* across depths and replicates, and an average of about 0.3% and 0.6% relative abundance of *Methylosinus* and *Methylobacter* respectively in the deeper 30-50cm soil range. Across both depths, cores and all replicates 10-18% of the total community was composed of methanotrophic genera. In addition to well established methanotroph genera, Bay et al recently recovered a good quality metagenome bin containing a particulate methane monooxygenase which was assigned to the proposed Gemmatimonadetes phylum (Bay et al., 2021). If the Gemmatimonadetes phylum does indeed contain methanotrophic members then it is worth noting that 2C 10-30 cm replicates A and B also contained a small amount of an unidentified putative Gemmatimonadaceae genus, assigned to this phylum.

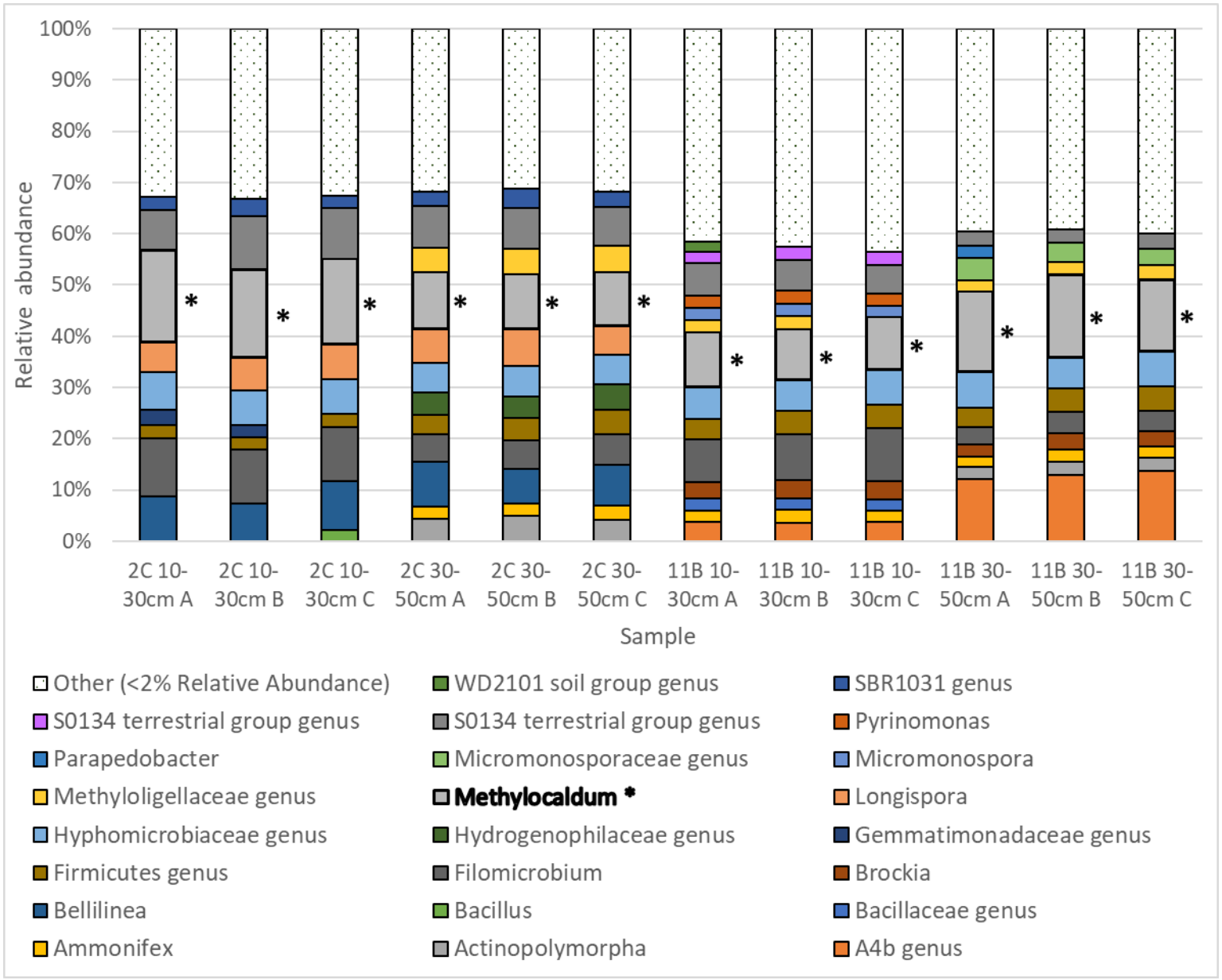

Figure 4.8 All bacteria identified at the genus level with 16S rRNA gene relative abundance above 2% in the core 2C and core 11B 16S rRNA V3-V4 amplicons. Also shown are similarly abundant groups of ASVs of unknown genera which could be grouped at a sequence similarity of 95% or above with each group representing a putative unknown genus (listed as "<Lowest identified taxonomic rank> genus"). Known methanotrophic genera are highlighted

Unlike in the case of the 11B/11C boundary soil core, we have a record of the *in-situ* temperatures of these soil core samples and we know that they were in the region of 50ºC. This allows us to link the relative abundances of methanotrophs present with this typical *in-situ* temperature. This amplicon analysis indicated that *Methylocaldum* may be the most abundant methanotroph at the hotter temperatures commonly seen in the biofilter (**Chapter 3.2**) which supported the findings of the initial DNA-SIP experiment to label active methanotrophs (**Chapter 5**). When compared with the methanotroph communities seen across similar depths for the 11B/11C boundary soil core (**Chapter 4.4.1**) the total relative abundance of methanotrophs in the 2C and 11B amplicons was both higher, more uniform and dominated by a single genus of methanotroph (*Methylocaldum*). The dominance by *Methylocaldum* at 50ºC is perhaps unsurprising as the other abundant methanotroph genera seen in the earlier 11B/11C amplicon set, are *Methylobacter* (composed of mesophilic or psychrophilic species) and *Crenothrix*, which has yet to be isolated but has been found in drinking water, lakes and agricultural soil (Bowman et al., 1993; Dörr et al., 2010; Oswald, 2017; Stoecker, 2006).

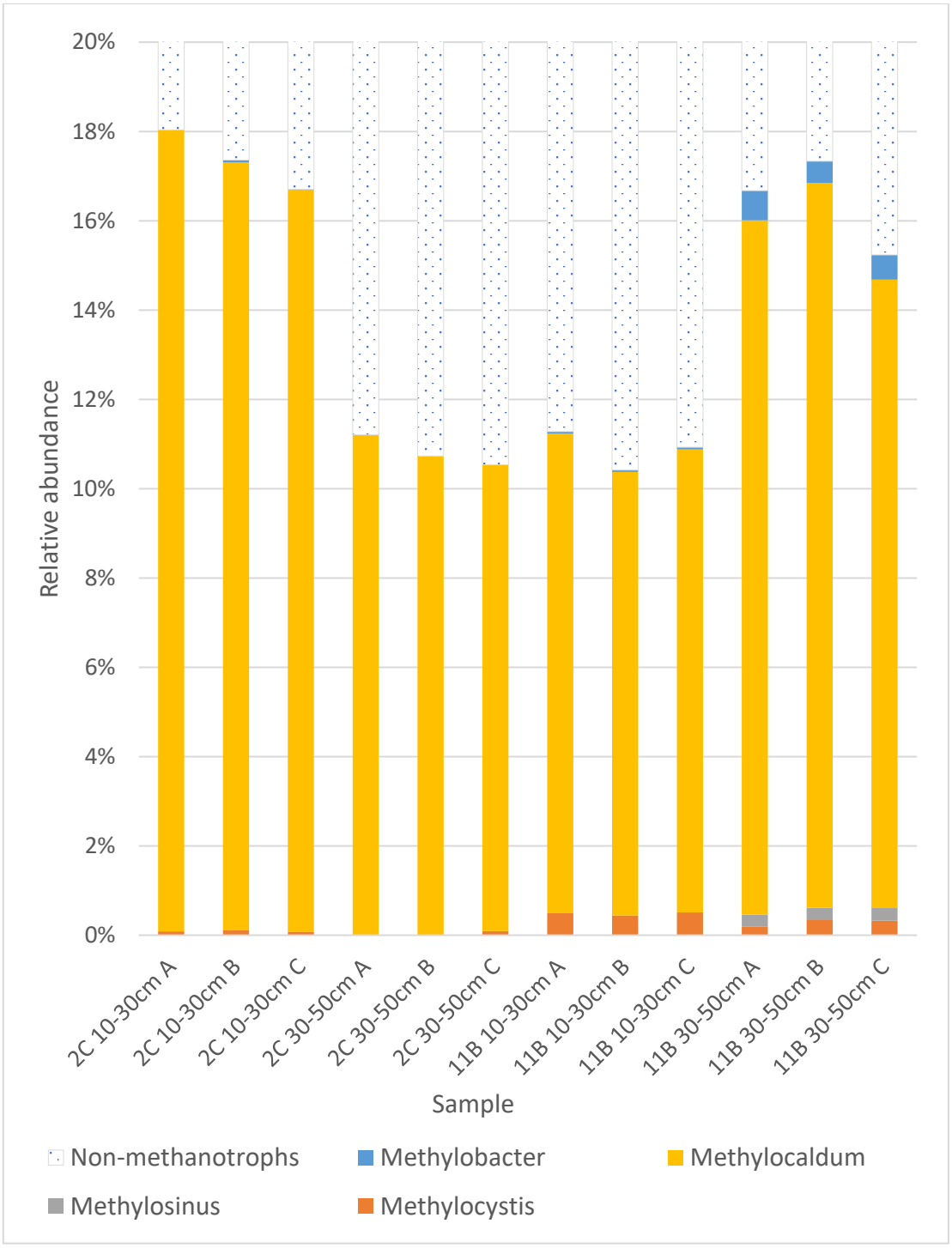

Figure 4.9 16S rRNA gene relative abundance (%) for all methanotrophic genera identified in the soil core 2C and core 11B 16S rRNA V3-V4 amplicons.

4.5 Biofilter soil metagenome sequencing and analysis

In addition to taxonomic profiling of the biofilter soil community using 16S rRNA gene amplicons, soil metagenome sequencing, assembly and analysis was also carried out on the core 2C samples (for additional methods see **Chapter 2.12.4**). The recovery of metagenome assembled genomes (MAGs) representing biofilter methanotrophs allowed identification of phylogenetically conserved marker genes other than the 16S rRNA gene sequence alongside reconstruction of their gene encoded metabolic potential.

4.5.1 Core 2C (17.5.19) metagenome sequencing (*in-situ* temp 50˚C)

Four DNA samples extracted from soil core 2C (sampled 17.5.19) were used for metagenome sequencing. (**Chapter 3.3.4**). 2C was selected for metagenome sequencing and analysis over core 11B (sampled on the same day), due to the higher soil CH_4 oxidation potential calculated for the 2C core sections indicating a greater degree of methanotroph activity (**Figure 3.4**).

The same pooled triplicate soil DNA extracts that provided the DNA template for core 2C amplicon sequencing in (**Chapter 4.4.2**), were used to provide the DNA for metagenome sequencing. Two (A and B) of the pooled DNA extracts from each depth (10-30cm and 30-50cm) were selected, adjusted to the concentration specified by the service provider (1 μg in 20 μl), and then sent as separate samples (2C 10-30cm A, 2C 30-50cm B, 2C 30-50cm A, 2C 30-50cm B) for shotgun metagenomic sequencing with mrDNA (**Chapter 2.10.7**).

4.5.2 Core 2C metagenome assembly and annotation

The resulting (R1 and R2) paired-end reads from each sample were then pre-processed as described in **Chapter 2.12.4**. Briefly, reads were trimmed and quality filtered using Trim Galore and the minoche filtering method and then assembled using metaSPAdes. The R1 and R2 trimmed and filtered reads from both samples were concatenated for each depth (to give A+B R1 and A+B R2 for 10-30 cm and 30-50 cm depths), and used in two separate metaSPAdes assemblies using standard parameters (one for the 10-30 cm depth and one for 30-50 cm depth samples). The resulting assemblies and reads then underwent binning using the MetaWRAP binning module, which conducts binning using the three different binning programs MaxBin2, metaBAT2 and CONCOCT. For each assembly, the resulting three sets of

bins were then refined into a single improved bin set using the metaWRAP bin refinement module.

Both the refined bins and initial metaSPAdes assemblies were then screened for the presence of the methanotroph marker genes *pmoA* and *mmoX* (McDonald et al., 2008), which encode subunits of the pMMO and sMMO respectively. The refined bin fasta files were first relabelled to include the bin of origin in the header for each contig, before they were all concatenated into a single fasta file for each set of refined bins, one for the 10-30 cm depth A+B refined bins and one for the 30-50 cm depth A+B refined bins. The concatenated 10-30 cm and 30-50 cm bin fastas as well as the 10-30 cm and 30-50 cm metaSPAdes assemblies were then each separately converted into NCBI-BLAST databases. Screening fasta files containing either *pmoA* or *mmoX* nucleotide sequences retrieved from genomes covering the range of known methanotroph genera were then produced. The *pmoA* and *mmoX* screening fasta files were then blasted against each of the four blast databases constructed, using the discontiguous megablast BLAST function, to obtain a list of candidate methane monooxygenase sequences. These candidate sequences were then blasted against the NCBI database with the nucleotide BLAST (blastn) function. **Table 4.1** lists the closest hits from the NCBI database for each candidate monooxygenase sequence found in the two metagenome assemblies, in addition to the contig of origin (and bin of origin for the refined bin database searches).

The taxonomic placement of the metagenome bins was then estimated using MIGA online and CheckM was used to estimate percentage completion and contamination. Bins (effectively metagenome assembled genomes or MAGs) containing putative *pmoA* or *mmoX* sequences and assigned a possible methanotrophic taxonomy were selected for further analysis along with MAGs lacking *pmoA* or *mmoX* but with possible methanotrophic taxonomy. MAG 9 from the 30-50 cm metagenome was also included despite possessing a non-methanotrophic taxonomy assignment (*Firmicutes, Bacilli*) as it contained a *pmoA* sequence with very high nucleotide similarity to that from a known methanotroph (*Methylomagnum* 83.02%, NODE_35631). Prokka was used to detect and annotate coding sequences in each of these candidate methanotroph MAGs. NCBI BlastP searches were then carried out on the translated nucleotide sequences of any *pmoA* or *mxaF* methanotrophic marker genes found, to provide further taxonomic information. Furthermore, the MAGs lacking the methanotroph marker genes *pmoA*, *mmoX* or *mxaF* were screened for the additional CH_4 metabolism genes *pmoB, pmoC, mmoY, mmoZ, mmoB, mmoC* and *mmoD* and were retained as candidate methanotrophs if any were found. The candidate methanotroph MAGs are listed in **Table 4.2** along with their MIGA

taxonomy assignment, CheckM completion and contamination scores and the results of BlastP marker searches.

Table 4.1 Closest hits from the NCBI database for each candidate monooxygenase sequence found in the 2C 10-30 cm depth and 30-50 cm depth metagenome assemblies. Those rows completely greyed out feature *pmoA* or *mmoX* with low translated amino acid similarity to known methanotrophs in the NCBI database (<60%) and are less likely to represent methane monooxygenases. (n.b. – not binned)

10-30 cm depth metagenome assembly - scaffolds and bins containing putative *pmoA* and *mmoX* sequences							
				identity and genera of closest blastn NCBI hit with assigned taxonomy			
scaffold	screen used	scaffold length	scaffold coverage	gene identity	% identity	taxonomy of closest hit	bin containing scaffold
NODE_29731	*pmoA*	3152	600.9	*pmoA*	83.02	*Methylomagnum*	6
NODE_722	*pmoA* (1/2)	52866	214.7	*pmoA*	67.54	*Methylococcus*	23
NODE_722	*pmoA* (2/2)	52866	214.7	*pmoA*	68.40	*Methylococcaceae*	23
NODE_28290	*pmoA*	3289	105.7	*pmoA*	95.97	*Methylocaldum*	n.b.
NODE_4556	*pmoA*	14648	8.3	*pmoA*	71.40	unassigned	n.b.
NODE_192276	*pmoA*	666	2.4	*pmoA*	97.15	*Methylocystis*	n.b.
NODE_365	*mmoX*	80222	340.1	*mmoX*	86.06	*Methylococcus*	6

30-50 cm depth metagenome assembly - scaffolds and bins containing putative *pmoA* and *mmoX* sequences							
				identity and genera of closest blastn NCBI hit with assigned taxonomy			
scaffold	screen used	scaffold length	scaffold coverage	gene identity	% identity	taxonomy of closest hit	bin containing scaffold
NODE_794	*pmoA (1/2)*	52501	426.3	*pmoA*	67.54	*Methylococcus*	9
NODE_794	*pmoA (2/2)*	52501	426.3	*pmoA*	68.40	*Methylococcaceae*	9
NODE_35631	*pmoA*	3108	381.9	*pmoA*	83.02	*Methylomagnum*	9
NODE_33061	*pmoA*	3320	41.4	*pmoA*	99.60	*Methylocaldum*	n.b.
NODE_167315	*pmoA*	839	36.7	*pmoA*	92.55	*Methylocaldum*	n.b.
NODE_30335	*pmoA*	3569	36.4	*pmoA*	98.12	*Methylocaldum*	n.b.
NODE_289161	*pmoA*	552	28.4	*pmoA*	89.35	*Methylocaldum*	n.b.
NODE_171429	*pmoA*	823	19.4	*pmoA*	92.91	*Methylocaldum*	n.b.
NODE_4226	*pmoA*	16881	15.8	*pmoA*	71.40	unassigned	27
NODE_289954	*pmoA*	551	6.1	*pmoA*	84.95	*Methylococcus*	n.b.
NODE_145076	*pmoA*	940	4.1	*pmoA*	89.76	*Methylomagnum*	n.b.
NODE_417	*mmoX*	77919	199.6	*mmoX*	85.93	*Methylococcus*	43

The fasta files containing the translated Prokka detected coding sequences for each MAG were then uploaded to the Kyoto Encyclopaedia of Genes and Genomes (KEGG) for KEGG K number assignment using BlastKOALA. Each K number in the database corresponds to an experimentally characterised protein, so the generated K numbers identify the corresponding sequences as orthologues of proteins of known function (based on sequence similarity). The K numbers from each MAG were next used to generate metabolic pathway maps using the KEGG pathway reconstruct tool. An inventory of key methanotroph enzymes and core metabolic pathways was built up for each candidate methanotroph MAG, with missing genes in the KEGG pathways manually searched for in the unassigned coding sequences using NCBI-BLAST. These inventories are shown in **Table 4.3**.

Table 4.2 The candidate methanotroph MAGs along with their MIGA taxonomy assignment, CheckM completion and contamination scores. Also shown are the results of methanotroph marker gene BLAST P searches against the NCBI database, displaying the top two genera and the nucleotide derived amino acid identity (%).

10-30 cm depth metagenome assembly candidate methanotroph MAGs

MAG	*pmoA* present	Closest top two genera NCBI hits (% identity)	*mmoX* present	Closest top two genera NCBI hits (% identity)	*MxaF* present	Closest top two genera NCBI hits (% identity)	MIGA online taxonomy assignment (P value < 0.05)	MAG size (bp)	Contigs	N50	GC content (%)	CheckM completion (%)	CheckM contamination (%)
6	yes	*Methylomagnum* (92.71) *Methylocaldum* (90.69)	yes	*Methylococcus* (90.32) *Methylocaldum* (91.68)	yes	*Methylomagnum* (91.18) *Methylocaldum* (90.52)	*Gammaproteobacteria*	3,359,035	39	262,143	64.97	98.14	0.18
36	no		no		no		*Gammaproteobacteria*	4,097,921	171	33,224	57.26	94.71	2.21

30-50 cm depth metagenome assembly candidate methanotroph MAGs

MAG	*pmoA* present	Closest top two genera NCBI hits (% identity)	*mmoX* present	Closest top two genera NCBI hits (% identity)	*MxaF* present	Closest top two genera NCBI hits (% identity)	MIGA online taxonomy assignment (P value < 0.05)	MAG size (bp)	Contigs	N50	GC content (%)	CheckM completion (%)	CheckM contamination (%)
9	yes	*Methylomagnum* (92.71) *Methylocaldum* (90.69)	no		no		*Bacilli*	2,292,215	170	37936	71.11	85.29	2.45
16	no		no		yes	*Methylocaldum* (100) *Methylomagnum* (90.91)	*Gammaproteobacteria*	3,632,470	383	12534	57.35	76.04	3.24
43	no		yes	*Methylococcus* (90.32) *Methylocaldum* (91.68)	yes	*Methylomagnum* (91.18) *Methylocaldum* (91.08)	*Gammaproteobacteria*	3,265,470	51	151526	65.06	98.14	0.23
50	no		no		no		*Gammaproteobacteria*	2,672,461	231	15470	55.69	81.23	4.54

NCBI BlastP hits (top two genera) for additional CH_4 metabolism genes in MAGs lacking *pmoA*, *mmoX* and *MxaF* marker genes.

MAG	*pmoC* present	Closest top two genera NCBI hits (% identity)	*xoxF* present	Closest top two genera NCBI hits (% identity)
10-30 cm MAG 36	yes (three)	*Methylocaldum* (94.00) *Methylotetracoccus* (69.01) *Methylocaldum* (91.67) *Methylumidiphilus* (82.35) *Methylocaldum* (97.25) *Methylumidiphilus* (82.75)	yes	*Methylocaldum* (96.94) *Ca. Methylospira* (85.00)
30-50 cm MAG 50	yes (two)	*Methylocaldum* (92.25) *Ca. Methylospira* (73.83) *Methylocaldum* (86.32) *Methylotetracoccus* (73.06)	yes	*Methylocaldum* (96.00) *Ca. Methylospira* (88.00)

Table 4.3 Inventories of key methanotroph enzymes and core metabolic pathways detected in the candidate methanotroph MAGs from the 2C 10-30 cm and 2C 30-50 cm metagenome assemblies. * pyrophosphate-dependent 6-phosphofructokinase as found in *Methylococcus capsulatus* (Bath) (Reshetnikov et al., 2008). (n.d. – not detected).

10-30 cm methanotrophic MAGs

	methane oxidation		methanol oxidation		formaldehyde oxidation			formate oxidation	carbon assimilation pathways			nitrogen metabolism					
MAG	particulate MMO pmoCAB	soluble MMO mmoXYBZDC	*MxaFI*	*XoxF*	H_4MPT linked	H_4F linked	formaldehyde dehydrogenase	formate dehydrogenase	Ribulose monophosphate	Serine	Calvin-Bensom-Bassham (CBB)	*hao*	denitrification	nitrogen fixation	assimilatory nitrate reduction	dissimilatory nitrate reduction	GS/GOGAT
6	one copy	one copy	one copy	one copy	complete	complete	n.d.	one copy	complete	partial	complete	one copy	partial	complete	n.d.	complete	complete
	two additional single *pmoC* genes present									fragmentary	PPi-PFK* instead of sedoheptulose-1,7-bisphosphatase		lacks nosZ for N_2O reduction	nifDKH			
36	n.d.	n.d.	n.d.	one copy	complete	complete	n.d.	two	complete	partial	complete	one copy	partial	complete	n.d.	partial	complete
	three single copies of *pmoC* present					lacks *glyA* for transer to serine cycle				fragmentary	PPi-PFK* instead of sedoheptulose-1,7-bisphosphatase		only *norB* and *norC* for nitric oxide reduction	nifDKH		only *nirB* and *nirD* for nitrite reduction	

30-50 cm methanotrophic MAGs

	methane oxidation		methanol oxidation		formaldehyde oxidation			formate oxidation	carbon assimilation pathways			nitrogen metabolism					
MAG	particulate MMO pmoCAB	soluble MMO mmoXYBZDC	*MxaFI*	*XoxF*	H_4MPT linked	H_4F linked	formaldehyde dehydrogenase	formate dehydrogenase	Ribulose monophosphate	Serine	Calvin-Bensom-Bassham (CBB)	*hao*	denitrification	nitrogen fixation	assimilatory nitrate reduction	dissimilatory nitrate reduction	GS/GOGAT
9	three	n.d.	n.d.	one	n.d.	partial	n.d.	n.d	complete	partial	near complete	one copy	partial	complete	partial	n.d.	partial
	only one *pmoA* gene has >58% aa identity to known methanotroph pmoCAB					lacking *mtdA* and *fchA*				fragmentary	lacking sedoheptulose-1,7-bisphosphatase		*nirK* for nitrite reduction	nifDKH	posesses *nirA* for nitrite reduction		lacks glutamate synthase
16	n.d.	n.d.	one copy	three	complete	partial	n.d.	one copy	complete	partial	complete	one copy	partial	partial	n.d.	partial	partial
	single copy of *pmoC* present					lacking *ftfl*				fragmentary	PPi-PFK* instead of sedoheptulose-1,7-bisphosphatase		*nirK* for nitrite and *norB/norC* for nitric oxide reduction	*nifHK*		only *nirB* and *nirD* for nitrite reduction	lacking *gltB* component of glutamate synthase
43	n.d.	one copy	one copy	one copy	complete	complete	n.d.	one copy	complete	partial	complete	one copy	partial	complete	partial	complete	complete
	two single *pmoC* genes present									fragmentary	PPi-PFK* instead of sedoheptulose-1,7-bisphosphatase		lacking *norC* and *norZ* for final steps	nifDKH	only *nasA* involved in initial reduction of nitrate		
50	n.d.	n.d.	n.d.	one copy	complete	partial	n.d.	four copies	near complete	partial	partial	one copy	partial	complete	partial	n.d.	partial
	two single *pmoC* genes present					lacking *ftfl* as well as *glyA* for transer to serine cycle			lacking H6PD hexose-6-phosphate dehydrogenase and *pgl* (6-phospho-gluconolactonase)	fragmentary	fragmentary		only contains *norC* involved in nitric oxide reduction	nifDKH	only posess *nasA* involved in initial reduction of nitrate		lacks *gltB* component of glutamate synthase

4.5.3 Analysis of candidate methanotroph MAGs from 10-30 cm and 30-50 cm core 2C metagenomes

4.5.3.1 Candidate methanotroph MAGs from the core 2C 10-30 cm depth metagenome

4.5.3.1.1 10-30 cm metagenome MAG 6

10-30 cm metagenome MAG 6 represents a gammaproteobacterial (MIGA online assigned taxonomy) methanotroph, as can be seen from (**Tables 4.2** and **4.3**) it's status as a methanotroph is due to possessing genes encoding enzymes of pathways for full CH_4 oxidation and carbon incorporation. MAG 6 contains a complete set of genes for particulate and soluble methane monooxygenases as well as genes encoding pathways for methanol (*mxaFI*, *xoxF*), formaldehyde (H_4MPT and H_4F pathways) and formate (formate dehydrogenase) oxidation. This MAG also contains genes suggesting a complete ribulose monophosphate pathway and CBB cycle, while several key genes involved in the serine pathway were not found (*hprA*, *gck*, *ppc* and *mtkB*), suggesting that this methanotroph relies on the ribulose monophosphate and CBB cycle for CH_4-derived carbon assimilation. This methanotroph also features the *nifH*, *nifK* and *nifD* genes encoding the nitrogenase structural units for dinitrogen fixation. An orthologue of the hydroxylamine oxidoreductase (*hao*) was also found, which could allow removal of the toxic hydroxylamine intermediate produced from *pmoCAB* co-metabolised ammonia (Stein et al., 2012). Like most studied (non-*methylocystis*) methanotrophs (Dam et al., 2012; Dumont et al., 2013) this MAG lacks a copy of *nosZ* for reduction of nitrous oxide to dinitrogen, leaving the potential for nitrous oxide production. 10-30 cm MAG 6 also features a complete GS/GOGAT glutamate cycle for ammonia incorporation with genes for glutamate synthase (*gltB* and *gltD*) and glutamine synthetase (*glnA*), as well as NADH dependent glutamate dehydrogenase and alanine dehydrogenase genes for ammonium assimilation via the α-ketoglutarate and pyruvate pathways (Murrell and Dalton, 1983b).

For the classic methanotroph and methylotroph marker genes *pmoA*, *mmoX* and *mxaF* (McDonald et al., 2008), the genera of the closest BLAST P hits (*Methylomagnum*, *Methylocaldum*, *Methylococcus* **Table 4.2**) suggest that 10-30 cm MAG 6 belongs to a member of the *Methylococcaceae*. All three of these genera contain species possessing both forms of methane monooxygenase (pMMO, sMMO) and potentially assimilating carbon through both

the ribulose monophosphate and CBB cycle routes (Henard et al., 2021; Khalifa et al., 2015; Takeuchi et al., 2019).

4.5.3.1.2 10-30 cm metagenome MAG 23

10-30 cm MAG 23 is also a MIGA online assigned member of the *Gammaproteobacteria* (**Table 4.2**). While no full pMMO (*pmoCAB*) or sMMO (*mmoXYBZDC*) gene clusters were found in this MAG, three single *pmoC* sequences were present (**Table 4.3**). The presence of downstream CH_4 carbon oxidation and metabolic genes including a methanol dehydrogenase (*xoxF*), genes for both the H_4MPT and H_4F formaldehyde oxidation pathways and two formate dehydrogenases support the possibility that this could be a methanotrophic MAG which has not received it's *pmoCAB* sequence(s) during the binning and bin refining steps of the metagenome assembly pipeline. This would not be that surprising, as short read metagenome assembly and binning (based on identical sequence overlap and equivalent abundances) struggles with both conserved multiple copy genes as well as repeat rich regions (Alkan et al., 2011). The *pmoCAB* region not only features highly conserved regions that make pmoA such a good taxonomic marker (McDonald et al., 2008), but methanotrophs often contain more than one copy of the *pmoCAB* cluster (Khadem et al., 2012; Murrell and Smith, 2010; Takeuchi et al., 2019). This is also the reason why 16S rRNA genes are less frequently recovered in metagenome MAGs, indeed in the candidate methanotroph MAGs from these two assemblies, only 30-50 cm MAG 9 contained 16S rRNA sequences. 10-30 cm MAG 23 also features genes representing complete ribulose monophosphate and CBB pathways, which would likely be favoured for carbon incorporation over the apparently incomplete serine pathway. This methanotroph may also be capable of dinitrogen fixation as this MAG contains the nitrogenase genes *nifH*, *nifK* and *nifD*. *hao* was also present, possibly allowing detoxification of any hydroxylamine that may be produced if this bacterium does indeed contain a functional *pmoCAB* cluster. *norB* and *norC* genes are also present in this MAG suggesting this bacterium may be capable of forming nitrous oxide from nitric oxide. A complete set of genes for ammonia incorporation via the GS/GOGAT glutamate cycle (*glnA* and *gltB* and *gltD*) were also present in this MAG as well as alanine and NADH dependent glutamate dehydrogenase genes for the alternative pyruvate and α-ketoglutarate pathways.

As this MAG lacked *pmoA*, *mmoX* or *mxaF*, the amino acid sequences of the lanthanide-dependent methanol dehydrogenase gene *xoxF* and the particulate methane monooxygenase

subunit C genes *pmoC* that were found in this MAG were BLAST P searched against the NCBI database as alternative taxonomy markers. The results of these searches are shown in **Table 4.2** and suggest that this bacterium might be a *Methylocaldum* species.

4.5.3.2 Candidate methanotroph MAGs from the core 2C 30-50 cm depth metagenome

4.5.3.2.1 30-50 cm metagenome MAG 9

30-50 cm MAG 9 is an unusual case as MIGA online assigned a *Bacilli* class taxonomy to this MAG (**Table 4.2**), which is unexpected for a potentially methanotrophic MAG as the *Bacilli* class belongs to the *Firmicutes* phylum which is not known to contain any methanotrophic species. The lack of genes encoding enzymes for formaldehyde or formate oxidation (**Table 4.3**) also suggests that this may not be a true methanotroph bin. Interestingly this was the only one of the candidate methanotroph MAGs containing partial 16S rRNA sequences, in this case two sequences. Blasting these sequences against the NCBI database (BLASTn) returned very different top hits for each, with one coming back with a 92.94% nucleotide identity to *Methylocaldum marinum*, while the other returned a 87.06% nucleotide identity to the bacterium *Limnochorda pilosa*, a moderately thermophilic *Firmicutes* bacterium (optimum growth temperature 45-50ºC) (Watanabe et al., 2015).

It appears likely that the *pmoA* gene with a high similarity to methanotrophic sequences (92.71% amino acid similarity to a *Methylomagnum pmoA* sequence) **Table 4.2** which corresponds to the *pmoA* from NODE_35631 in **Table 4.1** is likely a contaminant in this MAG and it is predominantly composed of non-methanotrophic *Bacilli* class sequences. This could have been due to a similar abundance of these *Bacilli* scaffolds compared to the *pmoA* containing NODE_35631. Looking at **Table 4.1**, it is interesting to note that the putative *pmoA* sequence from 10-30 cm NODE_29731 is the same as the putative *pmoA* sequence from 30-50 cm NODE_35631 and the two putative *pmoA* sequences (with <60% amino acid identity to known methanotrophic *pmoA*) from 10-30 cm NODE_722 match those on 30-50 cm NODE_794. In the metagenome from 10-30 cm the scaffold coverage of the scaffold containing the 92.71% *Methylomagnum pmoA* is approximately three times higher than that for the (<60% methanotroph amino acid identity) double *pmoA* scaffold (600.9 to 214.7) and these were binned into separate (*Gammaproteobacteria* and *Bacilli* class) MAGs. In the

metagenome from 30-50 cm the scaffold coverage of the scaffolds containing the corresponding *pmoA* sequences is much closer (426.3 to 381.9). As the metagenome binners use coverage as one of the parameters (along with tetranucleotide frequency) determining scaffold binning, a similar abundance of the methanotroph *pmoA* scaffold to the *Bacilli* class bacterium scaffolds in the metagenome from 30-50 cm could be responsible for incorrect binning of the relatively short scaffold NODE_35631 containing the 92.71% *Methylomagnum pmoA*. The short length of this scaffold (3,108 bp) may have reduced the likelihood of any tetranucleotide frequency difference between the organisms preventing incorrect bin assignment.

4.5.3.2.2 30-50 cm metagenome MAG 16

MAG 16 from the 30-50 cm metagenome was another gammaproteobacterial MAG lacking a full *pmoCAB* or *mmoXYBZDC* cluster but containing a single *pmoC* sequence and various genes and pathways for methanol, formaldehyde and formate oxidation, suggesting that this could be an incomplete methanotroph MAG, a possibility supported by the relatively low CheckM completion score for this MAG (only 76.04%) **Table 4.2** and **4.3**. Bearing in mind that this completion score suggests roughly 25% of genes may be missing, it is worth noting that genes encoding a full ribulose monophosphate and complete CBB pathway for carbon assimilation are present in contrast to the fragmentary serine pathway. Two of the three structural genes for nitrogenase (*nifH* and *nifK*) were also found. *hao* was present as a potential counter to hydroxylamine production by *pmoCAB* assuming there is such a cluster present in the full genome. *nirK*, *norB* and *norC* were also present indicating that this organism may be capable of nitrite reduction to nitrous oxide. The components of the GS/GOGAT cycle were not all present with the gene for the *gltB* subunit of glutamate synthase absent (although this could be an artifact of the low completion level of this MAG), genes for both alanine as well as NADH and NADPH dependent glutamate dehydrogenases for the alternative ammonia assimilation routes were also detected.

The *mxaF* methylotroph marker gene present in MAG 16 from the 30-50 cm metagenome demonstrated a 100% translated amino acid match with that from a *Methylocaldum* species in the NCBI database suggesting that 30-50 cm MAG 16 could be from a *Methylocaldum* species if it has been correctly binned.

4.5.3.2.3 30-50 cm metagenome MAG 43

MAG 43 from the 30-50 cm metagenome is yet another gammaproteobacterial methanotroph according to the MIGA online taxonomy assessment. This MAG contained a full *mmoXYBZDC* cluster but lacked a full *pmoCAB* region, although it did contain two single *pmoC* sequences. The *Gammaproteobacteria* taxonomic placement of this MAG and the presence of sMMO genes indicates that this MAG may be missing it's *pmoCAB* cluster as so far, the only known methanotrophs with only sMMO sequences belong to the *Alphaproteobacterial* genera *Methylocella* (Chen et al., 2010), *Methyloferula* (Dedysh et al., 2015), or *Methyloceanibacter* (Vekeman et al., 2016). This MAG features a single copy of both *mxaFI* and *xoxF* methanol dehydrogenase genes, a complete inventory of genes for the H_4MPT and H_4F pathways for formaldehyde oxidation as well as a single formate dehydrogenase. 30-50 cm MAG 43 seems to be from another methanotroph likely using the ribulose monophosphate or CBB pathway for CH_4 carbon assimilation, as with many of the other likely methanotroph MAGs seen here, these pathways are complete while the serine pathway is fragmentary (missing the key *hprA*, *gck*, *ppc* and *mtkB* genes). 30-50 cm has the *nifH nifK* and *nifD* nitrogenase structural genes indicating it may be capable of dinitrogen fixation. This MAG also contains *hao*, which could detoxify hydroxylamine produced by any elusive pMMO enzymes that this bacterium may possess. MAG 43 from the 30-50 cm metagenome lacks *nosZ* for nitrous oxide reduction but also lacks one of the subunits for nitrous oxide formation via nitric oxide reductase (*norC*). Genes encoding a complete GS/GOGAT (*glnA*, *gltB* and *gltD*) cycle as well as alanine and NADH dependent glutamate dehydrogenases for ammonium assimilation were also present.

The translated amino acid sequences of the *mmoX* and *mxaF* marker genes in 30-50 cm MAG 43 (**Table 4.2**) are closest to representatives from the *Methylomagnum*, *Methylocaldum* and *Methylococcus* genera suggesting that this MAG may be from a genus within the *Methylococcaceae*. Other than the absence of a *pmoCAB* cluster this MAG has some noticeable similarity to the 10-30 cm metagenome MAG 6 including: the taxonomy of the closest genera of NCBI BLAST hits against the *mmoX* and *mxaF* sequences, the MAG size and %GC content **Table 4.2**, as well as the presence of two single *pmoC* sequences and similar gene copy numbers and pathways for methanol, formaldehyde and formate oxidation **Table 4.3**. There was a possibility that these two MAGs are derived from the same or closely related organisms and the incorrect binning of 30-50 cm MAG 9 stripped 30-50 cm MAG 43 of it's *pmoCAB* cluster. This would be investigated using the Genome-to-Genome Distance Calculator to assess

the degree of similarity between 10-30 cm MAG 6 and 30-50 cm MAG 43 and by pairwise comparison of the *mmoX* and *mxaF* genes using BLAST P.

4.5.3.2.4 30-50 cm metagenome MAG 50

30-50 cm MAG 50 was also assigned gammaproteobacterial taxonomy using MIGA online (**Table 4.2**). This is another MAG lacking *mmoXYBZDC* or *pmoCAB* but possibly belonging to a methanotroph as it does contain genes for *pmoC* (two copies), a lanthanide dependant methanol dehydrogenase (*xoxF*) (**Table 4.3**) and the relatively low CheckM completion score of 81.23% (**Table 4.2**) suggests it could be an incomplete methanotroph MAG missing it's *pmoCAB* cluster or clusters. This MAG additionally contains a complete set of genes for the H_4MPT formaldehyde oxidation pathway and most of the genes for the H_4F linked pathway, lacking only formate-tetrahydrofolate ligase (*ftfl*) and *glyA* (for carbon transfer into the serine pathway). Multiple (four) formate dehydrogenase genes are also present. Of the three methanotroph carbon assimilation pathways (ribulose monophosphate, serine and CBB), only the ribulose monophosphate pathway is near complete. A full set of nitrogenase structural genes were also found (*nifH*, *nifK* and *nifD*), suggesting potential dinitrogen fixation potential. A copy of *hao* was detected alongside a single nitric oxide reductase subunit (*norC*). With regards to ammonia assimilation, genes for a near complete GS/GOGAT cycle (lacking the *gltB* subunit of glutamate synthase) were present along with those for alanine dehydrogenase and NADH and NAD(P)H dependent glutamate dehydrogenases. The potential low completion of this MAG may have contributed to some of the incomplete or partial metabolic pathways and missing genes in this MAG.

With *pmoA*, *mmoX* or *mxaF* absent from MAG 50 from the 30-50 cm metagenome, the particulate methane monooxygenase subunit C (*pmoC*) and lanthanide-dependent methanol dehydrogenase (*xoxF*) were once again used to suggest a higher resolution of taxonomic assignment than *Gammaproteobacteria* (**Table 4.2**), with the closest matches in the NCBI database against their translated amino acid sequences coming from *Methylocaldum*. Suggesting a likely *Methylococcaceae* origin and perhaps *Methylocaldum* identity.

4.5.4 Comparison of candidate methanotroph MAGs across both metagenome assemblies, and identifying the most abundant methanotrophs present.

The candidate methanotrophic MAGs generated from both metagenome assemblies (10-30 cm and 30-50 cm) were then compared against one another pairwise, using the genome-to-genome distance calculator, to assess the probability that they represent the same species or subspecies. This program carries out an *in-silico* genome-to-genome comparison and presents the similarity of the two genomes in a format matching traditional DNA-DNA hybridisation.

It was found that MAG 6 from the 10-30cm metagenome and MAG 43 from the 30-50 cm metagenome were highly likely to represent the same species (98.18% likelihood) and very likely to represent the same subspecies (79.42%). This was anticipated as the top NCBI blast hits for their methanotrophic marker genes (*mmoX* and *mxaF*) had very similar taxonomy **Table 4.2**. BLAST P comparisons of these two genes between MAG 6 from the 10-30 cm metagenome and MAG 43 from the 30-50 cm metagenome are shown alongside the Genome-to-Genome Distance Calculator estimate of genome similarity for these two MAGs in **Table 4.4**.

Table 4.4 BLAST P comparisons of the nucleotide derived amino acid sequences for *mmoX* and *mxaF* genes between MAG 6 from the 2C 10-30 cm metagenome and MAG 43 from the 2C 30-50 cm metagenome. Also shown is the Genome-to-Genome Distance Calculator estimate of genome similarity for these two MAGs.

Similarity of nucleotide derived amino acid sequences of *mmoX* and m*xaF* genes from 10-30 cm MAG 6 and 30-50 cm MAG 43	
mmoX	100.00%
MxaF	100.00%
Genome-to-Genome Distance Calculator comparison of 10-30 cm MAG 6 and 30-50 cm MAG 43	
Probability that DNA-DNA Hybridisation >70% (same species)	98.18%
Probability that DNA-DNA Hybridisation >79% (same subspecies)	79.42%

Finally, a rough estimate of the relative abundance of the methanotrophs represented by each of the recovered MAGs as a proportion of the total microbial community, was generated using CheckM. As CheckM estimates are based on the total number of raw reads that map to each MAG, these estimates are biased where MAGs are incomplete. Therefore the estimated average MAG read coverage (AMRC), normalised per million paired-end reads, for each bin in the two

metagenomes was calculated using the metaWRAP quant_bins module. This allowed a more accurate comparison of the relative abundance of the candidate methanotroph MAGs within and between each metagenome, as it is based on average read coverage at each nucleotide position and should suffer less bias where MAGs are incomplete. The methanotroph MAG CheckM relative abundance and AMRC values are shown in **Table 4.5**.

Table 4.5 average MAG read coverage (AMRC) and relative abundance for each of the candidate methanotroph MAGs in the 2C 10-30 cm depth and 30-50 cm depth metagenomes, calculated using the metaWRAP quant_bins function and CheckM respectively. MAG 9 from the 30-50 cm metagenome is believed to be a Firmicutes MAG contaminated with a methanotroph *pmoCAB* cluster and not a true non-chimeric methanotroph bin.

10-30 cm metagenome assembly			30-50 cm metagenome assembly		
MAG	Average MAG read coverage	Relative abundance (%)	MAG	Average MAG read coverage	Relative abundance (%)
6	28.0	5.27	9	34.6	7.09
36	4.3	0.81	16	2.1	0.37
			43	15.9	3.27
			50	1.3	0.26

Looking at the scaffold coverage for the reconstructed *pmoA* sequences in the 10-30 cm and 30-50 cm metagenome assemblies **Table 4.1** : the NODE_29731 *pmoA* sequence appears to be the most abundant *pmoA* sequence present in the 10-30 cm metagenome and the NODE_35631 *pmoA* sequence is likely the most abundant *pmoA* in the 30-50 cm metagenome, as the higher coverage NODE_794 putative *pmoA* sequences are probably not methane monooxygenase sequences (low nucleotide derived amino acid similarity to known methanotrophic *pmoA* sequences). A comparison of these two sequences using BLAST P indicates that they are highly similar (100% nucleotide-derived amino acid similarity). There was only one *mmoX* sequence detected in either the 10-30 cm or 30-50 cm metagenomes and again this sequence is highly similar between the metagenome assemblies (100% nucleotide-derived amino acid similarity).

In the 10-30 cm metagenome, both the most abundant *pmoA* and *mmoX* were recruited into the same MAG (10-30 cm MAG 6) during binning while in the 30-50 cm metagenome the *mmoX* sequence was recruited to a MAG (30-50 cm MAG 43) which displayed a very high genome-to-genome distance score when compared with 10-30 cm MAG 6 (suggesting same species and likely same subspecies). In contrast, in the 30-50 cm metagenome, the most abundant *pmoA*

sequence was perhaps incorrectly recruited into a predominantly *Firmicutes* MAG (30-50 cm MAG 9).

Taking this into consideration It appears that the most abundant methanotrophs found in both of these metagenome assemblies are the same or very closely related bacteria and represented by the MAG 6 from the 10-30 cm metagenome and MAG 43 from the 30-50 cm metagenome. The exact taxonomy of this MAG is difficult to pin down but it appears to be a member of the *Methylococcaceae* and most closely related to *Methylococcus*, *Methylocaldum* and *Methylomagnum*. The difficulty in assembling 16S rRNA sequences into short read metagenome bins prevented the use of this useful taxonomic benchmark to resolve this.

While the 10-30 cm and 30-50 cm metagenomes from core 2C resulted in reconstruction of MAGs that may represent the most abundant methanotroph present in the biofilter at 50ºC, the decision was made to carry out metagenome sequencing on the heavy $^{13}CH_4$ fraction of a $^{13}CH_4$ DNA-SIP enrichment of methanotroph soil incubated at the typical biofilter operating temperature of 50ºC (**Chapter 5**). It was hoped that enriching the DNA of the active methanotrophs through DNA-SIP, would improve the potential to retrieve accurate methanotroph MAGs containing complete *pmoCAB* clusters by artificially reducing the complexity of the community being studied. This would not only allow identification of the most abundant actively-methane-oxidizing methanotrophs but could also resolve the question of the *pmoA* MAG placement in MAG 6 from the 10-30 cm metagenome and MAG 43 from the 30-50 cm metagenome provided the same methanotroph was present in the DNA-SIP metagenomes.

4.6 Discussion

At the high temperatures (~50ºC) typically seen in the biofilter during uninterrupted operation (**Chapter 3**), the 16S rRNA amplicon studies on cores 2C and 11B described in this chapter suggest that *Methylocaldum* could be the dominant methane oxidising strain, purely due to the very high relative abundance of *Methylocaldum* 16S rRNA sequences compared to other methanotrophs at this temperature (10-18% : 0-1% relative abundance **Figure 4.9**). In addition, analysis of the core 2C 10-30 cm and 30-50 cm metagenomes found a *Methylococcaceae* methanotroph to be the likely origin of the most abundant *pmoA* and *mmoX* sequences found in the assembled metagenome scaffolds. There is a possibility that this methanotroph could have a *Methylocaldum* 16S rRNA signature as a matching MAG (based on Genome-to-

Genome Distance Calculator estimates) from a metagenome in (**Chapter 5**) possessed a partial *Methylocaldum* 16S rRNA sequence. Ultimately the $^{13}CH_4$ biofilter soil DNA-SIP labelling experiments (**Chapter 5**) were required to definitively determine which were the active methanotrophs in the biofilter through labelling their DNA with ^{13}C (linking CH_4 oxidation to methanotroph DNA).

The greater diversity of non-thermophilic or thermotolerant methanotrophs (*Methylobacter*, *Crenothrix* and *Methylocella*) detected in core 11B/11C by 16S rRNA amplicon sequencing (**Figure 4.7**) likely reflects the methanotroph communities at lower temperatures such as are observed following interruption to CH_4 and O_2 supply (**Chapter 3**).

Chapter 5: Identifying the active methanotroph community using DNA Stable Isotope Probing (DNA-SIP)

5.1 DNA stable isotope probing

DNA Stable Isotope Probing (DNA-SIP) experiments were designed, following the guidelines laid out in Neufeld et al. (2007), to identify active (methane metabolising) methanotrophs present in the biofilter. This involved the incubation of soil from the Strumpshaw biofilter with ^{13}C-labelled methane, with the expectation that active methanotrophs present would become labelled through metabolism and incorporation of this ^{13}C into their DNA. The heavier DNA of these labelled methanotrophs could then be isolated across a density gradient and analysed through amplicon and metagenome sequencing.

5.2 DNA-SIP and 16S rRNA gene amplicon analysis of the active methanotrophs in the top 10 cm of biofilter soil at 30°C, 37°C and 45°C

The top 10cm of the biofilter was the first target for DNA-SIP analysis of the active methanotroph community. This depth of biofilter soil was chosen as initial incubations of the top section of biofilter soil with methane had demonstrated a methane consumption of 184-309 nmoles h^{-1} g $soil^{-1}$ depending on the incubation temperature (**Chapter 3.3.2**). Additionally, Mr Elliot Brookes' preliminary work on the biofilter had resulted in the isolation of *Methylococcus capsulatus* (**Chapter 6**) from the top 5cm of soil.

5.2.1 $^{13}CH_4$ DNA-SIP incubation of soil from the top 10 cm of the biofilter at 30°C, 37°C and 45°C

While this experiment predated the availability of a combined temperature and gas probe (**Chapter 3**), initial observations suggested that the biofilter was operating at above ambient temperature. Fixed monitoring ports often indicated elevated temperatures, steam had been observed rising from the biofilter during winter operation and the surface of the biofilter was generally warm to the touch. For this reason it was decided to design this experiment as a variable temperature incubation. Three different temperatures (30°C, 37°C and 45°C) were selected within the range of values recorded at the monitoring ports across the biofilter. The

active methanotroph community at each of these temperatures could be examined to identify key methanotrophs involved in methane turnover within the biofilter and show how the community may shift as *in-situ* temperature changed. The labelled methanotrophs at the increasing temperatures could also be interpreted as snapshots of the active methanotroph community on the way to forming a methanotrophic "climax community" as the biofilter heats up following interruptions in operation.

The biofilter soil used for these variable temperature incubations came from the 60cm biofilter soil core (sampled from the sector 11B/11C boundary) taken from the centre of the biofilter on 19.2.18 (the same core which provided the material for the 16S rRNA amplicon sequencing experiment described in **Chapter 3.3.2**). The top most section of this core (0-10 cm depth) provided the soil material for this set of DNA-SIP incubations. As mentioned previously, soil methane oxidation potential was estimated for this soil to confirm the presence of active methanotrophs.

The experimental procedure followed that laid out in **Chapter 2.11**. Duplicate sets of $^{13}CH_4$ (labelled) and $^{12}CH_4$ (unlabelled control) incubation cultures were set up for each of three different temperature incubations: 30˚C, 37˚C and 45˚C (for a total of 12 incubation cultures as shown in **Figure 5.1**). Triplicate sets of incubation cultures would have been preferred, but the amount of soil sample that could be retrieved using the corer was limited, this limitation was overcome in a later DNA-SIP experiment (**Chapter 5.3.1**) by excavating the soil sample material with a spade.

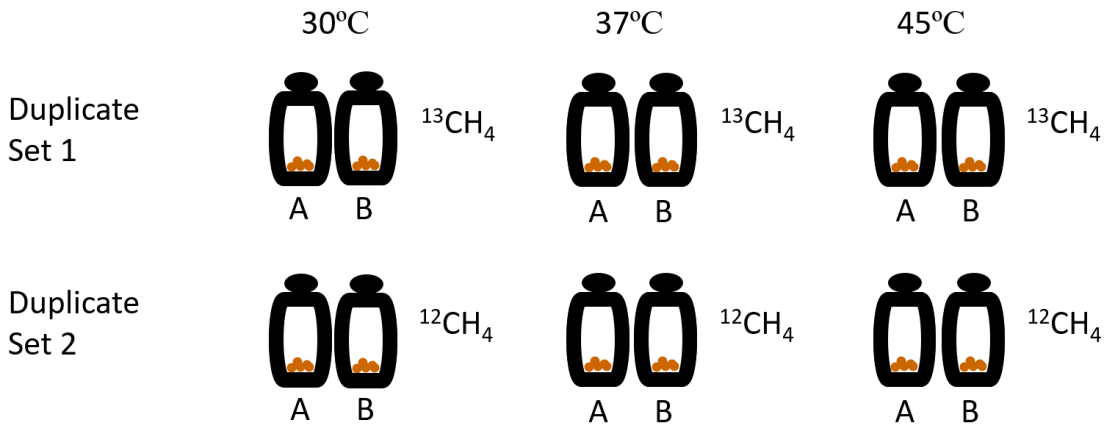

Figure 5.1 DNA-SIP incubations for the 11B/11C boundary core section 0-10 cm soil. The duplicate incubation cultures set up for the $^{13}CH_4$ and $^{12}CH_4$ treatments at each of the three incubation temperatures (30ºC, 37ºC and 45ºC) are shown.

Each incubation culture vial was set up (Chapter 2.11.1-2) with a 5 g soil aliquot prepared from section 0-15 cm of the 19.2.18 soil core. One pair of duplicates for each temperature were then gassed with an incubation volume of 6ml $^{13}CH_4$ into the headspace of each vial (5% of vial volume). The remaining vials were then gassed with an incubation volume of 6 ml $^{12}CH_4$ into the headspace of each vial. The via were then incubated at the appropriate temperatures (30,37 or 45˚C). 1 g timepoint samples were taken and vial re-gassing with 6ml incubation volumes was carried out as described in Chapter 2.11.2, resulting in soil removed from each incubation culture at three timepoints (T1, T2 and T3). The total incubation period lasted ten days. T1 soil was harvested after 4 days, T2 after 7 days and T3 after 10 days.

6 ml was selected for the methane incubation volume as it represents roughly 5% headspace in a 120 ml serum vial and is similar to *in-situ* methane concentrations (typically fed into the biofilter at 5 to 8%). Additionally, Neufeld et al. (2007) recommend labelling the target community with 5-500 µmoles C $gsoil^{-1}$, assuming a 50% incorporation of methane carbon into biomass of methanotrophs (Trimmer, 2015; Whalen, 1990), 6 ml (250 µmoles CH_4) incubation volumes will give 25, 56.3 and 97.9 µmoles C incorporated g $soil^{-1}$ for the T1, T2 and T3 harvested soil respectively. The lower end of the suggested labelling level (5-500 µmoles C $gsoil^{-1}$) was targeted in an attempt to limit the potential labelling of non-methanotrophs through cross-feeding on $^{13}CH_4$ derived ^{13}C containing metabolites and substrates made accessible by initial methanotroph driven oxidation of the $^{13}CH_4$. The duration

of labelling incubation was kept to a maximum of 10 days, with earlier timepoint sampling, to allow identification of the earliest point in the process where labelling of heavy fraction DNA in the $^{13}CH_4$ incubations can be observed (see **Figure 2.4 B**). The aim is to achieve adequate labelling of genuine methane oxidisers, while limiting the opportunity of non-methanotrophic cross-feeders to accumulate label through scavenging (or parasitising) methanotroph ^{13}C labelled metabolites and organic components.

DNA was then extracted from 0.5 g aliquots of soil from each timepoint sample across all vials. The quality of extracted DNA was validated by PCR of *pmoA* (Chapter 2.11.3). DNA (4 μg) extracted from each timepoint sample was then loaded into separate ultracentrifuge tubes containing a CsCl solution and subjected to ultracentrifugation and fractionation to separate out the DNA across a density gradient as outlined in Chapter 2.11.5. This resulted in each of the timepoint DNA extracts being separated out across 12 fractions of decreasing density. Once these fractions were separated, the refractive index (the ratio of the speed of light in a vacuum against the speed of light in the material in question) of each DNA sample was measured for all timepoints. Refractive index was measured across the fractions as a proxy for density which can be technically challenging to measure due to the small volumes of the fractions (Chapter 2.11.4). The DNA from the fractions from each timepoint was then precipitated and quantified as described in Chapter 2.11.5.

By plotting DNA concentration in fractions against refractive indices for each set of 12 fractions corresponding to a given timepoint and comparing the resulting plots for the ^{13}C and ^{12}C incubations at each temperature, the fractions containing heavy (^{13}C labelled) and light (^{12}C labelled) DNA could be identified as explained in Chapter 2.11.5 and Figure 2.5. This was carried out for each timepoint across each temperature treatment. The resulting plots are shown in **Figure 5.2**. By comparing the paired ^{13}C and ^{12}C plots for each timepoint from a given temperature treatment, the degree of ^{13}C labelling across timepoints was observed. Timepoint 2 was the earliest timepoint showing distinct ^{13}C labelling across all three temperature treatments, and was considered a good compromise between sufficient labelling of primary methane oxidisers and limited incubation period to reduce the opportunity for cross-feeders to become labelled with ^{13}C. Therefore, this timepoint was selected for DGGE analysis to confirm the suitability of these samples for 16S rRNA amplicon analysis of the active methanotroph community.

Denaturing gradient gel electrophoresis (DGGE) analysis was carried out on the identified heavy and light fractions from each Timepoint 2 sample as described in Chapter 2.11.6. Briefly, PCR was carried out on DNA from each of the identified heavy and light fractions, using 341GC-clamp and 518R primers (16S rRNA V3 region). The PCR products were then run on DGGE gels which are capable of separating out the amplified products in each PCR reaction based on sequence differences between them (capable of separating sequences with as little as a single base pair difference). This creates a "fingerprint" of the bacterial community for each fraction based on the range and abundance of amplified V3 16S rRNA gene sequences generated from the precipitated DNA. Comparing fingerprints from the ^{13}C-labelled heavy fractions with the ^{13}C-labelled light fractions and the ^{12}C-labelled heavy and light fractions can provide further evidence of the labelling of active community members: Whereas the band pattern was the same across all fractions of ^{12}C-incubations, the appearance of bands in the ^{13}C-labelled heavy fraction that do not appear or are noticeably fainter in all the other fraction fingerprints suggests that these bands belong to active methanotrophs that have incorporated the ^{13}C into their DNA. DGGE gels loaded and run with both the $^{13}CH_4$ and $^{12}CH_4$ heavy and light fraction PCR products from the separate incubation temperatures are shown in **Figures 5.3**, **5.4** and **5.5**, PCR product bands that appear enriched in the ^{13}C heavy fraction lanes are highlighted.

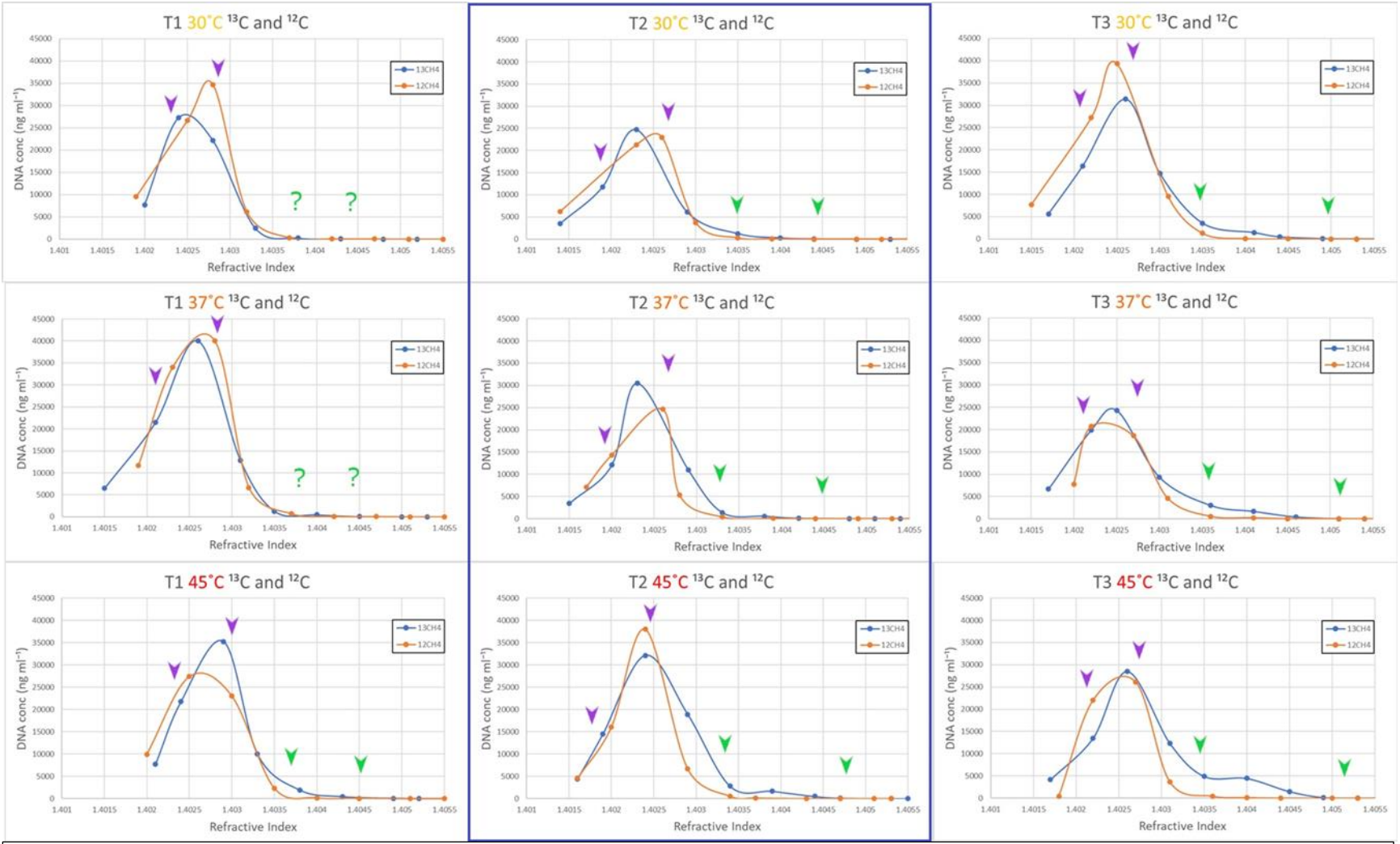

Figure 5.2 DNA concentration vs refractive index plots for the ^{13}C and ^{12}C timepoint samples from the 11B/11C boundary core DNA-SIP experiment. Purple arrows indicate range of "light fractions", while green arrows show the range of "heavy fractions". Green question marks indicate insufficient labelling of the $^{13}CH_4$ fed active community to allow identification of the heavy fraction by comparison with the ^{12}C plot. The blue box highlights the timepoint samples selected for DGGE and amplicon analysis (T2).

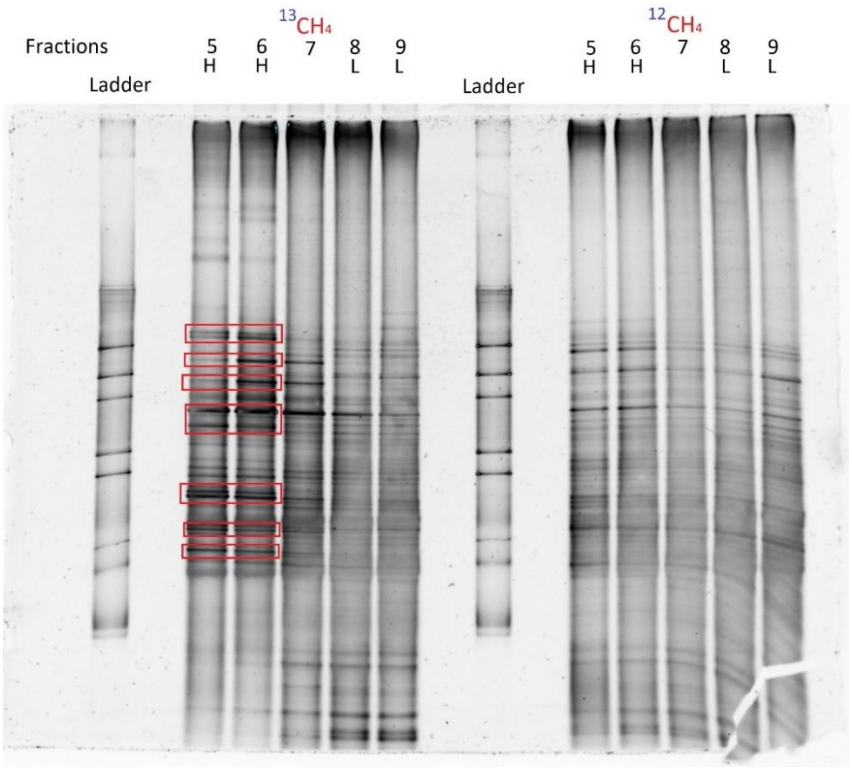

Figure 5.3 11B/11C boundary core DNA-SIP DGGE gel with $^{13}CH_4$ and $^{12}CH_4$ heavy and light fraction PCR products from T2 30˚C. Bands enriched or unique to the ^{13}C heavy fraction (potentially coming from active bacteria metabolising $^{13}CH_4$ derived ^{13}C) are highlighted red

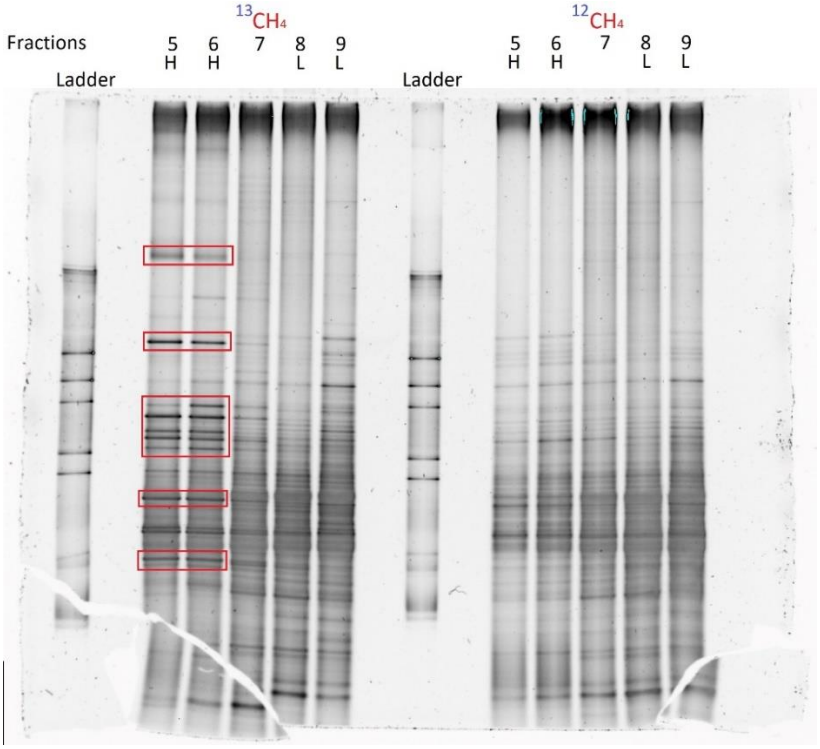

Figure 5.4 11B/11C boundary core DNA-SIP DGGE gel with $^{13}CH_4$ and $^{12}CH_4$ heavy and light fraction PCR products from T2 37˚C. Bands enriched or unique to the ^{13}C heavy fraction (potentially coming from active bacteria metabolising $^{13}CH_4$ derived ^{13}C) are highlighted red

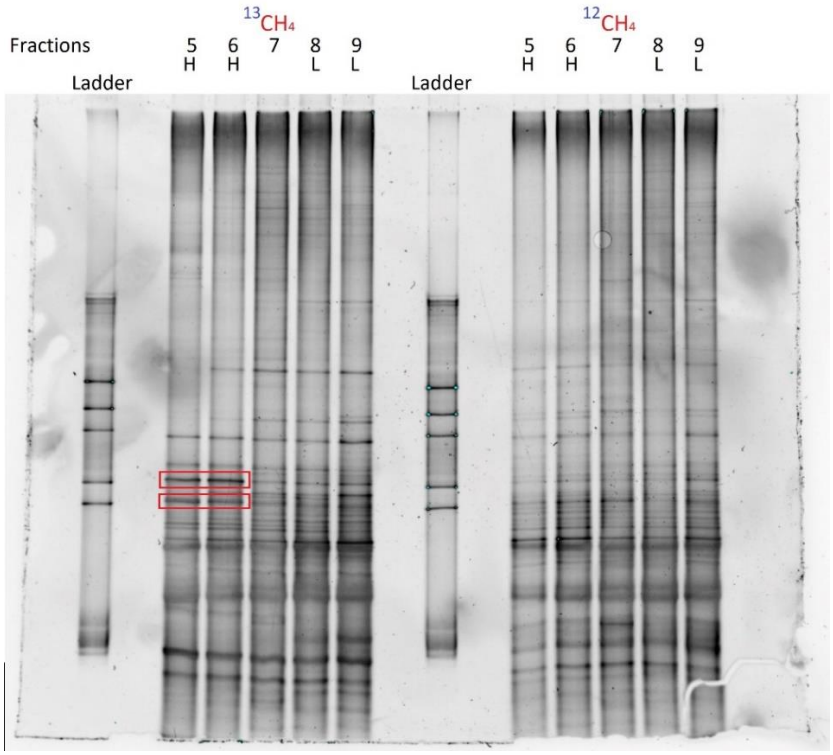

Figure 5.5 11B/11C boundary core DNA-SIP DGGE gel with $^{13}CH_4$ and $^{12}CH_4$ heavy and light fraction PCR products from T2 45˚C. Bands enriched or unique to the ^{13}C heavy fraction (potentially coming from active bacteria metabolising $^{13}CH_4$ derived ^{13}C) are highlighted red

The heavy and light fractions were then pooled separately for each individual Timepoint 2 replicate at the different temperature (30˚C, 37˚C and 45˚C) and CH_4 (^{12}C or ^{13}C) treatments. Care was taken to ensure equal volumes of the separate fractions were used to make up each combined heavy or light fraction mix. Heavy fractions were those with a refractive index range of 1.4048 to 1.4033, light fractions were those with a refractive index range of 1.4028 to 1.4018.

Each pooled light or heavy fraction mix was then used as template for PCR of 16S rRNA genes following the procedure described in Chapter 2.10.2, using 4 µl of heavy fraction mix or 4 µl of light fraction mix (diluted to match heavy fraction mix concentration) as template with PCR modifications: [25µl], [341F and 785R primers], [16S_72]. Six such reactions were carried out for each fraction mix to ensure sufficient PCR product for amplicon sequencing. These replicate PCR reaction products were then combined for each fraction mix. PCR clean-up was then carried out on the fraction mix PCR products using a High Pure PCR product purification kit (Chapter 2.10.6) to both purify and concentrate the PCR products.

20µl of each post-clean-up fraction mix PCR product was then diluted to 20 ng μl^{-1} (or left undiluted if lower than this) and sent for amplicon sequencing with "mrDNA" (Chapter 2.10.9).

5.2.2 16S rRNA amplicon analysis of the ^{13}C labelled community in DNA-SIP incubations at 30°C, 37°C and 45°C using soil from the top 10 cm of the biofilter.

The 16S rRNA amplicon generated using DNA extracted from the microbial community of the 0-10 cm section of the sector 11B/11C boundary core in Chapter 4.4.1 was used as a pre-incubation Timepoint 0 16S rRNA amplicon to supplement this analysis. The resulting 16S rRNA amplicons generated by mrDNA were analysed using DADA2 (**Chapter 2.12.3**). **Figure 5.6** Shows the relative abundance of all microorganisms above a relative abundance of 2%, identified at the genus level or as a strain associated clade in the Timepoint 0 and Timepoint 2 ^{13}C heavy fraction amplicons. The proportion of these most abundant bacteria was very similar within replicates at each temperature treatment, leading to the decision to use the average of replicate abundances for further analysis.

As can be seen, the most abundant bacteria in the T0 amplicon are assigned to the non-methanotrophic *Flavobacterium* genus (almost 37% relative abundance), while the most abundant methanotrophic genera present are *Methylocaldum*, *Crenothrix* and *Methylobacter*, accounting in total for a little over 11% of the methanotroph community when combined. This acts as a very good contrast with the ^{13}C heavy fraction amplicons from each temperature treatment where an enrichment in the active methanotrophs and associated bacteria would be expected due to ^{13}C labelling of DNA. In these enriched fractions, a much greater proportion of the most abundant bacteria belong to known methanotrophic genera: at 30ºC *Methylocella*, *Methylocystis*, *Methylocaldum* and *Crenothrix* (replicate A 38% and replicate B 42%); at 37ºC *Methylocella*, *Methylocystis*, *Methylocaldum* (replicate A 35% and replicate B 22%); and *Methylocaldum* (replicate A 22% and replicate B 35%) at 45ºC. The proportion of these most abundant microbes was similar within replicates at each temperature treatment, leading to the decision to use the average of replicate abundances to identify the enriched (^{13}C labelled) microbes in the $^{13}CH_4$ incubations and for further community analysis.

Bacteria identified in the 16S rRNA amplicon analysis were considered "enriched" and active in the metabolism of CH_4 derived carbon at a given temperature treatment if they met all of the following criteria: The 16S rRNA gene ASV made up at least 1% relative abundance in the ^{13}C heavy fraction amplicon and this relative abundance was at least 10% higher in the ^{13}C heavy fraction amplicon than in the ^{13}C light fraction or the ^{12}C heavy and light fractions. **Figure 5.7** shows all bacteria identified at the genus level or as a strain associated clade present at ≥1% relative abundance in at least one ^{13}C heavy fraction (amplicon replicates averaged). The

bacteria considered enriched at a given temperature incubation are highlighted in the respective ^{13}C heavy fractions. **Figure 5.7** also highlights that there is a stark (but anticipated) difference in bacterial community detected in the ^{13}C heavy fractions (enriched with bacteria labelled with ^{13}C derived from the supplied $^{13}CH_4$) compared with the unlabelled fractions, all of which possess similar bacterial community profiles.

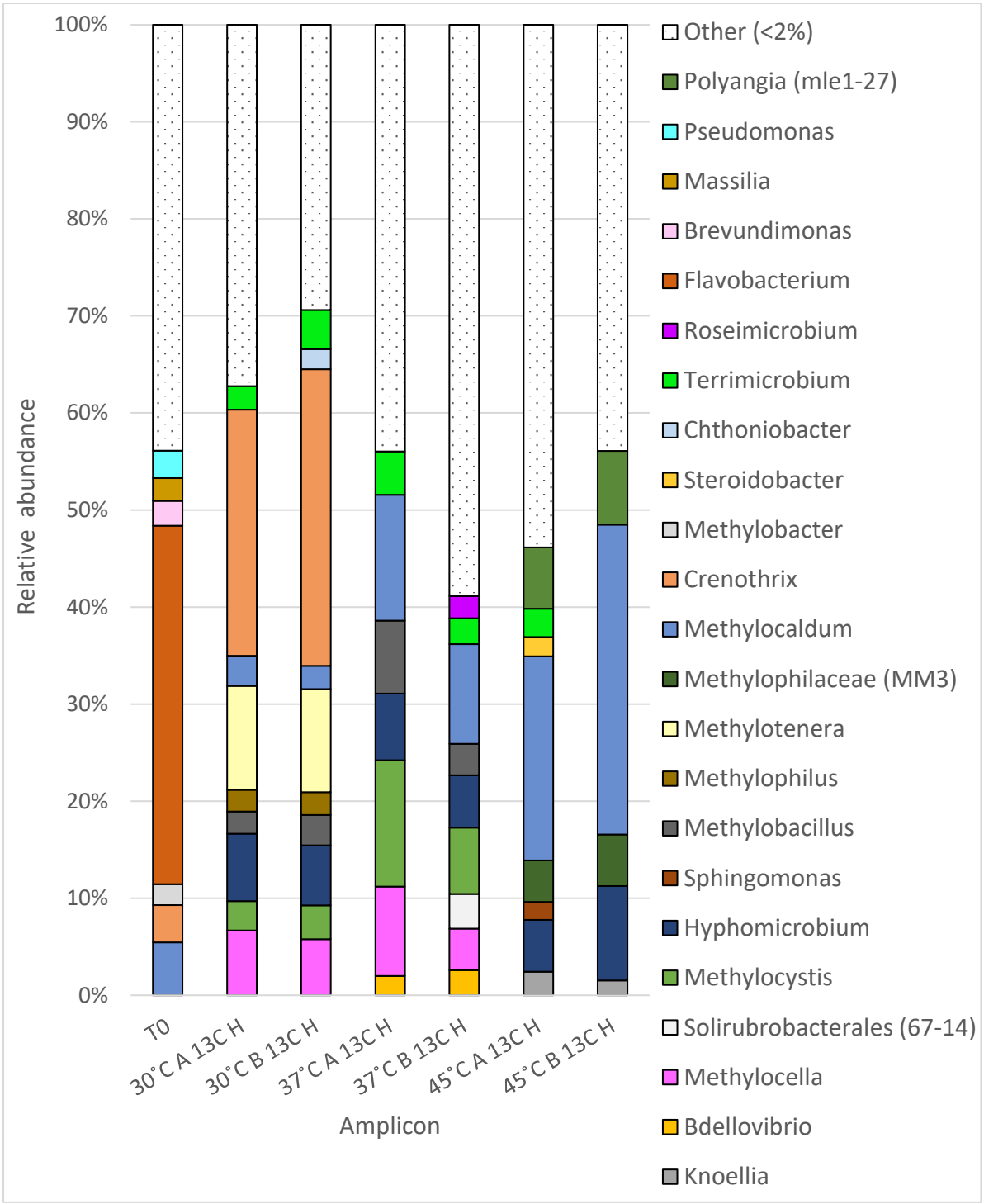

Figure 5.6 Relative abundance of all bacterial 16S rRNA genes above 2% identified at the genus level in the Timepoint 0 and Timepoint 2 ^{13}C heavy fraction amplicons. (11B/11C boundary core DNA-SIP experiment).

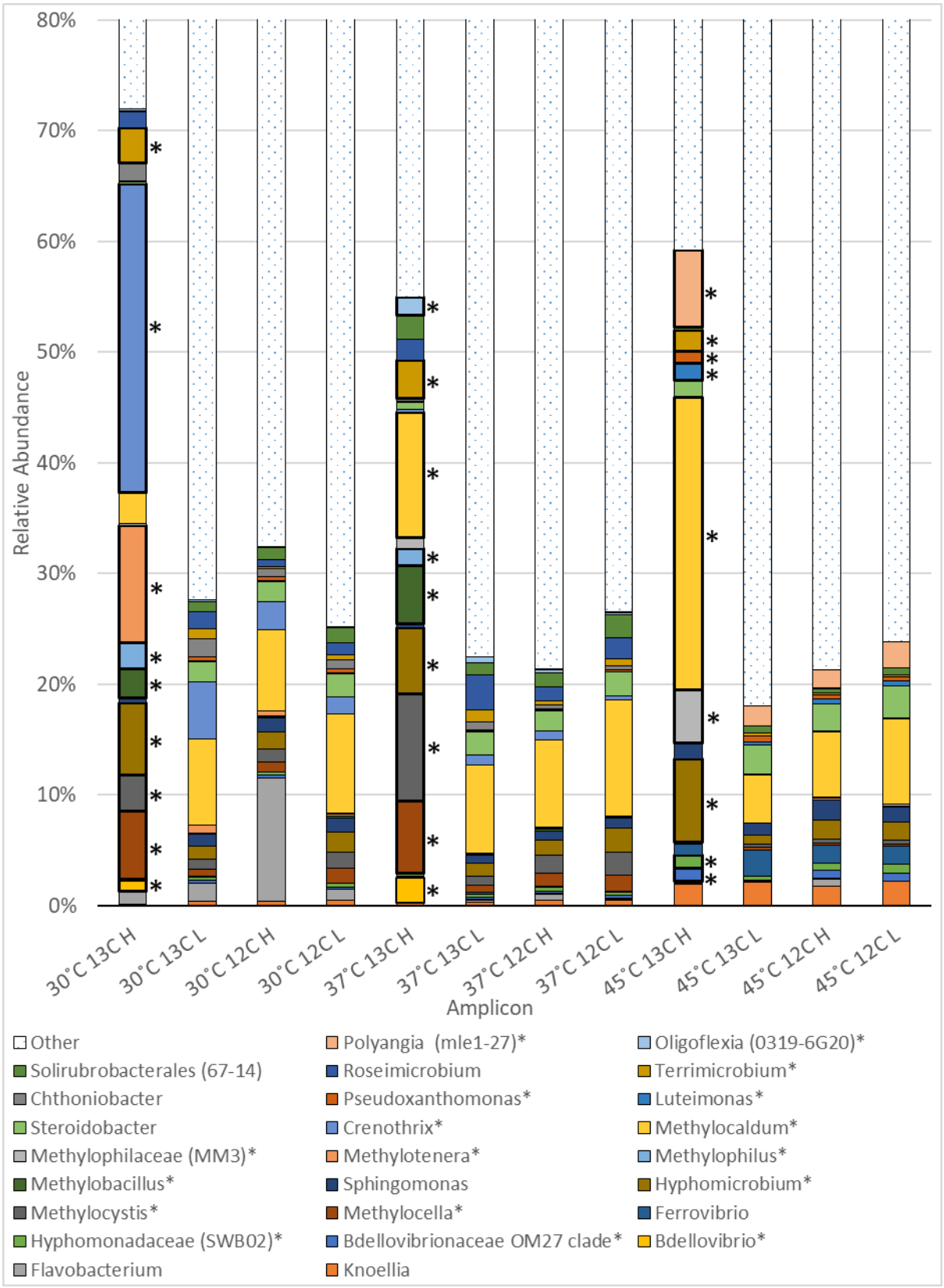

Figure 5.7 11B/11C boundary core DNA-SIP experiment. 16S rRNA gene amplicons showing genera and strain associated clades present at ≥1% relative abundance in at least one of the averaged ^{13}C heavy fraction amplicons. Genera considered enriched at a given temperature incubation are highlighted (*) in the respective ^{13}C heavy fractions.

Genera enriched in the 30ºC ^{13}C heavy fractions (**Figure 5.7**) include the methanotrophs *Crenothrix*, *Methylocella* and *Methylocystis* in addition to the non-methanotrophs *Bdellovibrio*, *Terrimicrobium* (Qiu et al., 2014), bacteria assigned to the Oligoflexia 0319-6G20 clade and the methylotrophs *Hyphomicrobium*, *Methylobacillus*, *Methylophilus*, and *Methylotenera*.

At 37ºC the enriched bacteria in the ^{13}C heavy fraction now includes the Methanotroph *Methylocaldum* as well as *Methylocella* and *Methylocystis*. The non-methanotrophs *Bdellovibrio*, *Terrimicrobium* and methylotrophs *Hyphomicrobium*, *Methylobacillus* and *Methylophilus* again make an appearance as enriched genera.

At the higher incubation temperature of 45ºC the only methanotroph that appears enriched in the ^{13}C heavy fractions is *Methylocaldum*, while the enriched non-methanotrophic methylotrophs *Hyphomicrobium* and *Methylophilaceae* (MM3) clade are joined by bacteria assigned to the *Bdellovibrionaceae* OM27 clade, *Terrimicrobium*, *Luteimonas*, the Polyangia (mle1-27) clade, *Pseudoxanthomonas* and the *Hyphomonadaceae* (SWB02) clade.

After analysing community members identified at the genus level, all ASVs that could not be resolved down to the genus level were compared across the averaged replicates of the ^{13}C and ^{12}C heavy and light amplicons from each incubation temperature, those that individually passed the same "enrichment criteria" laid out above were also considered to belong to active microorganisms metabolising CH_4 Carbon, these are shown alongside the previously identified enriched genera in **Table 5.1**.

The "enrich. diff." or "enrichment difference" column in **Table 5.1** shows the change in % relative abundance between the ^{13}C heavy fractions compared with the closest value observed across the other fractions for each genus or ASV considered enriched at each of the incubation temperatures used. This serves as an indicator of the degree of DNA incorporation of CH4-derived ^{13}C for each genus or ASV. This suggests that the most active of the enriched methanotrophs at 30ºC was *Crenothrix*, at 37ºC *Methylocystis* and at 45ºC *Methylocaldum*. There is also a fairly significant enrichment of the methylotrophs *Methylotenera* at 30ºC and *Hyphomicrobium* at 45ºC. **Table 5.1** highlights several bacterial 16S rRNA ASVs of unknown genera that appear to be enriched in the ^{13}C heavy fractions, although only the *Methyloligellaceae* family are known to contain methanotrophs (Vekeman et al., 2016), and are likely cross-feeders.

Table 5.1 Taxa enriched in the heavy fractions of the 30ºC, 37ºC and 45ºC $^{13}CH_4$ incubations, Relative abundance (%) shown for the heavy and light amplicons from each methane treatment (^{13}C and ^{12}C) at all temperatures (30ºC, 37ºC and 45ºC). The difference in relative abundance between the ^{13}C heavy and the next highest abundance from the other fractions is also included. The Relative abundance (%) values of these taxa in the Unfractionated T0 Amplicon are also shown for comparison purposes.

		30°C					37°C					45°C					T0
		13C H	13C L	12C H	12C L	enrich diff.	13C H	13C L	12C H	12C L	enrich diff.	13C H	13C L	12C H	12C L	enrich diff.	Unfractio-nated
Methanotroph genera	*Methylocella*	**6.23**	0.71	0.93	1.43	**4.80**	**6.82**	0.66	1.22	1.49	**5.33**	0.14	0.26	0.25	0.27		0.70
	Methylocystis	**3.25**	0.90	1.18	1.40	**1.86**	**10.05**	0.87	1.69	2.15	**7.90**	0.06	0.35	0.35	0.37		0
	Methylocaldum	2.76	7.83	7.42	9.12		**11.82**	8.08	7.92	10.69	**1.13**	**28.51**	4.46	5.96	7.92	**20.59**	5.45
	Crenothrix	**27.97**	5.23	2.56	1.57	**22.73**	0.31	0.91	0.85	0.41		0.07	0.06	0.14	0.09		3.84
	Bdellovibrio	**1.01**	0.02	0.01	0	**0.99**	**2.34**	0.10	0.07	0.03	**2.24**	0.20	0.04	0.06	0.01		0
	Bdellovibrionaceae OM27 clade	0.02	0.23	0.20	0.22		0.13	0.22	0.22	0.29		**1.23**	0.13	0.73	0.71	**0.50**	0
	Hyphomonadaceae (SWB02)	0.02	0.32	0.29	0.32		0.18	0.30	0.29	0.33		**1.28**	0.37	0.67	0.82	**0.47**	0
	Hyphomicrobium	**6.56**	1.20	1.56	1.84	**4.72**	**6.23**	1.17	1.31	2.20	**4.03**	**8.11**	0.80	1.72	1.61	**6.39**	0
	Methylobacillus	**2.72**	0.13	0.13	0.15	**2.57**	**5.43**	0.14	0.17	0.09	**5.26**	0.02	0.03	0.08	0.06		0
	Methylophilus	**2.29**	0	0.06	0	**2.24**	**1.59**	0.00	0.06	0.02	**1.53**	0	0	0	0		0
	Methylotenera	**10.65**	0.67	0.45	0.21	**9.98**	0.02	0.02	0.05	0.01		0.02	0	0.10	0		0.78
	Methylophilaceae (MM3)	0.22	0.07	0.04	0.06		0.99	0.05	0.10	0.06		**5.15**	0.04	0.18	0.18	**4.96**	0
	Luteimonas	0	0.10	0.14	0.11		0.01	0.04	0.10	0.09		**1.62**	0.20	0.51	0.41	**1.10**	0
	Pseudoxanthomonas	0.03	0.40	0.33	0.36		0.05	0.15	0.14	0.14		**1.15**	0.59	0.40	0.40	**0.56**	0.44
	Polyangia (mle1-27)	0.03	0.05	0.04	0.05		0.02	0.04	0.01	0.06		**7.50**	1.79	1.68	2.47	**5.02**	0
	Oligoflexia (0319-6G20)	0.01	0	0	0		**1.75**	0.52	0.30	0.21	**1.24**	0	0	0	0		0.03
	Terrimicrobium	**3.23**	0.97	0.18	0.47	**2.26**	**3.61**	1.12	0.38	0.62	**2.49**	**2.09**	0.24	0.17	0.16	**1.85**	0.42
individual ASVs identified as enriched	*Gemmatimonadaceae*	0.22	0.07	0.08	0.05		0.47	0.06	0.18	0.18		**1.22**	0.14	0.31	0.38	**0.84**	0
	Gemmatimonadaceae	0	0	0	0		0.02	0	0.01	0.03		**1.05**	0.14	0.64	0.40	**0.41**	0
	Gemmatimonadaceae	0.12	0.10	0.14	0.07		0.44	0.10	0.21	0.16		**1.58**	0.19	0.39	0.38	**1.20**	0.13
	Phycisphaeraceae	0.14	0	0.02	0.06		**1.88**	0.03	0.12	0.19	**1.69**	0.07	0.04	0.09	0.11		0
	Tepidisphaerales WD2101 soil group	0.08	0.35	0.25	0.31		**1.19**	0.72	0.50	0.77	**0.42**	0.25	0.45	0.37	0.39		0
	Methyloligellaceae	**1.01**	0.51	0.63	0.75	**0.26**	**1.58**	0.40	0.55	0.77	**0.81**	0.19	0.43	0.28	0.44		0.19
	Methyloligellaceae	**1.01**	0.38	0.58	0.59	**0.42**	**1.15**	0.36	0.49	0.51	**0.64**	0	0.27	0.26	0.26		0
	Rhodospirillales	**3.55**	0.07	0.15	0.10	**3.40**	0.03	0	0.02	0.02		0	0	0.04	0		0.48
	Methylophilaceae	**1.31**	0.01	0.03	0	**1.28**	0	0	0	0		0	0	0	0		0.08
	Sutterellaceae	0.08	0.12	0.10	0.14		0.44	0.19	0.21	0.27		**2.09**	0.28	0.51	0.61	**1.49**	0

Methylocaldum is a gammaproteobacterial genus of thermotolerant methanotrophs with several members capable of growth at over 60°C and incapable of growing below 30ºC (Takeuchi et al., 2014 b), The *Methylocaldum* present in these incubations fit such a thermotolerant profile, being the sole active methanotroph in the 45ºC incubations, still an active member of the methanotroph community at 37ºC but do not appear to be competitive at the lowest temperature (30ºC). *Crenothrix* have been identified as potentially facultative methanotrophs containing a phylogenetically distinct *pmoA* sequence (Stoecker, 2006). An example of this genus has yet to be isolated in pure culture, but they have been detected in a range of environments including arctic peat, temperate lake water and subtropical agricultural soil (one of the warmest environments where this methanotroph appeared abundant) (Dorr et al., 2010; Oswald et al., 2017; Rainer et al., 2020). If *Crenothrix* prefer lower-mesophilic and colder conditions, then the absence of this genus from the active methanotroph community in the higher temperature incubations (37 and 45ºC) is unsurprising. The genus *Methylocystis* contains facultative and obligate methanotrophs belonging to the *Alphaproteobacteria*. They are mesophilic bacteria capable of growth at 4-40°C (Belova, 2013; Tikhonova, 2021), which fits with their observed activity in the 30 and 37ºC incubations. *Methylocella* are facultative alphaproteobacterial methanotrophs which contain only the soluble methane monooxygenase (Dedysh, 2004). Isolates belonging to this genus grow at temperatures over the range of 4-30ºC (Dedysh, 2004) so the indication that one or more members of this genus were active methanotrophs in the 37ºC $^{13}CH_4$ incubation is noteworthy. One limitation in identifying the actively methane-oxidising methanotrophs from these results is that many of the methanotrophs labelled with ^{13}C at the different temperatures are potentially facultative. Their ability to grow on substrates other than methane means they cannot be definitively identified as the primary methane oxidisers, although they remain potential candidates.

Amongst the individual enriched ASVs that could not be identified at the genus level, the two ASVs assigned to the *Methyloligellaceae* family are of particular interest as this family has been found to contain the facultative methanotroph *Methyloceanibacter* species containing sMMO (Vekeman et al., 2016) as well as non-methanotrophic methylotrophic genera (Takeuchi et al., 2014a). This suggests that these bacteria may have become labelled either through direct methanotrophy or cross-feeding on ^{13}C labelled products of methane oxidation (such as methanol) or central metabolism from other (methanotrophic) bacteria. An example of this cross-feeding capability was observed in a study by Takeuchi et al where a

Methyloceanibacter species was thought to be cross-feeding on acetate from a *Methylocaldum* when co-cultured (Takeuchi et al., 2019).

Cross-feeding is a very likely explanation for the labelling of the various non-methanotrophs detected in these incubations; either through incorporation of methanotroph mediated $^{13}CH_4$ oxidation products such as methanol, formaldehyde and formate as well as ^{13}C labelled DNA and metabolic products originating from the active methanotrophs. This would also account for the ^{13}C labelling of numerous non-methanotrophic methylotrophs as they could be expected to exploit these methane oxidation products for their own growth, as they share similar metabolic pathways for the oxidation and metabolism of methanol, formaldehyde and formate with the methanotrophs (lacking only the capability to catalyse the initial CH_4 oxidation step) (Chistoserdova, 2011). Crossfeeding by methylotrophs and other bacteria has been observed in many $^{13}CH_4$ DNA-SIP labelling experiments ostensibly targeting methanotrophs (Deng et al., 2016; Dumont et al., 2011; Yang et al., 2022) suggesting that the active methanotrophs support a wider community of microbes which cannot directly utilize CH_4. Interestingly, the methylotrophic genus *Methylotenera*, which possessed the largest "enrichment difference" in the 30ºC incubations, was determined to be a cross-feeding "early responder" following CH_4 addition in microcosms containing methanotrophs in a study by Oskin et al (Oshkin et al., 2015). This and other highly enriched methylotrophs such as *Hyphomicrobium*, *Methylobacillus* and the clade associated with *Methylophilaceae* sp. MM3, isolated and identified as an obligate methylotroph *Methylobacillus* species by Macey et al, (Macey et al., 2018) may potentially support methanotrophic growth by preventing build-up of toxic intermediates such as methanol or formaldehyde (Grinsven, 2021).

While the scavenging of ^{13}C containing compounds such as methanol, acetate or sugars released by living or dead methanotrophs may account for most non-methanotroph crossfeeding and labelling in this experiment, some of the bacteria labelled in this experiment may have obtained their ^{13}C label through direct predation of the active methanotrophs present. *Bdellovibrio* are predatory bacteria (Koval et al., 2013; Lovering and Sockett, 2021), and have previously been found labelled with ^{13}C in $^{13}CH_4$ DNA-SIP experiments where they were suspected to be cross-feeding via predation of labelled methanotrophs (Morris et al., 2002). The uncultured OM27 clade bacteria are also thought to be members of the *Bdellovibrionaceae* (Gorokhova et al., 2021) and were identified as possibly predatory bacteria in a DNA-SIP where members of this clade became labelled with ^{13}C (Orsi et al., 2015). The Oligoflexia (0319-6G20) is a member of the wider Bdellovibrionota phylum (alongside *Bdellovibrio* and

the OM27 clade) which is known for its predatory members (Li et al., 2021). In addition, the Polyangia (Mle1-27) clade which appeared to accumulate a moderate amount of the ^{13}C label in the 45ºC incubation (**Table 5.1**) falls within the phylum Myxococcota, which is another phylum with many known predatory members (Waite, 2020).

5.3 $^{13}CH_4$ DNA-SIP investigation of the active methanotrophs at 50ºC and 37ºC using soil samples from hot (50ºC) zone of the biofilter at a depth of 50 cm

Further study of methanotrophic activity and *in-situ* temperature and gas measurements within the biofilter (**Chapter 3**) demonstrated significant methane removal occurring at greater depths and higher temperatures than the 0-10cm initially explored with DNA-SIP (of particular interest were the high temperatures seen at 50cm depth >50 ºC **Table 3.3**). Therefore, it was decided to explore the active methane metabolising community deeper in the biofilter at a hotter *in-situ* temperature, through a second $^{13}CH_4$ DNA-SIP experiment targeting this active region of the biofilter and incubated the soil at *in-situ* temperature.

5.3.1 $^{13}CH_4$ DNA-SIP incubation of soil from a 50 cm deep hot zone (50ºC) of the biofilter at 37°C and 50°C

Soil was sampled with a spade (to allow retrieval of a greater amount of soil) (**Chapter 2.7.1**) at a depth of 50 cm from biofilter sector B19 on 26.6.20 (**Chapter 3.3.7**) and the *in-situ* temperature of 50ºC (measured with a temperature probe (**Chapter 2.3.2**)) was used as an initial indicator of methanotrophic activity. The methane oxidation potential of this soil was assessed and found to be a respectable 2.61 μmoles h^{-1} g $soil^{-1}$ and the soil moisture content measured 25.76% , to confirm the presence of active methanotrophs and that the soil moisture was in the optimal range (10-27.5%) **(Chapter 3.3.7**).

Soil was then prepared for DNA-SIP incubation according to (**Chapter 2.11.1**-**2.11.2**) with three replicate sets of $^{13}CH_4$ and $^{12}CH_4$ fed incubation cultures set up for incubation at 37˚C and the same number for 50˚C (**Figure 5.8**), although no sterile dH_2O was added at the start of the incubation as the soil moisture was already at the upper end of the optimal range.

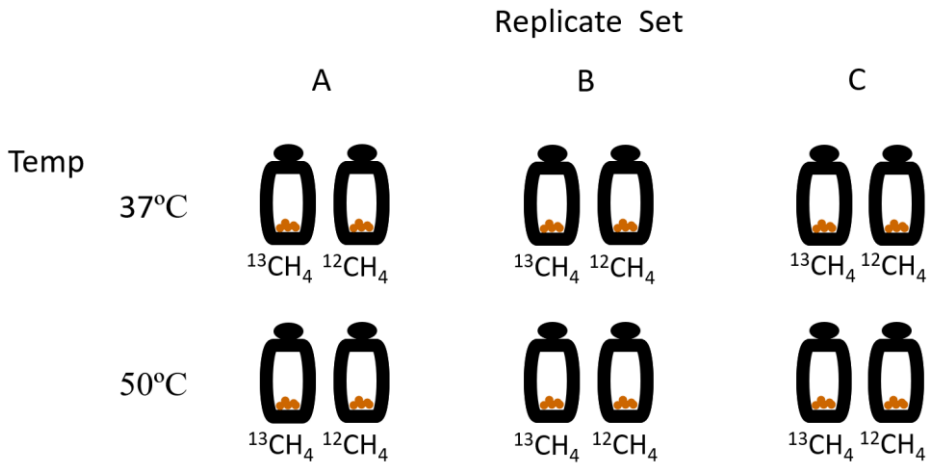

Figure 5.8 Incubations set up for B19 soil DNA-SIP. The triplicate incubation cultures set up for the $^{13}CH_4$ and $^{12}CH_4$ treatments at two incubation temperatures (37ºC and 50ºC) are shown.

In addition, three pre-incubation T0 soil samples were retained and stored at -20˚C. Each 120 ml incubation vial contained a 10 g soil aliquot and was fed with 5.4 ml (4.5% headspace) of the ^{13}C- or ^{12}C-methane. Due to the larger mass of soil in these incubations, two incubation volumes of CH_4 were allowed to be consumed before each timepoint soil harvesting. This resulted in the following incubation regimen: 5.4 ml CH_4, 5.4 ml CH_4, Timepoint 1 soil harvesting (1.45 g) 5.4 ml CH_4, 5.4 ml CH_4, Timepoint 2 soil harvesting (1.8 g), 5.4 ml CH_4, 5.4 ml CH_4, Timepoint 3 soil harvesting (6.75 g). Based on the same carbon conversion efficiency estimate for the active methanotrophs (50%) as used in the previous DNA-SIP (**Chapter 5.2.1**), Timepoint samples T1, T2 and T3 should have 22.5, 48.8 and 82.1 µmoles C incorporated g $soil^{-1}$ respectively.

DNA extractions were then carried out on 0.45 g soil for each timepoint sample across all vials, as well as on the retained T0 soil which additionally underwent humic acid removal (Zymo kit). The quality of extracted DNA was validated through PCR of *pmoA* genes (Chapter 2.11.3).

4 µg of DNA from each T1, T2 and T3 timepoint sample was then separated in density gradients via CsCl ultracentrifugation and fractionated into 12 fractions as outlined in Chapter 2.11.5. Once these fractions of decreasing density were separated, the refractive index of each was measured (Chapter 2.11.4). The DNA from the separated fractions from each timepoint was next precipitated and quantified as described in Chapter 2.11.5.

The heavy (^{13}C labelled) and light (^{12}C labelled) DNA fractions were identified as described in Chapter 2.11.5 and Figure 2.5, by plotting fraction DNA concentrations against refractive indices for each set of 12 fractions corresponding to a given timepoint and comparing the overlaid plots for the ^{13}C and ^{12}C incubations at each temperature. The DNA concentration vs RI graphs for each timepoint for both incubation temperatures are shown in **Figure 5.9**.This allowed identification of the earliest timepoint demonstrating ^{13}C labelling across both temperatures (timepoint 3).

Denaturing gradient gel electrophoresis (DGGE) analysis was carried out on the Timepoint 2 and Timepoint 3 heavy and light fractions from each DNA sample as described in **Chapter 2.11.6**. 16S rRNA V3 PCR products were generated from each DNA sample and run on DGGE gels. The resulting "fingerprints" of PCR products for the $^{13}CH_4$ and $^{12}CH_4$ heavy and light fractions from the 37ºC and 50ºC incubations are shown in **Figures 5.10** and **5.11**, PCR bands that appear enriched in the ^{13}C heavy fraction lanes are highlighted.

Based on observations from the DNA concentration vs RI graphs (**Figure 5.9**) and DGGE gels (**Figures 5.10** and **5.11**): Heavy fractions were defined as all fractions from the second fraction down (Refractive Index approximately 1.4050-1.4055) to a Refractive Index value of 1.4035. Light fractions are those with refractive index values from 1.4029 to 1.4015.

Heavy and light fraction DNA was pooled separately for each replicate at the three timepoints. Care was taken to ensure equal volumes of the separate fractions were used to make up each combined heavy or light fraction mix. Light and heavy fraction mixes along with the unfractionated T0 DNA were then used as templates for 16S rRNA PCR following the procedure in Chapter 2.10.2, using 2ng of DNA as template with PCR modifications: [25 µl], [341F and 785R primers], [16S_72]. Four such reactions were carried out and the products combined for each fraction mix and the T0 DNA, to ensure sufficient PCR product for amplicon sequencing. PCR products then underwent PCR clean-up and were concentrated using a High Pure PCR product purification kit (Chapter 2.10.6), before they were shipped to mrDNA for 16S rRNA gene amplicon sequencing.

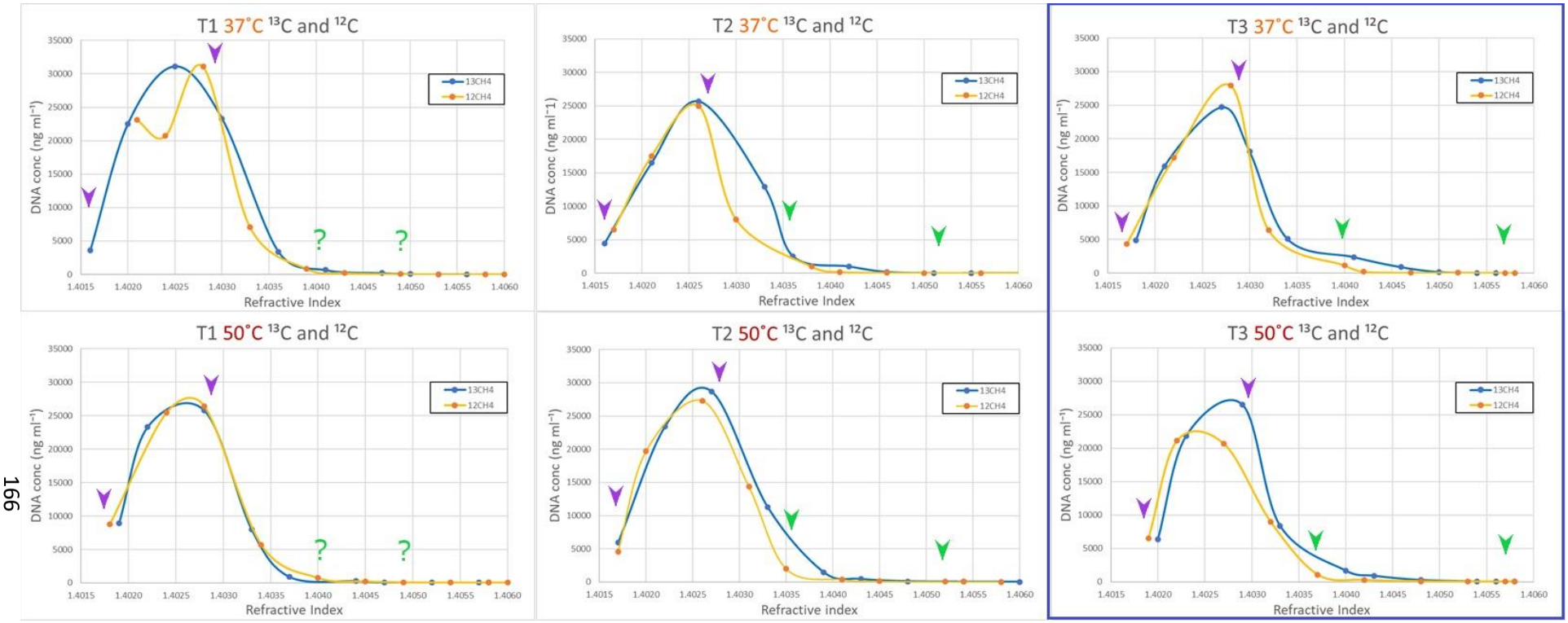

Figure 5.9 DNA concentration vs refractive index plots for the ^{13}C and ^{12}C Timepoint sample DNA fractions from the sector B19 soil DNA-SIP experiment. Purple arrows indicate range of "light fractions", while green arrows show the range of "heavy fractions". Green question marks indicate insufficient labelling of the $^{13}CH_4$ fed active community to allow identification of the heavy fraction by comparison with the ^{12}C plot. The blue box highlights the Timepoint samples selected for DGGE and amplicon analysis (T3).

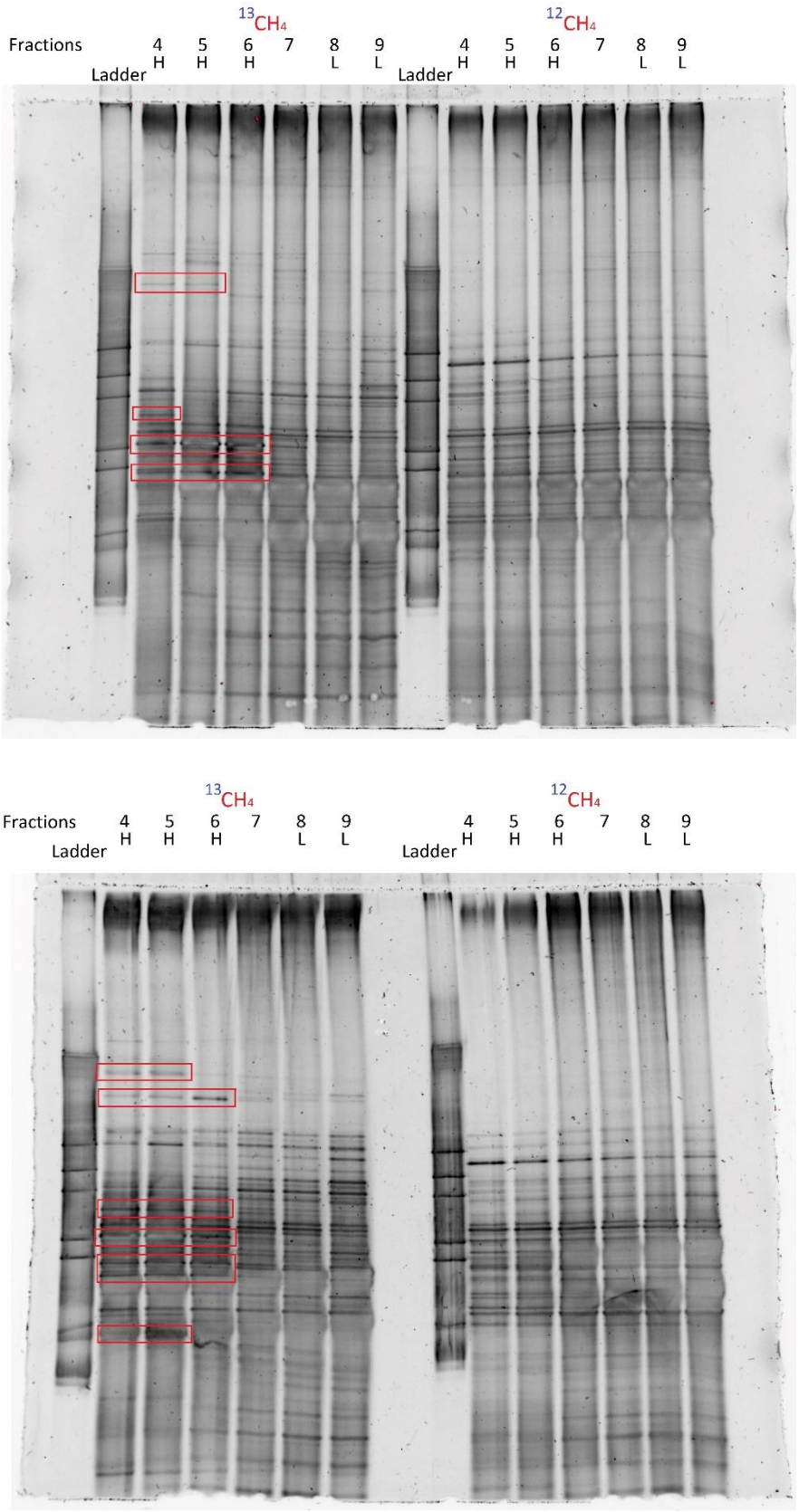

Figure 5.10 B19 soil DNA-SIP DGGE gel with $^{13}CH_4$ and $^{12}CH_4$ heavy and light fraction PCR products from T2 (top) and T3 (bottom) 37˚C fraction DNA. Bands enriched or unique to the ^{13}C heavy fraction (potentially coming from active bacteria metabolising $^{13}CH_4$ derived ^{13}C) are highlighted in red. Note the increased enrichment in T3.

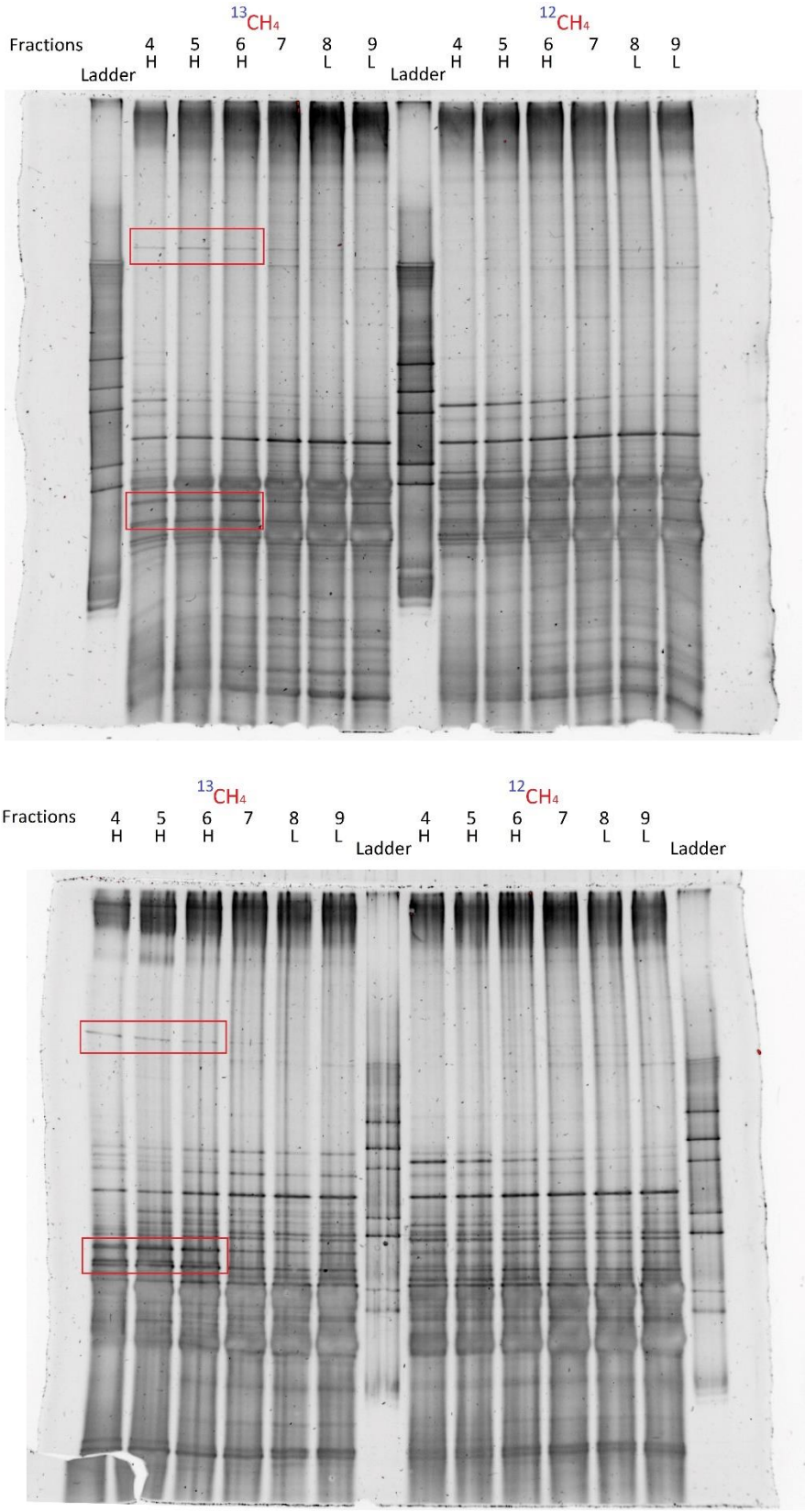

Figure 5.11 B19 soil DNA-SIP DGGE gel with $^{13}CH_4$ and $^{12}CH_4$ heavy and light fraction PCR products from T2 (top) and T3 (bottom) 50˚C fraction DNA. Bands enriched or unique to the ^{13}C heavy fraction (potentially coming from active bacteria metabolising $^{13}CH_4$ derived ^{13}C) are highlighted in red. Note the increased enrichment in T3.

5.3.2 16S rRNA amplicon analysis of the ^{13}C labelled community in DNA-SIP incubations at 37°C and 50°C using soil from a hot 50ºC and deep 50 cm region of the biofilter.

The resulting 16S rRNA gene amplicons from (**Chapter 5.3.1**) were analysed using DADA2 (**Chapter 2.12.3**). (**Figure 5.12**) shows the relative abundance of all microorganisms above 2% identified at the genus or strain associated clade level in the Timepoint 0 and Timepoint 3 ^{13}C heavy fractions. Much like the first DNA-SIP experiment, the communities revealed by amplicon analysis were very similar between incubation treatment replicates and so these were averaged for further analysis.

Methanotrophs detected above 2% relative abundance included *Methylobacter* in the 37ºC ^{13}C heavy fractions; *Methyloterricola* in the 50ºC ^{13}C heavy fractions and one of the T0 amplicons; and *Methylocaldum* in all the T0 and ^{13}C heavy fractions. In accord with the first DNA-SIP experiment (**Chapter 5.2**) many of the other abundant genera in these amplicons contain members capable of growth on methanol including the *Methylophilaceae* (MM2) and (MM3), *Hyphomicrobium*, *Sphingomonas*, *Bacillus* (Schendel, 1990) and *Filomicrobium* (Wu, 2009).

The same enrichment criteria as discussed earlier (**Chapter 5.2.2**) were also applied to these amplicons. **Figure 5.13** displays genera present at ≥1% relative abundance in at least one ^{13}C heavy fraction (amplicon replicates averaged). Genera identified as enriched at each temperature are highlighted in the respective ^{13}C heavy fractions.

Two genera were identified as enriched in the 50ºC ^{13}C heavy fractions, *Methylocaldum* and *Methyloterricola*, both of which are known methanotrophs.

The genus *Methyloterricola* contains one known species *Methyloterricola oryzae*, the type species is strain 73a and is a mesophilic methanotroph with a temperature growth range of 15-45ºC (Frindte et al., 2017).

The methanotrophs *Methylobacter* and *Methylocystis* were found to be enriched in the 37ºC ^{13}C heavy fractions alongside the non-methanotrophic genera *Pseudoxanthomonas* and *Methylophilaceae* (MM2) and (MM3) clades.

Enriched ASVs of unassigned genera were also identified in the heavy fractions of the 37ºC $^{13}CH_4$ fed incubations, as well as a sole *Methylocaldum* ASV which was found to be enriched in the 37ºC $^{13}CH_4$ incubations (this ASV also made up a large proportion of the *Methylocaldum* 16S rRNA sequences in the 50ºC heavy fraction). The relative abundances of these and the enriched genera are shown for the heavy, light and unfractionated amplicons from each methane treatment (^{13}C and ^{12}C) at both temperatures (37ºC and 50ºC) in **Table 5.2**.

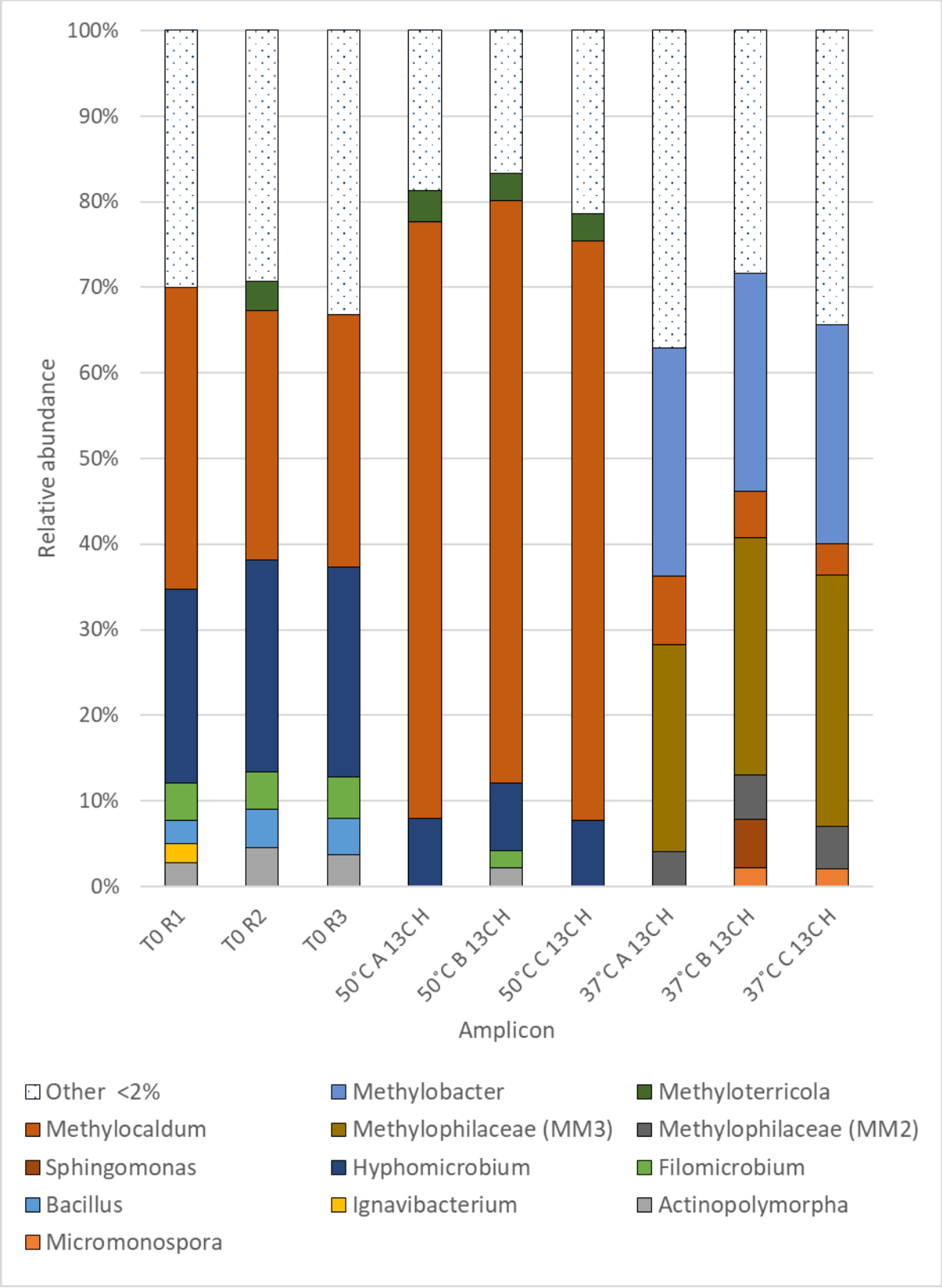

Figure 5.12 Relative abundance of all bacterial 16S rRNA genes above 2% identified at the genus and strain associated clade level in the Timepoint 0 and Timepoint 3 ^{13}C heavy fraction amplicons, from the sector B19 soil DNA-SIP experiment. Note similarity between replicates.

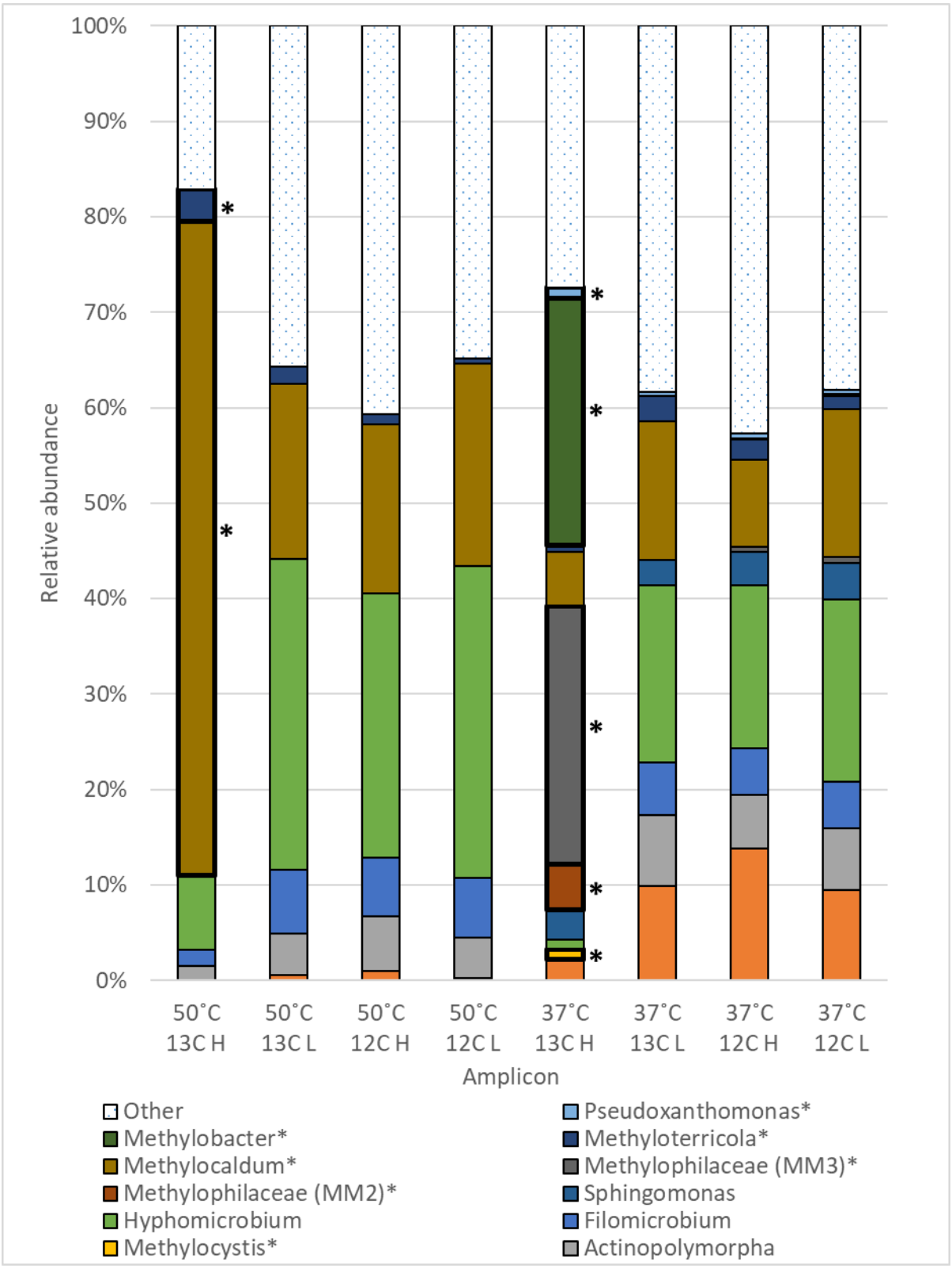

Figure 5.13 Sector B19 soil DNA-SIP experiment. Genera and strain associated clades present at ≥1% relative abundance in at least one of the averaged ^{13}C heavy fraction amplicons. Genera considered to be enriched at a given incubation temperature are highlighted (*) in the respective ^{13}C heavy fractions.

Table 5.2 Enriched genera, strain associated clades and individual ASVs of unknown genera in the heavy fractions of the 50°C and 37°C $^{13}CH_4$ fed incubations, Relative abundance (%) shown for the heavy and light amplicons from each methane treatment (^{13}C and ^{12}C) at both temperatures (37°C and 50°C). The difference in relative abundance between the ^{13}C heavy and the next highest abundance from the other fractions is also included. The average Relative abundance (%) of these taxa across the Unfractionated T0 Amplicons are also shown for comparison purposes. * While overall 16S rRNA gene sequences belonging to members of the *Methylocaldum* genus were not enriched in the 37°C heavy fraction, a single ASV (which was also enriched in the 50°C heavy fraction) was identified as enriched at 37°C.

		50°C					**37C**					**T0**
		13C H	13C L	12C H	12C L	enrich diff.	13C H	13C L	12C H	12C L	enrich diff.	Unfractionated
Methanotroph genera	*Methylocystis*	0	0	0	0		**1.09**	0	0	0	**1.09**	0
	Methylocaldum	**68.49**	18.26	17.69	21.24	**47.26**	5.70*	14.54	9.06	15.44		31.27
	Methyloterricola	**3.34**	1.81	1.01	0.52	**1.53**	0.61	2.65	2.17	1.42		2.30
	Methylobacter	0	0	0	0		**25.96**	0	0.12	0.15	**25.81**	0
	Methylophilaceae (MM2)	0	0	0	0		**4.78**	0	0	0	**4.78**	0
	Methylophilaceae (MM3)	0	0	0	0		**27.03**	0	0.60	0.66	**26.37**	0
	Pseudoxanthomonas	0	0	0	0		**1.08**	0.43	0.50	0.49	**0.58**	0
Individual ASVs identified as enriched	*Methylophilaceae*	0	0	0	0		**1.45**	0	0	0.34	**1.11**	0
	Methylophilaceae	0	0	0	0		**1.13**	0	0	0	**1.13**	0
	Methylophilaceae	0	0	0	0		**2.60**	0	0	0	**2.60**	0
	Methylomonadaceae	0	0	0	0		**1.25**	0	0	0	**1.25**	0
	Methylomonadaceae	0	0	0	0		**1.06**	0	0	0	**1.06**	0
	Methylomonadaceae	0	0	0	0		**1.14**	0	0.15	0	**0.98**	0
	Methylomonadaceae	0	0	0	0		**2.49**	0	0	0	**2.49**	0
	* 50 and 37°C enriched *Methylocaldum* ASV	**[18.74]**	0.94	2.86	1.77	**15.88**	**[3.54]***	0.25	1.06	1.10	**2.44**	[2.04]

Based on the enrichment values in **Table 5.2** *Methylocaldum* is the most active methanotroph in the 50ºC incubations. In the 37ºC incubations, *Methylobacter* is the most active methanotroph and the *Methylophilaceae* (MM3) clade also demonstrated a high degree of DNA labelling with $^{13}CH_4$-derived ^{13}C. This clade is centred on the obligate methylotrophic MM3 *Methylobacillus* isolate recovered from grassland soil by Macey et al (Macey et al., 2018). While the genus *Methylocaldum* was not enriched overall at 37ºC, a single *Methylocaldum* 16S rRNA ASV was found to meet the enrichment criteria in the 37ºC heavy fraction. This ASV was highly enriched in the 50ºC incubation, suggesting that the *Methylocaldum* strain of origin is an active methane oxidiser over a broad temperature range 37-50ºC. The 37ºC ^{13}C heavy fraction also contained enriched ASVs belonging to the families *Methylomonadaceae* which consists of methanotrophic genera and unassigned species of the methylotrophic *Methylophilaceae* (Doronina et al., 2014; Orata et al., 2018).

As discussed earlier, *Methylocaldum* is a thermotolerant or thermophilic genus, with optimal growth temperature of most strains in the 40-60ºC range (Houghten et al., 2019). It was found to be enriched in the 45ºC $^{13}CH_4$ incubation in the preliminary DNA-SIP experiment (**Table 5.1**) and present at significant abundance in biofilter soil sampled from a region of the biofilter with a high *in-situ* temperature of 50ºC (**Chapter 4.4.2**). Combining the observations from these 16S rRNA gene amplicon analyses *Methylocaldum* appears to be the best candidate for the primary methane oxidiser at the higher *in-situ* temperatures seen during sustained biofilter operation (~50ºC) (**Chapter 3**). The enrichment of a single *Methylocaldum* 16S rRNA ASV in the 37ºC $^{13}CH_4$ heavy fraction is an indication that at least one *Methylocaldum* strain present is a competitive methane oxidiser at high mesophilic temperatures, which correlates with the active *Methylocaldum* community observed at 37ºC in the preliminary DNA-SIP experiment (**Table 5.1**). The enrichment of the obligate methanotroph *Methylobacter* in the ^{13}C heavy fraction at 37ºC is in line with known optimal growth temperatures for *Methylobacter*, key strains having been characterised with growth optima from 20-37ºC (Bowman, 1993). It is interesting to note that the enriched community is considerably less complex in the 50ºC incubation compared with the 37ºC incubation, which featured abundant obligate methylotrophs, Methylophilaceae (MM2) and (MM3) clades, with apparently no non-methanotrophic genera enriched in the 50ºC ^{13}C heavy fraction. This was surprising as thermotolerant methylotrophs are known, such as the facultative methylotroph isolated from a methane oxidising enrichment by Islam et al which could grow at a temperature range of 30 to 60ºC and oxidise methanol at the growth optima of 55ºC (Islam et al., 2021) and the biofilter

is known to often operate at 50ºC and above (**Chapter 3**). The exact reason behind this observed difference is unclear.

5.3.3 Metagenome sequencing and analysis of methanotrophs from DNA-SIP incubations incubated at 37ºC and 50ºC using soil from a hot and deep region of the biofilter

In addition to 16S rRNA amplicon analysis of the heavy and light fractions of the 37°C and 50°C incubated DNA-SIP sector B19 soil samples, the opportunity was taken to carry out metagenome sequencing and assembly of DNA from the heavy fractions of the ^{13}C labelled 37 and 50°C biofilter soil incubations (for additional methods see **Chapter 2.12.4**). This would not only allow reconstruction of metagenome assembled genomes (MAGs) for the active methane-oxidising methanotrophs enriched in these heavy fractions, but could also improve the quality of the recovered methanotroph MAGs due to the increased proportion of their DNA in these fractions (through heavy ^{13}C incorporation) when compared with unenriched environmental samples. By carrying out further metagenome sequencing and assembly on the corresponding unfractionated total DNA extracts from these incubations, the degree of enrichment of recovered methanotroph MAGs in the heavy fractions could be estimated based on average read coverage when compared to matching MAGs from the unfractionated metagenomes. Finally, metagenome sequencing and assembly would be carried out on DNA extracted from the timepoint 0 (pre-incubation) soil sample (*in-situ* temperature of 50°C), to confirm the presence of the enriched methanotroph MAGs found in the 50°C heavy fraction metagenome. This would support the notion that these MAGs are the active methanotrophs in the biofilter at the operational temperature of 50°C.

5.3.3.1 Metagenome sequencing using Timepoint 3 ^{13}C 50˚C and 37˚C heavy fraction DNA, corresponding unfractionated DNA and Timepoint 0 DNA, from DNA-SIP incubations 50ºC and 37ºC

The remaining pre-fractionation DNA extracts from T3 $^{13}CH_4$ soil incubation replicates A, B and C were then pooled (1:1:1 sample DNA ratio) separately for the 50˚C and 37˚C samples, resulting in T3 50˚C ^{13}C unfractionated and T3 37˚C ^{13}C unfractionated samples. These unfractionated samples then underwent humic acid removal with a Zymo "OneStep PCR Inhibitor Removal Kit". Remaining T0 post-humic acid clean up DNA extract replicates (1, 2,

3) were also pooled (again, equal DNA ratio), as were the T3 50˚C $^{13}CH_4$ heavy fraction mixes for replicates A, B and C and the corresponding heavy fraction mixes for the T3 37˚C $^{13}CH_4$ replicates. The resulting five pooled DNA samples T3 50˚C $^{13}CH_4$ unfractionated (T3 50°C U), T3 37˚C $^{13}CH_4$ unfractionated (T3 37°C U), T3 50˚C $^{13}CH_4$ heavy fraction (T3 50°C H), T3 37˚C $^{13}CH_4$ heavy fraction (T3 37°C H) and T0 unfractionated (T0 U) were then adjusted to the service provider's specification and sent for shotgun metagenomic sequencing with Novogene (**Chapter 2.10.7**).

5.3.3.2 Assembly and annotation of the 50ºC and 37ºC DNA-SIP metagenomes

The R1 and R2 paired-end reads from each of the five metagenome sequencing samples (T0 U, T3 50°C H, T3 50°C U, T3 37°C H, T3 37°C U) underwent pre-processing as described in **Chapter 2.12.4**. Trim Galore and Minoche filtering with illumina-utils were used to trim and filter the reads. A range of different assemblers were trialled (SPAdes, IDBA and MEGAHIT) and MEGAHIT was selected for metagenome assembly, due to binned MEGAHIT assemblies producing a higher number of MAGs containing *pmoA* sequences that were assigned possible methanotroph taxonomy using MIGA online. The pre-processed paired-reads from each of the five samples were assembled separately using MEGAHIT with standard parameters. The generated contigs were then binned using metaBAT2 and MaxBin2 via the MetaWRAP binning module. An additional set of CONCOCT bins were then separately produced for each assembly and the fasta file headers changed to match MetaWRAP conventions, as the CONCOCT function in the MetaWRAP binning module has a conflict with the standard MEGAHIT assembly contig format. All three bin sets for each assembly (metaBAT2, MaxBin2 and CONCOCT) were then refined and combined into an improved bin set using the MetaWRAP bin_refinement module with completion and contamination thresholds were set at 70 and 10% respectively.

As was done for the Core 2C metagenomes (**Chapter 4.5.2**), The refined bins and MEGAHIT assemblies for each of the B19 metagenome samples were screened for methanotroph marker genes using *pmoA* and *mmoX* screening files (fasta files containing nucleotide sequences from known genera of methanotrophs). The MEGAHIT assembly and concatenated refined bins from each sample were used to generate nucleotide local BLAST databases for each metagenome assembly and these were then searched using the *pmoA* and *mmoX* screening files using the discontiguous megablast function. The candidate methane monooxygenase sequences

found in these searches were blasted against the NCBI database with the nucleotide BLAST function. The genera of the closest BLAST hit with known taxonomy for each candidate methane monooxygenase sequence is displayed in **Table 5.3** along with the contig of origin and the refined bin it was assigned to.

Table 5.3 Closest NCBI database hits for each candidate particulate or soluble methane monooxygenase sequence found in the five metagenomic assemblies. (n.b. – not binned)

Timepoint 0 metagenome assembly - contigs and bins containing putative *pmoA* and *mmoX* sequences							
				identity and genera of closest blastn NCBI hit with assigned taxonomy			
contig	Screen	contig length	contig coverage	gene identity	% identity	taxonomy of closest hit	bin containing contig
k141_610102	*pmoA*	2111	10635	*pmoA*	100.00	*Methylocaldum*	n.b.
k141_497913	*pmoA*	2917	3375	*pmoA*	82.88	*Methylomagnum*	n.b.
k141_492673	*pmoA*	2095	2547	*pmoA*	95.78	*Methylocaldum*	n.b.
k141_422157	*pmoA*	2548	223	*pmoA*	89.92	*Methylocaldum*	n.b.
k141_500816	*pmoA*	1530	60	*pmoA*	69.33	*Methylococcus*	n.b.
k141_142379	*pmoA*	2913	60	*pmoA*	86.67	*Methylomagnum*	n.b.
k141_545845	*pmoA*	1804	45	*pmoA*	97.38	*Methylocystis*	n.b.
k141_291264	*pmoA*	591	30	*pmoA*	86.98	*Methylomagnum*	n.b.
k141_321766	*pmoA*	689	30	*pmoA*	81.37	*Methylovulum*	n.b.
k141_590314	*mmoX*	68074	3148	*mmoX*	85.93	*Methylococcus*	37

50°C DNA-SIP timepoint 3 heavy fraction metagenome assembly - contigs and bins containing putative *pmoA* and *mmoX* sequences							
				identity and genera of closest blastn NCBI hit with assigned taxonomy			
contig	Screen	contig length	contig coverage	gene identity	% identity	taxonomy of closest hit	bin containing contig
k141_349106	*pmoA*	20453	5827	*pmoA*	82.88	*Methylomagnum*	41
k141_178296	*pmoA*	20836	5143	*pmoA*	100.00	*Methylocaldum*	36
k141_311342	*pmoA*	2566	446	*pmoA*	89.92	*Methylocaldum*	n.b.
k141_227352	*pmoA*	1842	124	*pmoA*	94.32	*Methylocaldum*	n.b.
k141_244949	*pmoA*	578	45	*pmoA*	98.19	*Methylocystis*	n.b.
k141_236723	*mmoX*	43303	5292	*mmoX*	85.93	*Methylococcus*	41

50°C DNA-SIP timepoint 3 unfractionated metagenome assembly - contigs and bins containing putative *pmoA* and *mmoX* sequences							
				identity and genera of closest blastn NCBI hit with assigned taxonomy			
contig	Screen	contig length	contig coverage	gene identity	% identity	taxonomy of closest hit	bin containing contig
k141_611117	*pmoA*	3061	6131	*pmoA*	100.00	*Methylocaldum*	n.b.
k141_554998	*pmoA*	67345	2228	*pmoA*	82.24	*Methylocaldum*	62
k141_393733	*pmoA*	3273	450	*pmoA*	89.92	*Methylocaldum*	n.b.
k141_33109	*pmoA*	2511	333	*pmoA*	95.97	*Methylocaldum*	n.b.
k141_292573	*pmoA*	1054	45	*pmoA*	87.43	*Methylomagnum*	n.b.
k141_656948	*pmoA*	645	30	*pmoA*	92.45	*Methylocystis*	n.b.
k141_434806	*pmoA*	321	15	*pmoA*	99.62	*Methylocaldum*	n.b.
k141_566925	*pmoA*	466	15	*pmoA*	96.38	*Methylosinus*	n.b.
k141_69083	*mmoX*	67579	2144	*mmoX*	86.21	*Methylococcus*	62

37°C DNA-SIP timepoint 3 heavy fraction metagenome assembly - contigs and bins containing putative *pmoA* and *mmoX* sequences							
				identity and genera of closest blastn NCBI hit with assigned taxonomy			
contig	screen used	contig length	contig coverage	gene identity	% identity	taxonomy of closest hit	bin containing contig
k141_438418	*pmoA*	67344	3896	*pmoA*	82.38	*Methylocaldum*	29
k141_803036	*pmoA*	179894	2923	*pmoA*	96.37	*Methylomicrobium*	35
k141_519497	*pmoA*	6464	2197	*pmoA*	87.87	*Methylovulum*	n.b.
k141_485561	*pmoA*	2731	726	*pmoA*	100.00	*Methylocaldum*	n.b.
k141_449175	*pmoA*	2232	420	*pmoA*	86.80	*Methylomagnum*	n.b.
k141_109504	*pmoA*	2717	298	*pmoA*	95.92	*Methylocystis*	n.b.
k141_808961	*pmoA*	71315	210	*pmoA*	91.47	*Methylocystis*	31
k141_105635	*pmoA*	4255	193	*pmoA*	98.20	*Methylocystis*	n.b.
k141_465053	*pmoA*	2566	104	*pmoA*	89.92	*Methylocaldum*	n.b.
k141_184292	*pmoA*	2002	45	*pmoA*	84.93	*Methylomagnum*	n.b.
k141_356899	*pmoA*	367	15	*pmoA*	95.64	*Methylocaldum*	n.b.
k141_591195	*pmoA*	1014	15	*pmoA*	89.91	*Methylomagnum*	n.b.
k141_163647	*mmoX*	67572	3912	*mmoX*	86.21	*Methylococcus*	29

37°C DNA-SIP timepoint 3 unfractionated metagenome assembly - contigs and bins containing putative *pmoA* and *mmoX* sequences							
				identity and genera of closest blastn NCBI hit with assigned taxonomy			
contig	Screen	contig length	contig coverage	gene identity	% identity	taxonomy of closest hit	bin containing contig
k141_691417	*pmoA*	3287	5670	*pmoA*	99.73	*Methylocaldum*	n.b.
k141_843498	*pmoA*	67346	1405	*pmoA*	82.24	*Methylocaldum*	48
k141_879687	*pmoA*	29344	749	*pmoA*	87.87	*Methylovulum*	29
k141_662438	*pmoA*	109486	330	*pmoA*	85.08	*Methylomonas*	32
k141_207954	*pmoA*	219949	315	*pmoA*	96.37	*Methylomicrobium*	32
k141_4610	*pmoA*	4690	274	*pmoA*	89.92	*Methylocaldum*	n.b.
k141_691362	*pmoA*	2094	252	*pmoA*	95.77	*Methylocaldum*	n.b.
k141_192725	*pmoA*	2445	178	*pmoA*	86.80	*Methylomagnum*	n.b.
k141_3313	*pmoA*	2973	45	*pmoA*	96.90	*Methylocystis*	n.b.
k141_160605	*pmoA*	677	30	*pmoA*	70.21	*Methylocapsa*	n.b.
k141_279167	*pmoA*	592	15	*pmoA*	87.14	*Methylomagnum*	n.b.
k141_496822	*mmoX*	67604	1409	*mmoX*	86.21	*Methylococcus*	48

MIGA online was used to estimate taxonomic placement of the metagenomic bins and bin percentage completion and contamination was estimated with CheckM. For the T0 and DNA-SIP heavy fraction (50°C and 37°C) metagenomes: high quality bins (>85% completion < 6% contamination) with a potentially methanotrophic taxonomic placement were selected for further analysis even if they lacked putative methane monooxygenase marker sequences (*pmoA* or *mmoX*). These high quality candidate methanotroph MAGs had their coding sequences identified and annotated using Prokka. The nucleotide derived amino acid sequences of detected methanotroph marker genes *pmoA* and *mxaF* were then searched against the NCBI database using BLASTP to provide additional taxonomic resolution for these MAGs. Those MAGs lacking the methanotroph and methylotroph marker genes *pmoA, mmoX* or *mxaF* were retained as candidate methanotrophs if they were found to contain other CH_4 metabolism genes (*pmoB*, *pmoC*, *mmoY*, *mmoZ*, *mmoB*, *mmoC* and *mmoD*). (**Table 5.4**) shows the MIGA taxonomy assignment, CheckM completion and contamination scores as well as the outcome of BLAST P marker gene searches against the NCBI database for each of the selected candidate methanotroph MAGs. As T0 MAG 59 lacked *pmoA mmoX* and *mxaF* genes, the pMMO C-subunit gene (*pmoC*) and the methylotroph marker gene *fhcD* (from the tetrahydromethanopterin pathway) (Dumont, 2014) were used instead for the BLASTP NCBI database search to provide taxonomic information. Note that the top hits from the closest two known genera in the NCBI database are shown for each marker gene BLAST result, to illustrate cases where taxonomy is harder to definitively assign due almost identical sequence similarity with more than one genera.

The translated coding sequences (determined by Prokka) were then assigned K numbers linking them to experimentally determined enzyme function using the BlastKOALA tool hosted at the Kyoto Encyclopaedia of Genes and Genomes (KEGG). Metabolic pathways for each MAG were then laid out using the KEGG pathway reconstruct tool and the assigned K numbers. Coding sequences that were not assigned K numbers were then screened for missing enzymes in the reconstructed pathways using BLAST and the NCBI database. **Table 5.5** shows the central methanotroph enzymes and core metabolic pathways detected in the high quality candidate methanotroph MAGs from the T0 assembly and the ^{13}C heavy fraction 50°C and 37°C assemblies.

Table 5.4 MIGA taxonomy assignment, CheckM completion and contamination scores and the results of BLAST P marker gene searches against the NCBI database for each of the high-quality candidate methanotroph MAGs.

Unfractionated T0 methanotrophic MAGs

MAG	*pmoA* present	closest top two genera NCBI hits (% identity)	*mmoX* present	closest top two genera NCBI hits (% identity)	*MxaF* present	closest top two genera NCBI hits (% identity)	MIGA online taxonomy assignment (P value < 0.05)	MAG size (bp)	contigs	N50	GC content (%)	CheckM completion (%)	CheckM contamination (%)
31	no		no		yes	*Methylocaldum* (92.85) *Methylotetracoccus* (86.19)	*Gammaproteobacteria*	3,913,343	173	35143	56.74	93.33	2.41
37	no		yes	*Methylococcus* (90.32) *Methylocaldum* (91.68)	yes	*Methylomagnum* (91.35) *Methylocaldum* (90.35)	*Gammaproteobacteria*	3,283,430	53	120176	65.27	98.14	2.16
59	no		no		no		*Gammaproteobacteria*	3,692,124	240	20318	57.29	86.98	2.26

T3 50°C $^{13}CH_4$ Heavy fraction methanotrophic MAGs

MAG	*pmoA* present	closest top two genera NCBI hits (% identity)	*mmoX* present	closest top two genera NCBI hits (% identity)	*MxaF* present	closest top two genera NCBI hits (% identity)	MIGA online taxonomy assignment (P value < 0.05)	MAG size (bp)	contigs	N50	GC content (%)	CheckM completion (%)	CheckM contamination (%)
21	no		no		yes	*Methylocaldum* (92.85) *Methylotetracoccus* (86.19)	*Gammaproteobacteria*	3,671,286	149	39382	56.66	85.16	3.10
36	yes	*Methylocaldum* (100) *Methylomagnum* (89.88)	no		yes	*Methylocaldum* (100.00) *Methylomagnum* (87.52)	*Gammaproteobacteria*	4,409,492	270	38438	57.29	95.59	5.15
41	yes	*Methylomagnum* (92.71) *Methylocaldum* (90.69)	yes	*Methylococcus* (90.32) *Methylocaldum* (91.68)	yes	*Methylomagnum* (91.35) *Methylocaldum* (90.35)	*Gammaproteobacteria*	3,121,787	50	136426	65.16	89.73	1.12

T3 37°C $^{13}CH_4$ Heavy fraction methanotrophic MAGs

MAG	*pmoA* present	closest top two genera NCBI hits (% identity)	*mmoX* present	closest top two genera NCBI hits (% identity)	*MxaF* present	closest top two genera NCBI hits (% identity)	MIGA online taxonomy assignment (P value < 0.05)	MAG size (bp)	contigs	N50	GC content (%)	CheckM completion (%)	CheckM contamination (%)
29	yes	*Methylomagnum* (92.71) *Methylocaldum* (90.69)	yes	*Methylococcus* (90.32) *Methylocaldum* (91.68)	yes	*Methylomagnum* (91.35) *Methylocaldum* (90.35)	*Gammaproteobacteria*	3,023,574	46	88916	65.2	92.26	0.36
31	yes	*Methylocystis* (94.92) *Methylosinus* (84.77)	no		yes	*Methylocystis* (94.07) *Methylosinus* (92.95)	*Methylocystaceae*	3,221,074	112	41443	65.27	95.99	1.2
35	yes (two)	*Methylomicrobium* (89.60) *Methylobacter* (90.80) --- *Methylomicrobium* (98.79) *Methylosarcina* (95.95)	no		yes	*Methylomicrobium* (98.34) *Methylosarcina* (92.36)	*Methylomicrobium*	3,699,438	55	102124	56.88	88.12	0.87

NCBI BlastP hits (top two genera) for additional CH_4 metabolism genes in MAGs lacking *pmoA*, *mmoX* and *MxaF* marker genes.

MAG	*pmoC* present	closest top two genera NCBI hits (% identity)	*fhcD* present	closest top two genera NCBI hits (% identity)
T0 MAG 59	yes (one)	*Methylocaldum* (92.86) *Ca. Methylumidiphilus* (87.50)	yes (one)	*Methylocaldum* (97.65) *Methylogaea* (88.59)

Table 5.5 Genes encoding enzymes involved in CH_4 oxidation and core metabolic pathways detected in the high quality candidate methanotroph MAGs from the Timepoint 0 metagenome and the Timepoint 3 ^{13}C heavy fraction 50°C and 37°C metagenomes

T0 methanotrophic MAGs

	methane oxidation		methanol oxidation		formaldehyde oxidation			formate oxidation	carbon assimilation pathways			nitrogen metabolism			
MAG	particulate MMO pmoCAB	soluble MMO mmoXYBZDC	*MxaFI*	*XoxF*	H_4MPT linked	H_4F linked	formaldehyde dehydrogenase	formate dehydrogenase	Ribulose monophosphate	Serine	Calvin-Bensom-Bassham (CBB)	*hao*	denitrification to nitrous oxide	nitrogenase structural genes	GS/GOGAT
31	–	×	✓	✓	✓	✓	×	✓	–	–	–	✓	–	✓	✓
37	–	✓	✓	✓	✓	✓	×	✓	✓	–	✓	✓	–	✓	✓
59	–	×	×	×	✓	✓	×	✓	✓	–	✓	✓	✓	–	–

T3 50°C $^{13}CH_4$ Heavy fraction methanotrophic MAGs

	methane oxidation		methanol oxidation		formaldehyde oxidation			formate oxidation	carbon assimilation pathways			nitrogen metabolism			
MAG	particulate MMO pmoCAB	soluble MMO mmoXYBZDC	*MxaFI*	*XoxF*	H_4MPT linked	H_4F linked	formaldehyde dehydrogenase	formate dehydrogenase	Ribulose monophosphate	Serine	Calvin-Bensom-Bassham (CBB)	*hao*	denitrification to nitrous oxide	nitrogenase structural genes	GS/GOGAT
21	–	×	–	✓	✓	✓	×	✓	✓	–	–	✓	–	✓	–
36	✓	×	✓	✓	✓	✓	×	✓	✓	–	✓	✓	✓	✓	✓
41	✓	✓	✓	✓	✓	✓	×	✓	✓	–	–	✓	–	✓	✓

T3 37°C $^{13}CH_4$ Heavy fraction methanotrophic MAGs

	methane oxidation		methanol oxidation		formaldehyde oxidation			formate oxidation	carbon assimilation pathways			nitrogen metabolism			
MAG	particulate MMO pmoCAB	soluble MMO mmoXYBZDC	*MxaFI*	*XoxF*	H_4MPT linked	H_4F linked	formaldehyde dehydrogenase	formate dehydrogenase	Ribulose monophosphate	Serine	Calvin-Bensom-Bassham (CBB)	*hao*	denitrification to nitrous oxide	nitrogenase structural genes	GS/GOGAT
29	–	✓	✓	✓	✓	✓	×	✓	✓	–	✓	✓	–	✓	✓
31	✓	×	✓	×	✓	✓	×	✓	–	✓	–	✓	×	✓	✓
35	✓	×	✓	✓	✓	–	×	✓	✓	–	–	✓	×	✓	–

5.3.3.3 Analysis of high-quality candidate methanotroph MAGs from the DNA-SIP Timepoint 0 (T0) metagenome and the T3 50°C and 37°C heavy fraction metagenomes.

5.3.3.3.1 Common features of the high-quality candidate methanotroph MAGs

While not all of the high quality methanotroph MAGs possessed a full *pmoCAB* (encoding pMMO) or *mmoXYBZDC* (encoding sMMO) cluster, they all contained at least one *pmoC* subunit (**Table 5.4**). The absence of full *pmoCAB* clusters, is likely due to the potential difficulty in successfully binning multicopy gene clusters in short read metagenome assemblies (Alkan et al., 2011), as *pmoCAB* is known to be multicopy in some methanotrophs (Khadem et al., 2012; Murrell and Smith, 2010; Takeuchi et al., 2019). Most of the MAGs also contained both *mxaFI* and *xoxF* genes, for calcium- and lanthanide-dependent methanol dehydrogenases, that could carry out the oxidation of methanol to formaldehyde. All of the high quality methanotroph MAGs contained genes encoding full tetrahydromethanopterin (H_4MPT)- and tetrahydrofolate (H_4F)-linked pathways for formaldehyde oxidation to formate, with the sole exception of T3 37ºC heavy fraction metagenome MAG 35 where the H_4F linked pathway was incomplete. No orthologues of formaldehyde dehydrogenase genes for direct conversion of formaldehyde to formate were detected in the methanotroph MAGs. This was not necessarily surprising, as while these genes have been found in non-methanotrophs such as *Pseudomonas putida* (Ito et al., 1994), to date the only methanotroph believed to use a similar enzyme was *Methylococcus capsulatus* (Zahn et al., 2001) and the formaldehyde oxidation activity observed in early experiments was later attributed to combined methanol dehydrogenase and methylene-H_4MPT dehydrogenase activity (Adeosun et al., 2004). Formate dehydrogenase genes encoding enzymes for the following and final step in the CH_4 oxidation pathway, formate oxidation to carbon dioxide, were also detected across all the methanotroph MAGs.

At least one full pathway for carbon assimilation was found in all but one of the methanotroph MAGs. In most cases this was the ribulose monophosphate pathway (with many of these MAGs possessing complete CBB cycles and very fragmentary serine pathways), while a single MAG possessed a complete serine cycle instead. This was anticipated, as the ribulose monophosphate pathway MAGs were determined to represent *Gammaproteobacterial* methanotrophs which typically use this pathway, while the serine pathway MAG was identified as belonging to a methanotroph of the *Alphaproteobacteria* (which are known to favour the serine pathway for carbon assimilation) (Stein et al., 2012) (**Table 5.5**). The MAGs with complete CBB cycles all

lacked sedoheptulose-1,7-bisphosphatase and instead contained an orthologue (≥79% amino acid identity) of the pyrophosphate-dependent 6-phosphofructokinase (PPi-PFK) gene which is believed to handle this step in *Methylococcus capsulatus* (Bath) (Reshetnikov et al., 2008). The incomplete CBB pathways in the T0 metagenome MAG 31 and T3 50ºC heavy fraction metagenome MAGs 21 and 41 also featured this alternative gene. The presence of CBB pathways in *Methylococcaceae* MAGs was particularly interesting as Henard et al recently demonstrated that the *Methylococaceae* methanotroph *Methylococcus capsulatus* (Bath) is in fact capable of fixing CO_2 using the RubisCO enzyme and this process appears to be required for growth (Henard et al., 2021). It will be interesting to see if this ability and requirement is detected in other *Methylococaceae* such as *Methylocaldum* spp. As this could represent both an additional mechanism for climate active gas (CO_2) removal and for label acquisition in $^{13}CH_4$ DNA-SIP experiments.

All three of the nitrogenase structural genes (*nifH*, *nifK* and *nifD*) were present in the methanotroph MAGs apart from MAG59 in the Timepoint 0 metagenome (which only contained the *nifH* and *nifK* subunits), indicating that these methanotrophs may be capable of atmospheric nitrogen fixation. A further ubiquitous nitrogen metabolism gene was hydroxylamine oxidoreductase (*hao*), which in methanotrophs is thought to have a role in removing the toxic hydroxylamine produced from pMMO co-metabolised ammonia (Stein et al., 2012). As is the case with most known methanotrophs (Dam et al., 2013), none of these MAGs contained *nosZ* genes for nitrous oxide reductase, suggesting that these methanotrophs are incapable of intracellular nitrous oxide removal and those possessing nitric oxide reductases (*norBC*) could be potential sources of nitrous oxide. All methanotroph MAGs contained genes encoding alanine dehydrogenase which in Type I (gammaproteobacterial) methanotrophs is known to be responsible for pyruvate pathway ammonia assimilation at higher ammonium concentrations (Murrell and Dalton, 1983b).

5.3.3.3.2 Timepoint 0 (T0) metagenome candidate methanotroph MAGs

5.3.3.3.2.1 Timepoint 0 MAG 31

Timepoint 0 MAG 31 was assigned a *Gammaproteobacteria* taxonomy by MIGA online. No full pMMO (*pmoCAB*) or sMMO (*mmoXYBZDC*) gene clusters were found in this MAG although two single *pmoC* genes were detected (**Table 5.4**).

The CH_4 carbon assimilation pathway(s) used by this bacterium could not be clearly determined, as the routes used by methanotrophs (the ribulose monophosphate, serine pathway and the CBB cycle) were incomplete in this MAG.

A *nirK* gene for nitrite reduction was present along with a sequence encoding an orthologue of the nitric oxide reductase C subunit (*norC*), a copy of *norB* was not found raising the possibility that this bacterium may be incapable of nitrous oxide production. Genes for the components of the ammonia assimilation GS/GOGAT cycle (*glnA*, *gltB*, *gltD*) were also detected in this MAG along with NADH and NAD(P)H dependent glutamate dehydrogenases which may be involved in the α-ketoglutarate ammonia assimilation pathway (Trotsenko and Murrell, 2008).

The two closest genera of BLAST P hits for the methylotroph marker gene *mxaF* (*Methylocaldum* and *Methylotetracoccus* (**Table 5.4**)) indicate that Timepoint 0 MAG 31 could be a member of the *Methylococcaceae*. In addition to this, the nucleotide-derived amino acid sequences of the two *pmoC* genes in this MAG were searched against the NCBI database using the BLAST P function. In both cases the genus that was the top hit for these sequences was *Methylocaldum*, with amino acid identities of 100.00 and 86.32%. This further reinforced the identity of *Methylococcaceae* and suggested that Timepoint 0 MAG 31 may be a *Methylocaldum* species.

5.3.3.3.2.2Timepoint 0 MAG 37

MIGA online assigned a *Gammaproteobacterial* taxonomy to Timepoint 0 MAG 37, which appeared to represent a methanotroph as it contains a full *mmoXYBZDC* cluster of genes for soluble methane monooxygenase, in addition to two single pMMO *pmoC* genes.

The *narGHI* and *nirK* genes, which encode enzymes for nitrate to nitric oxide denitrification, were discovered along with a copy of *norB*, which encodes one of the nitric oxide reductase

subunits, however the nitric oxide reductase *norC* gene which is also required for reduction of nitric oxide was not present. This MAG also contained the key genes (*glnA*, *gltB*, *gltD*) for the GS/GOGAT cycle as well as a NADH dependent glutamate dehydrogenase gene for ammonium assimilation.

Timepoint 0 MAG 37 possesses *mmoX* and *mxaF* marker genes (**Table 5.4**) with sequences closest to *Methylomagnum*, *Methylococcus* and *Methylocaldum* genera, suggesting that this MAG may lie within the *Methylococcaceae*.

5.3.3.3.2.3 Timepoint 0 MAG 59

Timepoint 0 MAG 59 was also assigned to the *Gammaproteobacteria* using MIGA online. This MAG lacks genes encoding the sMMO but does contain a single copy of the pMMO *pmoC* subunit (**Table 5.4**). While the further absence of either *mxaFI* or *xoxF* methanol dehydrogenase genes makes it harder to declare this MAG as definitely belonging to a methanotroph, this MAG does have one of the lowest CheckM assigned completion estimates for the candidate methanotroph MAGs analysed in detail (86.98% (**Table 5.4**)) so there is a possibility that they are missing in the MAG but present in the bacterium.

Only two (*nifH* and *nifK*) of the three structural nitrogenase genes were found in this MAG indicating that dinitrogen fixation may not be a feature of this bacterium.

This bacterium is a potential producer of nitrous oxide as it contains the genes *nirK* and *norBC* which encode enzymes for nitrite reduction to nitrous oxide. While NADH and NADPH dependent glutamate dehydrogenase genes were detected, this MAG did not contain a complete set of GS/GOGAT genes for ammonia assimilation, with the glutamate synthase subunits *gltB* and *gltD* absent. This is likely due to an incomplete MAG as the GS/GOGAT cycle is expected to be present in type I and type II methanotrophs (Trotsenko and Murrell, 2008).

As mentioned previously, Timepoint 0 MAG 59 did not contain *pmoA mmoX* or *mxaF* genes. Instead the *pmoC* gene and the *fhcD* gene (from the tetrahydromethanopterin pathway) were used in BLAST P searches against the NCBI database. The top hits for these sequences (*Methylocaldum*, *Methylogaea* and Ca. *Methylumidiphilus*) fall within the *Methylococcales* (Islam, 2015; Oren et al., 2020; Rissanen et al., 2018). With the higher similarity with *Methylocaldum*, particularly for the Methylotroph marker gene *fhcD* (97.65%), indicating that this bacterium may be a *Methylocaldum*

5.3.3.3.3 DNA-SIP 50°C heavy fraction metagenome candidate methanotroph MAGs

5.3.3.3.3.1 50°C ^{13}C H MAG 21

50°C ^{13}C H MAG 21 was given a *Gammaproteobacterial* taxonomy by MIGA online and while it lacks sMMO genes or a full *pmoCAB* cluster, it may still represent a methanotroph as it possesses three single *pmoC* subunit genes (**Table 5.4**). This MAG possesses three lanthanide -dependent methanol dehydrogenase (*xoxF*) genes, but only contains the *mxaF* gene for the large subunit of calcium dependent methanol dehydrogenase (the *mxaI* subunit gene is not present). The lack of *mxaI* in this MAG could be due to limitations in metagenome assembly and binning rather than absence from the methanotroph's genome as the *mxaF* gene was at the very end of a large contig, which could explain why the proximal *mxaI* gene was not found.

The gene *nirK* encoding a nitrite reductase and one of the subunits for nitric oxide reductase (*norB*) are present, but another gene required for the nitric oxide reductase (*norC*) is absent. However, the potential for this bacterium to generate nitrous oxide is hard to definitely determine due the relatively low completion of this MAG (85.16% (**Table 5.4**)). This MAG also lacks the *glnA* gene for glutamine synthetase leading to an incomplete GS/GOGAT cycle for ammonia assimilation, which is likely an artefact of incomplete MAG reconstitution (Trotsenko and Murrell, 2008). Both NADH and NAD(P)H dependent glutamate dehydrogenase genes, for the α-ketoglutarate ammonia assimilation pathway, were detected.

The *mxaF* gene detected in this MAG was found to be closest to sequences of *mxaF* from the *Methylocaldum* and *Methylotetracoccus* genera in the NCBI database (**Table 5.4**), suggesting this bacterium could belong to the *Methylococcaceae* (Ghashghavi et al., 2019). Nucleotide-derived amino acid sequences for each of the three *pmoC* sequences found in this MAG were then searched against the BLAST database. All three returned top hits against *Methylocaldum* species (amino acid identities of 92.25, 86.32 and 100.00%), further supporting the *Methylococcaceae* assignment and indicating this may be a *Methylocaldum* MAG.

5.3.3.3.3.2 50°C ^{13}C H MAG 36

Yet another *Gammaproteobacterial* MAG (according to MIGA online (**Table 5.4**)), 50°C ^{13}C H MAG 36 represents a methanotrophic bacterium as it features a full pMMO cluster (*pmoCAB*) as well as two single *pmoC* sequences (no sMMO genes were detected) (**Table 5.5**).

The presence of *nirK*, *norB* and *norC* orthologues indicate that this bacterium may be capable of generating nitrous oxide from nitrite and nitric oxide. Genes encoding a complete GS/GOGAT cycle (*glnA*, *gltB*, *gltD*) and NADH and NADPH dependent glutamate dehydrogenases for ammonia assimilation were also found in this MAG.

50°C ^{13}C H MAG 36 contains both *pmoA* and *mxaF* functional marker genes (**Table 5.4**), the nucleotide derived amino acid sequences of these genes both had a 100% identity with *Methylocaldum* sequences in the NCBI database, providing strong indication that this MAG represents a *Methylocaldum* bacterium. In further support of this taxonomic information, this MAG was one of only two candidate methanotroph MAGs which had a 16S rRNA gene sequence assigned to it. This sequence demonstrated a 96.19% nucleotide similarity to a *Methylocaldum* 16S rRNA gene sequence (the top hit following a nucleotide BLAST search of the NCBI database).

5.3.3.3.3.3 50°C ^{13}C H MAG 41

50°C ^{13}C H MAG 41 appeared to be a *Gammaproteobacterial* methanotroph possessing both a pMMO (pmoCAB) and a sMMO (*mmoXYBZDC*) gene cluster, with two additional single *pmoC* pMMO subunit genes detected in the MAG (**Tables 5.4** and **5.5**). This bacterium probably uses the ribulose monophosphate pathway for CH_4-derived carbon assimilation as it contains gene orthologues for the full pathway. The near complete CBB pathway could possibly be used if the missing but crucial ribulose-bisphosphate carboxylase large chain gene (*cbbL*) is due to low MAG completion (89.73% estimate) rather than absence from the bacterium's genetic inventory, while the serine cycle is a less likely route as several key genes are missing (*hprA*, *gck*, *ppc* and *mtkB*).

narGHI and *nirK*, which encode enzymes for nitrate to nitric oxide reduction, were detected along with a copy of *norB* (encoding a nitric oxide reductase subunit), however the required nitric oxide reductase *norC* subunit was absent. Finally, while no glutamate dehydrogenase

orthologues were found, this MAG did contain the *glnA*, *gltB* and *gltD* genes required for ammonia incorporation via the GS/GOGAT cycle.

This MAG contained *pmoA*, *mmoX* and *mxaF* marker genes (**Table 5.4**). The top two genera of NCBI database hits for each of these genes (following BLAST P searches with their nucleotide derived amino acid sequences) were from a mix of *Methylomagnum*, *Methylococcus* and *Methylocaldum* species. This suggested a likely *Methylococcaceae* taxonomy for this MAG. It was noted that the taxonomies of top hits for these marker genes matched those for the corresponding marker genes seen in Timepoint 0 MAG 37 and 37°C ^{13}C H MAG 29 as well as the core 2C metagenome MAGs 10-30 cm MAG 6 and 30-50 cm MAG 43 from **Chapter 4.5** (which were shown to likely belong to the same or closely related strains of bacteria). This suggests that these MAGs may all represent a particular strain or strains of a *Methylococcaceae* methanotroph species. This was investigated and the MAG similarity across metagenome assemblies estimated using the Genome-to-Genome Distance Calculator (**Chapter 5.3.3.5-6**).

5.3.3.3.4 DNA-SIP 37°C heavy fraction metagenome candidate methanotroph MAGs.

5.3.3.3.4.1 37°C ^{13}C H MAG 29

Based on MIGA online taxonomy analysis, 37°C ^{13}C H MAG 29 belongs to the *Gammaproteobacteria* (**Table 5.4**). This MAG likely represents a methanotroph as it possesses both a pMMO (*pmoCAB*) and a sMMO (*mmoXYBZDC*) gene cluster, as well as an additional single *pmoC* subunit (**Table 5.4** and **5.5**).

The genes *narGHI* and *nirK* encoding enzymes for nitrate and nitrite reduction were detected along with the *norB* gene which encodes a nitric oxide reductase subunit, however the *norC* gene which is also needed for nitric oxide reduction (and consequently nitrous oxide production) was absent leaving the potential nitrous oxide production capability of this methanotroph in doubt. Genes encoding enzymes involved in the GS/GOGAT cycle for ammonia incorporation were discovered although no gene orthologue for glutamate dehydrogenase could be found.

Similarly to MAG 41 from the 50ºC ^{13}C heavy fraction metagenome, 37°C ^{13}C H MAG 29 contained *pmoA*, *mmoX* and *mxaF* genes (**Table 5.4**) which had top BLAST P hits in the NCBI database among the *Methylomagnum*, *Methylococcus* and *Methylocaldum* genera, positioning this MAG as a likely *Methylococcaceae* bacterium. However, this MAG also contained a partial 16S rRNA gene sequence (429 bp), when used for a nucleotide BLAST search against the NCBI database the top hit was a 16S rRNA gene sequence from a *Methylocaldum* species with a nucleotide identity of 99.77%. If this 16S rRNA gene sequence has been correctly assigned to this MAG in the binning and refining steps, then this and matching MAGs from other metagenome assemblies may well belong to a *Methylocaldum* bacterium.

5.3.3.3.4.2 37°C ^{13}C H MAG 31

MIGA online assigned a *Methylocystaceae* taxonomy to this methanotrophic MAG which contains a pMMO (*pmoCAB*) gene cluster along with an additional single *pmoC* gene (**Table 5.4** and **5.5**). a single copy of the calcium-dependent methanol dehydrogenase genes *mxaFI* were present but no lanthanide-dependent methanol dehydrogenases were found. In agreement with the MIGA taxonomy assignment, it would appear that this MAG likely represents a type II alphaproteobacterial methanotroph as it possesses a full set of genes for the serine pathway for carbon assimilation but lacks almost all genes required for the ribulose monophosphate and CBB routes, such as genes for the key HPS and HPI enzymes (RuMP) and the *cbbL* and *cbbS* RubisCO genes (CBB) (White, 2007).

This methanotroph is unlikely to be capable of producing nitrous oxide as it lacks both the *norB* and *norC* genes encoding nitric oxide reductase. This MAG contains genes for both a NAD(P)H dependent glutamate dehydrogenase and a complete GS/GOGAT cycle (*glnA*, *gltB*, *gltD*).

The result of BLAST P searches against the NCBI database using the translated *pmoA* and *mxaF* genes from 37°C ^{13}C H MAG 31 (**Table 5.4**) suggest that this MAG may represent a *Methylocystis* species, as the top hits in both cases were from *Methylocystis* species with an amino acid identity around 94%. This fits very well with the MIGA online assignment of a *Methylocystaceae* taxonomy for this MAG.

5.3.3.3.4.3 37°C ^{13}C H MAG 35

A *Methylomicrobium* taxonomy was assigned to this MAG by MIGA online (**Table 5.4**). This MAG almost certainly represents a methanotroph as it contains two full pMMO gene clusters (*pmoCAB*). In contrast to the other methanotroph MAGs analysed in this section, while genes for a full H_4MPT linked formaldehyde oxidation pathway were discovered, *mtdA* and *ftfL* genes required for the H_4F linked pathway were missing. This MAG contains a full set of genes for the ribulose monophosphate pathway for CH_4 derived carbon assimilation which is the most likely route used by this bacterium as there are several genes missing from the CBB cycle and the only serine pathway genes detected were an enolase (*eno*) and phosphoenolpyruvate carboxylase (*ppc*).

No genes encoding enzymes for the denitrification pathway (and potentially nitrous oxide production) were found in this MAG. Genes encoding a NADH dependent glutamate dehydrogenase and a near complete GS/GOGAT cycle were detected with only the glutamate synthase gene *gltD* absent, although this ubiquitous cycle is probably complete in the methanotroph genome (Trotsenko and Murrell, 2008).

37°C ^{13}C H MAG 35 contained two *pmoA* marker gene sequences as well as an *mxaF* sequence. BLAST P searches using the nucleotide derived amino acid sequences from these genes against the NCBI database returned top hits with very high amino acid identity (>98%) from *Methylomicrobium* species for the *mxaF* and one of the *pmoA* sequences, while the other *pmoA* sequence was closest to sequences from *Methylomicrobium* and *Methylobacter* with a similarity of approximately 90% (**Table 5.4**). These results strongly support this MAG originating from a *Methylomicrobium* species. This further supports the MIGA online assignment of a *Methylomicrobium* taxonomy.

5.3.3.4 Analysis of lower quality candidate methanotroph MAGs from the Timepoint 0 (T0) metagenome and the DNA-SIP 50°C and 37°C heavy fraction metagenomes.

Potential methanotroph bins which failed to meet the high quality threshold (>85% completion and <6% contamination) were also examined to provide a full list of the methanotroph genomes reconstructed in these metagenome assemblies. While an in-depth analysis of the metabolic pathways encoded in these lower quality MAGs was not considered useful due to the lower completion and higher contamination estimates, they could still provide information on the

taxonomy and abundance of methanotrophs present in both the Timepoint 0 environmental DNA sample, as well as the Timepoint 3 (^{13}C enriched 37ºC and 50ºC) heavy fraction DNA samples. As was done with the high quality candidate methanotroph MAGs, Prokka was first used to find and annotate coding sequences for each MAG before putative *pmoA*, *mmoX* and *mxaF* functional marker sequences were searched against the NCBI database with BLAST P. MAGs without these marker genes were not discounted if they contained at least one orthologue of *pmoB*, *pmoC*, *mmoY*, *mmoZ*, *mmoB*, *mmoC* or *mmoD* (additional pMMO and sMMO genes). The results of the BLAST P searches against the NCBI database using the methanotroph marker genes are shown in (**Table 5.6**) for each of these lower quality candidate methanotroph MAGs along with their estimated completion and contamination scores (CheckM) and MIGA online taxonomy placement. Additionally, this table shows the results of BLAST P searches using the pMMO C-subunit gene (*pmoC*) and the methylotroph marker *fhcD* (tetrahydromethanopterin pathway) (Dumont, 2014) for those MAGs lacking *pmoA*, *mmoX* and *mxaF*.

As shown in **Table 5.6**, MAG 39 from the unfractionated timepoint 0 metagenome exceeded the contamination level for MIGA online taxonomy assignment. Instead CheckM was used to assess taxonomic placement of this MAG, which placed the represented bacterium in the *Gammaproteobacteria*. Furthermore, timepoint 0 metagenome MAG 39 could possibly represent a *Methylocaldum* species based on the *mxaF* gene present. MAG 7 from the 50ºC T3 heavy fraction metagenome may also represent a *Methylocaldum* species from the *Gammaproteobacteria* based on its *pmoC* and *fhcD* sequences. Looking at the three low quality candidate methanotrophs from the 37ºC T3 heavy fraction metagenome; MAG 9 appears to be a *Methylocaldum*, MAG 19 may be a *Methylococcaceae* species (in line with the origin of *pmoC* and *fhcD* hits above 80% AAI) (Ghashghavi et al., 2019) and MAG 39 might be a *Methylobacter*. T3 37°C ^{13}C heavy metagenome MAG 39 was later found to represent the same methanotroph as a MAG from the T3 37°C ^{13}C unfractionated metagenome (**Table 5.7**) which contained a *pmoCAB* cluster, with the nucleotide derived amino acid sequence of the *pmoA* subunit possessing a 100% amino acid identity to a *Methylobacter pmoA* sequence in the NCBI database, further supporting a *Methylobacter* taxonomic assignment.

Table 5.6 MIGA taxonomy assignment, CheckM completion and contamination scores and the results of BLAST P marker gene searches against the NCBI database for each of the lower-quality candidate methanotroph MAGs.

Unfractionated T0 methanotrophic MAGs

MAG	*pmoA* present	closest top two genera NCBI hits (% identity)	*mmoX* present	closest top two genera NCBI hits (% identity)	*MxaF* present	closest top two genera NCBI hits (% identity)	MIGA online taxonomy assignment (P value < 0.05)	MAG size (bp)	contigs	N50	GC content (%)	CheckM completion (%)	CheckM contamination (%)
39	no		no		yes	*Methylocaldum* (100.00) *Methylomagnum* (87.52)	contamination too high to assign taxonomy with MIGA	4087900	244	21727	57.04	89.66	9.14

T3 50°C $^{13}CH_4$ Heavy fraction methanotrophic MAGs

MAG	*pmoA* present	closest top two genera NCBI hits (% identity)	*mmoX* present	closest top two genera NCBI hits (% identity)	*MxaF* present	closest top two genera NCBI hits (% identity)	MIGA online taxonomy assignment (P value < 0.05)	MAG size (bp)	contigs	N50	GC content (%)	CheckM completion (%)	CheckM contamination (%)
7	no		no		no		*Gammaproteobacteria*	3261775	376	10498	57.2	73.95	2.55

T3 37°C $^{13}CH_4$ Heavy fraction methanotrophic MAGs

MAG	*pmoA* present	closest top two genera NCBI hits (% identity)	*mmoX* present	closest top two genera NCBI hits (% identity)	*MxaF* present	closest top two genera NCBI hits (% identity)	MIGA online taxonomy assignment (P value < 0.05)	MAG size (bp)	contigs	N50	GC content (%)	CheckM completion (%)	CheckM contamination (%)
9	no		no		yes	*Methylocaldum* (100.00) *Methylomagnum* (87.52)	*Gammaproteobacteria*	4306411	200	32455	57.12	96.16	7.51
19	no		no		no		*Methylococcales*	3334015	248	17447	60.71	80.91	2.23
39	no		no		no		*Methylococcales*	2797519	271	26240	51.07	72.19	5.28

NCBI BlastP hits (top two genera) for additional CH_4 metabolism genes in MAGs lacking *pmoA*, *mmoX* and *MxaF* marker genes.

MAG	*pmoC* present	closest top two genera NCBI hits (% identity)	*fhcD* present	closest top two genera NCBI hits (% identity)
T3 50°C heavy MAG 7	yes (one)	*Methylocaldum* (95.24) *Ca. Methylumidiphilus* (90.48)	yes (one)	*Methylocaldum* (97.65) *Methylogaea* (88.59)
T3 37°C heavy MAG 19	yes (one)	*Methylocaldum* (80.90) *Methylotetracoccus* (72.30)	yes (one)	*Methylomagnum* (90.94) *Methylogaea* (88.93)
T3 37°C heavy MAG 39	no		yes (one)	*Methylobacter* (99.33) *Methylotuvimicrobium* (94.30)

5.3.3.5 Comparison of candidate methanotroph MAGs across all five metagenome assemblies, and estimation of methanotroph relative abundance.

In order to identify MAGs from different metagenome assemblies that may represent the same methanotrophic bacterium, candidate methanotroph MAGs from the Timepoint 0 unfractionated, Timepoint 3 50ºC $^{13}CH_4$ heavy fraction and Timepoint 3 37ºC $^{13}CH_4$ heavy fraction metagenomes were compared with one another as well as with MAGs from the two Timepoint 3 (50ºC and 37ºC) $^{13}CH_4$ unfractionated DNA metagenomes. MAGs were compared pairwise using the Genome-to-Genome Calculator to provide an *in-silico* estimate of their similarity in line with DNA-DNA hybridisation methods. Where these estimates suggested a high likelihood of the MAGs representing the same subspecies (>70%), the amino acid sequences derived from functional gene markers present in both MAGs were also compared. CheckM was used to estimate the relative abundance of the recovered candidate methanotroph MAGs from each metagenome assembly. This estimate of relative abundance should only be viewed as a ballpark figure as the calculations make the assumption that each MAG is complete and assign the % based on the proportion of total reads mapping back to each MAG, when MAGs are incomplete (the MAGs in this study were assigned completion estimates between 70 and 98%) the relative abundance will be underestimated and if they are contaminated with many reads from other organisms it may be overestimated. To allow for a more accurate comparison of the MAG abundances within and between metagenome assemblies the Average MAG Read Coverage (AMRC) was calculated using the MetaWRAP quant_bins function. This calculates the average number of reads covering each nucleotide position along the length of each MAG and normalises this figure to be per 1 million reads used in the metagenome assembly. This normalised number can then be used to compare the abundance of MAGs within and between metagenome assemblies, the higher the MAG read coverage the more abundant the DNA of the represented species in the initial sequencing sample. As the coverage of the MAG is expected to be consistent along its length (and indeed coverage similarity is used to guide MAG binning), this method allows for comparison of MAG relative abundance without the bias associated with incomplete MAGs when using the CheckM total read mapping approach.

Note that colour coding was used to track MAGs representing the same methanotroph appearing in more than one metagenome comparison in this chapter.

5.3.3.5.1 Comparison of methanotroph MAGs from Timepoint 3 50ºC and 37ºC $^{13}CH_4$ heavy fraction metagenomes with MAGs from the corresponding unfractionated metagenomes and the DNA-SIP Timepoint 0 metagenome

The high-and-low-quality candidate methanotroph MAGs from the Timepoint 3 50ºC and 37ºC $^{13}CH_4$ heavy fraction metagenomes were first compared with MAGs from the corresponding Timepoint 3 50ºC and 37ºC $^{13}CH_4$ unfractionated metagenomes to find unfractionated metagenome MAGs representing the same methanotrophic bacteria. The estimated methanotroph MAG Average MAG read coverage (AMRC) was then used to identify candidate methanotroph MAGs in the two heavy fraction metagenomes representing active methanotrophs in these different temperature incubations, specifically those with DNA enriched (higher AMRC) in the heavy fraction metagenome, compared to the unfractionated metagenome (due to $^{13}CH_4$ derived ^{13}C incorporation). Each candidate methanotroph MAG from the 50ºC and 37ºC $^{13}CH_4$ heavy fraction metagenomes is listed in **Table 5.7** alongside the MAG representing the same methanotroph found in the unfractionated metagenome from the same incubation temperature, heavy fraction MAGs belonging to active methanotrophs are identified with an asterisk(*) for clarity. **Table 5.7** also shows the matching Timepoint 0 metagenome MAGs representing these same heavy fraction methanotrophs. Finally, an indication of the high level of amino acid similarity between the functional marker genes present across all MAGs attributed to the same methanotroph is provided, with the lowest % AAI of marker genes from pairwise comparison of the matching MAGs shown.

For each of the methanotrophic MAGs in the 50ºC $^{13}CH_4$ heavy fraction metagenome, matching MAGs were found in the 50ºC $^{13}CH_4$ unfractionated metagenome which demonstrated a high likelihood of representing the same subspecies (>78% probability and marker genes with 100% AAI). By comparing the MAG AMRC of the matching MAGs in the heavy fraction and unfractionated metagenomes it appears that three of the MAGs in the 50ºC heavy fraction (41, 36 and 21) metagenome are from methanotrophs with DNA enriched in this fraction, while the DNA of the fourth methanotroph MAG (7) was not enriched. This suggests that the heavy fraction enriched MAGs (*Methylocaldum* and *Methylococcaceae* species) represent active $^{13}CH_4$ oxidising methanotrophs from the 50ºC DNA-SIP incubation, while the MAG 7 methanotroph (also a *Methylocaldum* species) was less active. This is perhaps unsurprising as many *Methylocaldum* are known to be thermophilic or thermotolerant (Takeuchi et al., 2014b), the lower activity of MAG 7 could be due to this being one of the more mesophilic

Methylocaldum species, such as *Methylocaldum gracile* (Bodrossy et al., 1997), or a more extreme thermophilic *Methylocaldum* species that prefers temperatures well above 50ºC.

All four methanotrophic MAGs found in the 50ºC heavy fraction metagenome were also found in the Timepoint 0 unfractionated metagenome (generated from DNA extract from the biofilter soil community at 50ºC in-situ temperature), with two of the active methanotrophs in the 50ºC heavy fraction metagenome (yellow and blue labelled *Methylococcaceae* and *Methylocaldum*) detected at a high relative abundance in the Timepoint 0 metagenome. In contrast one of the methanotrophs (orange labelled *Methylocaldum*) with a high relative abundance in the Timepoint 0 metagenome did not appear to be enriched in the 50ºC heavy fraction metagenome and was considered to represent an inactive methanotroph under 50ºC DNA-SIP incubation conditions. The higher relative abundance of this methanotroph in the Timepoint 0 sample may be a legacy of previous higher or lower environmental temperatures more suitable for this methanotroph.

Comparing the AMRC of the Timepoint 0 MAGs with that of the corresponding MAGs from the 50ºC Timepoint 3 unfractionated metagenome, it was reassuring to note that the AMRC of the matching MAGs were within 30% for two of the three methanotrophs present above 1% relative abundance in the Timepoint 0 metagenome (labelled blue and yellow), which suggests that the 50ºC DNA-SIP incubations didn't dramatically alter the methanotroph community present when the soil was sampled at 50ºC. The single methanotroph present above 1% demonstrating a greater difference in relative abundance between the Timepoint 0 and 50ºC unfractionated MAGs (highlighted in orange) was also the only methanotroph that was not active in the DNA-SIP 50ºC incubations.

Matching MAGs for all but one of the methanotrophs found in the 37ºC $^{13}CH_4$ heavy fraction metagenome (all barring the *Methylocystis* MAG 31) were identified in the 37ºC $^{13}CH_4$ unfractionated metagenome. These included 37ºC heavy fraction MAGs 29 and 9 which likely represent two of the methanotrophs also found in the 50ºC $^{13}CH_4$ metagenomes (colour coded yellow and blue). Based on differences in AMRC between the matching heavy fraction and unfractionated metagenome MAGs, the DNA of the 37ºC heavy fraction MAGs 29 (*Methylococcaceae*), 35 (*Methylomicrobium*), 39 (*Methylobacter*) and 19 (*Methylococcaceae*) seem to be enriched and these likely represent the active methanotrophs in the 37ºC incubations, while the 37ºC heavy fraction MAG 9 methanotroph (blue labelled *Methylocaldum*) appears to be far less active at this temperature (37ºC) compared to the 50ºC

incubation metagenomes. As a MAG matching the heavy fraction *Methylocystis* MAG was not found in the unfractionated metagenome, it is hard to draw definite conclusions about the DNA enrichment status of this *Methylocystis* in the heavy fraction: it could be that a MAG was not found because the DNA from this methanotroph had a very low relative abundance in the unfractionated metagenome reads, alternatively it could have been more abundant but the idiosyncrasies of the metagenome assembly prevented recovery of a MAG meeting the bin_refinement threshold (70% completion, 10% contamination).

The lower AMRC of MAG 9 in the 37ºC heavy fraction metagenome compared with that for the matching MAG (19) in the unfractionated 37ºC metagenome suggests this methanotroph is not active in the 37ºC incubations. This may well be due to the incubation temperature, as these MAGs represents a thermophilic *Methylocaldum* species that appeared to be active in the 50ºC incubations. In contrast, the *Methylomicrobium* and *Methylobacter* with DNA enriched in the 37ºC heavy fraction metagenome MAGs (35 and 39) would be expected to be actively oxidising CH_4 at 37ºC as these are both mesophilic methanotroph genera (Bowman et al., 1993; Orata et al., 2018).

The apparent enrichment of the yellow labelled *Methylococcaceae* methanotroph DNA in the heavy fraction 37ºC incubation (MAG 29) is of particular interest as the DNA from this methanotroph was also found to be enriched in the heavy fraction of the 50ºC incubation. This indicates that this *Methylococcaceae* methanotroph has a broad temperature range over which it can compete for dominance in the active methanotroph community (37-50ºC), straddling the mesophilic and thermophilic ranges.

As might be expected, based on the difference in environmental temperature supporting the microbial community, fewer of the methanotrophs with MAGs in the Timepoint 0 metagenome (generated with DNA from biofilter soil that had been at 50ºC *in-situ*) were found among the methanotrophic MAGs recovered in the 37ºC incubated heavy fraction metagenome. Only two of these methanotrophs were found (yellow and blue highlighted *Methylococcaceae* and *Methylocaldum*) and only the yellow highlighted *Methylococcaceae* appeared to be an active methanotroph in the 37ºC incubation (enriched in the 37ºC heavy fraction metagenome). The AMRC of these methanotrophs shared between the 50ºC unfractionated, 37ºC unfractionated and Timepoint 0 (**Table 5.7**) metagenomes were lowest for the 37ºC unfractionated metagenome MAGs. Likely a direct result of a changing active methanotroph community due to a 13ºC drop in environmental temperature.

Table 5.7 Methanotroph MAGs from the 50ºC and 37ºC $^{13}CH_4$ heavy fraction metagenomes alongside MAGs believed to represent the same methanotroph found in the unfractionated metagenome from the same incubation temperature (>70% likelihood same subspecies, Genome-to-Genome Distance Calculator). AMRC stands for Average MAG Read Coverage (per million reads). Heavy fraction MAGs with an asterisk (*) are those MAGs believed to represent active methanotrophs at the given incubation temperature. They are considered active due to a higher AMRC in this heavy fraction metagenome compared with MAGs representing the same or very closely related methanotrophs in the unfractionated metagenome, suggesting their DNA density has been increased through active oxidation and incorporation of $^{13}CH_4$ derived carbon. Colour coding used to highlight the same or closely related methanotrophs appearing in multiple comparisons.

$^{13}CH_4$ 50ºC incubation Timepoint 3 metagenomes						Pre-incubation Timepoint 0 metagenome				Comparison of marker genes present in all MAGs (lowest pairwise % AAI)			
50ºC Heavy fraction metagenome **MAGs**	**Relative abundance** (%)	**AMRC** (Average MAG Read Coverage)	**50ºC Unfractionated** metagenome **MAGs**	**Relative abundance** (%)	**AMRC** (Average MAG Read Coverage)	**Timepoint 0** metagenome **MAGs**	**Relative abundance** (%)	**AMRC** (Average MAG Read Coverage)	**Taxonomy** (functional markers)	***pmoA***	***mmoX***	***mxaF***	***fhcD***
50ºC H **7**	0.3	2.2	50ºC U **40**	1.6	8.8	T0 **59**	5.6	28.2	*Methylocaldum*				100%
50ºC H **21 ***	0.5	3.2	50ºC U **17**	0.2	0.9	T0 **31**	0.4	1.9	*Methylococcaceae* likely *Methylocaldum*			100%	100%
50ºC H **36 ***	7.0	44.0	50ºC U **38**	6.7	37.4	T0 **39**	8.8	44.8	*Methylocaldum* (*Methylocaldum* 16S rRNA)			100%	100%
50ºC H **41 ***	6.9	43.9	50ºC U **62**	3.2	17.7	T0 **37**	4.5	22.8	*Methylococcaceae* (*Methylocaldum* 16S rRNA)		100%	100%	100%

$^{13}CH_4$ 37ºC incubation Timepoint 3 metagenomes						Pre-incubation Timepoint 0 metagenome				Comparison of marker genes present in all MAGs (lowest pairwise % AAI)			
37ºC Heavy fraction metagenome **MAGs**	**Relative abundance** (%)	**AMRC** (Average MAG Read Coverage)	**37ºC Unfractionated** metagenome **MAGs**	**Relative abundance** (%)	**AMRC** (Average MAG Read Coverage)	**Timepoint 0** metagenome **MAGs**	**Relative abundance** (%)	**AMRC** (Average MAG Read Coverage)	**Taxonomy** (functional markers)	***pmoA***	***mmoX***	***mxaF***	***fhcD***
37ºC H **9**	0.93	5.0	37ºC U **19**	5.8	25.7	T0 **39**	8.83	44.8	*Methylocaldum* (*Methylocaldum* 16S rRNA)				100%
37ºC H **19 ***	0.51	2.7	37ºC U **73**	0.15	0.8	n.d.	n.d.	n.d.	*Methylococcaceae*				99.66%
37ºC H **29 ***	5.51	29.1	37ºC U **48**	1.95	8.6	T0 **37**	4.51	22.8	*Methylococcaceae* (*Methylocaldum* 16S rRNA)		100%	99.83%	100%
37ºC H **31**	0.37	2.0	n.d.	n.d.	n.d.	n.d.	n.d.	n.d.	*Methylocystis*				
37ºC H **35 ***	3.91	20.3	37ºC U **32**	0.46	2.0	n.d.	n.d.	n.d.	*Methylomicrobium*	100% 100%		100%	100%
37ºC H **39 ***	6.56	35.8	37ºC U **29**	0.91	4.4	n.d.	n.d.	n.d.	*Methylobacter*				100%

5.3.3.6 Comparison of methanotroph MAGs from the DNA-SIP Timepoint 0 unfractionated metagenome and the sector 2C soil core metagenomes (Chapter 4)

The sector 19B DNA-SIP (pre-incubation) Timepoint 0 metagenome (from 50 cm depth) and the two sector 2C soil core metagenomes (10-30 cm and 30-50 cm depths), are all metagenomes of the microbial community in the biofilter soil operating at an *in-situ* temperature of 50ºC. While the estimated relative abundance and AMRC of methanotrophic MAGs in these metagenomes cannot be directly linked to the methane oxidation activity of the methanotrophs they represent, as is possible through comparison of the heavy fraction and unfractionated metagenome MAGs in a $^{13}CH_4$ DNA-SIP labelling experiment, they can still indicate which methanotrophic genera are the more populous amongst the recovered methanotrophic MAGs.

Methanotroph MAGs from the DNA-SIP Timepoint 0 unfractionated metagenome were compared with those found in the two sector 2C core metagenomes (**Chapter 4**), to identify MAGs representing the same methanotrophs across the different metagenomes. as mentioned in **Chapter 4** the 2C 10-30 cm metagenome MAG 6 and the 2C 30-50 cm metagenome MAG 43 were already identified as representing the same or a highly similar methanotroph strain. Methanotroph MAGs with a high probability (>70%) of representing the same methanotroph subspecies across these metagenomes are displayed in **Table 5.8** along with the estimated MAG relative abundance, and AMRC. Colour coding is again used to highlight those MAGs representing methanotrophs which also appeared in the DNA-SIP metagenome comparison table in this Chapter (**Table 5.7**).

The yellow labelled *Methylococcaceae* methanotroph which appeared to be an active methanotroph in both the 50ºC and 37ºC DNA-SIP incubations, based on higher AMRC in the heavy fraction metagenome compared with the unfractionated metagenome (**Table 5.7**), was found to be present at a high estimated relative abundance (3.27-5.27%) in all three metagenomes; 2C 10-30 cm, 2C 30-50 cm and Timepoint 0 (**Table 5.8**). While the blue labelled *Methylocaldum* methanotroph which had the highest relative abundance of any recovered methanotroph MAG in the DNA-SIP Timepoint 0 metagenome (8.83%), and was an active methanotroph in the 50ºC DNA-SIP incubation, was not identified in the shallower of the two core 2C metagenomes (10-30 cm) and while present in the deeper core 2C metagenome (30-50 cm) the MAG relative abundance was considerably lower (0.37%). The orange labelled *Methylocaldum* methanotroph, which featured a high relative abundance in the DNA-SIP Timepoint 0 metagenome (5.63%) but did not appear to be active in the 50ºC DNA-SIP $^{13}CH_4$

incubations (lower relative abundance in the heavy fraction vs the unfractionated metagenome (**Table 5.7**)), was only detected at a low relative abundance in the shallower 10-30 cm core 2C metagenome. Finally, the purple labelled "likely *Methylocaldum*" present at low relative abundance in the DNA-SIP Timepoint 0 metagenome and a potentially active methanotroph in the 50ºC DNA-SIP incubation, was detected at a comparably low relative abundance in the deeper of the core 2C metagenomes (30-50 cm). The main take home point of these comparisons is that the *Methylococcaceae* methanotroph represented by the yellow labelled MAGs seems to be fairly ubiquitous at 50ºC in the Strumpshaw biofilter, appearing to make up roughly 5% of the total microbial population in metagenomes assembled from microbial DNA extracted from soil samples taken at different coordinates (Sector 2C and 19B) and depths (10-30, 30-50 cm) within the biofilter. While MAGs representing the blue labelled *Methylocaldum*, the other most abundant active methanotroph from the DNA-SIP 50ºC incubation metagenomes, were only discovered in the DNA-SIP Timepoint 0 metagenome and the deeper of the core 2C metagenomes (although with a much lower relative abundance of 0.37%), the very high relative abundance seen in the Timepoint 0 and the 50ºC DNA-SIP metagenomes suggests that this may also be a major methane oxidiser at 50ºC. The ability of the yellow labelled *Methylococcaceae* methanotroph to remain one of the dominant CH_4 oxidisers at both thermophilic (50ºC) and mesophilic (37ºC) temperatures, may provide this methanotroph with a significant advantage in a system like the Strumpshaw biofilter where the in-situ temperature can vary during operation (**Chapter 3**). In fact, if the core 2C soil had only just heated up to 50ºC when sampled from the biofilter, this might explain the abundance of the yellow labelled *Methylococcaceae* and scarcity of the blue labelled *Methylocaldum*.

Table 5.8 Methanotroph MAGs from the sector B19 Timepoint 0 metagenome alongside MAGs believed to represent the same methanotroph found in the sector 2C soil core metagenomes (**Chapter 4**) (>70% likelihood same subspecies, Genome-to-Genome Distance Calculator). AMRC stands for Average MAG Read Coverage. Colour coding used to highlight the same or closely related methanotrophs appearing in multiple comparisons (including **Table 5.7**).

Sector B19 DNA-SIP Timepoint 0 metagenome			Sector 2C core section metagenomes									
Timepoint 0 metagenome **MAGs**	**Relative abundance** (%)	**AMRC** (Average MAG Read Coverage)	**2C 10-30 cm** metagenome **MAGs**	**Relative abundance** (%)	**AMRC** (Average MAG Read Coverage)	**2C 30-50 cm** metagenome **MAGs**	**Relative abundance** (%)	**AMRC** (Average MAG Read Coverage)	**Taxonomy** (functional markers)	Comparison of marker genes present in all MAGs (lowest pairwise % AAI)			
										pmoA	***mmoX***	***mxaF***	***fhcD***
T0 **31**	0.37	1.9	n.d.	n.d.	n.d.	2C 30-50 **50**	0.26	1.3	*Methylococcaceae* likely *Methylocaldum*				100%
T0 **37**	4.51	22.8	2C 10-30 **6**	5.27	28.0	2C 30-50 **43**	3.27	15.9	*Methylococcaceae* (*Methylocaldum* 16S rRNA)		100%	99.83%	100%
T0 **39**	8.83	44.8	n.d.	n.d.	n.d.	2C 30-50 **16**	0.37	2.1	*Methylocaldum* (*Methylocaldum* 16S rRNA)			100%	100%
T0 **59**	5.63	28.2	2C 10-30 **36**	0.81	4.3	n.d.	n.d.	n.d.	*Methylocaldum*				100%

5.4 Discussion

The DNA-SIP $^{13}CH_4$ labelling experiments in this Chapter demonstrate that the active CH_4 oxidising methanotrophs in the biofilter are linked to the *in-situ* temperature. Analysis of the 16S rRNA amplicons generated from the heavy and light fractions of $^{13}CH_4$ and $^{12}CH_4$ fed soil from the sector 11B/11C boundary core (**Chapter 5.2**) highlighted a different set of active methanotrophs at each of the three incubation temperatures used 30, 37 and 45ºC. With the active methanotrophs identified by enrichment of their 16S rRNA gene sequences in the corresponding temperature ^{13}C incubated heavy fraction compared to the ^{12}C incubated heavy fraction or accompanying light fractions. At 30ºC the most active methanotroph appeared to be *Crenothrix* with the mesophilic methanotrophs *Methylocella* and *Methylocystis* also active. At 37ºC, a mixture of mesophilic (*Methylocella* and *Methylocystis*) and thermophilic (*Methylocaldum*) methanotroph genera were most active. At 45ºC, only a thermophilic (*Methylocaldum*) methanotroph genus appeared to be active. It is probable that these diverse active methanotroph communities will become dominant at different points during biofilter operation due to the variable *in-situ* temperatures measured during biofilter operation (**Chapter 3.2**). This would tally with sequences from *Crenothrix*, *Methylobacter* and *Methylocaldum* having the highest relative abundance amongst the methanotrophic 16S rRNA gene sequences detected in 16S rRNA gene amplicons generated from microbial communities present in the biofilter at unknown environmental temperatures (**Chapter 4.4.1**), and a highest relative abundance of *Methylocaldum* sequences at a known *in-situ* temperature of 50ºC (**Chapter 4.4.2**). These findings suggest that, following biofilter switch-on, there could be a succession of active methanotroph communities from initially mesophilic genera to increasingly thermotolerant and thermophilic genera as the biofilter temperature rises during uninterrupted operation (driven by methanotroph CH_4 oxidation activity) (**Chapter 3.2.2**), leading to a possible *Methylocaldum* "climax" community at temperatures above 50ºC. Re-emergence of the mesophiles as dominant methanotrophs would then be expected following interruption of biofilter operation due to CH_4 supply interruption or non-optimal moisture conditions and the collateral drop in biofilter temperature due to cessation of methanotroph activity (**Chapter 3.4**).

The sector 19B soil DNA-SIP incubations at 50ºC and 37ºC demonstrated a similar partitioning of active methanotrophs into thermophilic (predominantly *Methylocaldum* with a smaller *Methyloterricola* contribution) and mesophilic (*Methylobacter* and small amounts of

Methylocystis) across the two temperatures (based on 16S rRNA amplicon sequencing). It was interesting to note that the *Methylocaldum* present did not appear to be active in the 37ºC incubations and *Methylobacter* was clearly the most active methanotroph detected at this temperature, which contrasts with the split between the active methanotroph genera *Methylocaldum*, *Methylocella* and *Methylocystis* observed at 37ºC in the earlier DNA-SIP experiment (**Table 5.1**). These differences may be due to the depth and temperature at which biofilter soil was retrieved for the two different DNA-SIP experiments, the earlier experiment (**Chapter 5.2**) making use of soil retrieved from the top 10cm of the biofilter at an unknown *in-situ* temperature and the second DNA-SIP incubation experiment used soil retrieved from a depth of 50 cm and an *in-situ* temperature of 50ºC. While the *in-situ* temperature of the shallower soil was not measured, temperature depth profiles suggest that the temperature of this region is often lower than at greater depth during operation (**Chapter 3.2 Tables 3.2-3.4**). It may be that the methanotrophic community in the 0-15 cm soil sample was better suited to mesophilic conditions than the community in the deeper potentially hotter 50ºC soil sample, resulting in noticeably different active methanotroph communities when these soils were incubated at 37ºC. The 0-15 cm soil may have had a larger population of mesophilic *Methylocaldum* species, while perhaps the *Methylobacter* in the 50 cm depth soil sample was better at weathering the in-situ 50ºC temperature than other mesophilic methanotrophs present and quicker to exploit a return to a lower temperature.

Metagenome sequencing and analysis of the sector 19B soil DNA-SIP $^{13}CH_4$ Timepoint 3 50ºC and 37ºC incubation heavy fraction DNA as well as the initial Timepoint 0 DNA extracts allowed recovery of a number of high quality methanotroph metagenome assembled genomes (MAGs) from these three metagenome assemblies. Comparison of the relative abundances of methanotrophs found in both the Timepoint 3 heavy fraction and unfractionated DNA metagenomes was used to determine which methanotrophs were likely to be actively oxidising CH_4 in the 50ºC and 37ºC DNA-SIP $^{13}CH_4$ incubations. In the 50ºC incubation, a common in-situ temperature within the biofilter during uninterrupted operation (**Chapter 3.2**), a *Methylococcaceae* methanotroph and a *Methylocaldum* methanotroph were active and abundant methanotrophs among the reconstructed MAGs. These methanotrophs were also the most abundant methanotrophs with reconstructed MAGs in the pre-incubation Timepoint 0 metagenome, which was derived from the biofilter microbial community present at an *in-situ* temperature of 50ºC, suggesting these methanotrophs may be major players in CH_4 turnover within the Biofilter at 50ºC. The same *Methylococaceae* methanotroph was also the most

abundant methanotroph found in the two core 2C metagenomes (discussed in **Chapter 4.5**), which were also generated from the DNA of the biofilter microbial community at an *in-situ* temperature of 50ºC. In the 37ºC incubation, the most abundant active methanotrophs with recovered MAGs were a *Methylobacter* a *Methylomicrobium* (both typically mesophilic) and the same *Methylococcaceae* methanotroph found to be active in the 50ºC incubation, suggesting that this *Methylococcaceae* is the most competitive methane oxidiser at both 50 and 37ºC. This may give the *Methylococcaceae* methanotroph an advantage over methanotrophs with narrower optimal temperature ranges, as the biofilter temperature can fluctuate during operation and the highest temperatures (50+ºC) are less likely to occur at shallower depths (**Chapter 3.2**).

A comparison of the active methanotrophic genera at 50 and 37ºC, as determined by the sector B19 DNA-SIP 16S rRNA gene amplicon and metagenome analyses summarised above, shows that they are not quite in agreement. Whereas both approaches seem to agree that *Methylocaldum* species account for most of the active methanotrophs in the 50ºC ^{13}C-fed incubations potentially including the *Methylococcaceae* methanotroph found in the metagenomes (which may possess a *Methylocaldum* 16S rRNA sequence), the two methods identify different active methanotroph communities for the 37ºC ^{13}C-fed incubations. The 16S rRNA gene analysis indicated that *Methylobacter* is highly active and *Methylocystis* as the only other active methanotroph at 37ºC, while the 37ºC DNA-SIP incubation metagenomes identified *Methylomicrobium*, the *Methylococcaceae* methanotroph with possible *Methylocaldum* 16S rRNA sequence and another unidentified *Methylococcaceae* as active methanotrophs in addition to *Methylobacter* and possibly *Methylocystis* (which was only recovered as a MAG in the 37ºC heavy fraction). It has been observed that the results from 16S rRNA gene amplicon sequencing and metagenome sequencing approaches for the same microbial community study do not always produce the same results (Durazzi et al., 2021). 16S rRNA gene sequencing analysis can be subject to a greater degree of bias due to the targeted nature of the amplification, with varying 16S rRNA gene PCR primer specificity across the different bacteria and archaea in the sample (Klindworth et al., 2013). It could be that PCR amplification of 16S rRNA gene sequences was unsuccessful for those active methanotrophs only identified by metagenome analysis in the 37ºC DNA-SIP incubations. With this in mind, the metagenome analysis may provide a more complete view of the active methanotrophs in the biofilter soil at 37ºC.

Finally, the presence of facultative methanotrophs among several of the ^{13}C labelled methanotroph genera found in the DNA-SIP amplicon and metagenome studies in this chapter, make a caveat necessary: It cannot be definitely determined if the active (but potentially facultative) methanotrophs belonging to the genera *Methylocystis*, *Methylocella*, *Crenothrix* found through ^{13}C DNA labelling in this chapter are truly oxidising CH_4, as they could potentially be gaining the ^{13}C label by effectively cross-feeding on downstream products of CH_4 oxidation or other substrates.

Chapter 6: Isolation and genome analysis of biofilter methanotrophs.

6.1 Initial isolation experiments

Preliminary enrichment and isolation work carried out by Elliot Brooks had resulted in successful isolation of a biofilter methanotroph, *Methylococcus capsulatus* (Norfolk). Briefly, Mr Brooks set up enrichment cultures in 120 ml serum vials containing NMS medium and soil taken from the top 5 cm of the biofilter, these were incubated at 25ºC with 20% headspace CH_4. Serial dilution and plating onto NMS agar resulted in individual bacterial colonies, one of which was identified as *Methylococcus capsulatus* (based on 16S rRNA sequence) which was then maintained in liquid NMS culture at 37ºC (**Chapter 2.7**). When grown on solid NMS agar (1.5%), colonies of *Methylococcus capsulatus* (Norfolk) are faun coloured with a slight orange tint as can be seen in **Figure 6.1**. This isolate was sent for Illumina whole-genome shotgun sequencing by MicrobesNG. All further isolate work was undertaken by the author.

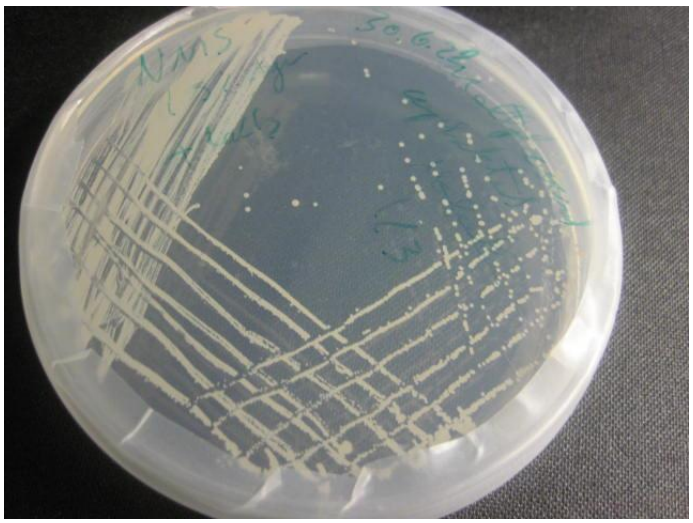

Figure 6.1 Colonies of *Methylococcus capsulatus* (Norfolk) grown on solid NMS agar (1.5%).

As *Methylococcus capsulatus* (Norfolk) was isolated from a biofilter system that heats up to temperatures above 60ºC during operation (**Chapter 3**) the temperature range at which this methanotroph would grow was explored. Sealed 120 ml serum vials containing 20 ml NMS medium were inoculated with 1 ml of NMS diluted *M.c* (Norfolk) inoculum from a purity

checked NMS starter culture (to give each serum vial an initial $O.D_{600}$ of ~0.1). The initial O.D of the inoculated medium in each vial was measured at 600nm and recorded. The headspace of each vial was gassed with 20 ml CH_4 and the vials were incubated at a range of temperatures (25, 30, 37, 45, 50 and 55ºC). The headspace CH_4 and culture $O.D_{600}$ were measured periodically to determine if *M.c* (Norfolk) was capable of growing at each incubation temperature, with increasing $O.D_{600}$ values indicating cell proliferation and headspace CH_4 depletion suggesting CH_4 oxidation activity (for methods see **Chapter 2.5**). An increase in measured $O.D_{600}$ values and a decrease in headspace CH_4 was observed in all incubation temperatures from 25-50ºC, while after two weeks no increase was observed in the 55ºC incubation $O.D_{600}$. These results indicated that *Methylococcus capsulatus* (Norfolk) was capable of growth over a 25-50ºC temperature range with an upper limit between 50 and 55ºC (the lower temperature limit for growth was not established). In addition to this, 20 ml NMS cultures inoculated with *M.c*. (Norfolk) (in 120 ml serum vials) were supplied with 5% v/v methanol (instead of CH_4) and incubated at 37ºC for 9 days, $O.D_{600}$ measurements and light microscope observation of culture cells indicated that *M.c.* (Norfolk) was capable of growing when supplied with this concentration of methanol. Such a high tolerance for methanol in *Methylococcus capsulatus* was unknown until it was very recently reported by Oshkin et al. (Oshkin et al., 2022) in the *Methylococcus capsulatus* MIR strain.

6.2 Isolating the biofilter soil methanotroph *Methylocaldum*

Isolation of thermophilic methanotrophs from the biofilter became a priority when it became apparent that the biofilter often operates at elevated temperatures (**Chapter 3**), for both genome sequencing and future study. To facilitate this, a biofilter core soil sample was taken adjacent to a hot temperature profile measured in sector 12D (30-80 cm depth temperature measurements) (**Table 3.2**). A methane oxidising isolate was recovered from a shaking 10 ml NMS enrichment culture incubated at 50˚C with 16.7% headspace CH_4 (**Chapter 2.7**). This enrichment culture was initially inoculated with 1 g of biofilter soil from the deepest segment (60-80 cm below biofilter surface) of the sector 12D soil core. After three subcultures the enrichment culture was serially diluted and spread onto NMS agar (1.8% w/v) and again incubated at 50˚C with 50% headspace CH_4 (**Chapter 2.7**). After two weeks, a large number of colonies could be seen on the dilution streak plates, many of these looked very similar to *M.c* (Norfolk) colonies (faun with an orange tint), however there were one or two distinct

brown colonies. One such brown colony on a 1 x 10^{-4} dilution plate was selected for further investigation. This colony was picked and streaked onto a fresh NMS agar plate (1.5% w/v) and incubated with 50% headspace CH_4 at 50˚C. Once uniform brown colonies were visible on the inoculated plate they were scraped off one third of the plate with a sterile loop and their DNA extracted using a Fast DNA SPIN Kit for Soil. (**Chapter 2.9.2**) This extracted DNA was used as a template for 16S rRNA PCR with the following PCR modifications: [50 µl volume reaction mix], [27F and 1492R primers], [16S_72 PCR protocol]. PCR products were validated by 1% agarose gel electrophoresis and underwent PCR cleanup (Roche high pure kit) and nanodrop DNA quantitation before being sent for overnight Sanger sequencing with Eurofins (**Chapter 2.10**). The resulting DNA sequence was then trimmed down to the higher quality bases (20-600bp) and used in a nucleotide BLAST search against the NCBI database (National Center for Biotechnology Information, 1988). The top hits against known strains returned were against the 16S rRNA genes of *Methylocaldum szegediense* KTM-1 and OR2 (Bodrossy et al., 1997; Jäckel et al., 2005) with 100% query cover E value of 0.0 and a 99.66 percent identity against both (**Chapter 2.12.1**).

The high similarity of the 16S rRNA genes between this biofilter isolate and known *Methylocaldum szegediense* strains suggested this isolate was likely be a *Methylocaldum* species and possibly a strain of *Methylocaldum szegediense*.

This putative *Methylocaldum* isolate was stored as a liquid culture with monthly subculturing at an incubation temperature of 50˚C. Purity was maintained by serial dilution plating and restreaking every three months (**Chapter 2.7.3**). When grown on solid NMS agar (1.8%), *Methylocaldum szegediense* (Norfolk) forms distinctive brown colonies as shown in **Figure 6.2**.

Figure 6.2 Colonies of *Methylocaldum szegediense* (Norfolk) grown on solid NMS agar (1.8%).

The temperature range over which *Methylocaldum* sp. (Norfolk) was capable of growth was investigated in the same manner as was done for *Methylococcus capsulatus* (Norfolk) (**Chapter 6.1**), with the exception that the NMS contained vitamin solution in the *Methylocaldum* sp. (Norfolk) inoculated vials (**Chapter 2.5.1**). The incubation temperatures used in this experiment were 37, 45, 50, 55, 58, 60, 62 and 65ºC. An increase in $O.D_{600}$ values was observed in the *Methylocaldum* sp. (Norfolk) inoculated cultures incubated at 37-62ºC indicating *Methylocaldum* sp. (Norfolk) is capable of growth over this temperature range. The lower limit of the growth range was not established while the upper limit lies between 62 and 65ºC, as no increase in O.D600 values were observed at 65ºC after two weeks of incubation.

6.3 *pmoCAB* in *Methylococcus capsulatus* (Norfolk)

The *Methylococcus capsulatus* (Norfolk) strain, originally isolated and sent for basic short-read-only genome sequencing by Elliot Brooks, was then submitted and mounted on the MicroScope platform by Muhammad Farhan Ul-Haque who also performed some initial annotation and identified a *pmoCAB* cluster. This genome sequence was then further interrogated by the author, but no second full *pmoCAB* cluster matching that found in *M.capsulatus* (Bath) could be identified, two contigs did appear to contain the very end of a *pmoCAB* cluster along with a suite of coding sequences matching those found adjacent to the *pmoCAB* clusters in *M.c* (Bath) illustrated in **Figure 6.3**.

This highlighted an issue with the *M.c* (Norfolk) short read genome sequence in that while it had a good CheckM completeness estimate (>99%), it was constructed from quite a few contigs (78) with over 46 of these shorter than 2000 bp, indicative of a fragmentary assembly. It was important to determine if there were one or two copies of *pmoCAB* in *M.c* (Norfolk). If there was only one *pmoCAB* cluster then this isolate could be an ideal model for *pmoCAB* knockout studies as double null *pmo* mutants have proven difficult to obtain in *M.c* (Bath) (Stolyar et al., 1999).

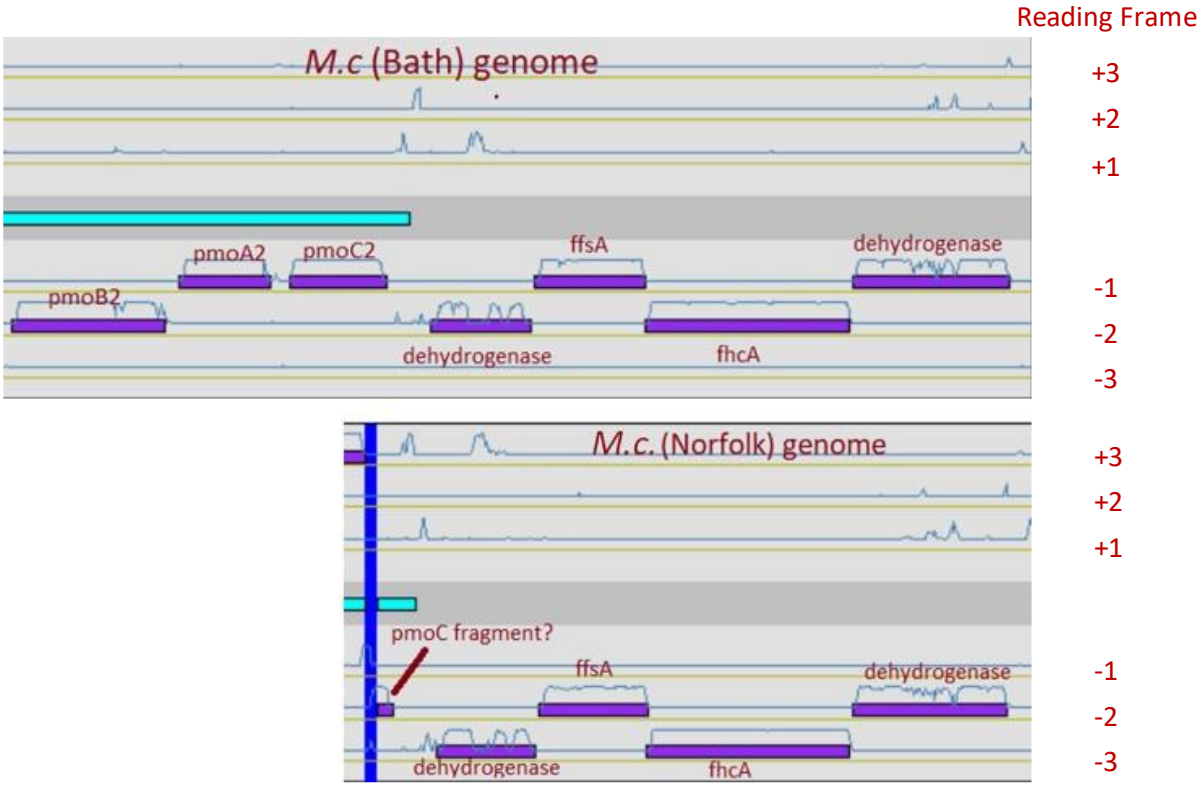

Figure 6.3 Example of one of the *Methylococcus capsulatus* (Norfolk) contigs ending with a severely truncated *pmoC* gene fragment, shown alongside a region of the *Methylococcus capsulatus* (Bath) genome with a matching suite of coding sequences adjacent to a full *pmoCAB* cluster. The vertical blue line in the *M.c.* (Norfolk) genome extract represents the end of a contig.

Two sets of primers were designed that would produce PCR products covering the region from a few hundred bp upstream of *pmoC* on the two different contig sequences with terminal *pmoC* fragments, through to the midpoint of *pmoA* (provided the truncated genes are in fact the two copies of *pmoC* adjacent to *pmoA*). These primer pairs (pmoCHF, pmoCHR1 and pmoCHF, pmoCHR2) are shown in **Table 2.3**. Two sets of colony PCR reactions using *Methylococcus capsulatus* (Norfolk) DNA were carried out using these primers, with PCR modifications: [50

µl reaction volume], [pmoCHF and pmoCHR1 or pmoCHF and pmoCHR2 primers], [PmoCABH1 PCR protocol] (**Chapter 2.10**). In addition, *Methylococcus capsulatus* (Bath) DNA was used as a positive control, as the pmoCHF (*pmoA* midpoint) primer had been designed using the *Methylococcus capsulatus* (Bath) *pmoA* sequences. The M.c (Norfolk) and M.c (Bath) PCR products were then ligated into vectors using the Promega pGEM-T Easy Vector System I and used to transform Top10 competent cells (**Chapter 2.10.5**). White colonies (blue/white screening) successfully transformed with one or the other of the two primer pair PCR products from both *M.c* (Norfolk) and *M.c* (Bath) were then used to provide templates for colony PCR reactions, modifications: [50 µl] [M13F, M13R primers] [16S_72col protocol]. Colony PCR products derived from the initial pmoCHF/pmoCHR1 and pmoCHF/pmoCHR2 PCR reactions for both *M.c* (Norfolk) and *M.c* (Bath) were then cleaned up using a Roche High Pure PCR Product Purification Kit and then sent for overnight Sanger DNA sequencing. In both *M.c*. (Norfolk) and *M.c*. (Bath) the two different PCR primer pairs (pmoCHF/pmoCHR1 and pmoCHF/pmoCHR2) successfully amplified genomic DNA. When the 5' and 3' ends of the *M.c*. Norfolk PCR products were sequenced they were found to match half of a *pmoA* gene and an adjacent *pmoC* gene sequence along with one or the other of the upstream sequences found next to the *pmoC* truncated fragments in the genome assembly. This demonstrated that there was at least half of a *pmoA* sequence next to each of these two *pmoC* sequences possessing different upstream genomic DNA regions in *M.c.* (Norfolk). This was a strong indication that there are two copies of *pmoCAB* in *M.c.* (Norfolk).

The absence of the second *pmoCAB* sequence coupled with the fact that the full *pmoCAB* cluster was on a very short contig lacking genome context lead to the decision to re-sequence the genome. The *M.c* (Norfolk) isolate was sent for enhanced genome sequencing with MicrobesNG, this coupled short Illumina and long Nanopore reads to generate a hybrid assembly on a single closed contig. The long but more error prone Nanopore reads allow for better bridging of repetitive regions while scaffolding a high read coverage of the shorter but accurate Illumina reads corrects any mistakes in the longer reads. The end result is improved reconstruction of repetitive regions and multicopy genes in the genome.

6.4.1 Genome analysis of biofilter methanotroph isolates

Both of the biofilter methanotroph isolates, *Methylococcus capsulatus* (Norfolk) and *Methylocaldum* sp. (Norfolk), were sent for enhanced (Illumina and Nanopore) genome

sequencing with MicrobesNG. This resulted in two high quality (>99% completion estimate) genomes, which were then mounted on the MicroScope platform for automated annotation and taxonomic analysis. An initial summary of genome stats and features is shown in **Table 6.1**. Both of these genomes were closed and encode two copies of the ribosomal RNA molecules (within each genome the 16S rRNA gene sequences were 100% identical). Additionally the MicroScope analysis pipeline assigned a *Methylococcus capsulatus* and *Methylocaldum szegediense* taxonomy to the two genomes (based on average nucleotide identity and genome topology).

Table 6.1 Genome stats and features for the two Strumpshaw biofilter methanotroph isolates, along with the taxonomy assigned to each by the MicroScope analysis pipeline.

Methylococcus **isolate**

Replicon	Seq length (bp)	% GC	number of CDS	ribosomal RNAs			CheckM		MicroScope assigned taxonomy
				16s rRNA	23s rRNA	5s rRNA	Completeness	Contamination	
chromosome	3,398,174	63.61	3324	2	2	2	99.9001	0	*Methylococcus capsulatus*

Methylocaldum **isolate**

Replicon	Seq length (bp)	% GC	number of CDS	ribosomal RNA			CheckM		MicroScope assigned taxonomy
				16s rRNA	23s rRNA	5s rRNA	Completeness	Contamination	
chromosome	4,869,648	57.16	5044	2	2	2	99.381	3.11419	*Methylocaldum szegediense*
plasmid	25,724	58.25	38	0	0	0			

The "genome clustering" function on the MicroScope platform was then used to compare the genomic similarity of a number of different methanotrophs with the Strumpshaw biofilter isolates. This tool uses MASH to measure pairwise genome distance and constructs a neighbour joining tree from the resulting distance matrix (**Figure 6.4**). This provided a good visual reference for the placement of the two isolates into the *Methylococcus capsulatus* and *Methylocaldum szegediense* species. This tree also highlighted a very close genome similarity between *Methylococcus capsulatus* (Norfolk) and *Methylococcus capsulatus* (Texas) (Foster and Davis, 1966) and between *Methylocaldum szegediense* (Norfolk) and *Methylocaldum szegediense* (O-12) (Eshinimaev et al., 2004).

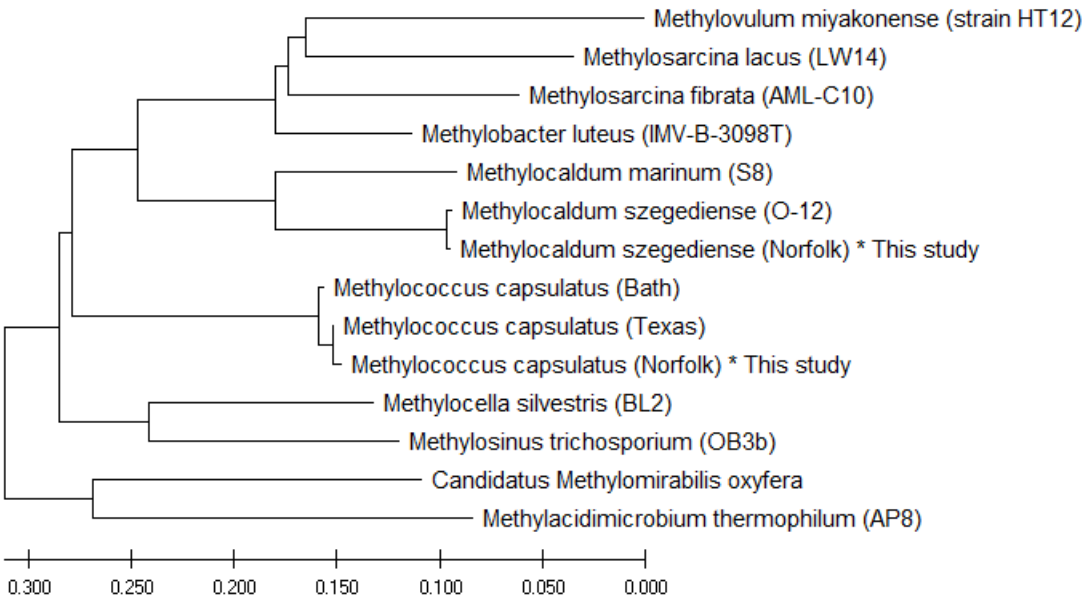

Figure 6.4 Neighbour-joining tree generated from a range of methanotroph genomes including the biofilter isolates *Methylococcus capsulatus* (Norfolk) and *Methylocaldum szegediense* (Norfolk) highlighting their taxonomic placement among the *M.capsulatus* and *M.szegediense* species.

6.4.2 Metabolic pathways predicted from the *Methylococcus capsulatus* (Norfolk) genome

6.4.2.1. Methane oxidation pathway

The genome of *Methylococcus capsulatus* (Norfolk) was found to contain two full copies of the *pmoCAB* cluster encoding the subunits of the pMMO, both of these clusters were in the typical 5' > 3' (*pmoC* > *pmoA* > *pmoB*) orientation (Lieberman and Rozenzweig, 2004). A single *pmoC* gene sequence remote from both clusters was also present. This methanotroph also contains genes encoding the sMMO, with a full set of structural genes in the common 5' > 3' *mmoXYBZDC* arrangement in the genome (Lee, 2016), followed by a conserved gene of unknown function and then the genes *mmoG*, *mmoQ*, *mmoS* and *mmoR* (with the *mmoQ* and *mmoS* genes encoded on the opposite DNA strand). *mmoG* encodes a GroEL-like protein and *mmoR* encodes a transcriptional regulator which were both found to be required for transcription of smmo genes and expression of functional sMMO in *Methylosinus trichosporium* OB3b (Stafford et al., 2003). *mmoS* and *mmoQ* are thought to encode a two-component signalling system involved in the "copper switch" (**Chapter 1.2.4.1**) between pMMO and sMMO expression in *Methylococcus* species (Csáki et al., 2003; Ukaegbu et al.,

2006). This arrangement of genes also occurs in the *M.c* (Bath) (Ward et al., 2004) and *M.c.* (Texas) (Kleiveland et al., 2012) genomes although a transposase gene is located between *mmoB* and *mmoZ* in *Methylococcus capsulatus* (Bath). In addition to the MMO genes a *mopE* gene was present. This gene encodes the outer membrane associated protein MopE, a copper chaperone thought to be part of a Cu uptake system, expressed under Cu limited conditions (Ve et al., 2012).

Methanol oxidation potential in the *M.c. Norfolk* genome is provided by a gene cluster (*mxaFJGIRSACKLD*) encoding the large (*mxaF*) and small (*mxaI*) calcium-dependent methanol dehydrogenase subunits and accessory genes (Amaratunga et al., 1997; Trotsenko and Murrell, 2008). A lanthanide-dependent methanol dehydrogenase *xoxF* gene was also detected, along with the *xoxJ* (a periplasmic binding protein) gene involved in *xoxF* dehydrogenase activation (Featherstone et al., 2019).

M.c (Norfolk) encodes full sets of genes for the tetrahydromethanopterin (*fae, mtdB, fch* and the formyltransferase/hydrolase complex) and tetrahydrofolate (*mtdA, fchA, ftfl*) linked formaldehyde oxidation pathways (Trotsenko and Murrell, 2008).

Finally, three sets of genes encoding formate dehydrogenase enzymes, for the final step in the CH_4 oxidation pathway (formate to carbon dioxide), also feature in this genome. Giving *Methylococcus capsulatus* (Norfolk) the genomic potential to oxidise CH_4 through to CO_2.

6.4.2.2. Methanotrophic carbon assimilation pathways

Genes encoding enzymes for a complete ribulose monophosphate pathway were identified in *M.c. Norfolk*, indicating that this is likely a primary route for CH_4 derived carbon assimilation in this organism. Genes encoding a complete Calvin-Benson-Bassham (CBB) cycle were also found. While the gene for sedoheptulose-1,7-bisphosphatase was missing, also absent in the *Methylococcus capsulatus* (Bath) genome (Ward et al., 2004), a copy of the gene encoding pyrophosphate-dependent 6-phosphofructokinase (PPi-PFK) found in *M.c* (Bath) and shown by Reshetnikov et al to be capable of catalysing the same step in the CBB cycle was present (98.57% nucleotide derived aa identity) (Reshetnikov et al., 2008). The similarity of this isolate to *Methylococcus capsulatus* (Bath) suggests that *M.c* (Norfolk) may also require the CBB cycle RubisCO for CO_2 fixation and growth (Henard et al., 2021). The genome inventory of *Methylococcus capsulatus* (Norfolk) does not include a complete serine pathway with genes

encoding glycerate dehydrogenase, glycerate-2-kinase, phosphoenolpyruvate carboxylase and two malate thiokinase subunits (*hprA, gck, ppc, mtkA* and *mtkB*) all absent from the genome.

6.4.2.3. Key nitrogen metabolism genes

The nitrogenase structural genes *nifH*, *nifK* and *nifD* were detected in this genome, indicating dinitrogen fixation potential. The hydroxylamine oxidoreductase (*hao*) gene for removal of toxic hydroxylamine was also present. Orthologues of the nitric oxide reductase genes *norB* and *norC* genes were detected in the genome, while no copies of *nirK* or *nirS* genes encoding nitrite reductase or the *nosZ* gene for nitrous oxide reductase were found, suggesting that *Methylococcus capsulatus* (Norfolk) could be a source of nitrous oxide production.

Methylococcus capsulatus (Norfolk) possesses an alanine dehydrogenase gene (*ald*) for ammonia assimilation via pyruvate, as well as the genes (*GDH2* and *gdhA*) encoding NADH and NADP glutamate dehydrogenases involved in ammonia assimilation via alpha-ketoglutarate and the GS/GOGAT cycle. The remaining key genes for the GS/GOGAT cycle, *glnA* encoding glutamine synthetase and *gltB* and *gltD* for glutamate synthase were also found.

6.4.2.4. Comparison of conserved marker genes with the closest relative of *Methylococcus capsulatus* (Norfolk).

The genome from extant methanotroph most similar to *Methylococcus capsulatus* (Norfolk) is the draft genome for *Methylococcus capsulatus* (Texas) produced by Kleiveland et al (Kleiveland et al., 2012) based on *in-silico* DNA-DNA hybridisation estimates generated using the Genome-to-Genome Distance Calculator (**Chapter 2.12.1**). **Table 6.2** shows a nucleotide and protein BLAST comparison of key methanotroph and methylotroph marker genes as well as DNA-DNA hybridisation estimation between these two genomes.

The DNA-DNA hybridisation results indicate that *Methylococcus capsulatus* (Norfolk) and (Texas) are very closely related strains. The absence of a second *pmoA* or 16S rRNA gene sequences in the *Methylococcus capsulatus* (Texas) draft genome is likely to be an artefact of this genome's fragmentary assembly, in much the same way that the initial short read *M.c.* (Norfolk) genome only contained one *pmoCAB* cluster, as the *M.c* (Texas) genome was assembled into 114 separate contigs using Illumina short reads only.

Table 6.2 Estimation of *Methylococcus capsulatus* (Norfolk) and *Methylococcus capsulatus* (Texas) DNA-DNA hybridisation and BLAST comparison of key methanotroph and methylotroph marker genes between the genomes. (n.p. - not present in genome).

Comparison of *Methylococcus capsulatus* (Norfolk) and *Methylococcus capsulatus* (Texas) genomes													
Probability DNA-DNA Hybridisation >70% **(same species)**	**Probability** DNA-DNA Hybridisation >79% **(same subspecies)**	Comparison of marker genes between genomes											
		pmoA1		***pmoA2***		***mmoX***		***mxaF***		***fhcD***		**16S rRNA 1/2**	**16S rRNA 2/2**
		nucleotide identity (%)	amino acid identity (%)	nucleotide identity (%)	amino acid identity (%)	nucleotide identity (%)	amino acid identity (%)	nucleotide identity (%)	amino acid identity (%)	nucleotide identity (%)	amino acid identity (%)	nucleotide identity (%)	nucleotide identity (%)
97.48%	74.47%	99.73	100	n.p. (Texas)		99.56	100	99.67	100	100	100	n.p. (Texas)	n.p. (Texas)

6.4.3 Metabolic pathways predicted from the *Methylocaldum szegediense* (Norfolk) genome

6.4.3.1 Methane oxidation pathway

Two particulate methane monooxygenase gene clusters (*pmoCAB*) were present in *Methylocaldum szegediense* (Norfolk), with three additional *pmoC* sequences (two of which are within 2.5kb of each other). No genes encoding elements of soluble methane monooxygenase were detected in this genome.

Multiple genes encoding enzymes involved in methanol oxidation were present in the *Methylocaldum szegediense* (Norfolk) genome, including a Ca-dependent MDH cluster (*mxaFJGIRSACKLD*). Two sets of *xoxFJ* were also discovered, encoding the lanthanide dependent methanol dehydrogenase (*xoxF*) and the periplasmic binding protein (*xoxJ*) which Featherstone et al suggest may have a role in XoxF cofactor incorporation (Featherstone et al., 2019).

The *M.szegediense* (Norfolk) genome contained *mtdA, fchA, ftfl* genes encoding the necessary enzymes of the tetrahydrofolate (H_4F)-linked formaldehyde oxidation pathway, as well as the *glyA* gene encoding serine hydroxymethyltransferase which allows carbon transfer to the serine cycle for assimilation. The tetrahydromethanopterin (H_4MPT)-linked formaldehyde oxidation pathway may also be used by this methanotroph as the genome contains *fae, mtdB, fch* and the formyltransferase/hydrolase complex genes required for this pathway.

The ability of this methanotroph to oxidise formate to CO_2 is suggested by the presence of three sets of genes encoding formate dehydrogenases.

6.4.3.2. Methanotrophic carbon assimilation pathways

Methylocaldum szegediense (Norfolk) has genes for a full ribulose monophosphate pathway for carbon assimilation, the primary route in Type I methanotrophs (Trotsenko and Murrell, 2008). The possession of genes encoding a complete CBB cycle, missing only the seduheptulose-1,7-bisphosphatase gene and encoding a possible alternative enzyme for this step (pyrophosphate-dependent 6-phosphofructokinase) (Reshetnikov et al., 2008), provides an alternative pathway in this methanotroph. Genes encoding a partial serine pathway for carbon

incorporation are present, but genes for several key enzymes are missing including *hprA* (glycerate dehydrogenase), *gck* (glycerate-2-kinase), *ppc* (phosphoenolpyruvate carboxylase) and the malate thiokinase subunit genes *mtkA* and *mtkB*.

6.4.3.3. Key nitrogen metabolism genes

Methylocaldum szegediense (Norfolk) may be capable of dinitrogen fixation as it contains all three structural nitrogenase genes (*nifH*, *nifK* and *nifD*), as well as hydroxylamine detoxification due to the presence of a hydroxylamine oxidoreductase (*hao*) gene. The presence of nitrite reductase (*nirK*) and nitric oxide reductase (*norB, norC*) genes suggests this methanotroph can reduce nitrite to nitrous oxide, with no *nosZ* to encode nitrous oxide reductase for removal of N_2O.

Genes encoding enzymes for ammonia assimilation via pyruvate (*ald*) and alpha-ketoglutarate (*GDH2* and *gdhA*) by alanine dehydrogenase and glutamate dehydrogenase respectively, were present, along with the remaining components of the GS/GOGAT cycle (*glnA*, *gltB* and *gltD*).

6.4.3.4. *Methylocaldum* plasmid sequence

Methylocaldum szegediense (Norfolk) also contains a smaller ~25kb chromosome which appears to be a plasmid, as it encodes genes for a plasmid replication initiator protein (*trfA*), replication protein (*repA*) and a toxin anti-toxin system (plasmid retention mechanism). While the products of many of the coding sequences are of unknown function, the plasmid does contain a gene encoding a putative siphovirus gp157 protein which is thought to provide increased bacteriophage resistance (Foley et al., 1998; Zhong et al., 2018).

6.4.3.5. Comparison of conserved marker genes with other *Methylocaldum* genomes.

The closest isolate genome to *Methylocaldum szegediense* (Norfolk) appears to be that of *Methylocaldum szegediense* (O-12) (NCBI accession GCA_000427385.1), based on DNA-DNA hybridisation estimates (**Chapter 2.12.1**). A nucleotide and protein BLAST comparison of key marker genes as well as DNA-DNA hybridisation estimation between these genomes is shown in **Table 6.3**.

Table 6.3 Estimation of *Methylocaldum szegediense* (Norfolk) and *Methylocaldum szegediense* (O-12) DNA-DNA hybridisation and BLAST comparison of key marker genes between the genomes. (n.p. – not present in genome)

Comparison of *Methylocaldum szegediense* (Norfolk) and *Methylocaldum szegediense* (O-12) genomes													
Probability DNA-DNA Hybridisation >70% **(same species)**	**Probability** DNA-DNA Hybridisation >79% **(same subspecies)**	Comparison of marker genes between genomes											
		pmoA1		***pmoA2***		***mmoX***		***mxaF***		***fhcD***		**16S rRNA 1/2**	**16S rRNA 2/2**
		nucleotide identity (%)	amino acid identity (%)	nucleotide identity (%)	amino acid identity (%)	nucleotide identity (%)	amino acid identity (%)	nucleotide identity (%)	amino acid identity (%)	nucleotide identity (%)	amino acid identity (%)	nucleotide identity (%)	nucleotide identity (%)
97.33%	73.55%	100	100	n.p. (O-12)		n.p. (Norfolk) (O-12)		99.94	100	100	100	99.93	n.p. (O-12)

Both the extremely high marker gene nucleotide and amino acid % identities (>99.93) and the DNA-DNA hybridisation estimate between these two genomes suggest that they are very closely related strains. As was the case for the *Methylococcus capsulatus* comparison (**Table 6.2**), the absence of the second *pmoA* and 16S rRNA gene sequences in the *Methyocaldum szegediense* (O-12) sequence may be due to the difficulty of recovering multicopy genes and repetitive regions in genome assemblies (Alkan et al., 2011), rather than a true absence from the genome of this methanotroph.

The genome of *Methylocaldum szegediense* (Norfolk) is also highly similar to the *Methylocaldum* metagenome assembled genome (MAG) 36 from the 50ºC DNA-SIP incubation heavy fraction metagenome (**Chapter 5**). This MAG was determined to represent one of the active methanotrophs at this incubation temperature. The comparison between the *Methylocaldum szegediense* (Norfolk) and 50 ºC heavy fraction MAG 36 is presented in **Table 6.4**. The isolate genome and this MAG are clearly very similar, as previously mentioned, the inclusion of gene duplicates (e.g. *pmoA2*) in genome or metagenome short-read assemblies is difficult to achieve (Alkan et al., 2011). The apparent difference in 16S rRNA sequence between these two genomes may be due a similar reason (if this 16S rRNA gene sequence has been miss-assembled). There is frequently such a risk with 16S rRNA gene sequences as they are from highly repetitive genome regions and due to being multicopy can tend towards being binned into MAGs belonging to more abundant microbes.

Table 6.4 *Methylocaldum szegediense* (Norfolk) and 50ºC heavy fraction metagenome MAG 36 DNA-DNA hybridisation and BLAST comparisons of key marker genes between these genomes. (n.p. – not present in genome)

Comparison of *Methylocaldum szegediense* (Norfolk) and 50ºC Heavy fraction metagenome MAG 36													
Probability DNA-DNA Hybridisation >70% **(same species)**	**Probability** DNA-DNA Hybridisation >79% **(same subspecies)**	Comparison of marker genes between genomes											
		pmoA1		***pmoA2***		***mmoX***		***mxaF***		***fhcD***		**16S rRNA 1/2**	**16S rRNA 2/2**
		nucleotide identity (%)	amino acid identity (%)	nucleotide identity (%)	amino acid identity (%)	nucleotide identity (%)	amino acid identity (%)	nucleotide identity (%)	amino acid identity (%)	nucleotide identity (%)	amino acid identity (%)	nucleotide identity (%)	nucleotide identity (%)
97.84%	76.95%	100	100	n.p. (50ºC H 36)		n.p. (Norfolk) (50ºC H 36)		99.94	100	100	100	93.11	n.p. (50ºC H 36)

6.5 Discussion

Two methanotrophs were successfully isolated from biofilter soil, *Methylococcus capsulatus* and *Methylocaldum szegediense*, both designated Norfolk strains.

It is interesting that *Methylococcus capsulatus* was isolated from the biofilter, since while the biofilter is often running at thermotolerant or thermophilic temperatures (37-55ºC) (**Chapter 3**), and this strain is capable of growth over much of that range (37-50º), *Methylococcus* was not present in the 16S rRNA gene PCR amplicons generated from biofilter microbial community DNA. Neither were any unambiguous *Methylococcus* metagenome assembled genomes (MAGs) recovered from the biofilter soil metagenomes, although there were some MAGs belonging to *Methylococcaceae* of unassigned genera which could potentially be *Methylococcus* species (**Chapters 4** and **5**). If *Methylococcus* species are not highly abundant in the biofilter soil, then their frequent appearance among serial dilution plate colonies during biofilter methanotroph isolation experiments may be due to bias in isolation methods. Perhaps these *Methylococcus* species are better growing in NMS medium or on NMS agar to become the dominant methanotrophs in enrichment and isolation experiments. Difference in pH could be the cause of this discrepancy as the enrichment cultures originally used to isolate the (Norfolk) strains had a pH of 6.8 while it appears that the biofilter is usually the other side of neutral at pH 7.5-8.0 (**Chapter 3.4**), if this strain prefers slightly acidic conditions it may not be competitive in the biofilter.

Methylocaldum szegediense (Norfolk) has high degree of similarity to a methanotroph which appeared to be active in a 50ºC DNA-SIP $^{13}CH_4$ labelling experiment using biofilter soil taken from a hot region of the biofilter demonstrating high methane oxidation potential. This, or a very closely related methanotroph, was also the most abundant methanotroph found among the metagenome-assembled genomes in the DNA-SIP Timepoint 0 metagenome assembly which was effectively the metagenome of the *in-situ* microbial community in the biofilter at 50ºC and a depth of 50 cm (**Chapter 5**). The ability of this isolate to grow at temperatures above 50ºC often observed in the biofilter during established operation (**Chapter 3**) mark this *Methylocaldum* strain as a potential contributor to biofilter CH_4 turnover at the higher operational temperatures. Indeed, this isolate demonstrated an ability to grow at 62ºC which is only ~ 5ºC lower than the highest temperature measured within the biofilter during this whole project (67.8ºC).

Chapter 7: Synopsis

The main objectives (**Chapter 1.2.8**) to be addressed in this project were:

1. Where is methane (CH_4) oxidised within the biofilter?
2. Which are the most active CH_4 oxidisers (methanotrophs) *in-situ*?
3. What parameters may be limiting the activity of methanotrophs?

7.1 Results

7.1.1 Where is CH_4 oxidised within the biofilter?

A combined gas/temperature probe was used to measure CH_4 and temperature at different depths within the biofilter, in order to build up depth profiles of temperature linked with CH_4 consumption across the biofilter (**Chapter 3**). As can be seen in **Figure 7.1**, this demonstrated that during prolonged operation most CH_4 consumption occurs in the top 50 cm of the biofilter at a temperature around 50°C.

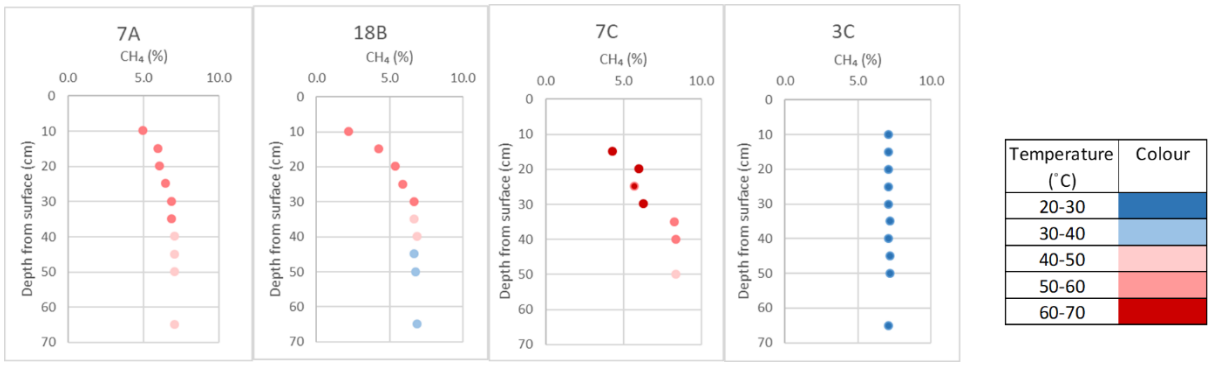

Figure 7.1 Examples of temperature/CH_4 consumption profiles. 7A, 7C and 18B represent the typical profiles observed within the biofilter, most CH_4 being removed at a high temperature in the 50cm below the biofilter surface. 3C represents an inactive region of the biofilter at ambient temperature with no CH_4 removal.

7.1.2 Which are the most active CH_4 oxidisers *in-situ*?

Based on 16S rRNA gene amplicon analysis, methanotrophs (active or otherwise) made up 5-10% of the biofilter soil bacteria, which represents a significant enrichment for a soil environment (**Chapter 4**). Feeding biofilter soil incubations with ^{13}C-methane labelled the DNA of active CH_4 metabolising methanotrophs (DNA-SIP, **Chapter 5**), this DNA was then separated to study the active community. 16S rRNA gene analysis of this DNA from incubations at different temperatures, suggested that the active methanotroph community within the biofilter shifts as temperature changes **(Figure 7.2)**.

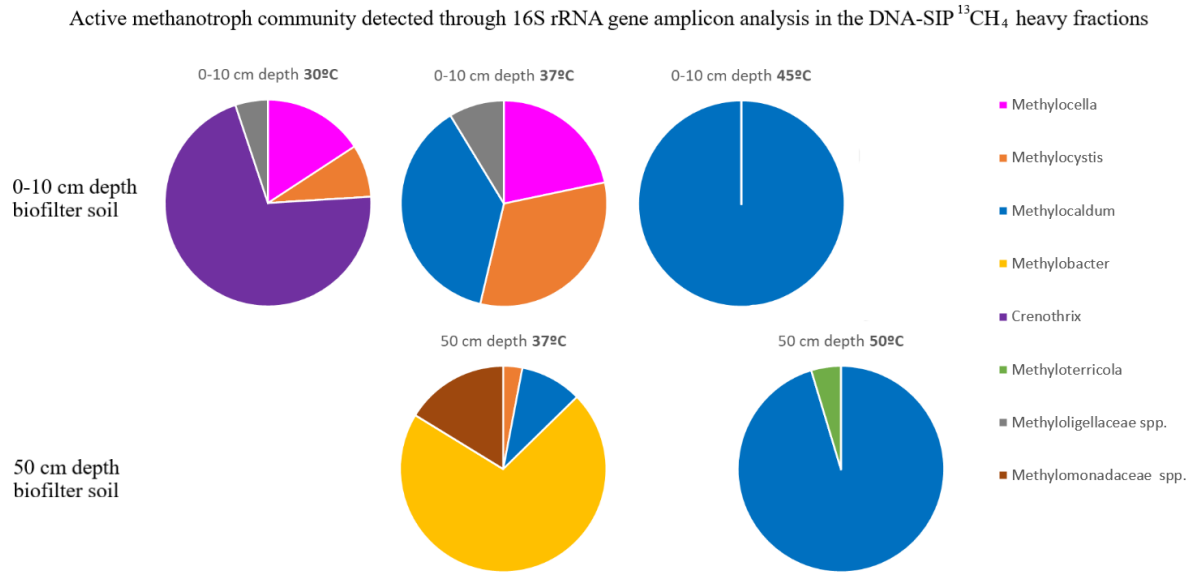

Figure 7.2 Relative abundance of 16S rRNA genes belonging to the different members of the active methanotroph community in the DNA-SIP $^{13}CH_4$ heavy fractions (**Chapter 5.2-3**).

While more diverse and variable communities were observed at lower temperatures, *Methylocaldum* species dominated the active community at (common *in-situ*) temperatures of 45˚C and 50°C. Metagenome analysis of ^{13}C enriched DNA fractions from the DNA-SIP experiment using soil taken from a hot region (50ºC) of the biofilter at a depth of 50 cm also suggested that a *Methylocaldum* and an unassigned *Methylococcaceae* species (possibly also *Methylocaldum*), were the most abundant active methanotrophs at 50ºC (**Chapter 5.3.3**). Furthermore, a methanotroph demonstrating a high degree of genomic similarity to this *Methylocaldum* was successfully isolated from biofilter soil. This isolate, *Methylocaldum szegediense* (Norfolk), was capable of growth at some of the highest temperatures recorded

within the biofilter (37-62ºC) (**Chapter 3** and **Chapter 6**). While the full extent of high heat adaptation in thermotolerant *Methylocaldum* species is unknown, Medvedkova and colleagues identified specific features thought to enhance thermotolerance in *Methylocaldum szegediense* (O-12), which might be shared with the Norfolk strain. At higher temperatures an increase in cytochrome c peroxidase activity was detected, which may serve to mitigate oxidative stress from reactive oxygen species formation; while the accumulation of sucrose could maintain metabolic enzyme activity, as it appeared to act as a thermoprotectant for formaldehyde and lactate dehydrogenases in cell free extracts (Medvedkova et al., 2009; Medvedkova et al., 2007).

These experiments suggested a wide range of methanotrophs were resident in the biofilter soil and that as conditions change within the biofilter, the best adapted methanotrophs dominate the active methane oxidising community. That being said, the heat generated by biological methane oxidation and respiration processes during biofilter operation appears to incubate the biofilter soil at around 50°C (**Chapter 3**), and so methane oxidation driven by thermophilic *Methylocaldum* is likely responsible for the bulk of biofilter CH_4 turnover during uninterrupted operation. Following disruption to operation (due to sub-optimal soil moisture or failure of gas supply) and concomitant biofilter cooling, the lower temperature adapted methanotrophs (*Methylobacter*, *Methylocella*, *Methylocystis* and *Crenothrix*) presumably take over CH_4 oxidation and heat the biofilter until the higher temperature is re-established. Interestingly the *Methylococcaceae* of unassigned genus which appeared active at 50ºC based on the DNA-SIP metagenome study (**Chapter 5.3**), also appeared to be competitive at the lower 37ºC incubation temperature, this suggested the methanotroph may have an advantage in this system which is prone to temperature fluctuations (**Chapter 3**).

7.1.3 What parameters may be limiting the activity of methanotrophs?

While a loss of CH_4 oxidation activity due to imbalance of the inflow gas CH_4:O_2 ratio was observed, a major physico-chemical parameter (in addition to temperature) effecting biofilter operation appears to be soil moisture content (**Chapter 3**). It was discovered that a higher CH_4 oxidation potential could be recovered in inactive dry biofilter soil by increasing soil moisture content (see **Figure 7.3**). Soil methane oxidation potential at different soil moisture levels was then characterised **Figure 7.4**, which proved useful in assessing the impact of wet and dry periods on biofilter CH_4 oxidation efficiency.

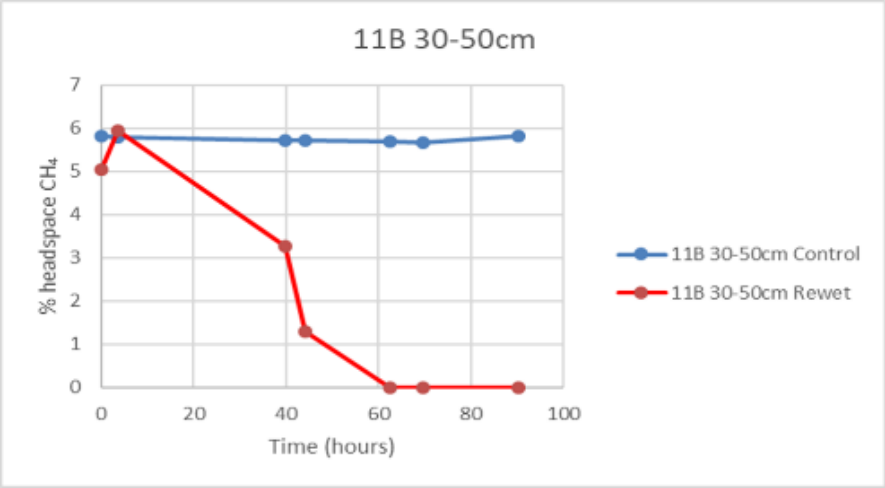

Figure 7.3 Effect of rewetting dry inactive soil on CH_4 oxidation potential. Blue line is unamended dry inactive soil, red line is dry inactive soil that has been rewetted with sterile water (adapted from **Figure 3.6**).

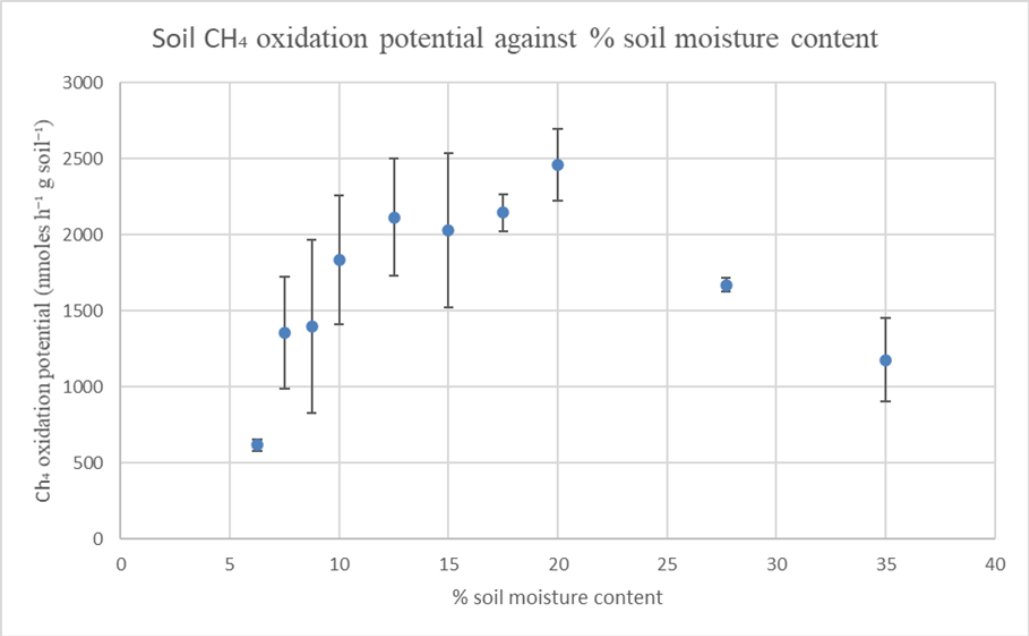

Figure 7.4 Biofilter soil CH_4 oxidation potential over a range of soil moisture levels, error bars show standard deviation (copy of **Figure 3.8**). CH_4 oxidation potential starts to drop off at lower (<10%) and higher (>27.5%) soil moisture content.

7.2 Conclusions and "take home points"

During typical operation the Strumpshaw biofilter establishes a *Methylococcaceae/Methylocaldum* active community at 50°C in the top 60 cm of the biofilter, this temperature is reached and maintained by biological activity (similar to the heat generated by microbes in a compost pile), and appears capable of oxidising >50% of CH_4 fed into the biofilter. Additionally, the biofilter soil moisture content was found to have a significant impact on biofilter CH_4 oxidation potential.

- With most CH_4 oxidation occurring in the top 60cm of the biofilter, future biofilter design should consider how much deeper than this is required to achieve even gas dispersion below the active zone. The full half-meter below this active zone at Strumpshaw may be excessive and the matrix material represents a major construction cost.
- Preventing stoppages in biofilter function (gas balance errors, power failures) is key to efficient running. Disrupting CH_4 supply results in a drop in biofilter temperature and noticeable reduction in biofilter soil CH_4 oxidation potential that can take many days/weeks to build back up (depending on shutdown length). The automation of biofilter inlet gas balancing has undoubtedly improved CH_4 oxidation efficiency, as shifting of the inlet gas O_2:CH_4 ratio away from the optimum (2:1) was a common problem.
- Soil moisture content represents a realistically manageable parameter for improved biofilter CH_4 turnover efficiency. Soil moisture content as low as 5% has been observed in the biofilter during dry periods alongside the expected drop in CH_4 oxidation, this represents a drop in efficiency of over 50% for extended periods (weather dependent). A simple sprinkler system could be implemented to wet down the biofilter during very dry spells. Similarly increasing drainage – perhaps through opening the leachate valve could mitigate the effects of waterlogged soils during very wet periods.

References

Adeosun E.K., Smith T.J., Hoberg A-M., Velarde G., Ford R., and Dalton H. (2004) *Formaldehyde dehydrogenase preparations from Methylococcus capsulatus (Bath) comprise methanol dehydrogenase and methylene tetrahydromethanopterin dehydrogenase*. Microbiology. 150. p707-13.

Alkan C., Sajjadian S., and Eichler E.E. (2011) *Limitations of next-generation genome sequence assembly*. Nature Methods. 8. p61-85.

Alneberg J., Bjarnason B. S., de Bruijn I., Schirmer M., Quick J., Ijaz U. Z., Loman N. J., Andersson A. F. and Quince C. (2013) *CONCOCT: Clustering cONtigs on COverage and ComposiTion.* arXiv: Genomics.

Amann R.I., Ludwig W., Schliefer K-H. (1995) *Phylogenetic Identification and In Situ Detection of Individual Microbial Cells without Cultivation*. Microbiological Reviews. 59. p143-69

Amaratunga K., Goodwin P.M., O'Connor C.D., and Anthony C. (1997) *The methanol oxidation genes mxaFJGIR(S)ACKLD in Methylobacterium extorquens*. FEMS Microbiology Letters. 146. p31-8.

Anthony C. (1982) *Biochemistry of Methylotrophs*. Academic Press.

Anthony C. (1992) *The structure of bacterial quinoprotein dehydrogenases*. International Journal of Biochemistry. 24. p29-39.

Anthony C., and Williams P. (2003) *The structure and mechanism of methanol dehydrogenase*. Biochimica et Biophysica Acta. 1647. p18-23.

Auman A.J., Speake C.C., and Lidstrom M.E. (2001) *nifH sequences and nitrogen fixation in Type I and Type II Methanotrophs*. Applied and Environmental Microbiology. 67. p4009-16.

Auman A.J., Stolyar S., Costello A.M. and Lidstrom M.E. (2000) *Molecular Characterization of Methanotrophic Isolates from Freshwater Lake Sediment.* ASM Applied and Environmental microbiology. 66. p5259-66.

Bay S.K., Dong X., Bradley J.A., Leung P.M., Grinter R., Jirapanjawat T., Arndt S.K., Cook P.L.M., LaRowe D.E., Nauer P.A., Chiri E., and Greening C. (2021) *Trace gas oxidizers are widespread and active members of soil microbial communities.* Nature Microbiology. 6. p246-56.

Banerjee R., Meier K.K., Munck E., and Lipscomb J.D. (2013) *Intermediate P* from Soluble Methane Monooxygenase Contains a Diferrous Cluster*. Biochemistry. 52. p4331-42.

Banerjee R., Proshlyakov Y., Lipscomb J.D., and Proshlyakov D.A. (2015) *Structure of the key species in the enzymatic oxidation of methane to methanol*. Nature. 518. p431-4.

Bartram A., Poon C. and Neufeld J. (2009) *Nucleic acid contamination of glycogen used in nucleic acid precipitation and assessment of linear polyacrylamide as an alternative co-precipitant.* Biotechniques. 47. p1019-22.

Baxter N.J., Hirt R.P., Bodrossy L., Kovacs K.L., Embley T.M., Prosser J.I., Murrell J.C. (2002) *The ribulose-1,5-bisphosphate carboxylase/oxygenase gene cluster of Methylococcus capsulatus (Bath).* Archives of Microbiology. 177. p279-89.

Belova S.E., Kulichevskaya I.S., Bodelier P.L.E., Dedysh S.N. (2013). *Methylocystis bryophila sp. nov., a facultatively methanotrophic bacterium from acidic Sphagnum peat, and emended description of the genus Methylocystis (ex Whittenbury et al. 1970)*. International Journal of Systematic and Evolutionary Microbiology. 63. p1096–104

de Bertoldi M., Vallini G., Pera A. (1983) *The Biology of Composting: A Review*. Waste Management and Research. 1. p157-76.

Bodrossy L., Holmes E.M., Holmes A.J., Kovács K.L., and Murrell J.C. (1997) *Analysis of 16S rRNA and methane monooxygenase gene sequences reveals a novel group of thermotolerant and thermophilic methanotrophs, Methylocaldum gen. nov*. Archives of Microbiology. 168. p493-503.

Bowman J.P., McCammon S.A., and Skerratt J.H. (1997) *Methylosphaera hansonii gen. nov., sp. nov., a psychrophilic, group I methanotroph from Antarctic marine-salinity, meromictic lakes*. Microbiology. 143. p1451-59.

Bowman J.P., Sly L.I., Nichols P.D, and Hayward A.C. (1993) *Revised Taxonomy of the Methanotrophs: Description of Methylobacter gen. nov., Emendation of Methylococcus, Validation of Methylosinus and Methylocystis Species, and a Proposal that the Family Methylococcaceae Includes Only the Group I Methanotrophs.* International Journal of Systematic Bacteriology. 43. p735-53.

Braakman R., and Smith E. (2013) *The compositional and evolutionary logic of metabolism*. Physical Biology. 10.

Brazeau B.J., and Lipscomb J.D. (2000) *Kinetics and Activation Thermodynamics of Methane Monooxygenase Compound Q Formation and Reaction with Substrates*. Biochemistry. 39. p13503-15.

Browell D., Georges M., Pawson D., and Shaughnessy J. (2009) *Control of landfill gas containing low concentrations of methane*. Environment Agency. 2009

Burrows K.J., Cornish A., Scott D., and Higgins I.J. (1984) *Substrate Specificities of the Soluble and Particulate Methane Mono-oxygenases of Methylosinus trichosporium OB3b*. Journal of General Microbiology. 130. p3327-33.

Callahan B.J., McMurdie P.J., Rosen M.J., Han A.W., Johnson A.J.A. and Holmes S.P. (2016) *DADA2: High resolution sample inference from Illumina amplicon data*. Nature Methods. 13. p581-3.

Camacho C., Coulouris G., Avagyan V., Ma N., Papadopoulos J., Bealer K., and Madden T.L. (2009) *BLAST+: architecture and applications.* BMC Bioinformatics. 10.

Cao L., Caldararu O., Rosenzweig A.C., and Ryde U. (2018) *Quantum Refinement Does Not Support Dinuclear Copper Sites in Crystal Structures of Particulate Methane Monooxygenase*. Angewandte Chemie International Edition. 57. p162-6.

Cappelletti M., Ghezzi D., Zannoni D., Capaccioni B., Fedi S. (2016) *Diversity of Methane-Oxidizing Bacteria in Soils from "Hot Lands of Medolla" (Italy) Featured by Anomalous High-Temperatures and Biogenic CO2 Emission*. Microbes and Environments. 31. p369-77.

Cebron A., Bodrossy L., Chen Y., Singer A.C., Thompson I.P., Prosser J.I., and Murrell J.C. (2007) *Identity of active methanotrophs in landfill cover soil as revealed by DNA-stable isotope probing*. FEMS Microbiol Ecol. 62. p12-23.

Chang W-H., Lin H-H., Tsai I-K., Huang S-H., Chung S-C., Tu I-P., Yu S. S-F., and Chan S.I. (2021) *Copper Centers in the Cryo-EM Structure of Particulate Methane Monooxygenase Reveal the Catalytic Machinery of Methane Oxidation*. Journal of the American Chemical Society. 143. p9922-32.

Chang J., Gu W., Park D., Semrau J.D., Dispirito A.A., and Yoon S. (2018) *Methanobactin from Methylosinus trichosporium OB3b inhibits N2O reduction in denitrifiers*. The ISME Journal. 12. p2086-9.

Chen Y., Crombie A., Rahman M.T., Dedysh S.N., Liesack W., Stott M.B., Alam M., Theisen A.R., Murrell J.C., and Dunfield P.F. (2010) *Complete Genome Sequence of the Aerobic Facultative Methanotroph Methylocella silvestris BL2*. American Society for Microbiology. 192. p3840-41.

Chen Y., Dumont M.G., Cébron A., and Murrell J.C. (2007) *Identification of active methanotrophs in a landfillcover soil through detection of expression of 16SrRNA and functional genes*. Environmental Microbiology. 9. p2855–69.

Chi Z-F., Lu W-J., and Wang H-T. (2015) *Spatial Patterns of Methane Oxidation and Methanotrophic Diversity in Landfill Cover Soils of Southern China*. J. Microbiol. Biotechnol. 25. p423-30.

Chistoserdova L. (2011) *Modularity of methylotrophy, revisited*. Environmental Microbiology. 13. p2603-22.

Chistoserdova L., Vorholt J.A., and Lidstrom M.E. (2005) *A genomic view of methane oxidation by aerobic bacteria and anaerobic archaea*. Genome Biology. 6.

Chistoserdova L.V., and Lidstrom M.E. (1994) *Genetics of the Serine Cycle in Methylobacterium extorquens AMi: Identification, Sequence, and Mutation of Three New Genes Involved in C1 Assimilation, orf4, mtkA, and mtkB*. Journal of Bacteriology. 176. p7398-404.

Chu F., Lidstrom M.E. (2016) *XoxF Acts as the Predominant Methanol Dehydrogenase in the Type I Methanotroph Methylomicrobium buryatense*. Journal of Bacteriology. 198. p1317-25.

Colby J., and Dalton H. (1979) *Characterization of the Second Prosthetic Group of the Flavoenzyme NADH-Acceptor Reductase (Component C) of the Methane Mono-oxygenase from Methylococcus capsulatus (Bath)*. Biochem. J. 177. p903-9.

Costello R.C. and Sullivan D.M. (2014) *Determining the pH Buffering Capacity of Compost Via Titration with Dilute Sulfuric Acid*. Waste and Biomass Valorization. 5. p505-13.

Crombie A.T, and Murrell J.C. (2014) *Trace-gas metabolic versatility of the facultative methanotroph Methylocella silvestris*. Nature. 510. p148-53.

Crowther G.J., Kosaly G., and Lidstrom M.E. (2008) *Formate as the Main Branch Point for Methylotrophic Metabolism in Methylobacterium extorquens AM1*. Journal of Bacteriology. 190. p5057-62.

Csáki R., Bodrossy L., Klem J., Murrell J.C., and Kovács K.L. (2003) *Genes involved in the copper-dependent regulation of soluble methane monooxygenase of Methylococcus capsulatus (Bath): cloning, sequencing and mutational analysis*. Microbiology. 149. p1785–95.

Culpepper M.A., and Rosenzweig A.C. (2012) *Architecture and active site of particulate methane monooxygenase.* Crit Rev Biochem Mol Biol. 47. 483-92.

Culpepper M.A., and Rosenzweig A.C. (2014) *Structure and Protein−Protein Interactions of Methanol Dehydrogenase from Methylococcuscapsulatus (Bath)*. Biochemistry. 53. p6211-19.

Czepial P.M., Mosher B., Crill P.M., and Harriss R.C. (1996) *Quantifying the effect of oxidation on landfill methane emissions.* Journal of Geophysical Research. 101. 16,721-29.

Dalton H. (1977) *Ammonia Oxidation by the Methane Oxidising Bacterium Methylococcus capsulatus Strain Bath*. Arch Microbiol. 114. p273-9.

Dam B., Dam S., Blom J., and Liesack W. (2013) *Genome analysis coupled with physiological studies reveals a diverse nitrogen metabolism in Methylocystis sp. strain SC2*. PLoS One. 8.

Dam B., Dam S., Kube M., Reinhardt R., and Liesack W. (2012) *Complete Genome Sequence of Methylocystis sp. Strain SC2, an Aerobic Methanotroph with High-Affinity Methane Oxidation Potential*. Journal of Bacteriology. 194. p6008-9.

Danilova O.V., Suzina N.E., Van De Kamp J., Svenning M.M., Bodrossy L., and Dedysh S.N.. (2016) *A new cell morphotype among methane oxidizers: a spiral-shaped obligately microaerophilic methanotroph from northern low-oxygen environments*. The ISME Journal. 10. p2734-43.

Darriba D., Posada D., Kozlov A.M., Stamatakis A., Morel B. and Flouri T. (2019) *ModelTest-NG: A New and Scalable Tool for the Selection of DNA and Protein Evolutionary Models*. Molecular Biology and Evolution. 37. p291-4.

Dassama L.M.K., Kenney G., Ro S.Y., Zielazinski E.L., and Rosenzweig A.C. (2016) *Methanobactin transport machinery*. PNAS. 113. p13027-32.

Dedysh S.N., Naumoff D.G., Vorobev A.V., Kyrpides N., Woyke T., Shapiro N., Crombie A.T., Murrell J.C. , Kalyuzhnaya M.G., Smirnova A.V., and Dunfield P.F. (2015) *Draft Genome Sequence of Methyloferula stellata AR4, an Obligate Methanotroph Possessing Only a Soluble Methane Monooxygenase.* Genome Announcements. 3.

Dedysh S.N., Berestovskaya Y.Y., Vasylieva L.V., Belova S.E., Khmelenina V.N., Suzina N.E., Trotsenko Y.A., Liesack W., and Zavarzin G.A. (2004) *Methylocella tundrae sp. nov., a novel methanotrophic bacterium from acidic tundra peatlands*. International Journal of Systematic and Evolutionary Microbiology. 54. p151–6.

Dedysh S.N., Liesack W., Khmelenina V.N., Suzina N.E., Trotsenko Y.A., Semrau J.D., Bares A.M., Panikov N.S., and Tiedje J.M. (2000) *Methylocella palustris gen. nov., sp. nov., a new methane-oxidizing acidophilic bacterium from peat bogs, representing a novel subtype of serine-pathway methanotrophs*. International Journal of Systematic and Evolutionary Microbiology. 50. p955-69.

Deng Y., Cui X., and Dumont M.G. (2016) *Identification of active aerobic methanotrophs in plateau wetlands using DNA stable isotope probing*. FEMS Microbiology Letters. 363.

Dennison C., David S., and Lee J. (2018) *Bacterial copper storage proteins*. Journal of Biological Chemistry. 293. p4616-27.

Deutzmann J.S., Hoppert M., and Schink B. (2014) *Characterization and phylogeny of a novel methanotroph, Methyloglobulus morosus gen.nov., spec.nov.* Systematic and Applied Microbiology. 37. p165-9.

Dever S.A., Swarbrick G.E., and Stuetz R.M. (2007) *Passive drainage and biofiltration of landfill gas: Australian field trial.* Waste Management. 27. p277-86.

Dinghua L., Liu C-H., Luo R., Sadakane K., and Lam T-W. (2019) *MEGAHIT: an ultra-fast single-node solution for large and complex metagenomics assembly via succinct de Bruijn graph* Bioinformatics. 31. p1674-6.

Dispirito A.A., Semrau J.D., Murrell J.C., Gallagher W.H., Dennison C., and Vuilleumier S. (2016) *Methanobactin and the Link between Copper and Bacterial Methane Oxidation.* Microbiology and Molecular Biology Reviews. 80. p387-409.

Doronina N., Kaparullina E., Trotsenko Y. (2014) *The Family Methylophilaceae*. In: The Prokaryotes. Springer. p869-80.

Dörr N., Glaser B., and Kolb S. (2010) *Methanotrophic Communities in Brazilian Ferralsols from Naturally Forested, Afforested, and Agricultural Sites*. Applied and Environmental Microbiology. 76. p1307-10.

Drewniak L., Maryan N., Lewandowski W., Kaczanowski S., and Sklodowska A. (2012) *The contribution of microbial mats to the arsenic geochemistry of an ancient gold mine*. Environmental Pollution. 162. p190-201.

Dumont M.G., (2014) *Primers: Functional Marker Genes for Methylotrophs and Methanotrophs*. In: McGenity T., Timmis K., Nogales B. (eds) *Hydrocarbon and Lipid Microbiology Protocols*. Springer Protocols Handbooks. p57-77.

Dumont M.G., Pommerenke B., and Casper P. (2013) *Using stable isotope probing to obtain a targeted metatranscriptome of aerobic methanotrophs in lake sediment*. Environmental Microbiology Reports. 5. p757-64.

Dumont M.G., Pommerenke B., Casper P., and Conrad R. (2011) *DNA-, rRNA- and mRNA-based stable isotope probing of aerobic methanotrophs in lake sediment*. Environmental Microbiology. 13. p1153-67.

Dunfield P.F., Belova S.E., Vorob'ev A.V., Cornish S.L., and Dedysh S.N. (2010) *Methylocapsa aurea sp. nov., a facultative methanotroph possessing a particulate methane monooxygenase, and emended description of the genus Methylocapsa*. International Journal of Systematic and Evolutionary Microbiology. 60. p2659–64.

Dunfield P.F., Yuryev A., Senin P., Smirnova A.V., Stott M.B., Hou S., Ly B., Saw J.H., Zhou Z., Ren Y., Wang J., Mountain B.W., Crowe M.A., Weatherby T.M., Bodelier P.L.E., Liesack W., Feng L., Wang L., and Alam M. (2007) *Methane oxidation by an extremely acidophilic bacterium of the phylum Verrucomicrobia.* Nature. 450. p879-82.

Dunfield P.F., Khmelenina V.N., Suzina N.E., Trotsenko Y.A., and Dedysh S.N. (2003) *Methylocella silvestris sp. nov., a novel methanotroph isolated from an acidic forest cambisol*. International Journal of Systematic and Evolutionary Microbiology. 53. p1231-9.

Durazzi F., Sala C., Castellani G., Manfreda G., Remondini D., and Cesare A.D. (2021) *Comparison between 16S rRNA and shotgun sequencing data for the taxonomic characterization of the gut microbiota*. Scientific Reports. 11.

El Ghazouani A., Basle A., Firbank S.J., Knapp C.W., Gray J., Graham D.W., and Dennison C. (2011) *Copper-Binding Properties and Structures of Methanobactins from Methylosinus trichosporium OB3b*. Inorg. Chem. 50. p1378-91.

Elmore B.O., Bergmann D.J., Klotz M.G., and Hooper A.B. (2007) *Cytochromes P460 and c0-beta; A new family of high-spin cytochromes c*. FEBS Letters. 581. p911-6.

Eren A.M., Vineis J.H., Morrison H.G. and Sogin M.L. (2013) *A Filtering Method to Generate High Quality Short Reads Using Illumina Paired-End Technology.* PLOS ONE. 8.

Eshinimaev B.T., Medvedkova K.A., Khmelenina V.N., Suzina N.E., OsipovG.A., Lysenko A.M., and Trotsenko Y.A. (2004) *New Thermophilic Methanotrophs of the Genus Methylocaldum*. Microbiology. 73. p448–56.

Ettwig K.F., Butler M.K., Paslier D.L., Pelletier E., Mangenot S., Kuypers M.M.M., Schreiber F., Dutilh B.E., Zedelius J., de Beer D., Gloerich J., Wessels H.J.C.T., van Alen T., Luesken F., Wu M.L., van de Pas-Schoonen K.T., Op den Camp H.J.M., Janssen-Megens E.M., Francoijs K.J., Stunnenberg H., Weissenbach J., Jetten M.S.M., and Strous M. (2010) *Nitrite-driven anaerobic methane oxidation by oxygenic bacteria*. Nature. 464. p543-8.

Featherston E.R., Rose H.R., McBride M.J.,Taylor E.M., Boal A., and Cotruvo J.A. (2019) *Biochemical and structural characterization of XoxG and XoxJ and their roles in activity of the lanthanide-dependent methanol dehydrogenase, XoxF*. ChemBioChem. 20. p2360-72.

Foley S., Lucchini S., Zwahlen M-C., and Brüssow H. (1998) *A Short Noncoding Viral DNA Element Showing Characteristics of a Replication Origin Confers Bacteriophage Resistance to Streptococcus thermophilus*. Virology. 250. p377-87.

Foster J.W., and Davis R.H. (1966) *A Methane-Dependent Coccus, with Notes on Classification and Nomenclature of Obligate, Methane-Utilizing Bacteria*. Journal of Bacteriology. 91. p1924-31.

Fox B.G., Surerus K.K., Munck E., and Lipscomb J.D. (1988) *Evidence for a p-Oxo-bridged Binuclear Iron Cluster in the Hydroxylase Component of Methane Monooxygenase*. The Journal of Biological Chemistry. 263. p10553-6.

Fox B.G., Froland W.A., Dege J.E., and Lipscomb J.D. (1989) *Methane Monooxygenase from Methylosinus trichosporium OB3b*. The Journal of Biological Chemistry. 264. p10023-33.

Frindte K., Maarastawi S.A., Lipski A., Hamacher J., and Knief C. (2017) *Characterization of the first rice paddy cluster I isolate, Methyloterricola oryzae gen. nov., sp. nov. and amended description of Methylomagnum ishizawai*. International Journal of Systematic and Evolutionary Biology. 67. p4507-14.

Gebert J., Singh B.K., Pan Y., and Bodrossy L. (2009) *Activity and structure of methanotrophic communities in landfill cover soils*. Environmental Microbiology Reports. 1. p414-23.

Gebert J., Groengroeft A., and Miehlich G. (2003) *Kinetics of microbial landfill methane oxidation in biofilters*. Waste Management. 23. p609-19.

Ghashghavi M., Belova S.E., Bodelier P.L.E, Dedysh S.N., Kox M.A.R., Speth D.R., Frenzel P., Jetten M.S.M., Lücker S., and Lüke C. (2019) *Methylotetracoccus oryzae Strain C50C1 Is a Novel Type Ib Gammaproteobacterial Methanotroph Adapted to Freshwater Environments*. mSphere. 4.

Ghashghavi M., Jetten M.S.M., and Lüke C. (2017) *Survey of methanotrophic diversity in various ecosystems by degenerate methane monooxygenase gene primers*. AMB Express. 7.

Goodwin P.M., and Anthony C. (1995) *The biosynthesis of periplasmic electron transport proteins in methylotrophic bacteria*. Microbiology. 141. p1051-64.

Gorokhova E., Motiei A., and El-Shehawy R. (2021) *Understanding Biofilm Formation in Ecotoxicological Assays With Natural and Anthropogenic Particulates*. Frontiers in Microbiology. 12.

Green J., and Dalton H. (1985) *Protein B of Soluble Methane Monooxygenase from Methylococcus capsulatus (Bath)*. The Journal of Biological Chemistry. 260. p15795-801.

Grinsven S.V., Damsté J.S.S., Harrison J., , Polerecky L., and Villanueva L. (2021) *Nitrate promotes the transfer of methane-derived carbon from the methanotroph Methylobacter sp. to the methylotroph Methylotenera sp. in eutrophic lake water*. Limnology and Oceanography. 66. p878-91.

Gu W., Farhan Ul Haque M., Dispirito A.A., Semrau J.D. (2016) *Uptake and effect of rare earth elements on gene expression in Methylosinus trichosporium OB3b*. FEMS Microbiology Letters. 363. p1-6.

Guindon S., Dufayard J-F., Lefort V., Anisimova M., Hordijk W., and Gascuel O. (2010) *New Algorithms and Methods to Estimate Maximum-Likelihood Phylogenies: Assessing the Performance of PhyML 3.0*. Systematic Biology. 59. p307-21.

Hall T.A. (1999) *BioEdit: a user-friendly biological sequence alignment editor and analysis program for Windows 95/98/NT.* Nucleic Acids Symposium Series. 41, p95–98

Hanson R.S., and Hanson T.E. (1996) *Methanotrophic bacteria*. Microbiological Reviews. 60. p439-71.

He R., Wang J., Pohlman J.W., Jia Z., Chu Y-X., Wooller M.J., and Leigh M.B. (2022) *Metabolic flexibility of aerobic methanotrophs under anoxic conditions in Arctic lake sediments*. ISME. 16. p78-90.

He Z., Cai C., Wang J., Xu X., Zheng P., Jetten M.S.M., and Hu B. (2016) *A novel denitrifying methanotroph of the NC10 phylum and its microcolony*. Scientific Reports. 6.

Henard C.A., Wu C., Xiong W., Henard J.M., Davidheiser-Kroll B., Orata F.D., and Guarnieri M.T. (2021) *Ribulose-1,5-Bisphosphate Carboxylase/Oxygenase (RubisCO) Is Essential for Growth of the Methanotroph Methylococcus capsulatus Strain Bath*. Applied and Environmental Microbiology. 87.

Henneberger R., Luke C., Mosberger L., and Schroth M.H. (2011) *Structure and function of methanotrophic communities in a landfill-cover soil*. FEMS Microbiol Ecol. 81. p52-65.

Higgins I.J., Best D.J., Hammond R.C., Scott D. (1981) *Methane-Oxidizing Microorganisms*. Microbiological Reviews. 45. p556-90.

Hoefman S., van der Ha D., Boon N., Vandamme P., De Vos P., and Heylen K., (2014) *Niche differentiation in nitrogen metabolism among methanotrophs within an operational taxonomic unit*. BMC Microbiology. 14. p1-11.

Holmes A.J., Costello A., Lidstrom M.E, Murrell J.C. (1995) *Evidence that particulate methane monooxygenase and ammonia monooxygenase may be evolutionarily related*. FEMS Microbiology Letters. 132. p203-8.

Houghten K.M., Carere C.R., Stott M.B., and McDonald I.R. (2019) *Thermophilic methanotrophs: in hot pursuit*. FEMS Microbiology Ecology. 95.

Howarth R.W. (2015) *Methane emissions and climatic warming risk from hydraulic fracturing and shale gas development: implications for policy*. Energy and Emission Control Technologies. 3. p45-54.

Huber-Humer M., Gebert J., Hilger H. (2008) *Biotic systems to mitigate landfill methane emissions*. Waste Management & Research. 26. p33-46.

Hutchens E., Radajewski S., Dumont M.G., McDonald I.R. and Murrell J.C. (2004) *Analysis of methanotrophic bacteria in Movile Cave by stable isotope probing*. Environmental Microbiology. 6. p111-120.

IPCC (2007) *Climate Change 2007: The Physical Science Basis. Contribution of Working Group I to the Fourth Assessment Report of the Intergovernmental Panel on Climate Change.* Cambridge University Press.

IPCC (2014) *Climate Change 2014: Synthesis Report. Contribution of Working Groups I, II and III to the Fifth Assessment Report of the Intergovernmental Panel on Climate Change*.

Islam T., Hernández M., Gessesse A., Murrell J.C., and Øvreås L. (2021) *A Novel Moderately Thermophilic Facultative Methylotroph within the Class Alphaproteobacteria*. Microorganisms. 9.

Islam T., Larsen Ø., Torsvik V., Øvreås L., Panosyan H., Murrell J.C., Birkeland N-K., and Bodrossy L. (2015) *Novel Methanotrophs of the Family Methylococcaceae from Different Geographical Regions and Habitats*. Microorganisms. 3. p484-99.

Ito K., Takahashi M., Yoshimoto T., and Tsuru D. (1994) *Cloning and High-Level Expression of the Glutathione Independent Formaldehyde Dehydrogenase Gene from Pseudomonas putida*. Journal of Bacteriology. 176. p2483-91.

Jäckel U., Thummes K., and Kämpfer P. (2005) *Thermophilic methane production and oxidation in compost*. FEMS Microbiology Ecology. 52. p175-184.

Jardine C.N., Boardman B., Osman A., Vowles J., and Palmer J. (2004) *Methane UK*, research report 30 Environmental Change Institute, Citeseer, Oxford.

Kalyuzhnaya M.G., Puri A.W., and Lidstrom M.E. (2015) *Metabolic engineering in methanotrophic bacteria*. Metabolic Engineering. 29. p142-152.

Kalyuzhnaya M.G., Khmelenina V., Eshinimaev B., Sorokin D., Fuse H., Lidstrom M., and Trotsenko Y. (2008) *Classification of halo(alkali)philic and halo(alkali)tolerant methanotrophs provisionally assigned to the genera Methylomicrobium and Methylobacter and emended description of the genus Methylomicrobium.* International Journal of Systematic and Evolutionary Microbiology. 58. p591-6.

Kalyuzhnaya M.G., Khmelenina V.N., Kotelnikova S., Holmquist L., Pedersen K., and Trotsenko Y.A. (1999) *Methylomonas scandinavica sp. nov., a New Methanotrophic Psychrotrophic Bacterium isolated from Deep Igneous Rock Ground Water of Sweden*. System. Appl. Microbiol. 22. p565-72.

Kanehisa M. (2019) *Toward understanding the origin and evolution of cellular organisms*. Protein Science. 28. p1947-51.

Kanehisa M., Sato Y., and Morishima K., (2016) *BlastKOALA and GhostKOALA: KEGG Tools for Functional Characterization of Genome and Metagenome Sequences*. Journal of Molecular Biology. 428. p726-31.

Kang D.D., Li F., Kirton E., Thomas A., Egan R., An H., and Wang Z. (2019) *MetaBAT 2: an adaptive binning algorithm for robust and efficient genome reconstruction from metagenome assemblies*. PeerJ. 7.

Kenney G.E., and Rosenzweig A.C. (2013) *Genome mining for methanobactins*. BMC Biology. 11. p1-17.

Khadem A.F., Wieczorek A.S., Pol A., Vuilleumier S., Harhangi H.R., Dunfield P.F., Kalyuzhnaya M.G., Murrell J.C., Francoijs K-J., Stunnenberg H.G., Stein L.Y., DiSpirito A.A., Semrau J.D., Lajus A., Médigue C., Klotz M.G., Jetten M.S.M., and Op den Camp H.J.M. (2012) *Draft Genome Sequence of the Volcano-Inhabiting Thermoacidophilic Methanotroph Methylacidiphilum fumariolicum Strain SolV*. Journal of Bacteriology. 194. p3729-30.

Khadem A.F., Pol A., Wieczorek A., Mohammadi S.S., Francoijs K-J., Stunnenberg H.G., Jetten M.S.M., and Op den Camp H.J.M. (2011) *Autotrophic Methanotrophy in Verrucomicrobia: Methylacidiphilum fumariolicum SolV Uses the Calvin-Benson-Bassham Cycle for Carbon Dioxide Fixation*. Journal of Bacteriology. 193. p4438-46.

Khadem A.F., Pol A., Jetten M.S.M., and Op den Camp H.J.M. (2010) *Nitrogen fixation by the verrucomicrobial methanotroph Methylacidiphilum fumariolicum SolV*. Microbiology. 156. p1052-9.

Khalifa A., Lee C.G., Ogiso T., Ueno C., Dianou D., Demachi T., Katayama A., and Asakawa S. (2015) *Methylomagnum ishizawai gen. nov., sp. nov., a mesophilic type I methanotroph isolated from rice rhizosphere*. 65. p3527–3534.

Khmelenina V.N., Kalyuzhnaya M.G., Starostina N.G., Suzina N.E., and Trotsenko Y.A. (1997) *Isolation and Characterization of Halotolerant Alkaliphilic Methanotrophic Bacteria from Tuva Soda Lakes*. Current Microbiology. 35. p257-61.

Kim H.J., Graham D.W., Dispirito A.A., Alterman M.A., Galeva N., Larive C.K., Asunskis D., and Sherwood P.M.A. (2004) *Methanobactin, a Copper-Acquisition Compound from Methane-Oxidizing Bacteria*. Science. 305. p1612-5.

Kits K.D., Klotz M.G., and Stein L.Y. (2015) *Methane oxidation coupled to nitrate reduction under hypoxia by the Gammaproteobacterium Methylomonas denitrificans, sp. nov. type strain FJG1*. Environmental Microbiology.17. p3219-32.

Kizilova A., Yurkov A., and Kravchenko I. (2013) *Aerobic Methanotrophs in Natural and Agricultural Soils of European Russia*. Diversity. 5. p541-56.

Kleiveland C.R., Hult L.T.O., Kuczkowska K., Jacobsen M., Lea T., and Pope P.B. (2012) *Draft Genome Sequence of the Methane-Oxidizing Bacterium Methylococcus capsulatus (Texas)*. Journal of Bacteriology. 194. p6626.

Klindworth A., Pruesse E., Schweer T., Peplies J., Quast C., Horn M., and Glöckner F.O. (2013) *Evaluation of general 16S ribosomal RNA gene PCR primers for classical and next-generation sequencing-based diversity studies*. Nucleic Acids Research. 41.

Knief C. (2015) *Diversity and Habitat Preferences of Cultivated and Uncultivated Aerobic Methanotrophic Bacteria Evaluated Based on pmoA as Molecular Marker*. Frontiers in Microbiology. 6.

Knightly D., Nedwell D.B., and Cooper M. (1995) *Capacity for Methane Oxidation in Landfill Cover Soils Measured in Laboratory-Scale Soil Microcosms*. Applied and Environmental Microbiology. 61. p592-601.

Kong J-Y., Su Y., Zhang Q-Q., Bai Y., Xia F-F., Fang C-R., He R. (2013) *Vertical profiles of community and activity of methanotrophs in landfill cover soils of different age*. Journal of Applied Microbiology. 115. p756-65.

Koval S.F., Hynes S.H., Flannagan R.S., Pasternak Z., Davidov Y., and Jurkevitch E. (2013) *Bdellovibrio exovorus sp. nov., a novel predator of Caulobacter crescentus*. International Journal of Systematic and Evolutionary Microbiology. 63. p146-151.

Krause S.M.B., Johnson T., Karunaratne Y.S., Fu Y., Beck D.A.C., Chistoserdova L., and Lidstrom M.E. (2017) *Lanthanide-dependent cross-feeding of methane-derived carbon is linked by microbial community interactions*. PNAS. 114. p358-63.

Lane D.J. (1991) *16S/23S rRNA sequencing*. Nucleic acid techniques in bacterial systematics. John Wiley & Sons. p115–75.

Latifah O., Ahmed O.H. and Majid N.M.A (2018) *Soil pH Buffering Capacity and Nitrogen Availability Following Compost Application in a Tropical Acid Soil*. Compost Science and Utilization. 26.

Lee J., Kim K., Chang I.S., Kim M-G., Ha K-S., Lee E.Y., Lee J., and Kim C. (2016) *Enhanced mass transfer rate of methane in aqueous phase via methyl-functionalized SBA-15*. Journal of Molecular Liquids. 215. p154-160.

Lee S-K., Nesheim J.C., and Lipscomb J.D. (1993a) *Transient Intermediates of the Methane Monooxygenase Catalytic Cycle*. The Journal of Biological Chemistry. 268. p21569-77.

Lee S-K., Fox B.G., Froland W.A., Lipscomb J.D., and Munck E. (1993b) *A Transient Intermediate of the Methane Monooxygenase Catalytic Cycle Containing an FPFP Cluster*. J. Am. Chem. Soc. 115. p6450-1.

Lee S.J. (2016) *Hydroxylation of methane through component interactions in soluble methane monooxygenases*. Journal of Microbiology. 54. p277-82.

Li Q-M., Zhou Y.L., Wei Z.F., and Wang Y. (2021) *Phylogenomic Insights into Distribution and Adaptation of Bdellovibrionota in Marine Waters*. Microorganisms. 9.

Lieberman R.L., and Rosenzweig A.C.(2004) *Biological Methane Oxidation: Regulation, Biochemistry, and Active Site Structure of Particulate Methane Monooxygenase*. Critical Reviews in Biochemistry and Molecular Biology. 39. p147-64.

Lieberman R.L., and Rosenzweig A.C. (2005) *Crystal structure of a membrane-bound metalloenzyme that catalyses the biological oxidation of methane*. Nature. 434. p177-82.

Limbri H., Gunawan C., Thomas T., Smith A., Scott J., and Rosche B. (2014) *Coal-Packed Methane Biofilter for Mitigation of Green House Gas Emissions from Coal Mine Ventilation Air*. PLoS ONE. 9.

Lin J-L., Radajewski S., Eshinimaev B.T., Trotsenko Y.A., McDonald I.R., and Murrell J.C. (2004) *Molecular diversity of methanotrophs in Transbaikal soda lake sediments and identification of potentially active populations by stable isotope probing*. Environmental Microbiology. 6. p1049-60.

Liu Y., Nesheim J.C., Lee S-K., Lipscomb J.D.. (1995) *Gating Effects of Component B on Oxygen Activation by the Methane Monooxygenase Hydroxylase Component*. The Journal of Biological Chemistry. 270. p24662-5.

Lovering A.L., and Sockett R.E. (2021) *Microbe Profile: Bdellovibrio bacteriovorus: a specialized bacterial predator of bacteria*. Microbiology. 167.

Macey M.C., Pratscher J., Crombie A., and Murrell J.C. (2018) *Draft Genome Sequences of Obligate Methylotrophs Methylovorus sp. Strain MM2 and Methylobacillus sp. Strain MM3, Isolated from Grassland Soil*. Microbiology Resource Announcements. 7.

Manzanera M. (2021) *Dealing with water stress and microbial preservation*. Environmental Microbiology. 23. p 3351–59.

Martin M. (2011) *Cutadapt removes adapter sequences from high-throughput sequencing reads*. EMBnet.journal. 17. p10-12.

Matsen J.B., Yang S., Stein L.Y., Beck D., and Kalyuzhnaya M.G. (2013) *Global molecular analyses of methane metabolism in methanotrophic alphaproteobacterium, Methylosinus trichosporium OB3b. Part I: transcriptomic study.* Frontiers in Microbiology. 4.

McDonald I.R., Bodrossy L., Chen Y., and Murrell J.C. (2008) *Molecular Ecology Techniques for the Study of Aerobic Methanotrophs*. Applied and Environmental Microbiology. 74. p1305-15.

Medvedkova K.A., Khmelenina V.N., Suzina N.E., and Trotsenko Y.A. (2009) *Antioxidant Systems of Moderately Thermophilic Methanotrophs Methylocaldum szegediense and Methylococcus capsulatus*. Microbiology. 78. p670-7.

Medvedkova K.A., Khmelenina V.N., and Trotsenko Y.A. (2007) *Sucrose as a Factor of Thermal Adaptation of the Thermophilic Methanotroph Methylocaldum szegediense O-12*. Microbiology. 76. p500-2.

Meier-Kolthoff J.P, Carbasse J.S., Peinado-Olarte R.L., and Göker M. (2021) *TYGS and LPSN: a database tandem for fast and reliable genome-based classification and nomenclature of prokaryotes*. Nucleic Acids Research. 50. pD801-7.

Met Office (n.d.) *Marham (Norfolk) UK climate averages*. Available at: https://www.metoffice.gov.uk/research/climate/maps-and-data/uk-climate-averages/u127sby66. Accessed 28.1.22.

Methanotroph Commons (2013), image , accessed 23rd May 2018 http://www.methanotroph.org/wp-content/uploads/2013/05/Fig-1_1.jpg

Meyer F., Paarmann D., D'Souza M., Olson R., Glass E.M., Kubal M., Paczian T., Rodriguez A., Stevens R., Wilke A., Wilkening J., and Edwards R.A. (2008) *The metagenomics RAST server – a public resource for the automatic phylogenetic and functional analysis of metagenomes*. BMC Bioinformatics. 9. p1-8.

Meyer-Dombard D.R., Bogner J.E., and Malas J. (2020) *A Review of Landfill Microbiology and Ecology: A Call for Modernization With 'Next Generation' Technology*. Frontiers in Microbiology. 11.

Minoche A.E., Dohm J.C., and Himmelbauer H. (2011) *Evaluation of genomic high-throughput sequencing data generated on Illumina HiSeq and Genome Analyzer systems.* Genome Biology. 12.

Miura Y., Wake H. and Kato T. (1991) *TBE, or not TBE; that is the question: Beneficial usage of tris-borate for obtaining a higher resolution of small DNA fragments by agarose gel electrophoresis*. 43. p1-6.

Mohammadi S.S., Pol A., van Alen T., Jetten M.S.M., and Op den Camp H.J.M. (2017) *Ammonia Oxidation and Nitrite Reduction in the Verrucomicrobial Methanotroph Methylacidiphilum fumariolicum SolV*. Frontiers in Microbiology. 8.

Morris S.A., Radajewski S., Willison T.W., and Murrell J.C., (2002) *Identification of the Functionally Active Methanotroph Population in a Peat Soil Microcosm by Stable-Isotope Probing*. Applied and Environmental Microbiology. 68. p1446-53.

Murrell J.C, and Smith T.J (2010) *Biochemistry and Molecular Biology of Methane Monooxygenase.* In Handbook of Hydrocarbon and Lipid Microbiology. Springer. p1045-55.

Murrell J.C., McDonald I.R., and Gilbert B. (2000) *Regulation of expression of methane monooxygenases by copper ions*. Trends in Microbiology. 8. p221-5.

Murrell J.C., and Dalton H. (1983a) *Purification and Properties of Glutamine Synthetase from Methylococcus capsulatus (Bath)*. Journal of General Microbiology. 129. p1187-96.

Murrell J.C., and Dalton H. (1983b) *Ammonia Assimilation in Methylococcus capsulatus (Bath) and other Obligate Methanotrophs*. Journal of General Microbiology. 129. p1197-206.

Muyzer G., de Waal E.C., and Uitterlinden A.G. (1993) *Profiling of Complex Microbial Populations by Denaturing Gradient Gel Electrophoresis Analysis of Polymerase Chain Reaction-Amplified Genes Coding for 16SrRNA*. ASM Applied and Environmental Microbiology. 59. p695-700.

Myung J., Wang Z., Yuan T., Zhang P., Van Nostrand J.D., Zhou J., and Criddle C.S. (2015) *Production of Nitrous Oxide from Nitrite in Stable Type II Methanotrophic Enrichments*. Environmental Science & Technology. 49. p10969-75.

Nakagawa T., Mitsui R., Tani A., Sasa T., Tashiro S., Iwama T., Hayakawa T., and Kawai K (2012). *A Catalytic Role of XoxF1 as La3+-Dependent Methanol Dehydrogenase in Methylobacterium extorquens Strain AM1*. PLOS ONE. 7.

National Research Council (US) Committee on Toxicology.(1984) *Emergency and Continuous Exposure Limits for Selected Airborne Contaminants: Volume 1*. METHANE. Available from: https://www.ncbi.nlm.nih.gov/books/NBK208285/. Accessed 28.01.22

National Center for Biotechnology Information (NCBI)[Internet]. (1988) Bethesda (MD): National Library of Medicine (US), National Center for Biotechnology Information. [cited 2022 Jan 28]. Available from: https://www.ncbi.nlm.nih.gov/

Neufeld J.D., Vohra J., Dumont M.G., Lueders T., Manefield M., Friedrich M.W., and Murrell J.C. (2007) *DNA stable-isotope probing*. Nature Protocols. 2. p860-6.

Nguyen H-H.T., Elliott S.J., Yip J. H-K., and Chan S.I. (1998) *The Particulate Methane Monooxygenase from Methylococcus capsulatus (Bath) Is a Novel Copper-containing Three-subunit Enzyme*. The Journal of Biological Chemistry. 273. p7957-66.

Nunn D.N., Day D., and Anthony C. (1989) *The second subunit of methanol dehydrogenase of Methylobacterium extorquens AM1*. Biochem. J. 260. p857-62.

Nurk S., Meleshko D., Korobeynikov A., and Pevzner P.A. (2017) *metaSPAdes: a new versatile metagenomic assembler*. Genome Research. 27. p824-34.

Nyerges G., and Stein L.Y. (2009) *Ammonia cometabolism and product inhibition vary considerably among species of methanotrophic bacteria*. FEMS Microbiol Lett. 297. p131-6.

Nyerges G., Han S-K., and Stein LY. (2010) *Effects of Ammonium and Nitrite on Growth and Competitive Fitness of Cultivated Methanotrophic Bacteria*. Applied and Environmental Microbiology. 76. p5648-51.

Omel'chenko M.V., Vasil'eva L.V., Zavarzin G.A., Savel'eva N.D., Lysenko A.M., Miytushina L.L., Khmelenina V.N., and Trotsenko, Y.A. (1996) *A novel psychrophilic methanotroph of the genus Methylobacter*. Mikrobiologiya. 65. p384-9.

Omelchenko M.V., Vasilyeva L.V., and Zavarzin G.A. (1993) *Psychrophilic Methanotroph from Tundra Soil*. Current Microbiology. 27. p255-9.

Orata F.D., Meier-Kolthoff J.P., Sauvageau D., and Stein L.Y., (2018*) Phylogenomic Analysis of the Gammaproteobacterial Methanotrophs (Order Methylococcales) Calls for the Reclassification of Members at the Genus and Species Levels*. frontiers in Microbiology. 9.

Oren A., Garrity G.M., Parker C.T., Chuvochina M., and Trujillo M.E. (2020) *Lists of names of prokaryotic Candidatus taxa*. International Journal of Systematic and Evolutionary Microbiology. 70. p3956–4042.

Orsi W.D., Smith J.M., Liu S., Liu Z., Sakamoto C.M., Wilken S., Poirier C., Richards T.A., Keeling P.J., Worden A.Z., and Santoro A.E. (2016) *Diverse, uncultivated bacteria and archaea underlying the cycling of dissolved protein in the ocean*. The ISME Journal. 10. p2158-73.

Oshkin I.Y., Suleimanov R.Z., Khmelenina V.N., Mardanov A.V., Pimenov N.V.,Dedysh S.N. (2022) *Complete Genome Sequence of Methylococcus capsulatus MIR, a Methanotroph Capable of Growth on Methanol*. Microbiology Resource Announcements. Vol 11.

Oshkin I.Y., Beck D.A.C., Lamb A.E., Tchesnokova V., Benuska G., McTaggart T.L., Kalyuzhnaya M.G., Dedysh S.N., Lidstrom M.E., and Chistoserdova L. (2015) *Methane-fed microbial microcosms show differential community dynamics and pinpoint taxa involved in communal response*. The ISME Journal. 9. p1119-29.

Oswald K., Graf J.S., Littmann S., Tienken D., Brand A., Wehrli B., Albertsen M., Daims H., Wagner M., Kuypers M.M.M., Schubert C.J., and Milucka J. (2017) *Crenothrix are major methane consumers in stratified lakes*. The ISME Journal. 11. p2124–40.

Parks D.H., Imelfort M., Skennerton C.T., Hugenholtz P., and Tyson G.W. (2015) *CheckM: assessing the quality of microbial genomes recovered from isolates, single cells, and metagenomes*. Genome Research. 25. p1043-45.

Pehme K-M., Orupõld K., Kuusemets V., Tamm O., Jani Y., Tamm T., Kriipsalu M. (2020) *Field Study on the Efficiency of a Methane Degradation Layer Composed of Fine Fraction Soil from Landfill Mining*. Sustainability. 12. p6209.

Pol A., Barends T.R.M., Dietl A., Khadem A.F., Eygensteyn J., Jetten M.S.M., Op den Camp H.J.M. (2014) *Rare earth metals are essential for methanotrophic life in volcanic mudpots.* Environmental Microbiology. 16. p255-64.

Popov V.O., and Lamzin V.S. (1994) *NAD+-dependent formate dehydrogenase*. Biochem. J. 301. p625-43.

Poret-peterson A.T., Graham J.E., Gulledge J., and Klotz MG. (2008) *Transcription of nitrification genes by the methane-oxidizing bacterium, Methylococcus capsulatus strain Bath*. The ISME Journal. 2. p1213-20.

Qiu Y-L., Kuang X-Z., Shi X-S., Yuan X-Z., and Guo R-B. (2014) *Terrimicrobium sacchariphilum gen. nov., sp. nov., an anaerobic bacterium of the class 'Spartobacteria' in the phylum Verrucomicrobia, isolated from a rice paddy field*. International Journal of Systematic and Evolutionary Microbiology. 64. p1718–23.

Quast C., Pruesse E., Yilmaz P., Gerken J., Schweer T., Yarza P., Peplies J., and Glöckner F.O. (2013) *The SILVA ribosomal RNA gene database project: improved data processing and web-based tools.* Nucleic Acids Research. 41. pD590-6.

Quince C., Walker A.W., Simpson J.T., Loman N.J., and Segata N. (2017) *Shotgun metagenomics, from sampling to analysis*. Nature Biotechnology. 35. p833-44.

Radajewski S., Webster G., Reay D.S., Morris S.A., Ineson P., Nedwell D.B., Prosser J.I., and Murrell J.C. (2002) *Identification of active methylotroph populations in an acidic forest soil by stable-isotope probing*. Microbiology. 148. p2331-42.

Rahalkar M., Bussmann I., and Schink B. (2007) *Methylosoma difficile gen. nov., sp. nov., a novel methanotroph enriched by gradient cultivation from littoral sediment of Lake Constance*. International Journal of Systematic and Evolutionary Microbiology. 57. p1073-80.

Rainer E.M., Seppey C.V.W., Tveit A.T., and Svenning M.M. (2020) *Methanotroph populations and CH 4 oxidation potentials in high-Arctic peat are altered by herbivory induced vegetation change*. FEMS Microbiology Ecology. 96.

Rasigraf O., Kool D.M., Jetten M.S.M., Damste J.S.S., and Ettwig K.F. (2014) *Autotrophic Carbon Dioxide Fixation via the Calvin-Benson-Bassham Cycle by the Denitrifying Methanotroph "Candidatus Methylomirabilis oxyfera*. Applied and Environmental Microbiology. 80. p2451-60.

Ren T., Roy R., and Knowles R. (2000) *Production and Consumption of Nitric Oxide by Three Methanotrophic Bacteria*. Applied and Environmental Microbiology. 66. p3891-97.

Rissanen A.J., Saarenheimo J., Tiirola M., Peura S., Aalto S.L., Karvinen A., and Nykänen H. (2018) *Gammaproteobacterial methanotrophs dominate methanotrophy in aerobic and anaerobic layers of boreal lake waters*. Aquatic Microbial Ecology. 81. p257–76.

Rodriguez (2018) *The Microbial Genomes Atlas (MiGA) webserver: taxonomic and gene diversity analysis of Archaea and Bacteria at the whole genome level*. Nucleic Acids Research. 46. pW282-8.

Rosenzweig A.C., Frederick C.A., Lippard S.J., and Nordlund P. (1993) *Crystal structure of a bacterial non-haem iron hydroxylase that catalyses the biological oxidation of methane*. Nature. 366. p537-43.

Russo C.A.M., and Selvatti A.P. (2018) *Bootstrap and Rogue Identification Tests for Phylogenetic Analyses*. Molecular Biology and Evolution. 35. p2327-33.

Sanschagrin S., and Yergeau E. (2014) *Next-generation Sequencing of 16S Ribosomal RNA Gene Amplicons*. Journal of Visualized Experiments. 90.

Saunois M., Stavert A.R., Poulter B., Bousquet P., Canadell J.G., Jackson R.B., Raymond P.A., Dlugokencky E.J., Houweling S., Patra P.K., Ciais P., Arora V.K., Bastviken D., Bergamaschi P., Blake D.R., Brailsford G., Bruhwiler L., Carlson K.M., Carrol M., Castaldi S., Chandra N., Crevoisier C., Crill P.M., Covey K., Curry C.L., Etiope G., Frankenberg C., Gedney N., Hegglin M.I., Höglund-Isaksson L., Hugelius G., Ishizawa M., Ito A., Janssens-Maenhout G., Jensen K.M., Joos F., Kleinen T., Krummel P.B., Langenfelds R.L., Laruelle G.G., Liu L., Machida T., Maksyutov S., McDonald K.C., McNorton J., Miller P.A, Melton J.R., Morino I., Müller J., Murguia-Flores F., Naik V., Niwa Y., Noce S., O'Doherty S., Parker R.J., Peng C., Peng S., Peters G.P., Prigent C., Prinn R., Ramonet M., Regnier P., Riley W.J., Rosentreter J.A., Segers A., Simpson I.J., Shi H., Smith S.J., Steele L.P., Thornton B.F., Tian H., Tohjima Y., Tubiello F.N., Tsuruta A., Viovy N., Voulgarakis A., Weber T.S., van Weele M., van der Werf G.R., Weiss R.F., Worthy D., Wunch D., Yin Y., Yoshida Y., Zhang W., Zhang Z., Zhao Y., Zheng B., Zhu Q., Zhu Q., and Zhuang Q. (2020) *The Global Methane Budget 2000–2017*. Earth System Science Data. 12. p1561-623.

Scheller S., Goenrich M., Boecher R., Thauer R.K., and Jaun B. (2010) *The key nickel enzyme of methanogenesis catalyses the anaerobic oxidation of methane*. Nature. 465. p606-9.

Schendel F.J., Bremmon C.E., Flickinger M.C., Guettler M., and Hanson R.S. (1990) *L-Lysine Production at 50°C by Mutants of a Newly Isolated and Characterized Methylotrophic Bacillus sp.* Applied and Environmental Microbiology. 56. p963–70.

Scheutz C., and Kjeldsen P. (2005) *Biodegradation of Trace Gases in Simulated Landfill Soil.* Journal of the Air & Waste Management Association. 55. p878-85.

Scheutz C., Kjeldsen P., De Visscher A., Gebert J., Hilger H.A., Huber-Humer M., and Spokas K. (2009) *Microbial methane oxidation processes and technologies for mitigation of landfill gas emissions*. Waste Management & Research. 27. p409-55.

Schloss P.D., and Handelsman J. (2005) *Introducing DOTUR, a Computer Program for Defining Operational Taxonomic Units and Estimating Species Richness*. Applied and Environmental Microbiology. 71. p1501-6.

Seemann T. (2014) *Prokka: rapid prokaryotic genome annotation*. Bioinformatics. 30. p2068-69.

Semrau J.D. (2011) *Bioremediation via methanotrophy: overview of recent findings and suggestions for future research*. Frontiers in Microbiology. 2. p1-7.

Semrau J.D., Jagadeven S., Dispirito A.A., Khalifa A., Scanlan J., Bergman B.H., Freemeier B.C., Baral B.S., Bandow N.L., Vorobev A., Haft D.H., Vuilleumier S., and Murrell J.C. (2013) *Methanobactin and MmoD work in concert to act as the 'copper-switch' in methanotrophs*. Environmental Microbiology. 15. p3077-86.

Sharp C.E, Smirnova A.V., Graham J.M., Stott M.B., Khadka R., Moore T.R., Grasby S.E., Strack M., and Dunfield P.F. (2014) *Distribution and diversity of Verrucomicrobia methanotrophs in geothermal and acidic environments*. Environmental Microbiology. 16. p1867-78.

Singh A.K., Nakhate S.P., Gupta R.K., Chavan A.R., Poddar B.J., Prakash O., Shouche Y.S., Purohit H.J., and Khardenavis A.A. (2022) *Mining the landfill soil metagenome for denitrifying methanotrophic taxa and validation of methane oxidation in microcosm*. Environmental Research. 215.

Söhngen N.L. (1906) *Uber bakterien welche methan ab kohlenstoffnahrung und energiequelle gerbrauchen (On bacteria which use methane as a carbon and energy source)*. Z. Bakteriol. Parazitenk. (Infektionster). 15. p513-17.

Song Y., Kaster A.K., Vollmers J., Song Y., Davison P.A., Frentrup M., Preston G.M., Thompson I.P., Murrell J.C., Yin H., Hunter C.N., and Huang W.E. (2017) *Single-cell genomics based on Raman sorting reveals novel carotenoid-containing bacteria in the Red Sea*. Microbial Biotechnology. 10. p125-37.

Stafford G.P., Scanlan J., McDonald I.R., and Murrell J.C. (2003) *rpoN, mmoR and mmoG, genes involved in regulating the expression of soluble methane monooxygenase in Methylosinus trichosporium OB3b*. Microbiology. 149. p1771-84.

Stanley S.H., Prior S.D., Leak D.J., and Dalton H. (1983) *Copper stress underlies the fundamental change in intracellular location of methane mono-oxygenase in methane-oxidizing organisms: studies in batch and continuous cultures*. Biotechnology Letters. 5. p487-492.

Stein L.Y., Yoon S., Semrau J.D., Dispirito A.A., Crombie A., Murrell J.C., Vuilleumier S., Kalyuzhnaya M.G., Op den Camp H.J.M., Bringel F., Bruce D., Cheng J-F., Copeland A., Goodwin L., Han S., Hauser L., Jetten M.S.M., Lajus A., Land M.L., Lapidus A., Lucas S., Medigue C., Pitluck S., Woyke T., Zeytun A., and Klotz M.G. (2010) *Genome sequence of the obligate methanotroph Methylosinus trichosporium strain OB3b*. Journal of Bacteriology. 192. p6497-98.

Stein L.Y., and Klotz M.G. (2011) *Nitrifying and Denitrifying pathways of methanotrophic bacteria*. Biochem. Soc. Trans. 39. p1826-31.

Stein L.Y., Roy R., and Dunfield P.F. (2012) *Aerobic Methanotrophy and Nitrification: Processes and Connections*. eLS.

Stirling D.I., and Dalton H. (1978) *Properties of the Methane Mono-oxygenase from extracts of Methylosinus trichosporium and evidence for Its Similarity to the Enzyme from Methylococcus capsulutus (Bath)*. Eur. J. Biochem. 96. p205-12.

Stoecker K., Bendinger B., Schöning B., Nielsen P.H., Nielsen J.L., Baranyi C., Toenshoff E.R., Daims H., Wagner M. (2006) *Cohn's Crenothrix is a filamentous methane oxidizer with an unusual methane monooxygenase.* PNAS. 103. p2363–7.

Stolyar S., Coste A.M., Peeples T.L., and Lidstrom M.E. (1999) *Role of multiple gene copies in particulate methane monooxygenase activity in the methane-oxidizing bacterium Methylococcus capsulates Bath*. Microbiology. 145. p1235-44.

Su Y., Zhang X., Xia F-F., Zhang Q-Q., Kong J-Y., Wang J., and He R. (2014) *Diversity and activity of methanotrophs in landfill cover soils with and without landfill gas recovery systems*. Systematic and Applied Microbiology. 37. p200-7.

Takeuchi M., Ozaki H., Hiraoka S., Kamagata Y., Sakata S., Yoshioka H., and Iwasak W. (2019) *Possible cross-feeding pathway of facultative methylotroph Methyloceanibacter caenitepidi Gela4 on methanotroph Methylocaldum marinum S8*. PLoS ONE. 14.

Takeuchi M., Katayama T., Yamagishi T., Hanada S., Tamaki H., Kamagata Y., Oshima K., Hattori M., Marumo K., Nedachi M., Maeda H., Suwa Y., and Sakata S. (2014 a) *Methyloceanibacter caenitepidi gen. nov., sp. nov., a facultatively methylotrophic bacterium isolated from marine sediments near a hydrothermal vent*. International Journal of Systematic and Evolutionary Microbiology. 64. p462-8.

Takeuchi M., Kamagata Y., Oshima K., Hanada S., Tamaki H., Marumo K., Maeda H., Nedachi M., Hattori M., Iwasaki W., Sakata S. (2014b) *Methylocaldum marinum sp. nov., a thermotolerant, methane-oxidizing bacterium isolated from marine sediments, and emended description of the genus Methylocaldum.* International Journal of Systematic and Evolutionary Microbiology. 64. p3240–6

Tamura K. Stecher G., and Kumar S. (2021) *MEGA11: Molecular Evolutionary Genetics Analysis Version 11*. Molecular Biology and Evolution. 38. p3022-27.

Taubert M., Grob C., Howat A.M., Burns O.J., Dixon J.L., Chen Y., and Murrell J.C. (2015) *XoxF encoding an alternative methanol dehydrogenase is widespread in coastal marine environments*. Environmental Microbiology. 17. p3937-48.

Teeseling M.C.F., Pol A., Harhangi H.R., van der Zwart S., Jetten M.S.M., Op den Camp H.J.M., and van Niftrik L. (2014) *Expanding the Verrucomicrobial Methanotrophic World: Description of Three Novel Species of Methylacidimicrobium gen. nov.* Applied and Environmental Microbiology. 80. p6782-91.

Tikhonova E.N, Grouzdev D.S., Avtukh A.N., Kravchenko I.K. (2021) *Methylocystis silviterrae sp.nov., a high-affinity methanotrophic bacterium isolated from the boreal forest soil*. International Journal of Systematic and Evolutionary Biology. 71.

Tinberg C.E., and Lippard S.J. (2009) *Revisiting the Mechanism of Dioxygen Activation in Soluble Methane Monooxygenase from M. capsulatus (Bath)*: Evidence for a Multi-Step, Proton-Dependent Reaction Pathway. Biochemistry. 48. p12145-58.

Trimmer M., Shelley F.C., Purdy K.J., Maanoja S.T., Chronopoulou P-M., and Jonathan G (2015) *Riverbed methanotrophy sustained by high carbon conversion efficiency*. The ISME Journal. 9. p2304-14.

Tringe S.G., and Hugenholtz P. (2008) *A renaissance for the pioneering 16S rRNA gene*. Current Opinion in Microbiology. 11. p442-6.

Trotsenko Y.A., and Murrell J.C. (2008) *Chapter 5 Metabolic Aspects of Aerobic Obligate Methanotrophy*. Advances in Applied Microbiology. 63. p183-229.

Turgeon N., Bihan Y.L., Buelna G., Bourgault C., Verreault S., Lessard P., Nikiema J., and Heitz M. (2011) *Application of methanotrophic biofilters to reduce GHG generated by landfill in Quebec City (Canada)*. Transactions on Ecology and the Environment. 147. p387-97.

Ukaegbu U.E., Henery S., and Rosenzweig A.C. (2006) *Biochemical Characterization of MmoS, a Sensor Protein Involved in Copper-Dependent Regulation of Soluble Methane Monooxygenase*. Biochemistry. 45. p10191-8.

Ul Haque M.F., Kalidass B., Vorobev A., Baral B.S., Dispirito A.A., and Semrau J.D. (2015) *Methanobactin from Methylocystis sp. Strain SB2 Affects Gene Expression and Methane Monooxygenase Activity in Methylosinus trichosporium OB3b*. Applied and Environmental Microbiology. 81. p2466-73.

U.S. Department of Agriculture Soil Survey Staff (2009) *Soil Survey Field and Laboratory Methods Manual*. Soil Survey Investigations Report No. 51.

Uritskiy G.V., DiRuggiero J., and Taylor J. (2018) *MetaWRAP—a flexible pipeline for genome-resolved metagenomic data analysis*. Microbiome. 6.

Vallenet D., Calteau A., Dubois M., Amours P., Bazin A., Beuvin M., Burlot L., Bussell X., Fouteau S., Gautreau G., Lajus A., Langlois J., Planel R., Roche D., Rollin J., Rouy Z., Sabatet V., and Medigue C. (2020) *MicroScope: an integrated platform for the annotation and exploration of microbial gene functions through genomic, pangenomic and metabolic comparative analysis*. Nucleic Acids Research. 48. pD579-89.

Ve T., Mathisen K., Helland R., Karlsen O.A., Fjellbirkeland A., Røhr A.K., Andersson K.K., Pedersen R-B., Lillehaug J.R., and Jensen H.B. (2012) *The Methylococcus capsulatus (Bath) Secreted Protein, MopE*, Binds Both Reduced and Oxidized Copper*. PLOS ONE. 7.

Veillette M., Girard M., Viens P., Brzezinski R., and Heitz M. (2012) *Function and limits of biofilters for the removal of methane in exhaust gases from the pig industry*. Applied Microbiology and Biotechnology. 94. p601–11.

Vekeman B., Kerckhof F.M., Cremers G., de Vos P., Vandamme P.,Boon N., Op den Camp H.J.M., and Heylen K. (2016) *New Methyloceanibacter diversity from North Sea sediments includes methanotroph containing solely the soluble methane monooxygenase*. Environmental Microbiology. 18. p4523-36.

Vita N., Platsaki S., Basle A., Allen S.J., Paterson N.G., Crombie A.T., Murrell J.C., Waldron K.J., and Dennison C. (2015) *A four-helix bundle stores copper for methane oxidation*. Nature. 525. p140-3.

Vorholt J.A. (2002) *Cofactor-dependent pathways of formaldehyde oxidation in methylotrophic bacteria*. Arch Microbiol. 178. p239-49.

Vorholt J.A., Marx C.J., Lidstrom M.E., and Thauer R.K.(2000) *Novel Formaldehyde-Activating Enzyme in Methylobacterium extorquens AM1 Required for Growth on Methanol*. Journal of Bacteriology. p6645-50.

Vorobev A.V., Baani M., Doronina N.V., Brady A.L., Liesack W., Dunfield P.F., and Dedysh S.N. (2011) *Methyloferula stellate gen. nov., sp. nov., an acidophilic, obligately methanotrophic bacterium that possesses only a soluble methane monooxygenase*. International Journal of Systematic and Evolutionary Microbiology. 61. p2456-63.

Waite D.W., Chuvochina M., Pelikan C., Parks D.H., Yilmaz P., Wagner M., Loy A., Naganuma T., Nakai R., Whitman W.B., Hahn M.W., Kuever J., and Hugenholtz P. (2020) *Proposal to reclassify the proteobacterial classes Deltaproteobacteria and Oligoflexia, and the phylum Thermodesulfobacteria into four phyla reflecting major functional capabilities*. International Journal of Systematic and Evolutionary Biology. 70. p5972-6016.

Wang Y., Ji Y., Wharfe E.S., Meadows R.S., March P., Goodacre R., Xu J., and Huang W.E. (2013) *Raman Activated Cell Ejection for Isolation of Single Cells*. Anal. Chem. 85. p10697-701.

Wang W., Iacob R.E., Luoh R.P., Engen J.R., and Lippard S.J. (2014) *Electron Transfer Control in Soluble Methane Monooxygenase*. American Chemical Society. 136. p9754-62.

Wang Y., Huang W.E., Cui L., and Wagner M. (2016) *single cell stable isotope probing in microbiology using Raman microspectroscopy*. Current Opinion in Biotechnology. 41. p34-42.

Wang X., Cao A., Zhao G., Zhou C., and Xu R. (2017) *Microbial community structure and diversity in a municipal solid waste landfill*. Waste Management. 66. p79-87.

Walters K.J., Gassner G.T., Lippard S.J., and Wagner G. (1999) *Structure of the soluble methane monooxygenase regulatory protein B*. PNAS. 96. p7877-82.

Ward N., Larsen O., Sakwa J., Bruseth L., Khouri H., Durkin A.S., Dimitrov G.,Jiang L., Scanlan D., Kang K.H., Lewis M., Nelson K.E., Methe B., Wu M., Heidelberg J.F., Paulsen I.T., Fouts D., Ravel J., Tettelin H., Ren Q., Read T., Deboy R.T., Seshadri R., Salzberg S.L., Jensen H.B., Birkeland N.K., Nelson W.C., Dodson R.J., Grindhaug S.H., Holt I., Eidhammer I., Jonasen I., Vanaken S., Utterback T., Feldblyum T.V., Fraser C.M., Lillehaug J.R., and Eisen J.A. (2004) *Genomic Insights into Methanotrophy: The Complete Genome Sequence of Methylococcus capsulatus (Bath)*. PLoS Biology. 2.

Watanabe M., Kojima H., and Fukui M. (2015) *Limnochorda pilosa gen. nov., sp. nov., a moderately thermophilic, facultatively anaerobic, pleomorphic bacterium and proposal of Limnochordaceae fam. nov., Limnochordales ord. nov. and Limnochordia classis nov. in the phylum Firmicutes*. International Journal of Systematic and Evolutionary Microbiology. 65. p2378-84.

Whalen S.C., Reeburgh W.S., and Sandbeck K.A. (1990) *Rapid Methane Oxidation in a Landfill Cover Soil*. Applied and Environmental Microbiology. 56. p3405-11.

White D. (2007) *The Physiology and Biochemistry of Prokaryotes 3rd edition*. Oxford University Press.

Wise M.G., McArthur J.V., and Shimkets L.J. (2001) *Methylosarcina fibrata gen. nov., sp. nov. and Methylosarcina quisquiliarum sp. nov., novel type I methanotrophs*. International Journal of Systematic and Evolutionary Microbiology. 51. p611–21.

Wise M.G., McArthur J.V., and Shimkets L.J. (1999) *Methanotroph Diversity in Landfill Soil: Isolation of Novel Type I and Type II Methanotrophs Whose Presence Was Suggested by Culture-Independent 16S Ribosomal DNA Analysis*. Applied and Environmental Microbiology. 65. p4887-97.

Wittenbury R., Phillips K.C., and Wilkinson J.F. (1970) *Enrichment Isolation and some properties of Methane-utilizing bacteria*. Journal of General Microbiology. 61. p205-18.

Wood D.E., Lu J., and Langmead B. (2019) *Improved metagenomic analysis with Kraken 2*. Genome Biology. 20.

Wu M.L., Ettwig K.F., Jetten M.S.M., Strous M., Keltjens J.T., and van Niftrik L. (2011) *A new intra-aerobic metabolism in the nitrite-dependent anaerobic methane-oxidizing bacterium Candidatus 'Methylomirabilis oxyfera'*. Biochem. Soc. Trans. 39. p243-8.

Wu M.L., van Teeseling M.C.F., Willems M.J.R, van Donselaar E.G., Klingl A., Rachel R., Geerts W.J.C., Jetten M.S.M., Strous M., and van Niftrik L. (2012) *Ultrastructure of the Denitrifying Methanotroph "Candidatus Methylomirabilis oxyfera," a Novel Polygon-Shaped Bacterium*. Journal of Bacteriology. 194. p284-91.

Wu M.L., Wessels H.J.C.T., Pol A., Op den Camp H.J.M., Jetten M.S.M., van Niftrik L., and Keltjens J.T. (2015) *XoxF-Type Methanol Dehydrogenase from the Anaerobic Methanotroph "Candidatus Methylomirabilis oxyfera"*. Applied and Environmental Microbiology. 81. p1442-51.

Wu X-L., Yu S-L., Gu J., Zhao G-F., and Chi C-Q. (2009) *Filomicrobium insigne sp. nov., isolated from an oil-polluted saline soil*. International Journal of Systematic and Evolutionary Microbiology. 59. p300-5.

Wu Y-W., Simmons B.A., Singer S.W. (2015) *MaxBin 2.0: an automated binning algorithm to recover genomes from multiple metagenomic datasets*. Bioinformatics. 32. p605-7.

Yang Y., Chen J., Pratscher J., and Xie S. (2022) *DNA-SIP reveals an overlooked methanotroph, Crenothrix sp., involved in methane consumption in shallow lake sediments*. Science of the Total Environment. 814.

Yu Z., Pesesky M., Zhang L., Huang J., Winkler M., and Chistoserdova L. (2020) *Complex Interplay between Nitric Oxide, Quorum Sensing, and the Unique Secondary Metabolite Tundrenone Constitutes the Hypoxia Response in Methylobacter*. mSystems. 5.

Zahn J.A., Bergmann D.J., Boyd J.M., Kunz R.C., and Dispirito A.A. (2001) *Membrane-Associated Quinoprotein Formaldehyde Dehydrogenase from Methylococcus capsulatus Bath*. Journal of Bacteriology. 183. p6832-40.

Zhang X., Kong J-Y., Xia F-F., Su Y., and He R. (2014) *Effects of ammonium on the activity and community of methanotrophs in landfill biocover soils*. Systematic and Applied Biology. 37. p296-304.

Zigah P.K., Oswald K., Brand A., Dinkel C., Wehrli B., and Schubert C.J. (2015) *Methane oxidation pathways and associated methanotrophic communities in the water column of a tropical lake*. Limnology and Oceanography. 60. p553-72.

Zhong K.X., Suttle C.A, Baudoux A-C., Derelle E., Colombet J., Cho A., Caleta J., Six C., and Jacquet S. (2018) *A New Freshwater Cyanosiphovirus Harboring Integrase*. Frontiers in Microbiology. 9.

Bioinformatics Data Access

NCBI Bioproject Accessions:

11B/11C boundary soil core

PRJNA936813 : Biofilter sector 11B/11C boundary soil core

16S rRNA gene amplicon analyses **Chapter 4.4.1** and **Chapter 5.2.2**

2C and 11B soil cores

PRJNA936822 : Biofilter sector 2C and 11B soil cores

16S rRNA gene amplicon and metagenome analyses **Chapter 4.4.2** and **Chapter 4.5**

19B soil

PRJNA936830 : Biofilter sector B19 soil

16S rRNA gene amplicon and metagenome analyses **Chapter 5.3**

ENA draft genome project references:

***Methylocaldum szegediense* (Norfolk)**

PRJEB52687

***Methylococcus capsulatus* (Norfolk)**

PRJEB60078